Improved Mass Transport Efficiency in Copper Solvent Extraction

A Thesis Submitted for the Degree of Doctor of Philosophy

by

Ross John Gordon, *MChem*

School of Chemistry

Faculty of Science and Engineering

The University of Edinburgh

November 2008

Abstract

This thesis considers methods which can be employed to increase the mass of copper transferred into and out of the organic phase during the load and strip stages of commercial solvent extraction processes. Conventional 5-alkylsalicylaldoxime reagents transfer 1 mol of divalent copper per 2 mol of ligand in a neutral complex of the type $[Cu(L\text{-}H)_2]$ *via* a pH-swing process. New *tri*acidic ligands have been designed which triple the molar transport of copper to form $[Cu_3(L\text{-}3H)_2]$. Until recently copper recovery by solvent extraction has been confined to oxidic ores which are leached with sulfuric acid. New leaching technologies generate high tenor copper sulfate feed streams from sulfidic ores. The conventional 5-alkylsalicylaldoxime reagents do not work effectively in conjunction with these leach processes as they do not consume the acid which is generated on loading the oxime. To address this problem ditopic zwitterionic ligands have been designed which can transfer both metal cation and attendant anion. These new metal salt reagents are diacidic, therefore not only transfer metal salts but also increase the molar transport relative to the conventional reagents. Equilibrium-modifiers are often added to improve the mass transport efficiency of conventional solvent extraction processes. The nature of their interaction with the species in solution is poorly understood. This thesis investigates their interaction with the free ligands and copper complexes to gain an understanding of their mode of action in order to rationalise the design of future modifiers to optimise recovery efficiencies.

Increased molar transport is addressed in Chapter 2. The diacidic ligand 5-methylsalicylaldehyde-pivaloylhydrazide (**L2**) and its *di*nuclear copper complex $[Cu_2(\mathbf{L2}\text{-}2H)_2]$ were synthesised and characterised to gain an understanding of their speciation in solution. X-ray structural analysis of $[Cu_2(\mathbf{L2}\text{-}2H)_2]$ confirmed that the phenolate oxygen atoms bridge the copper centres rather than the amidato oxygen atoms of the hydrazone. Variable temperature magnetic susceptibility data confirm that the copper centres are antiferromagnetically coupled as expected for the Cu-O-Cu angle (99.6(2)°). An understanding of the coordination geometry of the *di*nuclear systems lead to design of *tri*acidic ligands. A series of 3-hydrazono- and 3-hydroxyanil- 5-alkylsalicylic acids were synthesised. The prototype ligand 5-methyl-

3-octanoylhydrazonosalicylic acid (**L6**) was demonstrated to triple molar transport and increase mass transport by 2.5 fold. Solvent extraction results indicate that copper is sequentially loaded as pH is increased. The plateaux observed in loading curves suggest formation of stable *mono*-, *di*-, and *tri*-nuclear copper complexes within the pH-ranges 1.75 - 2.75, 3.25 - 4.0 and > 4.25 respectively. The triacidic ligands were also demonstrated to double the molar transport of the conventional salicylaldoximes when used in 1:1 blends by formation of a ternary complex.

Chapter 3 describes the incorporation of two tertiary amine groups into *di*acidic salicylaldehydehydrazone ligands to form dinucleating metal *salt* extractants. Piperidinomethyl, piperazinomethyl and dihexylamino groups were incorporated into various positions of the ligand including 3- and/or 5- positions of the salicylaldehyde or incorporated into the hydrazone. Solvent extraction results obtained for 3,5-bis((dihexylamino)methyl)salicylaldehyde-octanoic hydrazone (**L20**) are consistent with transfer of 1 mol of copper sulfate per mol of ligand in the organic phase between pH 2.0 and 2.5. This result is indicative of the formation of $[Cu_2(\mathbf{L20})_2(SO_4)_2]$.

Conventional salicylaldoximes are "strong" copper extractants which require concentrated acid electrolyte to efficiently strip the copper from the organic phase. However, as the use of concentrated acid affects the quality of the copper cathodes, oxygen-containing equilibrium modifiers are often added. These facilitate copper stripping without adversely affecting the loading. The affect of 2-ethylhexanol (2-EH) and trioctylphosphine oxide (TOPO) on the extractive ability of 5-*t*-octylsalicylaldoxime (**19**) in *n*-heptane is reported. Both are found to decrease copper extraction more under stripping conditions than loading conditions. 2-EH shows little affect at pH greater than 2.5. TOPO does not significantly affect copper loading at pH greater than 3.0. Evidence for the formation of the adduct $[Cu(\mathbf{19}\text{-}H)_2)(TOPO)]$ was obtained from UV/Vis, IR, EPR and sonic spray mass spectrometry.

Declaration

Since graduating from the University of Edinburgh in 2005 with an MChem (Hons.) in Environmental Chemistry with Industrial Experience the author has been engaged in a programme of full time research under the supervision of Professor Peter A. Tasker at the University of Edinburgh, and Mr. Ronald M. Swart and Mr. John Campbell at CYTEC Industries Inc., Manchester.

I hereby declare that except where reference is made to other sources, the work contained in this document is the original work of the author. It has been composed by the author and has not been submitted previously in whole or in part for another degree or qualification from this or any other university or institute of learning. In accordance with the regulations this thesis does not exceed 70,000 words in length.

Ross John Gordon

November 2008

Acknowledgements

I would like to extend my most sincere thanks to Professor Peter Tasker for always being available to discuss any problems throughout the last three years, no matter how busy his schedule was. His patience and support are unrivalled!

I thank Peter again, along with Mr. Ron Swart and Mr. John Campbell at CYTEC Industries Inc., not only for their expertise and guidance but also giving me the opportunity to do this PhD.

I would also like to thank past and present members of the Tasker group who inspired me to start this adventure, kept me amused throughout and for listening to my moaning! In particular Dr.'s Rachel Cooper, Dorothy Henry, Ross Forgan and David Henderson. Fraser White deserves a special thank you for solving all my crystal structures. I also thank all the friends that I have met whilst at Edinburgh University, there are too many to mention.

I extend my gratitude to Dr. Philip Camp for calculating association constants. Mr. John Miller and Mr. Juraj Bella for their help with NMR and Lorna Eades for solving ICP-OES problems. I also thank Lesley Yellowlees for help with EPR and for her support throughout my years at the University of Edinburgh.

For financial support with this project I would like thank CYTEC and the EPSRC. I also thank CYTEC, The Royal Society of Chemistry and the University of Edinburgh Chemistry Department for financial assistance to present my work at a number of conferences.

Finally, my greatest apologies and thanks all my family and friends, and also to those who, unfortunately are no longer here to witness this moment, for their understanding, support and for still being there after the long periods without contact throughout the years that I have been a student. Last but not least, I thank my girlfriend, Jenny for all her patience, support, encouragement and discipline over the last three years.

Contents

Ligands Studied

L1-L13

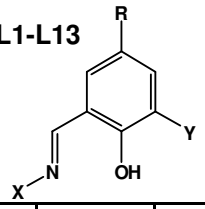

L	R	Y	X
L1	*t*-Oct	COOH	OH
L2	Me	H	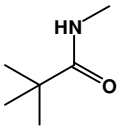
L3	*t*-Bu	H	
L4	Me	COOH	
L5	*t*-Bu	COOH	
L6	Me	COOH	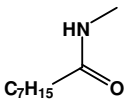
L7	*t*-Oct	COOH	
L8	nonyl	COOH	
L9	Me	COOH	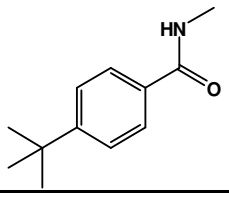
L10	*t*-Oct	COOH	
L11	Me	COOH	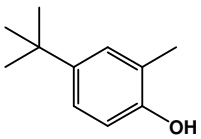
L12	*t*-Oct	COOH	
L13	nonyl	COOH	

18

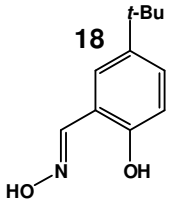

19

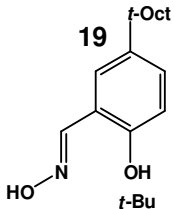

L14

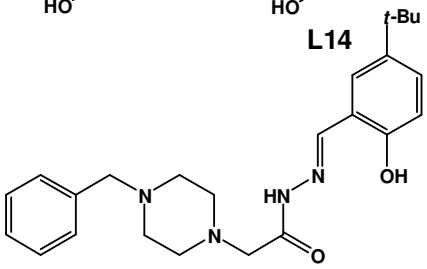

L15

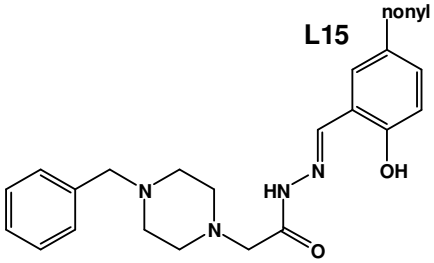

L16

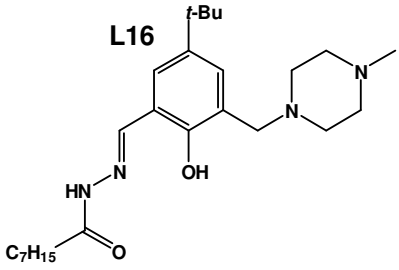

L17

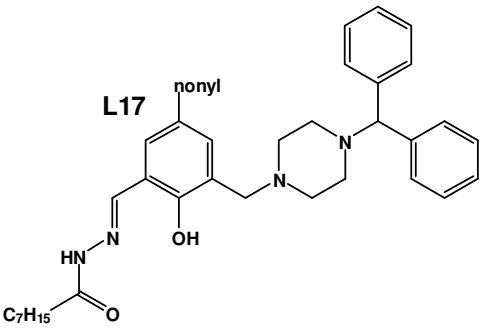

L18

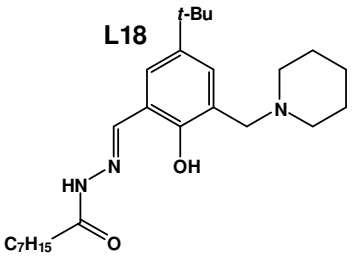

L19

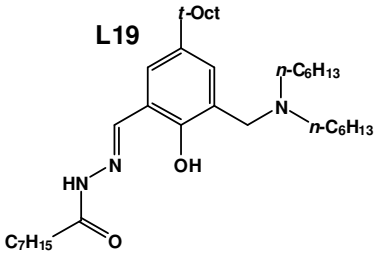

L20

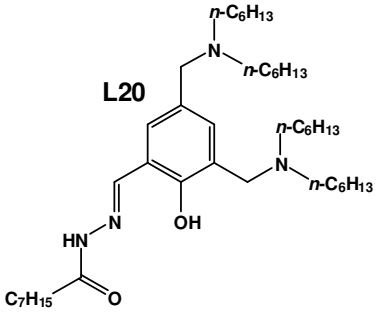

Abbreviations

Δ	change in
δ	chemical shift
°	Degrees
°C	degree centigrade
$	US. Dollars
<	less than
≤	less than or equal to
>	greater than
≥	greater than or equal to
%	percent
±	plus or minus
~	approximately
√	square route
ε	extinction coefficient (UV/Vis)
v	wavenumber (IR)
χ_M	Magnetic Susceptibility
λ	wavelength
μ_B	Bohr magneton
1D	one-dimensional
2D	two-dimensional
2-EH	2-ethylhexanol
Å	Angstrom
A	hyperfine coupling constant (EPR)
anal.	Analysis
aq	aqueous phase

Ar	aromatic; aryl
B_0	applied magnetic field
b.p.	boiling point
br	broad (spectroscopy)
C_6H_5	phenyl
C_9H_{19}	nonyl
ca.	circa (about)
calc.	calculated
cf.	confer (compare)
CHN	Carbon, Hydrogen, Nitrogen (elemental analysis)
CID	Collision Induced Dissociation (MS)
cis	cisoid
cm^{-1}	wavenumber (IR)
CSD	Cambridge Structural Database
d	doublet (NMR)
D	distribution coefficient
Dc	direct current
DCM	dichloromethane
DFT	Density Functional Theory
DMSO	dimethylsulfoxide
ΔE	difference in energy
ed.	editor(s)
e.g.	for example
emu	electromagnetic unit
EPR	Electron Paramagnetic Resonance
Equiv.	molar equivalent
ESI	electrospray (MS)

et al	*et alli* (and others)
EtOH	ethanol
FAB	Fast Atom Bombardment (MS)
FTIR	Fourier Transform Infrared
ΔG_{free}	Gibbs free energy
g	gram; g-factor (EPR)
G	Gauss (EPR)
GHz	gigahertz
g L^{-1}	grams per litre
GPa	gigapascal
HMT	hexamethylenetetramine
hr	hour
I	nuclear spin quantum number
ICP-OES	inductively coupled plasma optical emission spectroscopy
i.e.	that is
in situ	in the natural place
in vacuo	under vacuum
IR	infrared
iso-	isomer
K	degree Kelvin
K	association constant
kJ mol^{-1}	kilojoules per mole
L	ligand, liquid, litre
m	metre, medium(IR), milli (10^{-3}), multiplet (NMR),
m	*meta*
M	molar
Me	methyl

MeOH	methanol
MHz	megahertz (NMR)
mm Hg	millimetre of mercury
mol	mole
mol dm^{-3}	mole per litre
MS	mass spectrometry
M_s	molecular spin number
MW	molecular weight
m/z	mass to charge ratio
n	normal, nano (10^{-9})
NOBA	3-nitrobenzylalcohol
NMR	nuclear magnetic resonance
o	*ortho*
obs.	observed
org	organic phase
p	*para*
P50	5-nonylsalicylaldoxime
pH	$-\log_{10}[H^+]$
$pH_{½}$	pH when D = 0
pK_a	$-\log_{10}K_a$
pls	pregnant leach solution
pp.	inclusive pages
ppm	parts per million
py	pyridine
q	quartet (NMR)
s	singlet (NMR); strong (IR); second; solid
SX	solvent extraction

t	triplet (NMR)
t	tertiary
T	temperature
t-Bu	tertiary butyl
TBP	tri-*n*-butylphosphate
TDA	*iso*-tridecanol, 2,4-diethyl-6-methyloctan-1-ol
tert	tertiary
TFA	trifluoroacetic acid
TFA^-	trifluoroacetate anion
THF	tetrahydrofuran
t-Oct	tertiary octyl
TOPO	trioctylphosphine oxide
trans	transoid
TXIB	2,2,4-trimethyl-1,3-pentanediol diisobutyrate
UV/Vis	ultraviolet-visible
via	by way of
Vol.	volume
vs.	versus
w	weak (IR)
XRD	X-ray Diffraction

Chapter 1 Introduction

Advances in leaching technologies and plant engineering used for solvent extraction have not been fully exploited because extractants are often not available to meet the requirements of the new flowsheets. The reagents currently used to process copper are essentially identical to those when hydrometallurgy for base metal recovery was in its infancy.[1] Consequently, the capacity of plants is often limited by reagents and a lack of understanding of how blending of reagents and addition of modifiers influence their extractive properties.

The objective of this thesis is to improve the efficiency of existing industrial methods and develop new reagents for the recovery of copper by solvent extraction. Presently, reagents are blended or their extraction properties altered by the addition of modifiers to tune their strength. Formulation of such blends is essentially an empirical process as there is relatively little understanding of how such modifiers interact at a molecular level with other entities in the extraction and stripping stages. Such interactions have been investigated in this thesis in an attempt to rationalise modifier design. In addition, new ligands have been developed which increase the amount of copper transported through the hydrometallurgical circuit per load/strip cycle relative to existing reagents. This principle has been extended for application in processes to transport copper *salts* where innovative leaching technologies require both metal cations and attendant anion(s) to be extracted.

This chapter provides background on the chemistry of copper, its applications and methods available for extraction from its ores. Figure 1.1 is provided to illustrate the scale of copper recovery operations. Small improvements can dramatically improve the efficiency and economic viability of the associated processes.

Figure 1.1: Image of the Chuquicamata copper mine in Chile.

1.1 Copper

Copper, the 29th element in the periodic table, is a paramagnetic transition metal with electronic configuration $3d^{10}$ $4s^{1}$ and spin of s = ½. It has two stable isotopes, Cu^{63} and Cu^{65}, and can be found in oxidation states of I to IV. It is believed to be the 22nd most abundant element,[2] present at 68ppm[3] in the Earth's crust where it is possible to find it in its elemental form but is most commonly found as Cu(II) ($3d^{9}$) in chalcopyrite, $CuFeS_2$.[4] Copper exhibits excellent conducting properties of both electricity and heat, second only to silver but exceeding those of gold and aluminium.[4] High purity electrical grade copper (>99.95%) is soft, ductile and malleable, properties which lend it to being rolled and drawn for electrical wiring applications. It is also used as a roofing material owing to the corrosion resistance of the turquoise-green insoluble layer of basic hydroxycarbonate ($Cu(OH)_2.CuCO_3$) formed by oxidative weathering which retards further corrosion. [2, 4, 5]

Historically, copper is believed to be the first metal extensively used by man with some finds in Iraq dating back 10,000 years.[4, 6] It was used to make implements for hunting and fishing as well as decorative items such as keepsakes and jewellery[4] due

to its characteristic lustre, malleability and ductility. Later, during the Bronze Age, copper was crafted into many household items.[4]

Apart from gold, copper is the only metal which does not carry a metallic-grey colour, it is red and can be alloyed to give stronger materials which are similarly lustrous and malleable, yet more resistant to corrosion than the native metals.[2, 4, 6] Brass is formed when copper is alloyed with zinc to give a coloured alloy which can be tuned from red to yellow respective of the amount of zinc present (5-45%).[4] Bronze is formed when copper and tin (<10%) are alloyed to give a brown material which is stronger and more corrosion resistant than brass.[4] These properties have been extensively exploited in coinage for centuries.

Demand for copper continues to increase because of its widespread applications which include; building and construction, power generation and distribution, telecommunications, transportation and industrial and domestic electrical equipment.[7] Global economic growth has fuelled the increase in its demand and market price,[8] stimulated in particular by the development of Asia-Pacific countries.[9, 10] Consequently, a demand of 17 million tonnes outstripped the 15 million tonnes produced in 2006[9] and market prices reached an all time high of $8,820 per metric tonne on the 6th of March 2008.[11] However, if the demand for copper continues to increases at current rates, global reserves could be exhausted within the next 30-60 years.[8, 10] Recycling must be considered to address this problem because it consumes only about 30% of the energy required to process ore reserves.[12] However, currently only *ca*. 53% of discarded copper is reused[8] and *ca*. 26% of the discarded copper will never be reused.[7] Alternatively, the production lifetimes of the reserves can be extended through the development of new technologies to exploit low grade ores which are currently restricted by excessive environmental or financial expense.[7]

1.2 Extractive Metallurgy

Copper has a high affinity for sulfur[6] and for this reason forms sulfidic ores under the reducing conditions as experienced during the formation of the Earth. As life on Earth evolved, photosynthesis caused the atmosphere to become predominantly oxidising.[13] Subsequent groundwater leaching of the ore bodies resulted in weathering of the near-surface deposits to yield three layers; a superficial oxidic layer with an underlying mixed oxidic/sulfidic transition layer on top of the deep sulfidic deposits. Large ore bodies are known and mined in the Asian-Pacific, Former Eastern block countries, South Africa and the west coasts of the Americas.[6, 9, 10] Copper is present in most ores in small quantities, generally less than 1% by mass, so requires purification.[6] Extractive metallurgy involves separation and concentration of the desired metal followed by reduction to elemental form and finally refining to yield a product of high purity.[14] Metal extraction has been practiced for over 7000 years in the form of high temperature pyrometallurgical smelting[15] and more recently by hydrometallurgical processes, many of which use solvent extraction in the separation and concentration operations.

1.2.1 Pyrometallurgy

Pyrometallurgy is best suited to the recovery of copper from sulfidic ores. Before reduction and refinement, the ore is successively crushed, ground and milled to yield a wetted slurry of ore particles of 0.25 mm diameter in size.[6] Selective separation of metal sulfide minerals from silicaceous waste material, "gangue", is achieved by froth flotation in an aerated aqueous medium containing hydrophobic[16] additives agitated by impellers. The skimmed oil-based froth contains 20-30% copper. This is dewatered before undergoing a two stage purification process by smelting.[6] The concentrate is roasted in an oxygen rich environment at high temperature (*ca.* 1300°C) with recycled converter "slag" and lime to form an immiscible layer of impurities over a "matte" of molten high grade copper(I)/iron(II) sulfides. The dense matte is drawn off into a converter which is fed with air and a silica "flux".[17] Under controlled conditions FeS is converted into a siliceous slag, which is recycled back

into the smelter. Subsequently, at temperatures above 1250°C, Cu_2S is converted into sulfur dioxide and molten copper, which is cast into blister anodes of 98% purity. The exothermic conversion of metal sulfide to metal oxide and sulfur dioxide releases enough energy to make both processes thermodynamically autogenous. [18, 19]

If electrical grade copper (>99.95%) is required, it is necessary to further purify the blister anodes. This is done by electro-deposition of copper on a stainless steel cathode in a sulfuric acid electrolyte.[19] The impurities dissolved in the electrolyte sink to the bottom of the cells where the resulting "slimes" are collected to recover precious metals of value.

1.2.2 Hydrometallurgy

Hydrometallurgy is a well established industrial process used for the recovery of aluminium, titanium, chromium, cobalt, nickel, copper, zinc, palladium, silver, cadmium, platinum, gold, lead, and uranium from their ores or pyrometallurgical wastes.[16, 20, 21] In general these processes involve dissolution of the desired metal ion into aqueous solutions followed by separation, concentration and purification by; precipitation, cementation, electrowinning, reverse osmosis, ion exchange or solvent extraction.[22] The particular technology implemented depends on the target metal and its chemical composition in the source material. Hydrometallurgy is also applied in cleanup operations for the recovery of heavy metals from contaminated industrial wastelands and acid mining drainage systems.[21]

1.3 Copper Recovery from Oxidic Ores

Solvent extraction can effect the separation and concentration of copper from oxidic, transition (mixed sulfidic/oxidic) or sulfidic ores directly into electrical grade copper suitable for commercial use as part of a hydrometallurgical flowsheet.[16] Between 20[9, 19] and 30%[22] of primary copper recovery now involves hydrometallurgy using cation exchange solvent extraction reagents in a pH-swing process. In this process copper is

dissolved in dilute sulfuric acid to yield a "pregnant leach solution" (pls). This solution is fed to a mixer-settler where it is agitated with a water-immiscible organic phase containing an extractant which is selective for copper. Cu(II) transfers from the aqueous phase into the organic phase *via* cationic exchange with suitable ionisable functional groups on the extractant ligand.[16] After phase disengagement the resulting acidic aqueous phase is recycled onto the leach pad. The copper-containing organic phase is separated from the aqueous phase using an overflow weir and continues to another mixer-settler where the metal is stripped from the organic phase by contact with a sufficiently acidic sulfuric acid solution which re-protonates the extractant to generate a pure copper sulfate solution. The organic phase is recycled and the aqueous copper sulfate solution is taken into the electrolytic tankhouse as the electrolyte where conductivity grade copper cathodes are electro-deposited. These processes are shown in Figure 1.2 and the corresponding equilibria given in Figure 1.3.

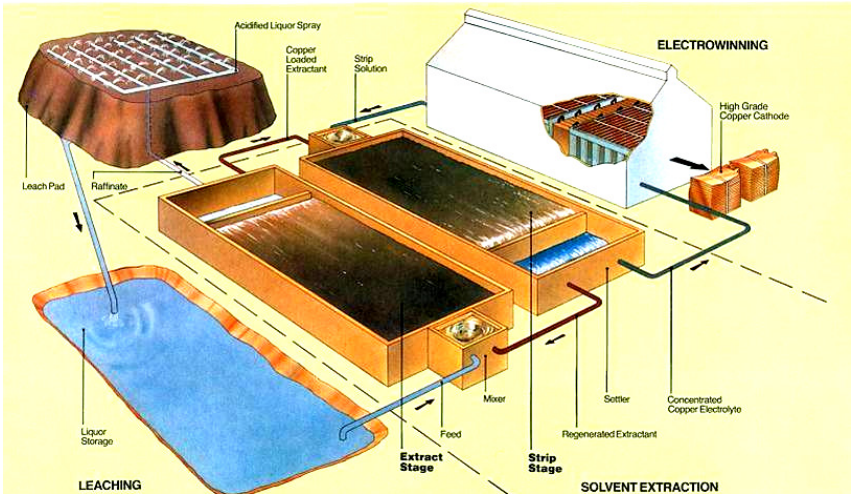

Figure 1.2: Schematic representation of the closed loop circuit for the leach/solvent extraction/strip/electrowin steps used to process copper from oxidic ores.[23]

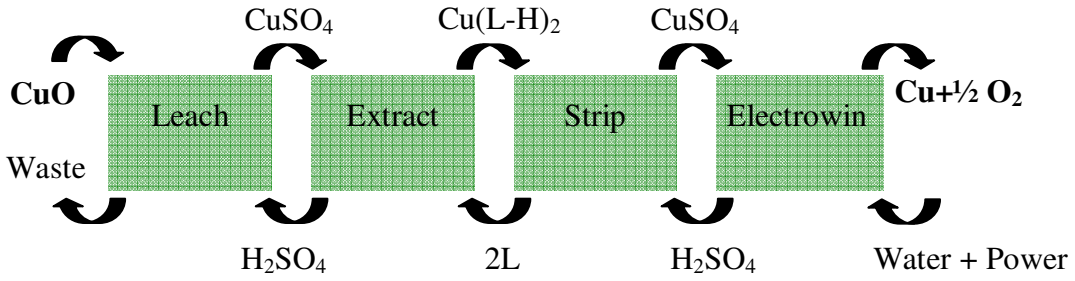

Leach	$CuO + H_2SO_4$	$\rightleftharpoons$	$CuSO_4 + H_2O$
Extraction	$CuSO_4 + 2L_{(org)}$	$\rightleftharpoons$	$[Cu(L\text{-}H)_2]_{(org)} + H_2SO_4$
Strip	$[Cu(L\text{-}H)_2]_{(org)} + H_2SO_4$	$\rightleftharpoons$	$CuSO_4 + 2L_{(org)}$
Electrowin	$CuSO_4 + H_2O$	$\rightleftharpoons$	$Cu + ½O_2 + H_2SO_4$
Overall	**CuO**	$\rightleftharpoons$	**$Cu + ½O_2$**

Figure 1.3: The reactions and materials balance for the process shown in Figure 1.2.

1.4 Benefits of Processing Copper by Solvent Extraction

Hydrometallurgical recovery of copper from oxidic ores is an extremely efficient process as demonstrated by the exceptional materials balance achieved and can be applied to low grade ores which contain as little as 0.3 to 0.7% copper.[19, 24] A fundamental source of economy in this process arises because the mined ore can be leached directly without further refining. This greatly reduces energy consumption since large scale crushing machinery is not required on the mine site. Moreover, the entire processing plant can be located near the site and the facility size can be tailored to suit the mine capacity, reducing the cost incurred through transportation of low grade materials. Theoretically the only material consumed in a hydrometallurgical plant once it is fully operational is the power used for pumping and mixing solutions and for the electrolytic reduction. All other resources are recycled. Loss of solvent, both aqueous and organic, is inevitable as is degradation of the extractant, nonetheless these losses are minimal and have only a minor impact on the overall economic viability of hydrometallurgy. This can allow small, remote ore

bodies to be exploited commercially and with less environmental impact than smelting.

Pyrometallurgical alternatives generally require ores of at least 1% copper content to be profitable. These plants consume electricity, silica as the flux and oxygen to generate silicaceous iron slags and sulfuric acid as waste by-products.[19] To put the scale of these wastes into perspective, it is estimated that 20% of total sulfur consumed globally in 2005 (*ca*. 72 million tonnes) was in the form of sulfuric acid, generated by base metal smelters and a large portion of this from copper processing sites.[9] Other extremely energy intensive operations required prior to pyrometallurgical processes include the concentration steps of crushing, grinding, milling and froth flotation. Moreover, the raw ores or resulting concentrates are generally required to be transported to smelters remote from the mine site.[9, 25] This incurs further expenditure, both economic and environmental, from the fossil fuels used. The main reason smelters are remote from mines is because the associated plant costs are very high.[26] Consequently the only way to recoup the initial investment is to build a smelter located between ore bodies which can be customised to process the individual ores from different sites.[9] In 2006, at a time when energy prices were considerably lower than now, the investment required per annual tonne (tpa) of copper produced by hydrometallurgy was \$1000-\$2500[27] compared to \$3000-\$5000[26, 27] for pyrometallurgy. Beyond 250,000 tpa, smelters have greater economies of scale.

It is increasingly necessary to consider the carbon balance of both processes in a society aware of global warming and legislatively directed towards using "greener" more environmentally friendly technologies and renewable energy sources. One report[28] from 2004 concludes that when the life cycle assessments of both technologies are compared, solvent extraction is more energy intensive. One reason for this assumption was the…

"inefficiency of [power] transmission over long distances or if it is generated on site, the inefficiency of diesel generation… [and] power generation *via* black coal combustion is not only relatively inefficient it also releases substantial amounts of CO_2, SO_2, particulate airborne pollution including metallic pollutants such as radium, thorium and uranium."[28]

These arguments may be true at present but also could be directed at pyrometallurgy, especially if the electricity generated at hydrometallurgical sites is from solar or wind based resources. The selection of the sources of the data used and the audience to which it was aimed must be questioned as another quote from the papers states that…

"human induced "global warming" is most likely a fallacy [and] the author strongly disagrees with the concept that CO_2 and other "greenhouse gases" produced by human activity can change the global climate in any measurable way"[28]

Considering the limited availability of high grade ores at present[10] and the declining grade of ores accessible in future, along with the increased cost of transportation, it is difficult to conceive that current pyrometallurgical processes are an economically competitive alternative to hydrometallurgical methods which are more energy efficient, produce less waste and can be located next to small mine sites.

1.5 Solvent Extractants

Conventional solvent extractants can be separated into three classes; cation and anion exchange reagents and solvating reagents.[14] Conventional phenolic oximes and the hydrazone ligands discussed in Chapters 2 and 4 are classed as pH-swing cation exchange reagents as they deprotonate to generate organic soluble, charge-neutral complexes through inner sphere coordination of metal cations.

$$2L_{(org)} + M^{2+}_{(aq)} \rightleftharpoons [M(L\text{-}H)_2]_{(org)} + 2H^{+}_{(aq)}$$

Phenolic oximes are discussed further in Section 1.6.[22]

Anion exchange reagents can form outer-sphere contact ion-pairs through electrostatic attractions between an organic soluble cation and stable metal chloridometallates.[14, 29, 30] Examples include tetraalkylammonium salts which can be used in chloride controlled processes or trialkylamines in pH-controlled processes such as the Alamine® reagents:[16]

$$FeCl_4^- + [R_4N]Cl_{(org)} \rightleftharpoons [R_4N][FeCl_4]_{(org)} + Cl^-$$

$$R_3N_{(org)} + H^+ + FeCl_4^- \rightleftharpoons [R_3NH][FeCl_4]_{(org)}$$

Outer sphere coordination is an efficient method of transporting inert chloridiometallate anions, MCl_x^{y-}, containing precious metals but not chloridocopper(II)ates. This is because such chlorido anions are less readily formed by copper than by other transition metal ions, e.g. $FeCl_4^-$. Moreover, inner-sphere reaction replacing chloride ligands in chloridocopper(II)ates can lead to the formation of stable species from which it would be extremely difficult to strip the metal.[30]

Zwitterionic ligands discussed in Chapter 3 function as both cation and anion exchange reagents. More detail of these is given in Section 1.8.3.

The third class of extractants are solvating reagents, which are charge neutral-molecules[14] that transfer metal salts into the organic phase *via* inner- or outer-sphere coordination. One of the most intensively applied solvating reagents is tributylphosphate (TBP) as used in the nuclear industry for extraction of thorium and uranium concentrates and wastes:[14, 17, 31]

$$UO_2^{2+} + 2NO_3^- + 2TBP_{(org)} \rightleftharpoons [UO_2(NO_3)_2(TBP)_2]_{(org)}$$

Solvating reagents to process copper(II) chloride are discussed further in Section 1.8.1.

1.5.1 Extractant Design Criteria

When designing new ligands for application in copper recovery by solvent extraction several issues need to be addressed. To achieve selectivity for copper(II) over the other metals present in the pregnant leach solution the ligand must contain the correct number of deprotonatable functional groups of suitable Lewis basicity[32] to yield a charge-neutral complex. It would be thermodynamically favourable if these atoms were in a prearranged geometry to complex a square planar copper(II) cation via 5- and 6-membered chelate rings to exploit the chelate effect.

Once a target molecule has been designed and synthesized, it is necessary to establish its performance relative to the current industrial reagents applied in solvent extraction. There are several requirements which need to be addressed:[23]

- Safety - the extractant must be non-toxic, non-volatile and non-flammable.
- Selectivity - the extractant must be selective for the desired metal cation, or cation and anion in the case of metal salt extractants.
- Separation - the organic and aqueous phase should separate rapidly and efficiently.
- Solubility - both extractant and complex should be soluble in water-immiscible solvents and display negligible solubility in any aqueous phase which it may come into contact.
- Speed - extraction and stripping should be kinetically favourable.
- Stability - the extractant should be stable to hydrolysis and oxidation over a wide temperature range.
- Strength - the extractant strength should be such that it allows efficient loading and stripping under the conditions implemented.
- Synthesis - it should be possible to produce the extractant cheaply and safely on a large scale.
- System - the extractant should either be able to be employed in existing solvent extraction plants without extensive reengineering or should be capable of being used as part of a total system in which all components of the pls can be accounted for and preferably used to generate articles of commerce.

1.6 Phenolic Oxime pH-Swing Reagents

The most extensively used hydrometallurgical copper extractants are phenolic oximes.[1, 16, 22] In non-polar organic solvents these molecules associate through intermolecular hydrogen bonds between the oximic hydrogen and phenolic oxygen atoms.[33-36] The resulting pre-organised geometry is ideal for deprotonation and insertion of a square planar Cu(II) ion[36] *via* a cationic exchange equilibrium as shown in Figure 1.4 to form a neutral 1 copper to 2 ligand complex. Branched alkyl groups in the R' position impart solubility in the hydrocarbon solvents used industrially. The R'' substituent can be altered to tune the "strength" of the reagent.

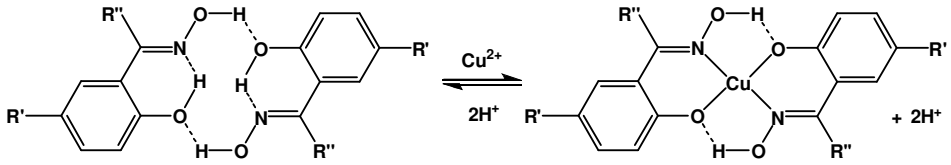

Figure 1.4: Complexation of copper(II) by phenolic oxime extractant.

The relative affinity of pH-swing extractants for different metal cations can be assessed by determination of the metal loading as a function of pH. Plotting the metal loaded as a percentage of the theoretical maximum based on the concentration of the extractant against the pH of the aqueous phase after equilibration results in an S-shaped graph (Figure 1.5). These "S-curves" allow reagent strength to be compared from the $pH_{½}$ values, the pH at which 50% of the extractant is loaded. A lower $pH_{½}$ corresponds to a higher "strength" for a particular metal. Phenolic oxime reagents are selective for copper over other first transition series metals at low pH and adhere to the Irving-Williams series (Figure 1.6).[37]

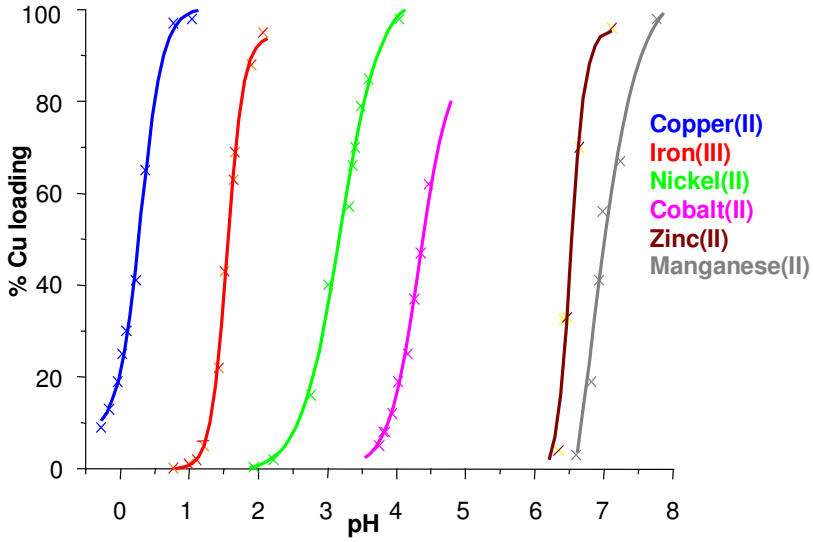

Figure 1.5: Loading S-curves for the first row transition metals by Cytec Industries Inc.'s P50 reagent, 5-nonylsalicylaldoxime where R'=C_9H_{19} and R''=H in Figure 1.4.[22]

$$Ba^{2+} < Sr^{2+} < Ca^{2+} < Mg^{2+} < Mn^{2+} < Fe^{2+} < Co^{2+} < Ni^{2+} < Cu^{2+} > Zn^{2+}$$

Figure 1.6: The Irving-Williams series for divalent transition metals.[37]

The strength of the reagents can be tuned by changing the nature of the R'' substituent seen in Figure 1.4. The strongest class of reagent are salicylaldoximes, where R'' = H. If R'' is substituted by an alkyl or aromatic group, the weaker ketoxime and benzophenone oxime classes of reagent are formed respectively. In practice salicylaldoximes are the most used and their strengths are tuned by the addition of equilibrium modifiers.

1.7 Increasing Mass Transport Efficiency

The materials balance achieved in solvent extraction circuits which process copper oxide using sulfuric acid and salicylaldoximes is extremely good (see Figure 1.3). However, in practice salicylaldoximes are extremely strong extractants and require equilibrium modifiers to be added to improve copper stripping. Moreover multiple load and strip cycles are required to maximise copper recovery. The mass of copper which is transported across the circuit per unit mass of ligand used is known as the "mass transport efficiency".

1.7.1 The Role of Modifiers in Copper Solvent Extraction

Salicylaldoximes are very strong copper extractants which require concentrated sulfuric acid electrolytes to strip the copper effectively from the organic phase. Equilibrium modifiers are blended with salicylaldoximes to tune their strength, increasing the $pH_{½}$ value and facilitating stripping at a higher pH.[38] Equilibrium modifiers are generally oxygen-contain molecules which behave as hydrogen bond donors and/or acceptors.

Previous studies have suggested that equilibrium modifiers interact with extractant molecules through hydrogen bonds.[39] This favourable interaction lowers the concentration of "active" extractant which is free to complex copper.[40] They have also been found to affect interfacial tension, interfacial activity of the extractant and influence the kinetics of extraction.[41, 42] This thesis focuses on the interaction between equilibrium modifiers and salicylaldoxime copper complexes. Molecular modelling and experimental data are discussed in Chapter 4.

1.7.2 Increasing Molar Transport

The phenolic oximes currently used extract 1 mol of copper per 2 mol of ligand as shown in Figure 1.4. Recent developments in leaching technology (see Section 1.8.2) and plant engineering require new reagents to be developed which increase the mass transport efficiency of pH-swing type reagents. The approach considered in this thesis is to design new polyacidic multiloading ligands which are capable of transporting more copper per extractant molecule. To achieve this, additional deprotonatable sites are required to form neutral copper complexes of high copper to ligand ratio which are soluble in the hydrocarbon organic phase. Previous work at the University of Edinburgh has increased molar transport two fold to 2 Cu : 2L using diacidic 2-hydroxyanils[43] and salicylaldehyde-hydrazones,[44] A and B respectively in Figure 1.7.

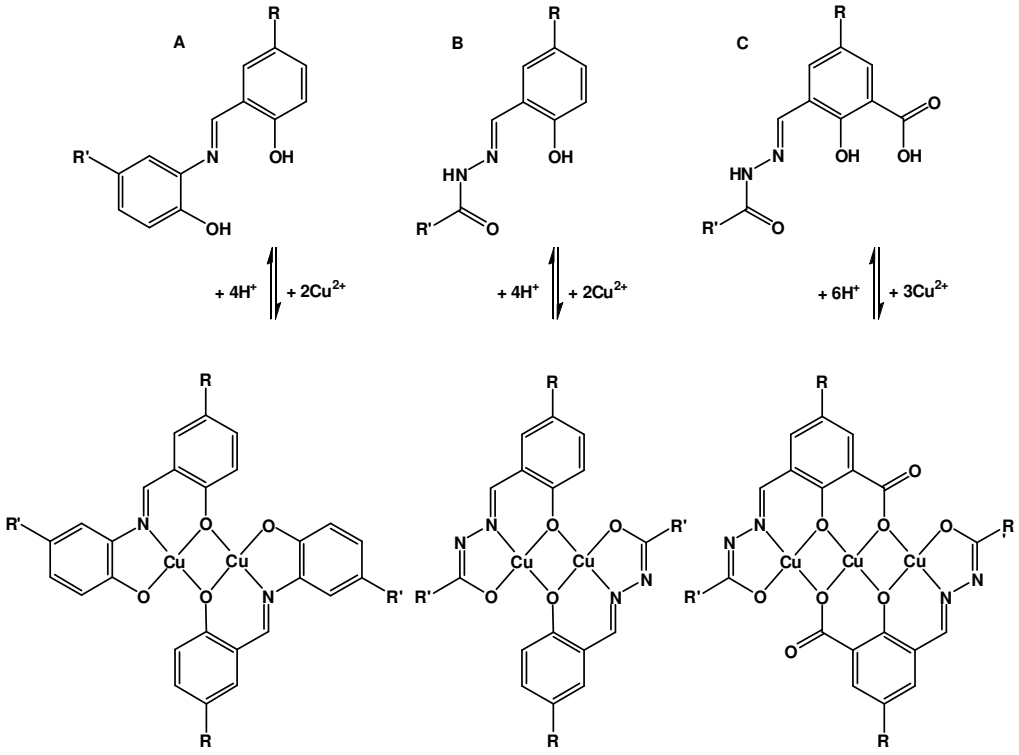

Figure 1.7: Previously studied diacidic 2-hydroxyanil[43] (A) and salicylaldhydehydrazone[44] (B) ligands and the triacidic 3-hydrazono-5-alkylsalicylic acid ligands (C) investigated in Chapter 2 and their expected fully loaded structures.

In this thesis the molar transport has been increased to 3 Cu : 2 L by incorporation of an additional deprotonatable group into the basic architecture of the salicylaldehyde hydrazones to generate 3-hydrazono-5-alkylsalicylic acids of type C Figure 1.7.

1.8 Processing Copper from Sulfidic Ores

High grade copper sulfide ores are traditionally treated *via* pyrometallurgical routes which are often not cost effective for processing low grade ores. Consequently, hydrometallurgical alternatives have been pursued. New leaching technologies have had to be developed to process sulfidic ores effectively because only 25-30% copper recovery is achieved using dilute sulfuric acid.[16, 45] The new leaching technologies can be split into two types, chloride- or sulfate-generating streams.

1.8.1 Chloride Leaching

Rapid oxidative chloride leaching of chalcopyrite ($CuFeS_2$) under oxidising conditions using chloride salts (Scheme 1.1) has been demonstrated to solubilise >95% of copper in the CLEAR process.[46]

$$CuFeS_2 + 4FeCl_3 \longrightarrow 5FeCl_2 + CuCl_2 + 2S$$

Scheme 1.1: Leaching of chalcopyrite by ferric chloride to generate $CuCl_2$ in the CLEAR process.

The CUPREX process is a chloride-swing controlled method which precipitates elemental sulfur from chalcocite (Cu_2S) to generate $CuCl_2$, the processes and related equilibria are presented in Figure 1.8.[16]

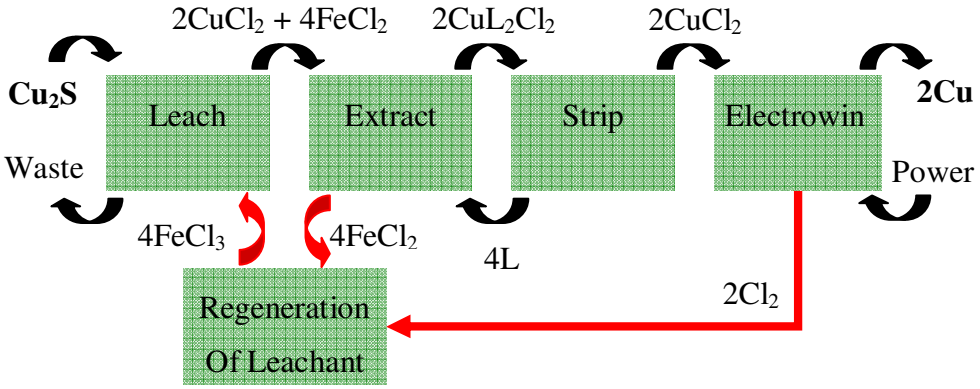

Leach	$4FeCl_3 + Cu_2S_{(s)}$	⇌	$2CuCl_2 + 4FeCl_2 + S_{(s)}$
Extraction	$2CuCl_2 + 4L_{(org)}$	⇌	$2[CuL_2Cl_2]_{(org)}$
Strip	$2[CuL_2Cl_2]_{(org)}$	⇌	$2CuCl_2 + 4L_{(org)}$
Electrowin	$2CuCl_2$	⇌	$2Cu_{(s)} + 2Cl_{2(g)}$
Leach Regen	$4FeCl_2 + 2Cl_{2(g)}$	⇌	$4FeCl_3$
Overall	$\mathbf{Cu_2S_{(s)}}$	→	$\mathbf{2Cu_{(s)} + S_{(s)}}$

Figure 1.8: Simplified flow sheet and corresponding equilibria for recovery of copper from sulfidic ores by the CUPREX process.[16]

The $CuCl_2$ generated in the chloride leaching process can be selectively extracted using the "solvating reagent" CLX50, Figure 1.9.[47-49]

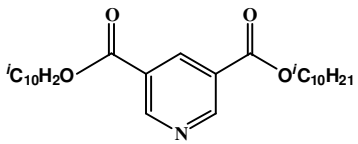

Figure 1.9: The $CuCl_2$ solvating extractant CLX50.

There are several practical safety hazards and engineering problems associated with the handling and processing of the extremely corrosive media encountered in these processes. However, most of these can be overcome by using polymer linings.[46, 47] Another problem encountered when copper is recovered by electrolysis from chloride media is that it is deposited as reactive dendritic grains rather than smooth cathodic plates as obtained from sulfate electrolytes.[50] These are difficult to harvest

and often need further refining.[51] Alternative sulfate-based leaching technologies avoid the complications arising from the presence of corrosive chloride media.

1.8.2 Sulfate Leaching

A recent publication by Dreisinger[26] reviews the applicability of sulfate-based copper recovery processes. These can be separated into biological or chemical and high or low pressure processes which generate a $CuSO_4$ electrolyte for treatment in solvent extraction / electrowinning circuits.

The Mount Gordon copper process employs low pressure stepwise oxidative leaching of chalcocite (Cu_2S) to copper sulfate *via* covellite (CuS) by a regenerated ferric sulfuric acid solution under 8 atm pressure at 90°C using oxygen generated on-site.[26]. This plant is no longer in use as the ore type which it was originally designed to process has been exhausted.

The "Total Pressure Oxidation" process was developed in the 1950's and is used today at the Phelps Dodge Bagdad plant in Arizona.[26] This requires high temperature and pressure autoclaves at 200-230°C and 30-40 atm to oxidise all sulfide minerals to metal sulfates and sulfuric acid.[52]

Alternatively, biotechnology can be used, as successfully demonstrated for the liberation of gold from sulfide ores by mesophiles (*ca*. 40°C) in the BIOX® process. Unfortunately, these bacteria are not effective for oxidation of primary copper sulfides. For this purpose, the BioCOP™ process was developed by BHP Billiton[24] which employs thermophilic archaea at higher temperatures (ca. 65-80°C) to generate metal sulfates and sulfuric acid as commercialised in Chile to treat ores from the Chuquicamata mine.[26] The microorganisms catalyse the oxidiation of the ferrous ion into the ferric ion which oxidises the chlocopyrite:

$$CuFeS_2 + 4Fe^{3+} \rightleftharpoons 5Fe^{2+} + Cu^{2+} + 2S$$

$$2Fe^{2+} + 2H^{+} + \tfrac{1}{2}O_2 \rightleftharpoons 2Fe^{3+} + H_2O$$

$$2S + 3O_2 + 2H_2O \rightleftharpoons 2H_2SO_4$$

Oxidative bioleaching and pressure leaching processes are capable of generating high tenor feeds[16] containing copper at concentrations of up to 65 g L^{-1} compared to *ca.* 5 g L^{-1} in conventional solvent extraction circuits.[16] Conventional pH-swing reagents are not suitable to process such streams as for every gram of copper recovered, 1.54 g of sulfuric acid is liberated, causing a build up of acid at the front end of the circuit.[16] This is especially undesirable in the bioleaching process as the pH increase caused by the acid build up would kill the enzymes. This compromises the excellent materials balance achieved for leaching oxidic ores (Figure 1.3) as shown in

Figure 1.10.

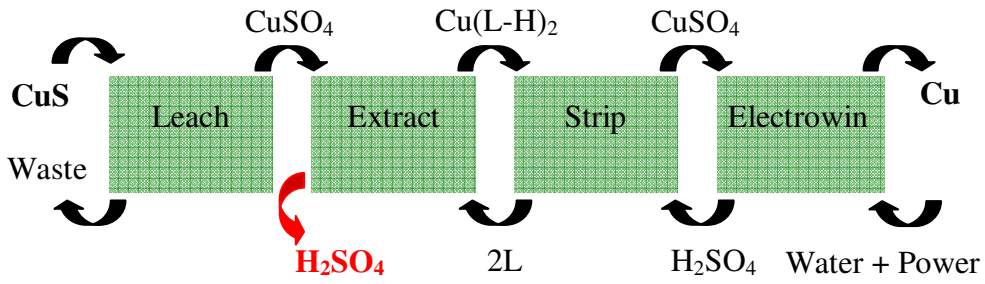

Leach	$CuS + 2O_2$	⇌	$CuSO_4$
Extraction	$CuSO_4 + 2L_{(org)}$	⇌	$[Cu(L\text{-}H)_2]_{(org)} + H_2SO_4$
Strip	$[Cu(L\text{-}H)_2]_{(org)} + H_2SO_4$	⇌	$CuSO_4 + 2L_{(org)}$
Electrowin	$CuSO_4 + H_2O$	⇌	$Cu + ½O_2 + H_2SO_4$
Overall	$\mathbf{CuS + 3/2O_2 + H_2O}$	⇌	$\mathbf{Cu + H_2SO_4}$

Figure 1.10 Materials balance for the hydrometallurgical extraction of copper from sulfidic ores, signifying the build-up of sulfuric acid in the circuit.

To avoid acid build up at the front end of the circuit and improve copper transport, new ditopic metal *salt* extractants have been investigated.[53, 54] These transport both copper and its attendant (sulfate) anion across the circuit (see Scheme 1.2).

1.8.3 Multiloading Copper(II) Salt Extractants

Novel reagents which extract metal salts have previously been studied in the Tasker group. These are generally ditopic ligands with separate cation and anion binding sites. They can exist in a zwitterionic form, where the positively and negatively charged binding sites ensure that the complex formed with a metal salt is an overall charge-neutral species.

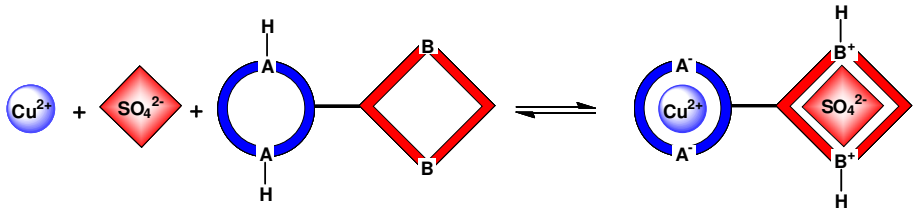

Scheme 1.2: Formation of a neutral copper sulfate complex in a zwitterionic form of a ditopic ligand.

Systems previously investigated to transfer copper sulfate have generated $[Cu(L)(SO_4)]$,[55] $[Cu(L)_2(SO_4)]$[56] and $[Cu_2(L)_2(SO_4)]$[43] species. The aim of the work discussed in Chapter 3 is to create ligands which can transport 2 moles of copper sulfate to form $[Cu_2(L)_2(SO_4)_2]$ species. The ligands used to achieve this are described in Chapter 3. These are based on diacidic salicylaldehyde hydrazones of the type shown in Figure 1.11 which are functionalised (X, Y and Z in Figure 1.11) to carry amino substituents which on protonation provide anion binding sites.

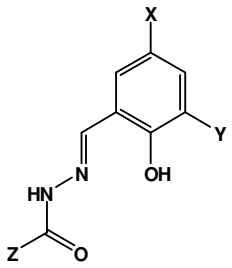

Figure 1.11: Basic structure of the metal salt extractants reported in this thesis in Chapter 3. X, Y and Z can be alkyl, monoamine or diamine.

1.9 Thesis Outline

Polyacidic multiloading copper extractants (Section 1.7.2) are discussed in Chapter 2. Methods to increases mass transport of current phenolic oxime reagents are considered and previous research[43, 44] into dinuclear copper extractants is reviewed. Details of the synthesis and characterisation of new diacidic ligands **L2** and **L3**, analogous to the diacidic salicylaldehydehydrazones previously studied,[44] is followed by X-ray diffraction and magnetic susceptibility data of the dinuclear copper complex $[Cu_2(\mathbf{L2}\text{-}2H)_2]$. The synthesis, characterisation and extraction studies of novel triacidic copper extractants **L4**-**L13** are discussed and solid state structures of the species isolated are provided. The potential for the triacidic ligands to double the molar transport efficiency of a commercial process is explored by blending them in a 1:1 ratio with the current phenolic oxime reagents.

Chapter 3 is introduced by a description of polytopic zwitterionic ligands and a review of metal salt extractants. This chapter extends the multiloading capabilities of the diacidic salicylaldehydehydrazones discussed in Chapter 2 to create a new class of metal salt extractant. Details of the synthesis and characterisation for ligands **L14**-**L20** are provided. Solvent extraction results for **L14**-**L20** are discussed and the industrial viability of **L19** and **L20** are investigated.

Chapter 4 probes the formation of modifier adducts with salicylaldoximes and their copper complexes. Previous work investigating the effects of modifiers on extraction efficiency and interactions between non-metal species in extraction processes are reviewed. The findings of a molecular modelling study[57] commissioned by industrial sponsors CYTEC Industries Inc. are discussed. Experimental evidence for adduct formation is sought by IR, UV/Vis, NMR, EPR and sonic-spray mass spectrometry.

Preparative methods and characterisation of the compounds synthesised in this work are provided in Chapter 5, as are details of the experimental apparatus, parameters and procedures employed.

1.10 References

1. G. A. Kordosky, Epomin 2000, International Conference on Clean Technologies for the Mining Industry, Santiago, Chile, 2000.
2. D. Nicholls, *Complexes and First-Row Transition Elements*, 1981 edn., The MacMillan Press LTD, London, 1974.
3. N. N. Greenwood and A. Earnshaw, *Chemistry of the Elements*, First edn., Butterworth-Heinemann, Oxford, 1995.
4. J. W. Laist, *Copper, Silver and Gold*, 1st edn., Van Nostrand, New York, 1954.
5. D. F. Shriver and P. W. Atkins, *Inorganic Chemistry*, Third edn., Oxford University Press, Oxford, 1999.
6. M. Grayson and D. Eckroth, *Kirk-Othmer Encyclopaedia of Chemical Technology*, 3rd edn., Wiley: New York, 1978.
7. R. B. Gordon, M. Bertram and T. E. Graedel, *Proc. Natl. Acad. Sci. U. S. A.*, 2006, **103**, 1209-1214.
8. T. E. Graedel, D. van Beers, M. Bertram, K. Fuse, R. B. Gordon, A. Gritsinin, A. Kapur, R. J. Klee, R. J. Lifset, L. Memon, H. Rechberger, S. Spatari and D. Vexler, *Environ. Sci. Technol.*, 2004, **38**, 1242-1252.
9. P. J. Mackey, *CIM Magazine*, 2007, **2**, 35-42.
10. D. Cohen, *The New Scientist*, 2007, **194**, 34-41.
11. London Metal Exchange, Annual report, 2008.
12. R. A. Frosch, W. C. Clark, J. Crawford, A. Sagar, F. T. Tschang and A. Webber, *Philos. Trans. R. Soc. London Ser. A*, 1997, **355**, 1335-1347.
13. J. F. Kasting, *Science (New York, N.Y.)*, 1993, **259**, 920-926.
14. M. J. Nicol, C. A. Fleming and J. S. Preston, *Comprehensive Coordination Chemistry*, 1987, **6**, 779-942.
15. S. M. Hong, J. P. Candelone, C. C. Patterson and C. F. Boutron, *Science*, 1996, **272**, 246-249.
16. P. A. Tasker, P. G. Plieger and L. C. West, *Comprehensive Coordination Chemistry II*, 2004, **9**, 759-808.
17. T. W. Swaddle, *Inorganic Chemistry: An Industrial and Environmental Perspective*, Academic Press Inc., London, 1996.
18. S. G. Galbraith and P. A. Tasker, *Supramolecular Chem.*, 2005, **17**, 191-207.
19. R. R. Moskalyk and A. M. Alfantazi, *Miner. Eng.*, 2003, **16**, 893-919.
20. C. S. Brooks, *Sep. Sci. Technol.*, 1993, **28**, 579-593.
21. M. Cerna, *Environ. Mon. Ass.*, 1995, **34**, 151-162.
22. J. Szymanowski, *Hydroxyoximes and Copper Hydrometallurgy*, CRC Press, London 1993.

23. F. Habashi, *A Textbook of Hydrometallurgy*, Metallurgie Extractive, Quebec, 1994.
24. M. E. Clark, J. D. Batty, C. B. van Buuren, D. W. Dew and M. A. Eamon, *Hydromet.*, 2006, **83**, 3-9.
25. S. Prasad and B. D. Pandey, *Miner. Eng.*, 1998, **11**, 763-781.
26. D. Dreisinger, *Hydromet.*, 2006, **83**, 10-20.
27. I. Hyvarinen and M. Hamalainen, *Hydromet.*, 2005, **77**, 61-65.
28. L. W. John, *Publications of the Australasian Institute of Mining and Metallurgy*, 2004, **6**/**2004**, 19-33.
29. K. J. Bell, A. N. Westra, R. J. Warr, J. Chartres, R. Ellis, C. C. Tong, A. J. Blake, P. A. Tasker and M. Schroeder, *Angew. Chem., Int. Ed. Int.*, 2008, **47**, 1745-1748.
30. P. A. Tasker, C. C. Tong and A. N. Westra, *Coord. Chem. Rev.*, 2007, **251**, 1868-1877.
31. H. Singh and C. K. Gupta, *Mineral Processing and Extractive Metallurgy Review*, 2000, **21**, 307-349.
32. R. G. Pearson, *J. Am. Chem. Soc.*, 1963, **85**, 3533-&.
33. A. G. Smith, P. A. Tasker and D. J. White, *Coord. Chem. Rev.*, 2003, **241**, 61-85.
34. P. O'Brien and J. R. Thornback, *Hydromet.*, 1982, **8**, 331-339.
35. P. O'Brien, J. R. Thornback and J. Szymanowski, *J. Coord. Chem.*, 1983, **13**, 11-15.
36. B. McCudden, P. Obrien and J. R. Thornback, *Dalton Trans.*, 1983, 2043-2046.
37. H. Irving and R. J. P. Williams, *J. Chem. Soc.*, 1953, 3192-3210.
38. J. Szymanowski, *Crit. Rev. Anal. Chem.*, 1995, **25**, 143-194.
39. M. B. Bogacki and J. Szymanowski, *Solv. Extrac. R&D, Japan*, 1996, **3**, 10-22.
40. A. M. Sastre, Szymanowski, J., *Solvent Extr. Ion Exch.*, 2004, **22**, 737-759.
41. K. Prochaska and K. Staszak, *J. Colloid Interface Sci.*, 2005, **285**, 1-8.
42. J. Szymanowski, *Solvent Extr. Ion Exch.*, 2000, **18**, 729-751.
43. D. C. R. Henry, PhD Thesis, The University of Edinburgh, 2007.
44. J. L. Wood, PhD Thesis, The University of Edinburgh, 2005.
45. G. A. Kordosky, *International Solvent Extraction Conference, Cape Town, South Africa, Mar. 17-21, 2002*, 2002, 853-862.
46. J. Liddicoat and D. Dreisinger, *Hydromet.*, 2007, **89**, 323-331.
47. J. Szymanowski, *J. Radioanal. Nucl. Chem.*, 1996, **208**, 183-194.
48. R. F. Dalton, R. Price, E. Hermana and B. Hoffman, *Mining Eng.*, 1988, **40**, 24-28.

49. R. F. Dalton, G. Diaz, R. Price and A. D. Zunkel, *J. Metallurgy*, 1991, **43**, 51-56.

50. A. Borowiak-Resterna, G. Kyuchoukov and J. Szymanowski, *International Solvent Extraction Conference, Cape Town, South Africa, Mar. 17-21, 2002*, 2002, 988-994.

51. O. Hyvaerinen and M. Haemaelaeinen, *Hydromet.*, 2005, **77**, 61-65.

52. J. O. Marsden, R. E. Brewer and N. Hazen, *Hydromet. 2003, Proceedings of the International Symposium, Vancouver, BC, Canada, Aug. 24-27, 2003*, 2003, **2**, 1429-1446.

53. D. J. White, N. Laing, H. Miller, S. Parsons, S. Coles and P. A. Tasker, *Chem. Commun.*, 1999, 2077-2078.

54. S. G. Galbraith, PhD Thesis, The University of Edinburgh, 2004.

55. S. G. Galbraith, P. G. Plieger and P. A. Tasker, *Chem. Commun.*, 2002, 2662-2663.

56. R. S. Forgan, J. E. Davidson, S. G. Galbraith, D. K. Henderson, S. Parsons, P. A. Tasker and F. J. White, *J. Chem. Soc., Chem. Commun.*, 2008, 4049-4051.

57. D. Tackley, Intertek ASG, 2006, Confidential Communication.

Chapter 2 Multiloading Copper Extractants

2.1 Introduction

This chapter discusses new triacidic metal extractants designed to give improved throughput in commercial plants operating pH-swing solvent extraction processes for copper recovery. New classes of reagents may also be required to respond to pregnant leach solutions (pls) generated from novel leaching technologies. The ability of the new reagents to extract copper cations into a water-immiscible organic phase and their industrial applicability are investigated.

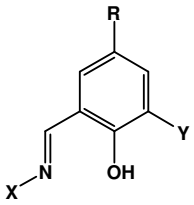

Table 2.1: Ligands **L1**-**L13** discussed in this chapter.

L	R	Y	X	L	R	Y	X
L1	*t*-Oct	COOH	OH	**L9**	Me	COOH	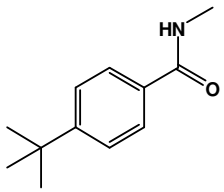
L2	Me	H	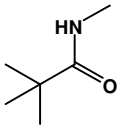				
L3	*t*-Bu	H		**L10**	*t*-Oct	COOH	
L4	Me	COOH					
L5	*t*-Bu	COOH					
L6	Me	COOH	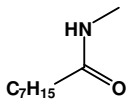	**L11**	Me	COOH	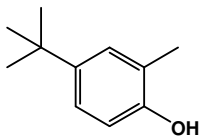
L7	*t*-Oct	COOH		**L12**	*t*-Oct	COOH	
L8	nonyl	COOH		**L13**	nonyl	COOH	

The work includes:

- synthesis and characterisation of 3 diacidic ligands **L1**-**L3** and 10 novel triacidic ligands **L4**-**L13** (see Table 2.1),
- the study of copper loading *via* pH-swing based solvent extraction into chloroform solutions of the ligands from aqueous sulfate streams,

- investigations into their ability to complex first row transition metals and their propensity to selectively extract copper over other transitions metals,
- the ability of the new ligands to increase the molar and mass transport of copper in blends with current commercial extractants and,
- discussion of the solution speciation of the copper complexes in loaded organic solutions and the solid state.

Many attempts have been made to optimise the productivity of metal extraction plants by improving kinetics of the extract and strip processes as well as phase disengement.[1] Some have included formulation of extractant blends although few have focussed on the development of a new class of ligand. Work done previously[2-4] at the University of Edinburgh (see Section 2.3) to improve throughput by increasing metal to ligand stoichiometry has been expanded in this project.

2.2 Increasing Mass Transport

The "mass transport efficiency" of an extractant is the mass of metal it can carry through the extract and strip stages of the hydrometallurgical cycle per unit mass of ligand. This is dependent on the metal to ligand stoichiometry of the extracted species and the molecular mass of the ligand and metal.

Consequently, increasing the mass of copper transported by an extractant will enhance the productivity of a conventional plant, leading to improved energy efficiency, lower production costs and/or increased profit margins. Successful design and application of a new class of reagent which improves mass transport may not only be limited to use in conventional sulfuric acid solvent extraction plants; they could also find application in processes employing new leaching technologies where conventional phenolic oximes are not effective.

2.2.1 Ligand Design for High Mass Transport Efficiency

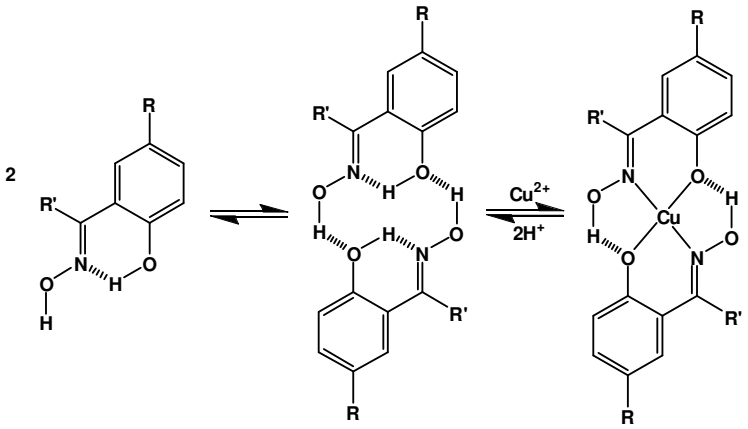

Figure 2.1: Preorganisation of the phenolic oxime dimer and pH-swing process by which copper is complexed.

Conventional pH-swing phenolic oxime extractants form charge neutral $[Cu(L\text{-}H)_2]$ copper complexes in the organic phase *via* a cationic phase transfer process (Figure 2.1).[5] As the phenolic proton of these reagents is the only site capable of being ionised within the pH-range accessible in conventional plants, the metal to ligand stoichiometry is limited and two mol of ligand are required to liberate 1 mol of copper. The percentage by mass of copper transferred by the commercial aldoxime reagent **P50** (R = C_9H_{19}, R' = X = H, Figure 2.2) *via* the $[Cu(L\text{-}H)_2]$ complex is calculated to be 12.1 wt.%. This efficiency is slightly lower in related ketoximes and significantly lower for benzophenone oximes, e.g. with R' = CH_3 and R' = C_6H_5 respectively as they have higher molecular weights.

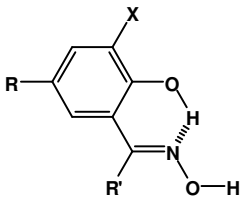

Figure 2.2: General phenolic oxime structure.

To increase the mass transport efficiency of conventional phenolic oximes it is necessary to decrease their molecular weight or increase the metal to ligand stoichiometry. The simplest way to decrease the molecular weight would be to

reduce the chain length of R and R'. This, however, would detrimentally reduce their solubility and that of the resulting complexes in the organic solvents used commercially. An alternative route to lower the molecular weight would be to use non-aromatic analogues. This generic aliphatic structure was used in the first oxime proposed for copper recovery by solvent extraction,[6] LIX 63 (Figure 2.3), developed by General Mills. This reagent did not selectivity extract copper in the presence of iron and could not be used to extract copper below pH 3.5[7, 8] as a result of its low hydrolytic stability which is characteristic of aliphatic oximes.[1]

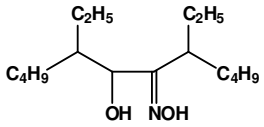

Figure 2.3: LIX63, the first oxime proposed for copper solvent extraction by General Mills.

Consequently, the only practicable approach to increase mass transport is to increase the metal to ligand stoichiometry thereby increasing the molar ratio of copper in the complex. An essential design criterion for ligands used in pH-swing extraction is the requirement to form overall charge-neutral, organic-soluble complexes. Therefore, in order to increase the Cu:L stoichiometry it is necessary to have a higher anionic charge on L as shown in Scheme 2.1. This requires incorporation of additional, easily ionisable, acidic functional groups. Formation of the simplest polynuclear complexes Cu_nL or Cu_nL_2 are considered in Scheme 2.1, these represent the most predictable cases, and are those discussed in this thesis.

$$nCu^{2+} + LH_{2n} \rightleftharpoons Cu_nL + 2nH^+$$

$$nCu^{2+} + 2LH_n \rightleftharpoons Cu_nL_2 + 2nH^+$$

Scheme 2.1: Increasing Cu to L stoichiometry of neutral complexes by incorporation of additional ionisable protons on L to produce polynuclear complexes.

Formation of a mononuclear 1Cu:1L complex could be possible through the development of quadridentate ligands with two ionisable protons within a cavity as shown in Scheme 2.2. Such ligands capable of selectively extracting copper have

been synthesised.[9-13] These are unlikely to be applied industrially as they are expected to have prohibitively high production cost and display very slow kinetics for metal stripping. Moreover if they were tailored for industrial use they are likely to have a molecular weight comparable to or exceeding that of two **P50** ligands due to addition of alkyl chains to impart solubility.

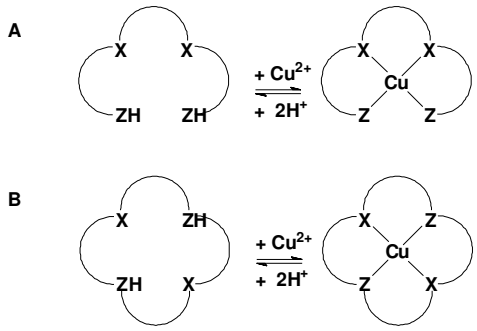

Scheme 2.2: LH_2 ligands capable of forming mononuclear [Cu(L-2H)] complexes (X and Z can be equivalent).

An alternative approach would be to increase the loading capacity of the current reagents through the introduction of an ionisable site *ortho* to the phenolic group (X in Figure 2.2). An example, where X is a carboxylic acid, is shown in Figure 2.4. Such ligands have been reported[14] to form dinuclear copper complexes (R = H). The resulting charge neutral copper complex $[Cu_2(L\text{-}2H)_2]$ has a greater Cu:L stoichiometry (2:2) than that formed by the conventional salicylaldoxime reagent **P50** (1:2).

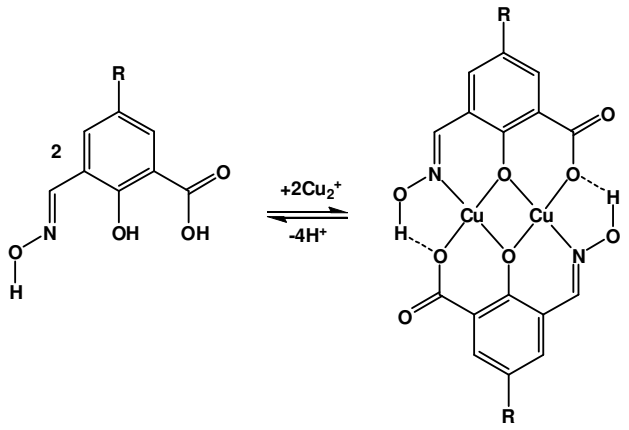

Figure 2.4: Formation of dinuclear copper complexes from 3-formyl-5-alkyl-salicylic acid oximes.[14]

In this work **L1** was prepared by the route shown in Scheme 2.3 from *t*-octylphenol *via* successive formylation (Levin *et al*),[15] oxidation, formylation (Lindoy adaptation of the Duff reaction)[16] and oximation.[17] Unfortunately the copper(II) complexes of **L1** were not sufficiently soluble in chloroform for further investigations to be pursued.

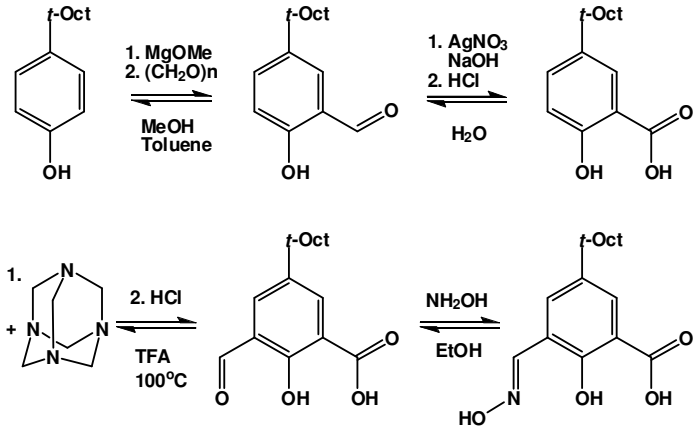

Scheme 2.3: Synthetic procedure for **L1**.

2.3 Previously Studied Dinucleating Cu Extractants 1-7

Tridentate, doubly ionisable salicylaldehyde octanoic hydrazone ligands (**1**-**6**)[3] and salicylaldehyde-2-hydroxyanil derivative (**7**)[4] shown in Figure 2.5 have been studied by the Tasker group at the University of Edinburgh.

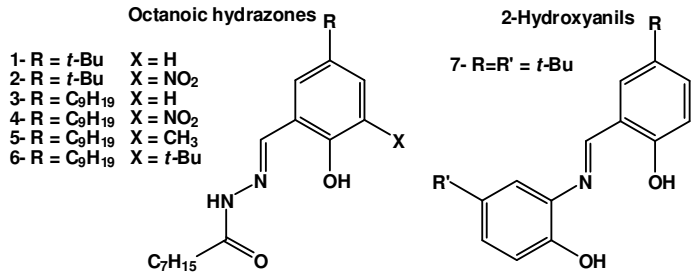

Figure 2.5: Previously studied dinucleating octanoic hydrazone (**1**-**6**)[3] and 2-hydroxyanil (**7**)[4] copper extractants.

Investigations of the hydrazone ligands (**1**-**6**) followed a screening study[2] for potential replacements of the phenolic oximes (**P50**) for application in copper recovery from sulfate streams. This study was initiated as a result of an observation made by workers at CYTEC Industries Inc. (previously Avecia) using the semicarbazone ligand shown in Figure 2.6 which extracted more copper than could be expected by formation of the complex which was predicted (Figure 2.6, right).

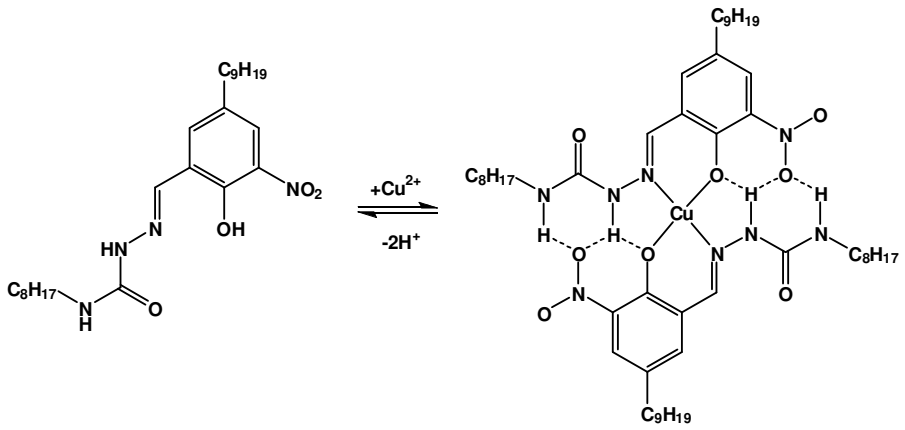

Figure 2.6: Semicarbazone extractant showing 100% of theoretical loading based on expected 1:2 Cu:L stoichiometry.[18]

2.3.1 Speciation of Cu Complexes Formed by 1-6

One of the initial objectives of the work carried out[3] at the University of Edinburgh using the octanoic hydrazone ligands **1**-**6** was to determine the metal to ligand stoichiometry of the species extracted by the semicarbazone ligand developed by CYTEC shown in Figure 2.6. Drawing analogies with the structures found for 3-formyl-5-alkyl-salicylic acid oxime (Figure 2.4),[14] it is possible to conceive a similar phenolate bridged species for **1**-**6** as shown by the comparison of **A** and **B** in Scheme 2.4. A search of the CSD[19] gave 200 hits for phenolate bridged copper centres in an NO_3 coordination environment. Of these only 21 were square planar.

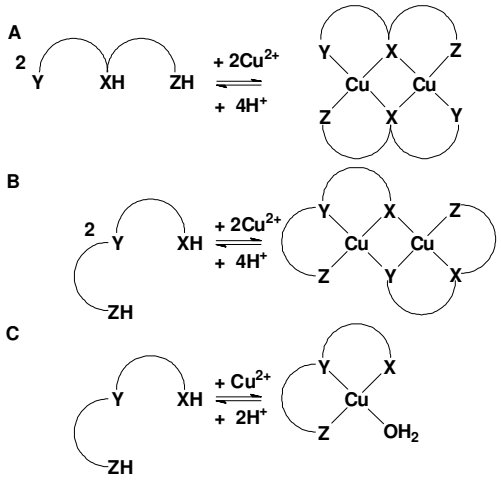

Scheme 2.4: Possible copper complex conformations formed by tridentate ligands.

Few crystal structures of dinuclear copper complexes derived from salicylaldehyde hydrazones have been published.[20-23] These have the general conformation of **B** and most are only deprotonated at the phenol to give square pyramidal or octahedral copper centres due to coordination of counter anions. An example is shown in Figure 2.7.

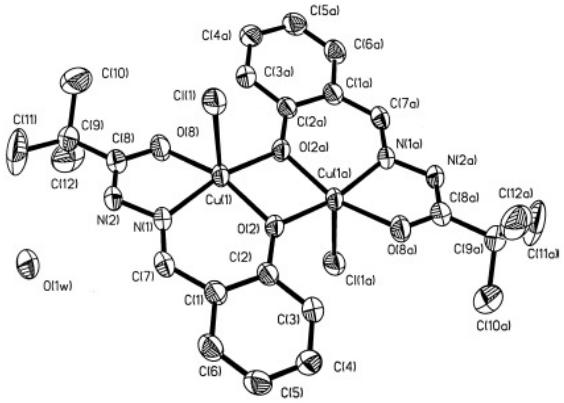

Figure 2.7: Typical structure of a dinuclear copper(II) complex formed from a singly deprotonated acylhydrazone of salicylaldehyde with square pyramidal copper centres and apical anion (Cl^-).[23]

The di-anionic ligands **1**-**6** could also form mononuclear copper(II) complexes in which the fourth coordination site of the square planar geometry is occupied by a water molecule or another neutral donor atom[24] (**C**, Scheme 2.4). In a salicylaldehyde hydrazone example where water is coordinated in the fourth equatorial site,[22] the phenol again is the only site ionised and the copper centre is square pyramidal. This is discussed further and an example given in Section 2.8.2.

The Electron Paramagnetic Resonance (EPR) spectra of solutions of known copper concentration taken from solvent extraction experiments at different equilibrium pH values were analysed. These confirmed that ligands **1**-**7** extract copper as 2Cu:2L species as demonstrated by the relationship between the concentration of Cu(II) cations extracted into the organic phase and the EPR spectrum of the solution. The signal intensity grew as a function of copper concentration in the organic phase until the metal to ligand ratio reached 1:2, thereafter decreased to a minimum when the metal to ligand ratio increased to 2:2. See Figure 2.8 for the EPR spectra measured for **4**.

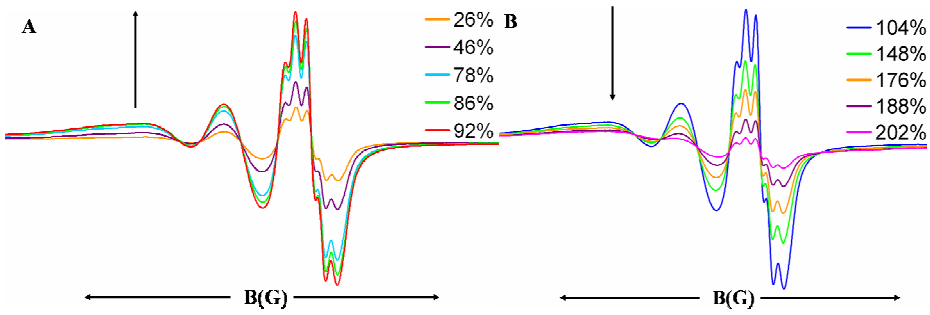

Figure 2.8: Illustration of the relationship between copper loading by **4** and intensity of the EPR spectra measured where 100 and 200% represent the formation of the mononuclear [Cu(**4**-H)$_2$] and dinuclear [Cu$_2$(**4**-2H)$_2$] complexes respectively.

This behaviour is consistent with antiferromagnetic spin coupling of the two paramagnetic copper centres. Spin coupling behaviour has been extensively reported for dinuclear copper centres within close proximity.[25] Evidence for the formation of the [Cu$_2$(L-2H)$_2$] species was provided by a study of the ternary system formed when a tridentate pyrazolone is introduced as shown in Scheme 2.5. Overall the system was found to extract the same quantity of copper into the organic phase but the EPR

signal did not decrease when the copper to ligand stoichiometry increased beyond 1Cu:2L, confirming that the copper centres were not coupled and therefore not complexed within the same molecular unit. The mononuclear complex shown in Scheme 2.5 could also be generated by the addition of 3-*iso*-propyl-2-pyrazol-5-one to a solution of the dinuclear complex.

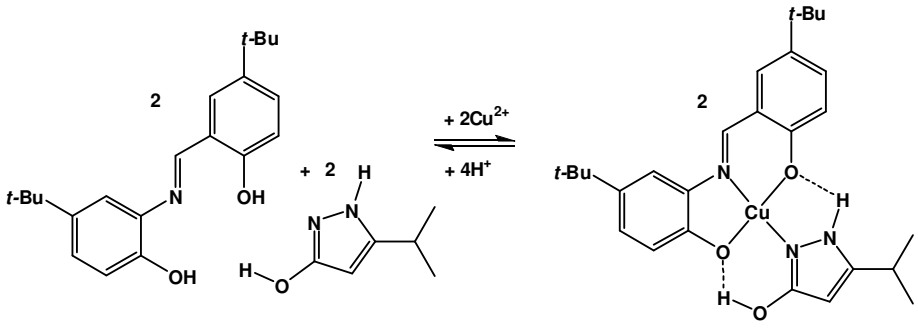

Scheme 2.5: Possible structure of the ternary mononuclear copper complex formed when 3-*iso*-propyl-2-pyrazol-5-one is introduced into chloroform solutions of ligands **1**-**7** as an auxiliary ligand. The example shown is for Ligand **7**.

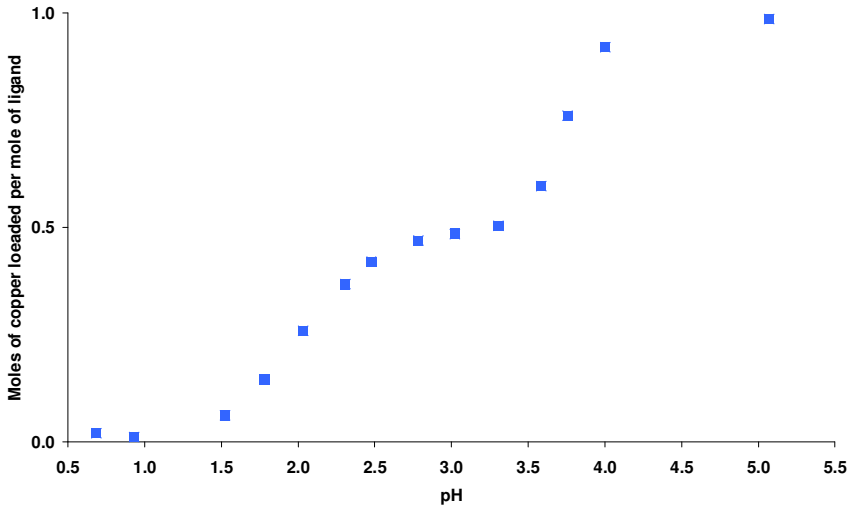

Figure 2.9: The pH-dependence of copper loading by 0.05 M chloroform solutions of **4** from aqueous sulfate solutions (*ca.* 0.0625 M).[3]

The pH-profile for copper(II) extraction by **4** shows a double inflection (Figure 2.9). The first plateau corresponds with a 1Cu:2L complex and the second a 2Cu:2L complex. This indicates a two step loading process and the formation of a stable

[Cu(**4**-H)$_2$] species, expected to be stabilised by intermolecular hydrogen bonding shown in Figure 2.10, before the [Cu$_2$(**4**-2H)$_2$] complex is formed at higher pH. Such bifurcated hydrogen bond buttressing has been observed in a similar cobalt complex formed by 5-methyl-3-nitro-salicylaldoxime (R = Me, X = NO_2, Figure 2.2) as shown in Figure 2.11, and more recently[26, 27] [Cu(L-H)$_2$] where R = *t*-Bu; X = H, Me, *t*-Bu, Br and OMe as well as the pyridine adduct [Cu(L-H)$_2$(py)$_2$] where R = *t*-Bu; X = NO_2 (Figure 2.2).[28] Formation of such a species in solution is supported by EPR analysis which is consistent with a copper atom being coordinated to two equivalent nitrogen atoms.

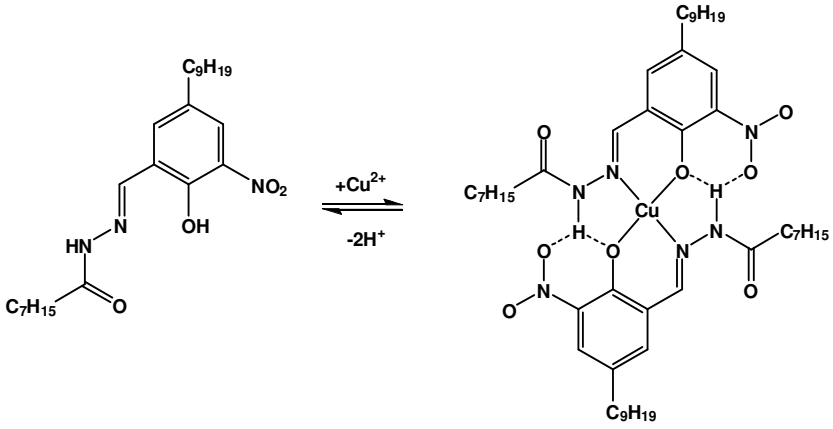

Figure 2.10: Predicted structure for the mononuclear copper complex formed by **4**, expected to be stabilised by intermolecular hydrogen bonds.

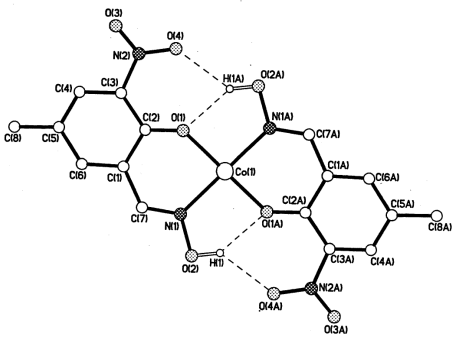

Figure 2.11: Bifurcated hydrogen buttressing between oxime NOH and nitro and phenolate oxygen atoms.[28]

There are two possible ways in which the two copper centres can be bridged in the dinuclear copper complexes formed by **1**-**7**, see Scheme 2.6. Of the two isomers, **A** is

the most reported in the CSD. There are no structures of type **B** published in which an amidato oxygen bridges two copper centres.[21]

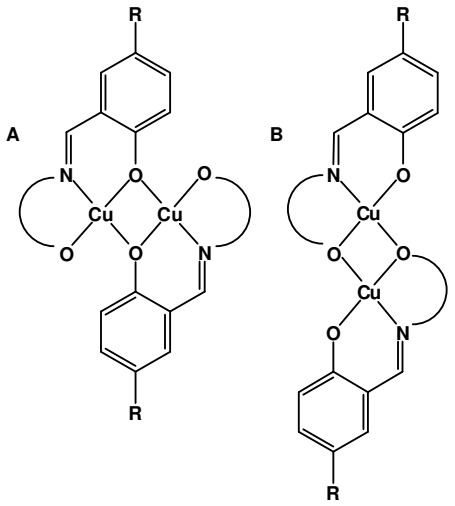

Scheme 2.6: Possible copper bridging modes for tridentate ONO ligands**.**

Ligands **1**, **3** and **5**-**7** are expected to adopt the geometry represented by **A**. This conformation is unlikely for the nitro substituted ligands **2** and **4** as the nitro oxygen atoms are anticipated[29, 30] to interfere sterically with the hydrazone oxygen atom as illustrated in Figure 2.12.

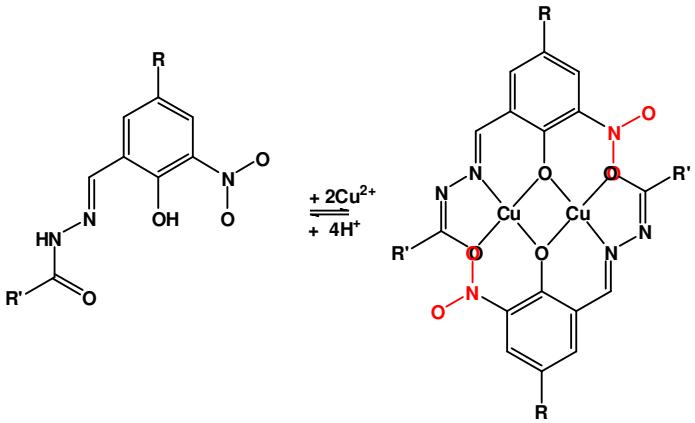

Figure 2.12: Depiction of the steric interference expected between NO_2 and hydrazone oxygen atoms for ligands **2** and **4**.

Attempts to obtain single crystals to undertake X-ray structure determinations of the copper complexes formed by the acyl hydrazone (**1**-**6**) and hydroxyanil (**7**) ligands

were unsuccessful. This is unfortunate because it leaves some ambiguity about the structure of the dinuclear complexes. Whilst the main objective of this thesis is extension of the work on the *di*acidic systems by development of new *tri*acidic ligands, the design of such systems requires an understanding of the coordination chemistry involved in the dinuclear complexes. To achieve this, analogues of the diacidic salicylaldehyde hydrazone ligands were synthesised with substituents which are more likely to lead to crystalline copper(II) complexes.

2.3.2 Preparation and Characterisation of New Ligands L2 and L3

To increase the probability of crystallising dinuclear copper complexes of the salicylaldehyde hydrazone ligands (**1**-**6** in Figure 2.5), the length of the alkyl chains was reduced. 2,2-Dimethyl-propanoic hydrazide (**8**) was prepared by the method of Li *et al*[31] and reacted with the appropriate salicylaldehyde to give ligands **L2** and **L3** (Scheme 2.7).

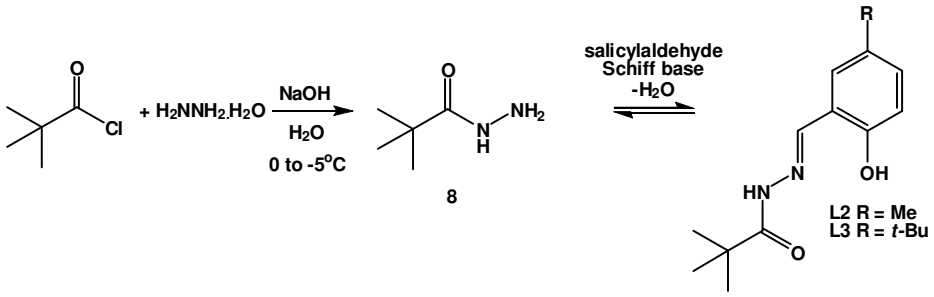

Scheme 2.7: Preparative method for 2,2-dimethyl-propanoic hydrazide (**8**) and ligands **L2** and **L3.**

Both precursors and ligands were characterised by ^{1}H and ^{13}C NMR, IR spectroscopy, electrospray mass spectrometry and CHN analysis. The X-ray crystal structure of **L2** (Figure 2.13) has orthorhombic symmetry with space group P_{nma}. There are four molecules in the unit cell. The molecule is entirely planar (excluding the *t*-Bu methyl groups) with zero deviation from the least squares plane. The structure shows intramolecular H-bonding between the phenol hydrogen and imine nitrogen (O1•••N22, 2.653(3) Å) and intermolecular H-bonding interaction between N23 and O25 (3.307(3) Å) of the amidato units of neighbouring units. The ONO

coordination site is preorganised for complexation of a square planar metal, although the angle (101.68(9)°) is greater than the ideal geometry of 90°.

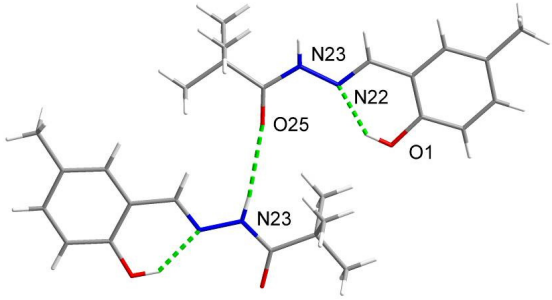

Figure 2.13: Crystal structure of **L2** showing intra- and inter-molecular hydrogen bonds associated with the N22•••O1 and N23•••O25 contacts of 2.653(3) and 3.307(3) Å.

2.3.3 Preparation and Characterisation of $[Cu_2(L2\text{-}2H)_2]$

The copper complex $[Cu_2(\mathbf{L2}\text{-}2H)_2]$ was prepared by stirring stoichiometric quantities of ligand and copper acetate in ethanol under reflux for 30 min. The resulting green precipitate was recrystallised from chloroform to give needles suitable for analysis by X-ray diffraction. The structure is shown in Figure 2.14.

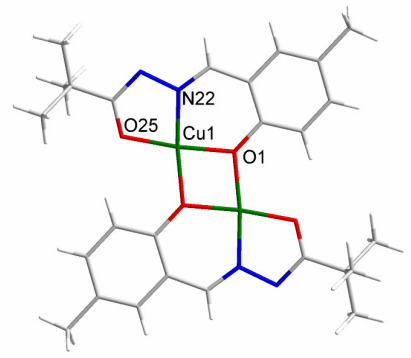

Figure 2.14: X-ray structure of phenolate bridged dinuclear copper complex $[Cu_2(\mathbf{L2}\text{-}2H)_2]$ formed by **L2**.

The crystal system is triclinic with space group $P\bar{1}$ and has one molecule per unit cell. $[Cu_2(\mathbf{L2}\text{-}2H)_2]$ has a centrosymmetric structure with phenolate oxygen atoms (O1) bridging two four-coordinate copper centres (see Table 2.2 for bond lengths and angles). The Cu–Cu distance is 2.965(2) Å which is within the range 2.788-3.365 Å

reported for 98 phenolate bridged dinuclear four-coordinate copper complexes in the CSD but is less than the mean value of 3.040 Å. The value is also within the range 2.853-3.073 Å reported for 20 phenolate bridged $Cu_2N_2O_6$ structures but again is less than the mean value, 3.005 Å.

The Cu1-O1-Cu1 angle of 99.6(2)° is significantly less than the ideal 120° for sp^2 hybridisation of the phenolate oxygen atom. Angles around the Cu centres range from 80.4(2)° to 104.9(2)° for O1-Cu1-O1' and O1-Cu1-O25, indicating significant distortion from ideal square planar geometry. The $Cu_2N_2O_4$ complex unit is almost planar with the maximum deviation from the least square plane through Cu1, O1, N22, O25, Cu1', O1', N22', O25' atoms being -0.0217 and 0.0079 Å for atoms O1 and N22 with mean deviation of 0.0151 Å. The $Cu_2N_2O_4$ plane is at an angle of 3.2° from that of the aromatic ring. Comparison of the ONO angle in the free ligand and complex reveal it has been reduced from 101.65(7)° upon complexation to 92.80(30)°.

Table 2.2: Bond lengths and angles in the coordination spheres of the copper atoms in $[Cu_2(\mathbf{L2}\text{-}2H)_2]$**.**

Lengths /Å		Angles /°	
Cu1•••Cu1'	2.965(2)	Cu1-O1-Cu1'	99.6(2)
Cu1-O25	1.906(6)	O1-Cu1-O1	80.4(2)
Cu1-N22	1.906(7)	O1-Cu1-O25	104.9(2)
Cu1-O1	1.916(5)	O25-Cu1-N22	81.6(3)
		N22-Cu1-O1	93.1(3)

The structure contains a phenolate bridging mode consistent with one previously published in literature as shown in Figure 2.7.[23] However, in $[Cu_2(\mathbf{L2}\text{-}2H)_2]$ the ligand is deprotonated at both the phenol and amide to yield four coordinate copper centres with distorted square planar geometry unlike the published structure in which the ligand is only deprotonated at the phenol, resulting in square pyramidal copper with chloride anions in the apical position.

2.3.4 Magnetic Properties of $[Cu_2(L2\text{-}2H)_2]$

Variable temperature, solid-state direct current (dc) magnetic susceptibility measurements were collected on a Quantum Design MPMS SQUID magnetometer equipped with a 7 T dc magnet. Samples were prepared and measured with the help of Lindsay Egan. Data were interpreted and simulated with the assistance of Dr. Euan Brechin and Ross Inglis at the University of Edinburgh. Diamagnetic corrections were applied to the observed paramagnetic susceptibilities using Pascal's constants.[25] Studies were performed on a vacuum dried polycrystalline sample of $[Cu_2(\mathbf{L2}\text{-}2H)_2]$ in the 5-300 K temperature range under an applied field of 1.0 T. The results are plotted as the $\chi_M T$ product vs. T in Figure 2.15.

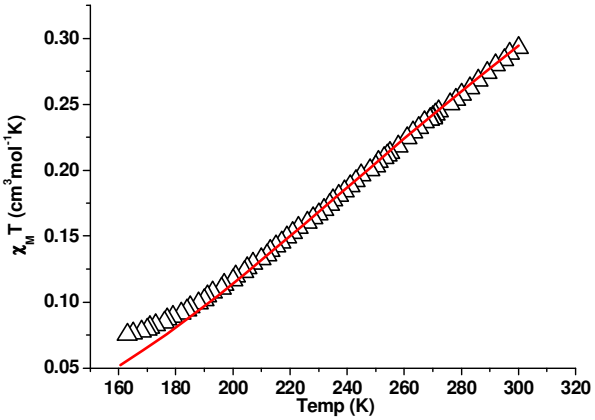

Figure 2.15: Plot of $\chi_M T$ *vs* T for $[Cu_2(\mathbf{L2}\text{-}2H)_2]$. The solid line represents a simulation of the experimental data in the temperature range 300-160 K; see text for details.

The $\chi_M T$ value of 0.29 cm^3 K mol^{-1} at 300 K is less than half the spin-only value (g = 2.00) expected for a dinuclear Cu(II) complex (0.75 cm^3 K mol^{-1}), indicative of relatively strong antiferromagnetic exchange between the two metals. This is as expected because the Cu-O-Cu bond angle of 99.6° is greater than the ferromagnetic to antiferromagnetic exchange crossover angle of ~97.5° suggested by Hatfield and Hodgson for hydroxo/alkoxo bridged Cu(II) dimers.[32, 33] The value of $\chi_M T$ decreases linearly with temperature to 160 K when the sample becomes diamagnetic, indicating population of the S = 0 ground state. The small plateau observed at temperatures below ~170 K is attributed to a small fraction of paramagnetic impurities that are almost always observed in S=0 systems with large exchange.

$$\hat{H} = -2J(\hat{S}_1 \cdot \hat{S}_2) \qquad \textbf{Equation 2.1}$$

The data were successfully simulated using the program MAGPACK[34, 35] employing the 1*J* model of Equation 2.1, affording the parameters J = -235 cm^{-1} and g = 2.218. These are entirely consistent with the numerous Cu-O(R)-Cu systems in the literature.[36-38]

2.4 Increased Mass Transport of Copper by Dinucleating Extractants

It has been established that the diacidic ligands, **1**-**7**, previously studied and those developed for this current work, **L1**-**L3**, can form dinuclear copper complexes of the type $[Cu_2(L\text{-}2H)_2]$. Consequently, the number of mol of copper transported per mol of extractant is double that of the of the conventional phenolic oxime reagent (**P50**) which forms $[Cu(L\text{-}H)_2]$ complexes. To be beneficial in a commercial solvent extraction plant the *mass* of copper transported per unit mass of ligand should also be greater. The *mass* transport of each ligand is calculated in Table 2.3.

Table 2.3: Masses of copper (g) transported per unit mass of extractant (kg) for the diacidic ligands **1**-**7** and **L1**-**L3** and the increases in mass transport efficiency relative to the commercial extractant, **P50**.

Ligand	M.W.	Cu : L	Cu (g) per L (kg)	Fold increase
P50	263	1 : 2	121	0
1	318	2 : 2	200	1.65
2	363	2 : 2	175	1.45
3	389	2 : 2	163	1.35
4	434	2 : 2	146	1.21
5	403	2 : 2	158	1.30
6	445	2 : 2	143	1.18
7	325	2 : 2	196	1.62
L1	293	2 : 2	217	1.79
L2	234	2 : 2	272	2.24
L3	276	2 : 2	230	1.90

Of the dinuclear complexes investigated previously,[3, 4] few are sufficiently soluble in the water-immiscible hydrocarbon solvents used industrially to be of commercial importance, with the possible exception of **3** and **4**. Nevertheless, they successfully increase mass transport efficiency and could be developed for industrial application through integration of additional alkyl groups provided these do not increase the molecular weight to the point where the benefit of the increased mass transport efficiency is lost. As the increase in mass transport efficiency for the diacidic ligands is relatively small (1.18 up to 2.24 fold) there will be limited scope to increase the solubility in this way. Partly as a consequence of this, the triacidic ligands described in this chapter were developed to further increase the molar transport capacity by forming complexes of the type $[Cu_3(L\text{-}3H)_2]$.

2.5 Trinucleating Cu Extractants L4-L13

The design principles incorporated in the *di*nucleating systems discussed previously were applied to create *tri*nucleating ligands which are the subject of the remainder of this chapter. An additional deprotonatable group capable of bridging two metal cations is required to convert a *di*nucleating ligand into a *tri*nucleating ligand as outlined in Section 2.2.1. This was achieved by incorporating a carboxylic acid as the group ZH in Scheme 2.8, *ortho* to the hydroxyl of the 5-alkylsalicylaldehyde precursors to give a series of 3-imine-substituted-5-alkylsalicylic acids extractants, **L4**-**L13** shown in Table 2.1. The salicylic acid 3,5-di-*iso*-propylsalicylic acid has been demonstrated to extract copper into hydrocarbon solvent.[39]

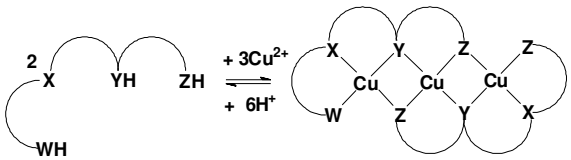

Scheme 2.8: Formation of charge-neutral linear *tri*nuclear copper complexes from *tri*acidic ligands.

The general preparative procedure for ligands **L4**-**L13** is given in Scheme 2.9, a more detailed description of each of the steps involved for each ligand is discussed in Section 2.5.1.

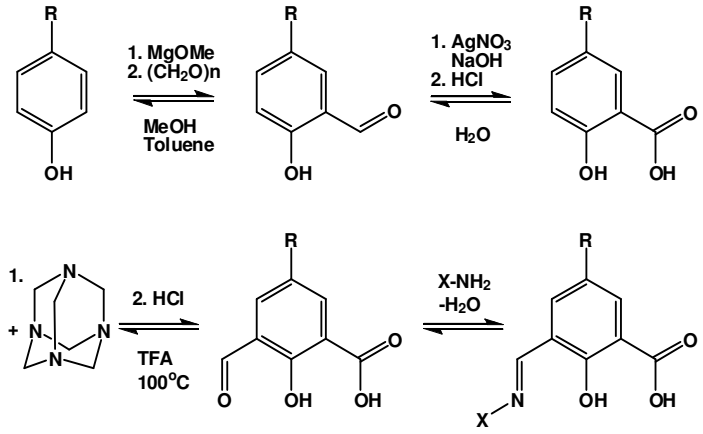

Scheme 2.9: General preparative scheme for **L4**-**13**.

2.5.1 Ligand Synthesis

Synthesis of the target triacidic ligands where the substituent *para* to the phenol oxygen atom is a methyl group (**L4**, **L6**, **L9** and **L11**) involved a two step process from 5-methylsalicylic acid. The starting material was formylated *via* an adaptation of the Duff reaction[40] described by Lindoy and co-workers[16] to yield 3-formyl-5-methylsalicylic acid (**9**) in approximately 70% yield. The reaction mechanism is given in Scheme 2.10. The resulting aldehyde was treated with the appropriate hydrazide or 2-hydroxyaniline to give the target molecule *via* a Schiff base condensation in yields of > 70%. 2,2-Dimethyl-propanoic hydrazide (**8**) was prepared as previously mentioned in Section 2.3.2, octanoic hydrazide, 4-*t*-butylbenzoic hydrazide and 2-amino-4-*t*-butylphenol were used as supplied by Sigma-Aldrich.

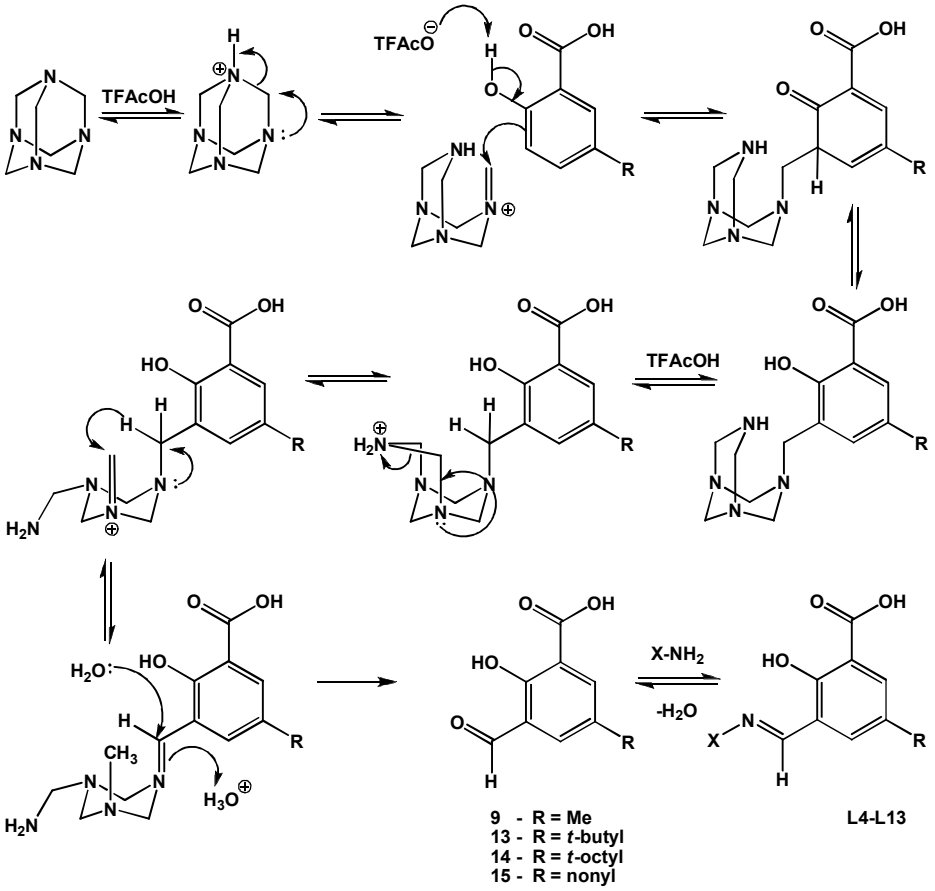

Scheme 2.10: Reaction mechanism[41] for the 3-formylation of 5-alkylsalicylic acids *via* the adaptation of the Duff reaction described by Lindoy and co-workers.[16]

Triacidic ligands where the substituent in the 4 position to the phenol oxygen atom is *t*-butyl (**L5**), *t*-octyl (**L7**, **L10** and **L12**) were prepared *via* a 4 step synthesis from the 4-substituted alkyl phenols which were sourced from Sigma-Aldrich and used as supplied. The phenols were *ortho*-formylated using the method of Levin and co-workers[15] from magnesium methoxide and paraformaldehyde *via* the magnesium-salicylaldehyde salt. The mechanism is shown in Scheme 2.11. The resulting salicylaldehydes and 5-nonylsalicylaldehyde, used to synthesise **L8** and **L13**, were oxidised by silver nitrate in aqueous sodium hydroxide to yield the salicylic acids; 5-*t*-butylsalicylic acid (**10**), 5-*t*-octylsalicylic acid (**11**) and 5-nonylsalicylic acid (**12**). These were treated as shown in Scheme 2.10 to yield the 3-formyl-5-*t*-butylsalicylic acid (**13**), 3-formyl-5-*t*-octylsalicylic acid (**14**) and 3-formyl-5-nonylsalicylic acid

(**15**) precursors and generate the target ligands upon treatment with the relevant primary amine Schiff bases.

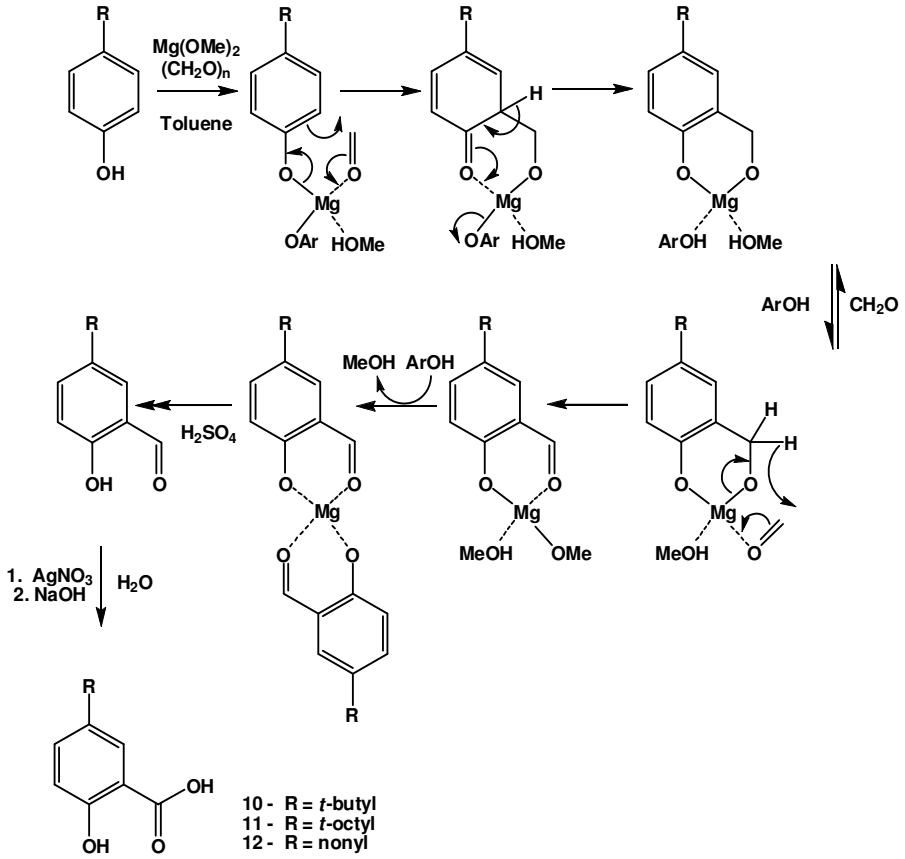

Scheme 2.11: Magnesium-mediated *ortho*-formylation[15] followed by oxidation to give the intermediates; 5-*t*-butylsalicylic acid (**10**), 5-*t*-octylsalicylic acid (**11**) and 5-nonylsalicylic acid (**12**).

Initial attempts to isolate **L6** *via* reflux of 3-formyl-5-methylsalicylic acid and octanoic hydrazide in methanol, ethanol or acetonitrile resulted in the formation of 3,3'-(azinodimethylidyne)bis(5-methylsalicylic acid) (**16**) and *di*-(octan-1-one)azine (**17**) (Figure 2.16) as previously observed when using salicylaldehyde.[23] Carrying out the reaction in toluene using Dean-Stark apparatus for water removal also yielded **16** and **17**, as recognised by the resulting strongly coloured orange solution. **L6** was successfully isolated from the filtrate of a reaction carried out at reduced temperature (< 40°C) of a suspension of the starting materials and magnesium sulfate in chloroform. This was possible as the starting materials are sparingly soluble in chloroform whilst **L6** is soluble.

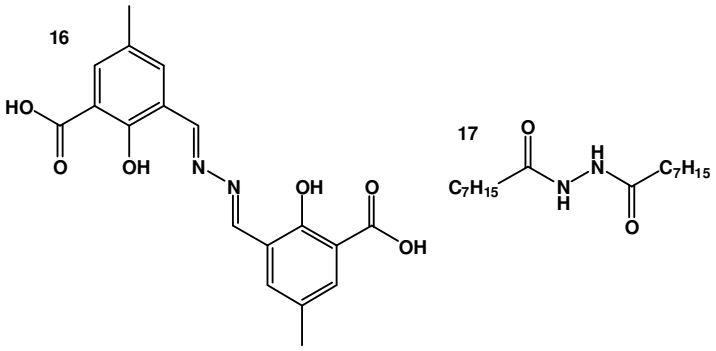

Figure 2.16: Undesired products 3,3'-(azinodimethylidyne)bis(5-methylsalicylic acid) (**16**) and *di*-(octan-1-one)azine (**17**) obtained from initial attempts to synthesise **L6**.

The crystal structure of the DMSO adduct of **16** is shown in Figure 2.17. There are two molecules per unit cell and the crystal system is monoclinic with space group $P2^1/c$. The molecule is planar with maximum deviation from the least square plane through the molecule (excluding hydrogen atoms) being ± 0.0446 Å for N62 with mean deviation of 0.0241 Å. There is an intramolecular hydrogen bond between O1 and O23 (2.5927(17) Å) and a hydrogen bond from the carboxylic acid O22 to the DMSO solvate O2S (2.5518(17) Å).

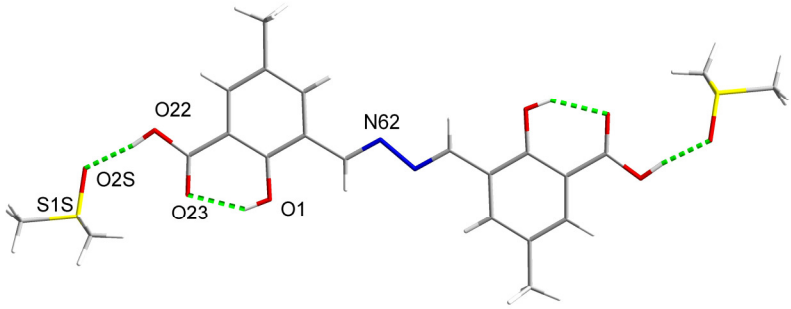

Figure 2.17: Crystal structure of DMSO adduct of 3,3'-(azinodimethylidyne)bis(5-methylsalicylic acid) (**16**).

2.5.2 Characterisation by NMR Spectroscopy

All ligands and precursors were characterised by ^{1}H and ^{13}C spectroscopy. NMR spectroscopy was particularly useful in following the processes which involved substitution of the aromatic rings. This was evident through observation of the decreasing number of protons on the ring from four in the alkyl-phenol to three in the salicylaldehydes and salicylic acids to two in the 3-formyl-5-alkylsalicylic acids. The characteristic aldehydic proton (10-10.5 ppm) disappears upon conversion to the carboxylic acid and the resonance shifts to 8.5-9 ppm when treated with Schiff-bases to form the imine as shown in Figure 2.18 for **L5**. Comparison of the ^{13}C NMR spectra (Figure 2.19) with that of the Distortionless Enhancement by Polarisation Transfer (DEPT) 135 ^{13}C NMR experiment (Figure 2.20) was valuable for identification of tertiary and quaternary carbons in aromatic, aldehyde, carboxylic acid and imine environments.

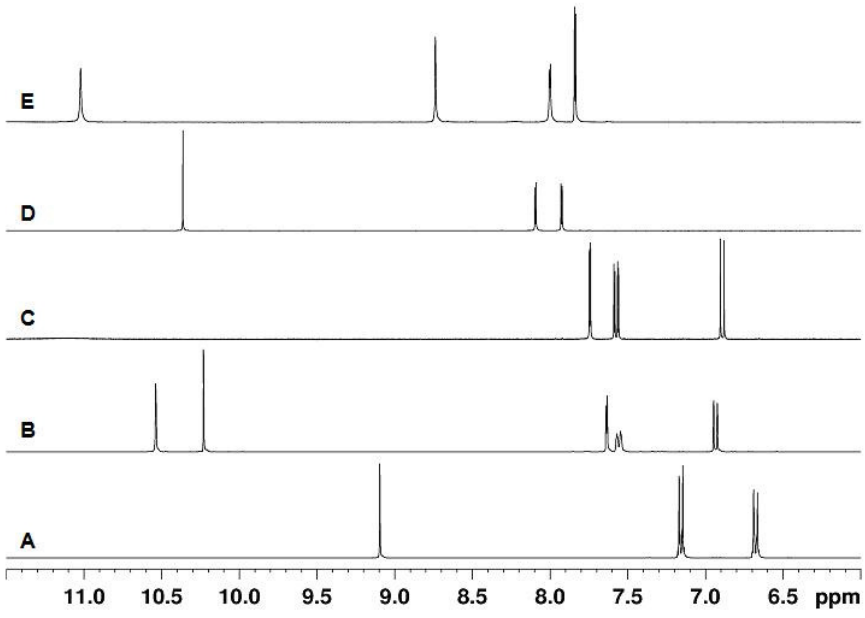

Figure 2.18: ^{1}H NMR spectra of **L5** (E) and the precursors; 4-*t*-butylphenol (A), 5-*t*-butylsalicylaldehyde (B), 5-*t*-butylsalicylic acid (C) and 3-formyl-5-*t*-butylsalicylic acid (D).

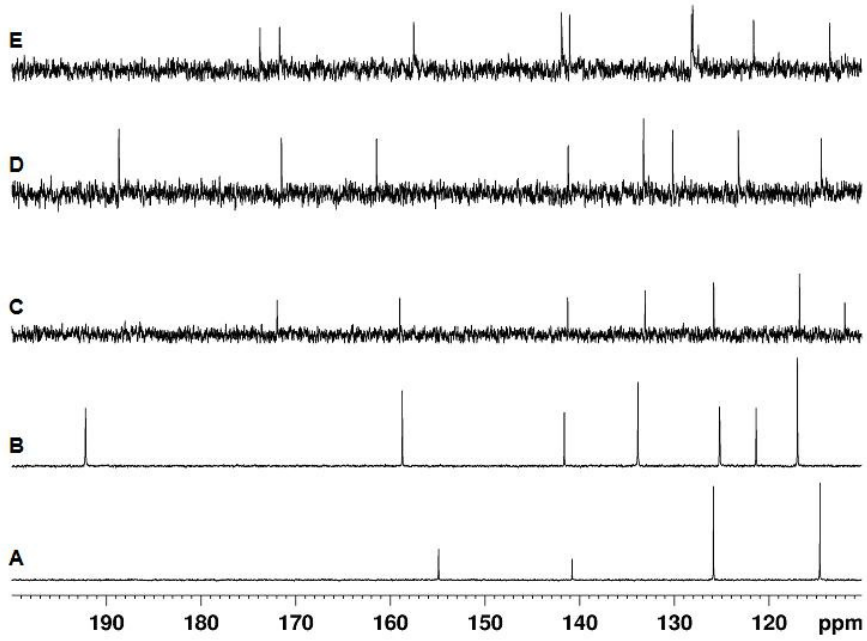

Figure 2.19: ^{13}C NMR spectra of **L5** (E) and the precursors; 4-*t*-butylphenol (A), 5-*t*-butylsalicylaldehyde (B), 5-*t*-butylsalicylic acid (C) and 3-formyl-5-*t*-butylsalicylic acid (D).

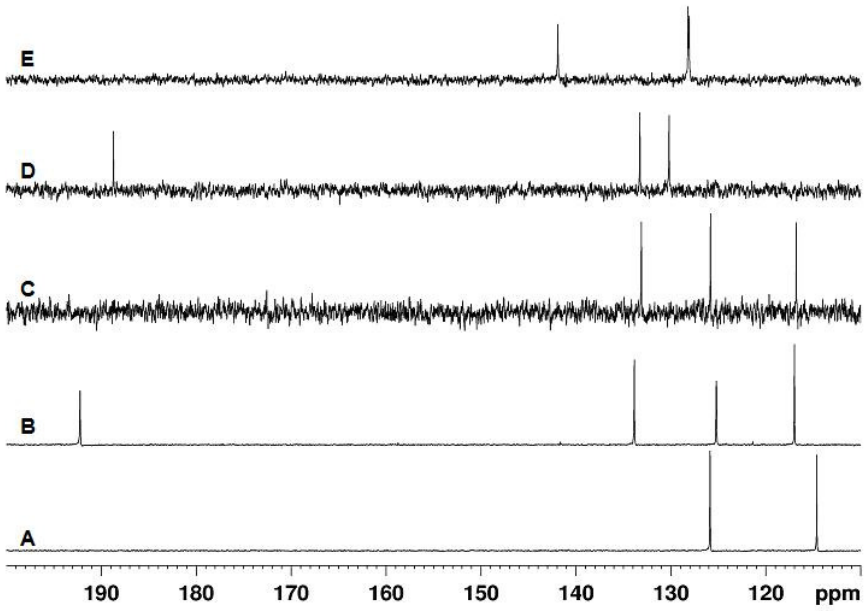

Figure 2.20: DEPT 135 NMR spectra of **L5** (E) and the precursors; 4-*t*-butylphenol (A), 5-*t*-butylsalicylaldehyde (B), 5-*t*-butylsalicylic acid (C) and 3-formyl-5-*t*-butylsalicylic acid illustrating the aldehydic CH *ca*. 190 ppm (B and D) and the imine CH (*ca*. 142 ppm).

2.5.3 Crystal Structures of L5, L6 and L11

L5 was isolated as a methanol solvate (Figure 2.21) and an ethanol solvate (Figure 2.22 and Figure 2.23). Both crystallise with four molecules in the unit cell as monoclinic systems with space group $P2^1/c$. Ignoring the six methyl units in the *t*-butyl groups and all protons, both solvates show maximum deviation from the least squares plane of the molecule by the azomethine carbon atoms, C61 (-0.3692 and -0.2775 Å) and amido oxygen atoms, O65 (0.7468 and 0.6717 Å) with mean deviations from the plane of ±0.2163 and ±0.1807 Å for the methanol and ethanol solvates respectively. This difference might be due to stronger hydrogen bonds formed to a smaller and more polar methanol molecule and also because the methanol molecule forms three intermolecular H-bonds; two to the imino unit of one molecule O1S•••N62 (2.931(2) Å), O1S•••O65 (2.880(2) Å) and the third to the carboxylic acid group of another molecule O1S•••O23, 2.578(3) Å. The ethanol molecule only forms two H-bonds, O1S bridges between N62 (2.878(3) Å) of one molecule and O22 (2.606(4) Å) of another.

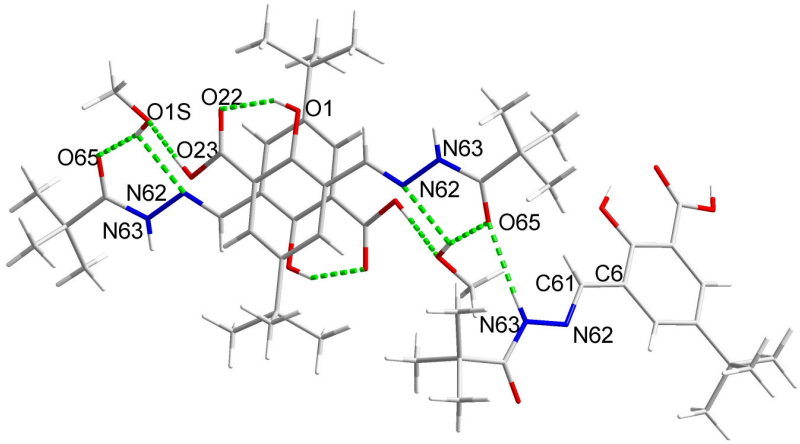

Figure 2.21: Part of the structure of **L5**•CH_3OH showing the intramolecular contacts between the phenolic and carboxylic groups (O1•••O23, 2.587(3) Å). Intermolecular crosslinking by three H-bonds through the methanol solvate molecules; O1S•••N62 (2.931(2) Å), O1S•••O65 (2.880(2) Å) and O1S•••O23, 2.578(3) Å. Intermolecular H-bonding between the amido groups N63•••O65, 2.982(2) Å is also shown.

Both solvates form intramolecular H-bonds from the phenoxy to the carbonyl of the carboxylic acid, O1•••O23 distances of 2.587(3) and 2.570(2) Å are measured for the

ethanol and methanol solvates respectively. Both also form intermolecular H-bonds between amido groups, the N62•••O65 distance is longer for the methanol solvate (2.982(2) Å) than the ethanol solvate (2.881(4) Å).

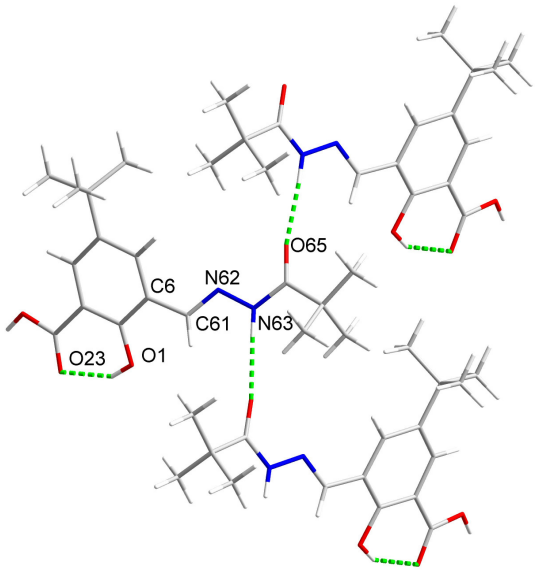

Figure 2.22: Part of the structure of **L5**•C_2H_5OH showing the intermolecular H-bonding between the amido groups (N62•••O65, 2.881(4) Å) and intramolecular contacts between the phenolic and carboxylic groups (O1•••O23, 2.587(3) Å).

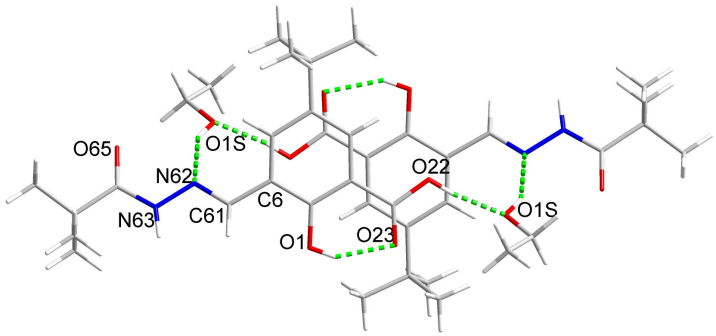

Figure 2.23: Part of the structure of **L5**•C_2H_5OH showing the crosslinking by H-bonding through ethanol solvate molecules (N62•••O1S, 2.878(3); O1S•••O22, 2.606(4) Å).

Both solvates of **L5** adopt a geometry in which the ONO donor set is not preorganised to form a linear trinuclear copper complex as depicted in Scheme 2.8, similar to **L6**. However, unlike **L6**, only one 180° rotation, about the C6-C61 bond,

is required to obtain the preorganised geometry suitable for accommodation of a square planar Cu(II) centre.

L6 crystallised from pyridine as the pyridinium adduct as shown in Figure 2.24. There are two molecules in the unit cell which has triclinic symmetry with $P\bar{1}$ space group. The ligand molecule is surprisingly planar, omitting hydrogen atoms, given the presence of the alkyl chain which has the potential to impart significant disorder. Maximum deviations from the carbon, nitrogen and oxygen plane of the molecule were measured for O65 (0.2187 Å) and C68 (-0.1673 Å) with mean deviation of ±0.0717 Å.

The hydrogen atom between the carboxylic acid (O23) and pyridine nitrogen (N1T) was placed on the carboxylic acid by judgment of crystallographer Fraser J. White. The reasoning for this is that, although the position of this hydrogen is slightly ambiguous, there are two peaks on the difference map of approximately equal intensity at appropriate distances from each of the hosts. One peak is present 0.71 Å from N1T and the other 0.91 Å from O23. For X-ray data collected at 150 K, 0.84 Å is the approximate distance of an OH hydrogen atom and 0.88 Å for an NH hydrogen atom. The peak observed for the former deviates less (0.07 Å) from the ideal position of an OH than the latter does from that of an NH (0.17 Å). The peak intensity of the OH position is also slightly higher than the NH. Consequently, the hydrogen atom was placed on the oxygen and constrained to be 0.84 Å from O23 as expected for an OH hydrogen atom.

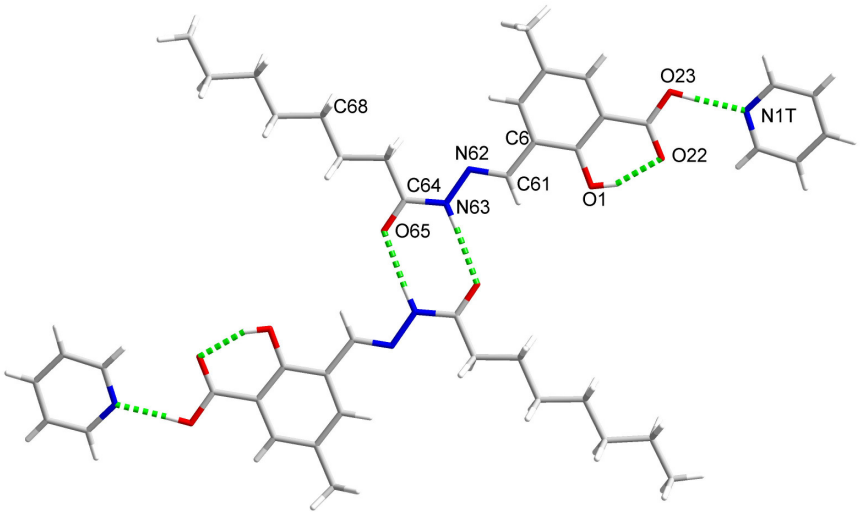

Figure 2.24: The extended conformation of the pyridine solvate of **L6 s**howing intermolecular (N63•••O65, 2.870(3) Å) and intramolecular (O1•••O22, 2.547(2) Å) H-bonding.

This judgment may be false as the pyridinium ion[42] is a weaker acid in water (K_a = 5.6 x 10^{-6}, pK_a = 5.25) than salicylic acid[43] (K_a = 1.07 x 10^{-3}, pK_a = 2.97). That predicted[44] for **L5**, see Table 2.5, (K_a = 1.20 x 10^{-3}, pK_a = 2.92) by the online chemical properties predictor SPARC is very similar to that of salicylic acid. Therefore it can be concluded that the acid is likely to be deprotonated in preference to the pyridinium ion in water. However, this rule cannot be readily translated into polar solvents. For example in DMSO, the solvent from which this product was recrystallised, the relative acidities of pyridine hydrochloride (pK_a = 3.5) and salicylic acid (pK_a = 6.8) are reversed.[43] As a result the judgment made by the crystallographer may be chemically sound.

L6 adopts a geometry in which the ONO donor set is not preorganised to form a linear trinuclear copper complex as depicted in Scheme 2.8. To adopt the desired conformation 180° rotation about 2 bonds is required, namely C6-C61 and N63-C64. **L6** appears to adopt a structure in the solid state which optimises the number and strength of intra- and inter-molecular hydrogen bonds. There is an intramolecular H-bond from the phenolic OH group to the carbonyl of the carboxylic acid O1•••O22, 2.547(2) Å and a pair of intermolecular H-bonds arise from the amido NH and C=O groups of a neighbouring molecule N63•••O65, 2.870(3) Å.

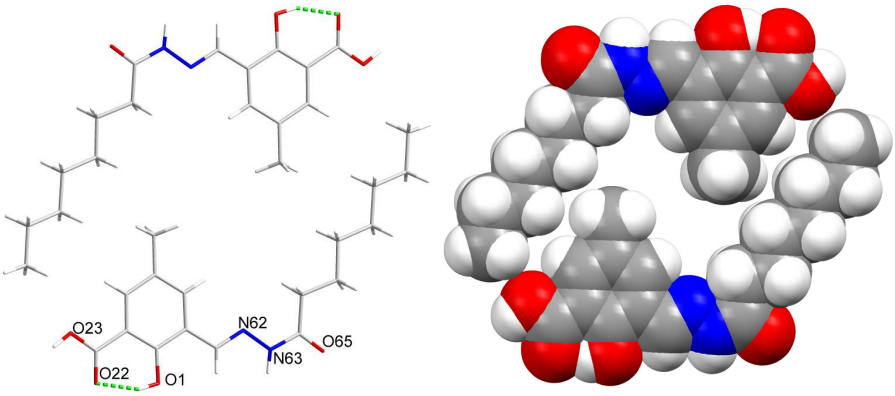

Figure 2.25: Crystal structure of **L6** illustrating the intermolecular packing interaction between the lipophilic sides in wireframe (left) and spacefill (right) representations.

The crystal structure of **L6** not only demonstrates intermolecular hydrogen bonds, but also favourable interactions between the hydrophobic edges of the molecules. The methyl group interdigitates with the cavity provided between the aromatic ring and alkyl chain of the neighbouring molecule as shown in Figure 2.25 within the same plane as the intermolecular interactions.

L11 (Figure 2.26) was not isolated as a solvate. There are 8 molecules per unit cell, the crystal system is monoclinic with space group *C*2/*c*. Unexpectedly, **L11** is in zwitterionic form in which the phenolic proton has transferred to the imino nitrogen atoms and three intramolecular H-bonds result. Hydrogen atoms H11 and H211 were found on the difference map, H232 was placed. The phenol oxygen atom (O12) forms intramolecular H-bonds with both the OH group of the carboxylic acid (O232) and the protonated (H211) imino nitrogen (N211). The imino nitrogen (N211) also forms an intramolecular hydrogen bond to phenol oxygen atom O11 and the hydrogen atom attached to it (H11) points away from $N211^{+}$-H211 as a result. There is also an intermolecular H-bond between the phenol oxygen atom, O11, and the carbonyl oxygen atom O222 of the carboxylic acid group of a neighbouring molecule with a distance of 2.689(3) Å. Although the ligand is in a zwitterionic form, the imino C=N bond of 1.303 Å does not deviate significantly from that of the structure obtained for analogous ligand **7**, 1.280(3) Å which is not zwitterionic.[4] The two aromatic rings of the molecule are inclined at an angle of 19.4° relative to each other.

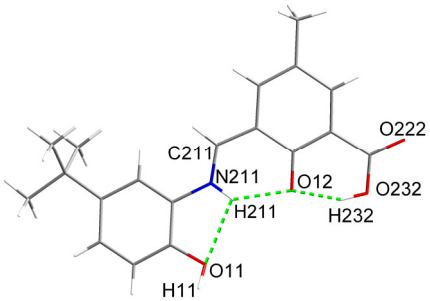

Figure 2.26: The crystal structure of **L11** showing it to be in a zwitterionic form with the phenolate oxygen atom (O12) forming intramolecular H-bonds to the imino nitrogen atom (N211•••O12, 2.634(9) Å) and to the carboxylic acid OH group (O12•••O232, 2.453(3) Å). The imino nitrogen also forms an intramolecular H-bond to phenol O11 (N211•••O11, 2.6617(14) Å).

The O11, N211, O12 angle is 88.816(4)° indicating that the ligand is almost ideally preorganised for complexation of a square planar Cu(II) cation. Placing a copper at the midpoint between O11 and O12 would give Cu•••O and Cu•••N distances of 1.853(2) and 1.910(6) Å respectively, which are shorter than the distances observed for Cu(II) to phenolate oxygen, 1.865(3)-1.92(1) Å, and oxime nitrogen atoms, 1.933(4)-1.968(4) Å, in structures of complexes with phenolic oximes of the types used commercially.[5]

Triacidic ligands **L6**, **L9** and **L11** were the prototype ligands designed to investigate solvent extraction. It was predicted that **L6** and **L9** could show stepwise loading with three plateaux in their pH-profiles, as in Figure 2.27. Such profiles are expected to arise as the three different deprotonatable sites are likely to have different pK_a's.

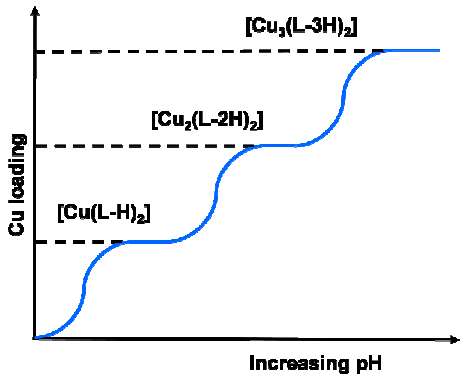

Figure 2.27: Idealised extraction curve expected for triacidic ligands derived from acyl hydrazones.

It was hoped that the additional aromatic ring in **L9** and **L10** would increase the probability of isolating crystalline samples to allow the solid state structures of the hydrazone complexes to be determined. **L11**-**L13** were expected to demonstrate different extraction properties due to the presence of two phenolic protons in similar chemical environments, with similar pK_a's, and as a result should deprotonate at roughly the same pH. As a consequence the extraction curve might be compatible with a two step loading process, with the first plateau due to a stable dinuclear copper complex [Cu_2(L-2H)$_2$] and the second due to the trinuclear complex [Cu_3(L-3H)$_2$]. Ligands **L4** and **L5** were designed to improve the chance of obtaining crystal structure determination of non-aromatic acyl hydrazones.

The very limited solubility of **L11** in chloroform (<0.0025 M) was the initial reason for development of *t*-octyl, **L12**, and nonyl, **L13**, derivatives. **L12** was suitably soluble in chloroform. However the resulting copper complexes formed a third phase during solvent extraction experiments. Efforts to obtain an extraction curve for **L13** were not pursued as this did not show markedly improved solubility over **L12**. Moreover, in a parallel project,[4] this type of ligand was demonstrated to have low hydrolytic stability when the complexes were contacted with strong acid to strip copper back out of the organic phase. The ligands hydrolysed and the constituent parts transferred into the aqueous phase in cases where the alkyl groups were *t*-butyl groups (**7**).

Of the acyl hydrazone ligands, **L6** was used to demonstrate proof-of-concept, thereafter **L7** was used for all other solvent extraction experiments due its higher solubility and convenience of synthesis over **L6** as undesired azine by-products (eg. **16** and **17**) were not encountered during the Schiff base condensation. Also, the ligand could be purified more easily by recrystallisation. *t*-Butylbenzoic hydrazide derivatives **L9** and **L10** did not form sufficiently soluble complexes in chloroform solutions to warrant further investigation.

The following section discusses the results from initial proof-of-concept solvent extraction experiments using **L6** which show that molar transport can be increased to 3Cu:2L. Thereafter **L7** was used to investigate the applicability of this type of

triacidic ligand as a metal extractant or as a blend with phenolic oximes in commercial processes through metal selectivity experiments.

2.6 Solvent Extraction by the Trinucleating Ligands L6 and L7

The pH dependence of solvent extraction was initially investigated for ligand **L6** to establish proof-of-concept and assess the ability of the new triacidic tetradentate ligands to bind 3 copper cations per 2 ligands to form $[Cu_3(\mathbf{L6}\text{-}3H)_2]$. This was established by stirring chloroform solutions of the ligand (5 ml, 0.01 M) with copper sulfate aqueous phases (5 ml, 0.015 M Cu) of varying pH. These were prepared from a stock solution of copper sulfate (3 ml, 0.025 M), deionised water and either sulfuric acid or potassium/sodium hydroxide in varying quantities to adjust the pH. The resulting organic and aqueous phases were stirred for 16 hrs to allow equilibration to be fully established, although extraction was evident after minutes from the yellow/green colour of the organic phase, see Scheme 2.12.

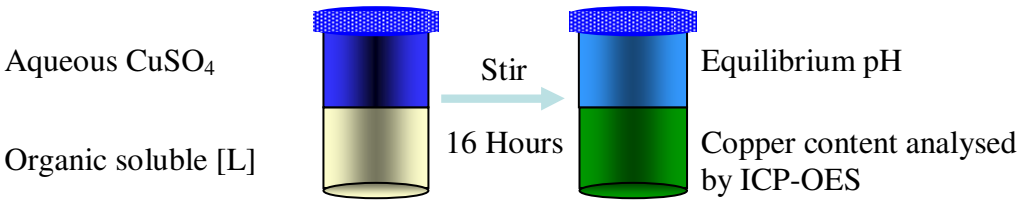

Scheme 2.12: Evaluation of copper loading by ligands **L6** and **L7** as a function of pH**.**

The phases were separated, the pH of the aqueous phase measured and a portion of the organic phase analysed for copper content by inductively coupled plasma optical emission spectroscopy (ICP-OES) by the procedure outlined in Chapter 5. The results obtained from ICP-OES analysis for the copper content of the organic phase are 5-10% greater than calculated for maximum loading. This is quite unexpected as the mass of ligand used in the extraction and that of the aliquot taken for analysis are measured and taken into account. This anomaly is not due to inaccurate oil-based copper standards as different batches gave consistent results but could be due to

entrainment of copper sulfate in the organic phase. It is possible that evaporation of the organic solvent occurs during overnight equilibration as the surfaces of the multi-stirrers do become noticeably warm. To minimise evaporation, the 50 ml glass jars used for the initial proof-of-concept extraction studies were replaced with smaller 14 ml screw-top vials, sealed with parafilm. This reduced the deviation from the expected values.

The data recorded are represented as the number of mol of copper per mol of ligand used. Formation of the trinuclear complex $[Cu_3(\mathbf{L6}\text{-}3H)_2]$ as a function of pH is plotted in Figure 2.28.

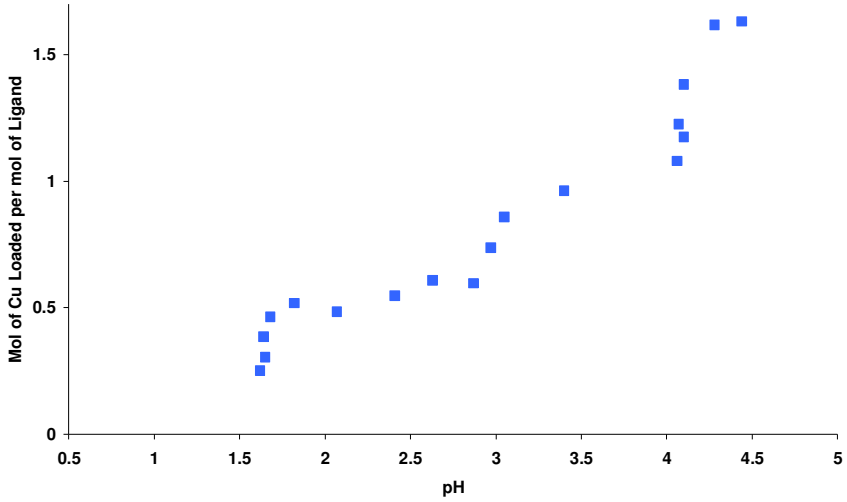

Figure 2.28: pH-dependent copper loading by a 0.010 M chloroform solution of **L6** from aqueous copper sulfate solutions (*ca.* 0.015 M).

Three inflection points and plateau regions are observed suggesting three stable species can be formed in the organic phase and their stability is dependent on the pH of the aqueous phase. The number of mol of copper loaded for each plateau (*ca.* 0.5, 1.0 and 1.5) is consistent with the formation of the *mono*-, *di*- and *tri*-nuclear complexes; $[Cu(\mathbf{L6}\text{-}H)_2]$, $[Cu_2(\mathbf{L6}\text{-}2H)_2]$ and $[Cu_3(\mathbf{L6}\text{-}3H)_2]$ within the pH ranges in which they are observed; pH 1.75-2.75, 3.25-4 and >4.25 respectively. It is also possible, of course, that species with higher molecular weight but similar stoichiometries are formed; a tetranuclear nickel complex was previously isolated[4] using the diacidic ligand **7**. Although higher molecular weight species are observed in mass spectra of copper complexes of the triacidic ligands, the peak intensity is

weak relative to that of the desired molecule. For example, isotopic distribution patterns are observed in the mass spectra of $[Cu_3(\mathbf{L6}\text{-}3H)_2]$ which are consistent with characteristic of multinuclear copper species $[Cu_3(\mathbf{L6}\text{-}2H)_3]H^+$, $[Cu_4(\mathbf{L6}\text{-}2H)_3]H^+$ and $[\{Cu_3(\mathbf{L6}\text{-}3H)_2\}_2]H^+$, nevertheless peak intensities are *ca.* $1/8^{th}$, 1/4 and $1/80^{th}$ respectively relative to the target molecular ion $[Cu_3(\mathbf{L6}\text{-}3H)_2]H^+$. Speciation is discussed further in Section 2.7.

2.6.1 Metal Selectivity by L7

The preliminary investigations described above indicate that the ligand **L6** is capable of tripling the *molar* transport of copper into the organic phase relative to the current commercial reagents and demonstrates the proof-of-concept that incorporating an additional acidic group which can bridge Cu(II) ions into a ligand superstructure can increase the copper : ligand stoichiometry in forming neutral, organic-soluble, complexes. To probe the industrial viability of the multiloading ligand architectures it is necessary to investigate the propensity of the ligands to extract other metal cations which are likely to be present within the pls. For this study late first row transition metals; iron(III), cobalt(II), nickel(II) and zinc(II) sulfate salts were used. The study was performed similarly to that for **L6** with ligand solutions (5 ml, 0.0025 M) and metal sulfate solutions (3 ml, 0.02 M). Lower ligand solution concentrations were used to limit the amount of ligand required per extraction experiment.

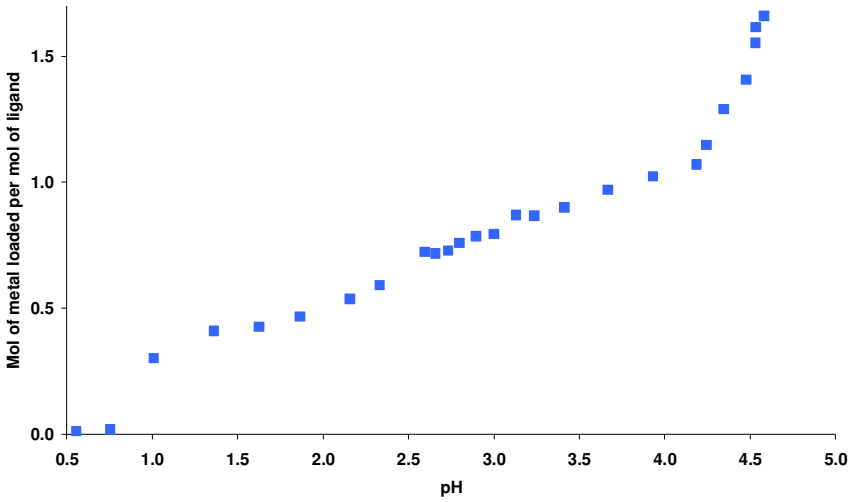

Figure 2.29: The pH-dependence of copper loading by 0.0025 M chloroform solutions of **L7** from aqueous sulfate solutions (*ca*. 0.012 M).

The solvent extraction curve obtained for **L7**, as seen in Figure 2.29, shows similar plateau regions corresponding to *mono*-, *di*- and *tri*-nuclear species in similar pH ranges to those for **L6**. However the profile of the "S-Curve" for conversion of [Cu(**L7**-H)$_2$] to [Cu$_2$(**L7**-2H)$_2$] is less well defined. "Complete" formation of [Cu(**L7**-H)$_2$] and [Cu$_2$(**L7**-2H)$_2$] is observed at slightly lower pH values than for **L6** <1.4 *cf*. 1.6 and 2.5 *cf*. 3.0 respectively. A dependence of pH$_{½}$ values on the concentration of the extractant has been observed in previous work[4] and the results presented here are consistent with the finding that pH$_{½}$ values decrease with decreasing ligand concentration.

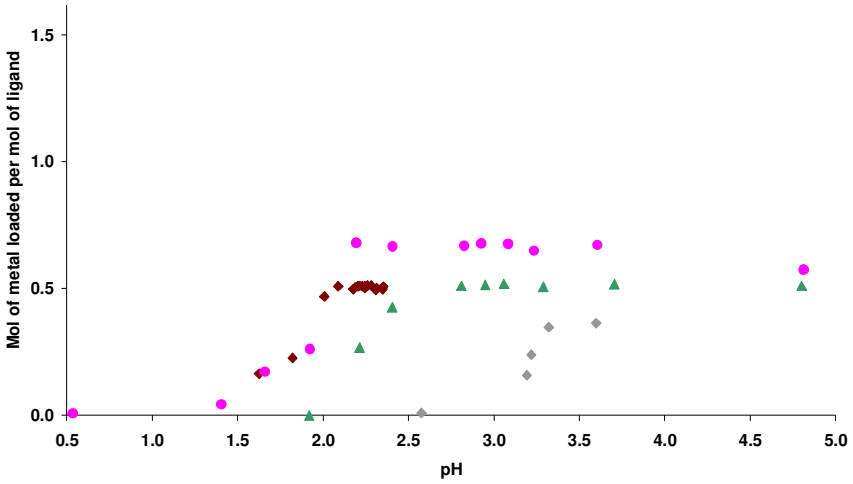

Figure 2.30: The pH-dependence of metal loading by 0.0025 M chloroform solutions of **L7** from single metal (Fe(III), ♦; Co(II), ●; Ni(II), ♦ and Zn(II), ▲) sulfate aqueous solutions (0.012 M).

Extraction results for **L7** from individual solutions of Fe(III), Co(II), Ni(II) and Zn(II) sulfate solutions are shown in Figure 2.30. The maximum loading of Fe, Ni and Zn is limited to 0.5 mol per mol of **L7** suggesting formation of [M(**L7**-H)$_2$] complexes. The result obtained for cobalt is slightly ambiguous as it suggests between one and two mol of ligand are required to extract each mol of Co.

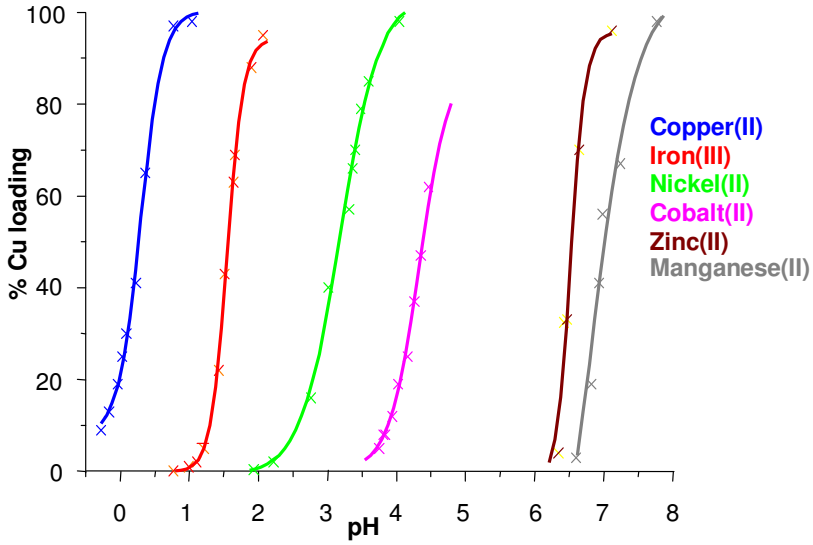

Figure 2.31: S-curves for various first row transition metals using commercial phenolic oxime reagent **P50** in kerosene.

Comparison of the pH-profiles show **L7** has greatest affinity for copper as this is extracted at the lowest pH, followed by iron and cobalt, zinc then nickel. The findings are consistent with relative stabilities of complexes formed by metal(II) cations predicted by the Irving-Williams series.[42, 45] However, the strength of metal binding found for **L7** is not consistent with those of the commercial reagent **P50** (Figure 2.31) in kerosene, particularly in the instances of Co and Zn ($pH_{½}$ *ca*. 2.0 c*f*. 4.5 and *ca*. 3.25 *cf*. 6.5 respectively). Even after taking into consideration the general finding that metals are loaded one pH unit lower in kerosene than in chloroform (*cf*. $pH_{½}$ values in Figure 2.31 and Figure 2.33 respectively), **L7** forms more stable complexes with Co and even more so with Zn than **P50**. The stability of the Co complexes may be attributed to the presence of the salicylic acid group which has a harder Lewis basic character than the oxime unit of **P50** due to the potential O_2^- (or even an O_2^{2-}) binding unit over the NO^- cavity[42] and consequently can form more stable complexes with the "harder" Lewis acid Co,[46] especially if the Co(II) has oxidised to "hard" Co(III)[47] as previously reported[48] with phenolic oximes. It is difficult to attribute the cause of the unexpectedly low $pH_{½}$ of the Zn(II) complex as it is a softer Lewis acid than Ni(II) and is generally expected to form complexes of similar stability to Ni(II) according to the Irving-Williams series[42] but may be due to the preference of Ni(II) to form strictly square planar or octahedral complexes, whereas Zn(II) can adopt distorted geometries more readily.[49]

It can be concluded from Figure 2.30 that **L7** should be selective for copper until the mononuclear complex [Cu(**L7**-H)$_2$] has formed. Extraction studies were performed from mixed metal feed solutions to establish whether or not the ligand would still be selective for copper when other metal cations are present and whether it would extract more than one type of metal to form heterogeneous metal complexes. The pH-profile for iron extraction (Figure 2.30) could not be extended beyond pH 2.5 as iron (oxy)hydroxides precipitate to form a third phase. This was also evident in preliminary extraction studies from mixed metal feed solutions containing Fe(III) sulfate which prevented the pH of the system being raised sufficiently to extract more than one copper cation. Consequently Fe(III) sulfate was omitted in the competitive binding studies. In the absence of Fe(III) sulfate it was possible to raise

the pH sufficiently to allow full loading of copper to form $[Cu_3(\mathbf{L7}\text{-}3H)_2]$ as can be seen in Figure 2.32. It can be concluded that **L7** shows striking selectivity for Cu(II) over Co(II), Ni(II) and Zn(II) cations.

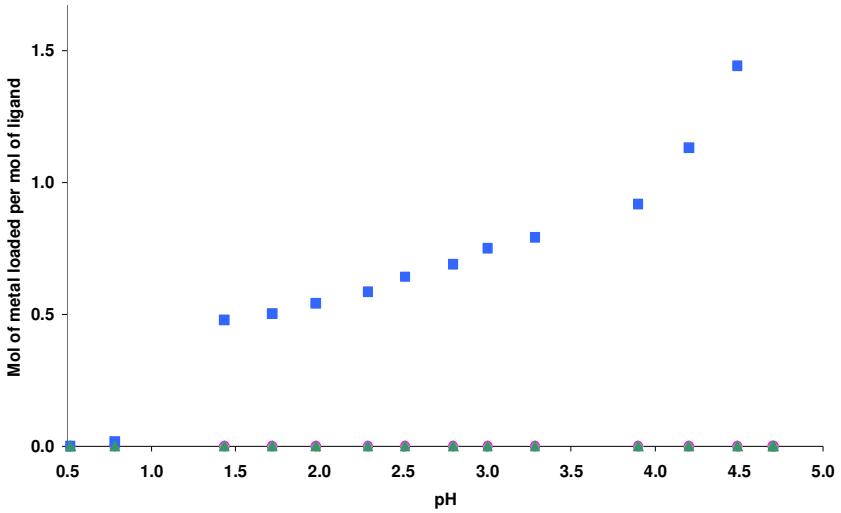

Figure 2.32: The pH-dependence of metal loading by 0.0025 M chloroform solutions of **L7** from a mixed metal feed solution containing (Cu(II), ■; Co(II), ●; Ni(II), ♦ and Zn(II), ▲) sulfate (0.012 M of each).

2.6.2 Extractant Strength

Metal selectivity studies indicate acyl hydrazone type ligands are selective for copper over Co(II), Ni(II) and Zn(II) in all pH ranges studied and for Fe(III) at low pH, a requirement for commercial use. To investigate further the practical industrial applicability of these ligands their "strength" relative to the commercial standard (**P50**) in chloroform solution was determined. Reagent strengths are conventionally compared using $pH_{½}$ values, the pH at which 50% loading is achieved. The lower the $pH_{½}$ value, the stronger the reagent. Figure 2.33 shows that the $pH_{½}$ of **P50** in chloroform is *ca.* 1.6, almost identical to the $pH_{½}$ for the analogous mononuclear complex $[Cu(L\text{-}H)_2]$ formed by **L6**.

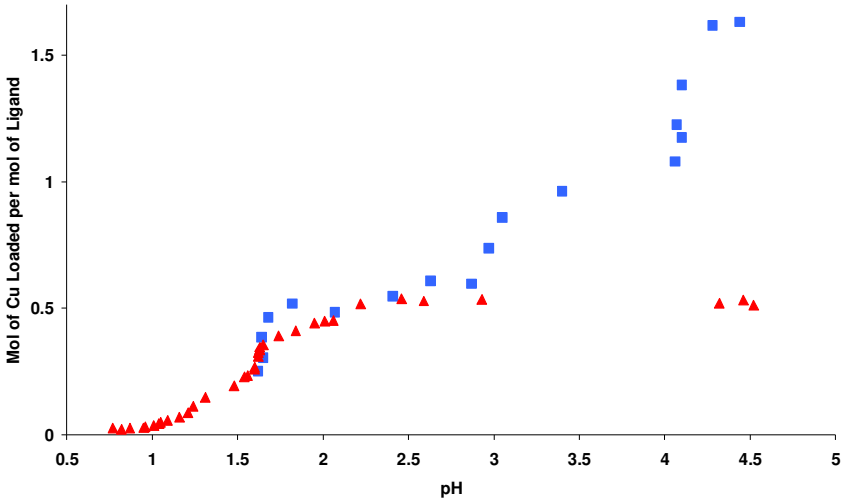

Figure 2.33: Comparison of the pH-dependence of copper loading by chloroform solutions of ligand **L6** (♦) (0.010 M) and **P50** (■) (0.010 M) from copper sulfate solutions (0.015 M), indicating that both have very similar $pH_{½}$ values for formation of $[Cu(L\text{-}H)_2]$.

The strength of **L7** was compared to that of the isomerically pure **P50** analogue *t*-octylsalicylaldoxime **19** to ensure impurities present within the commercial reagent did not influence the $pH_{½}$ value. The S-curves shown in Figure 2.34 were obtained using more dilute (0.0025 M) ligand solutions. **L7** is seen to be significantly stronger than **19** when forming the mononuclear complex $[Cu(L\text{-}H)_2]$.

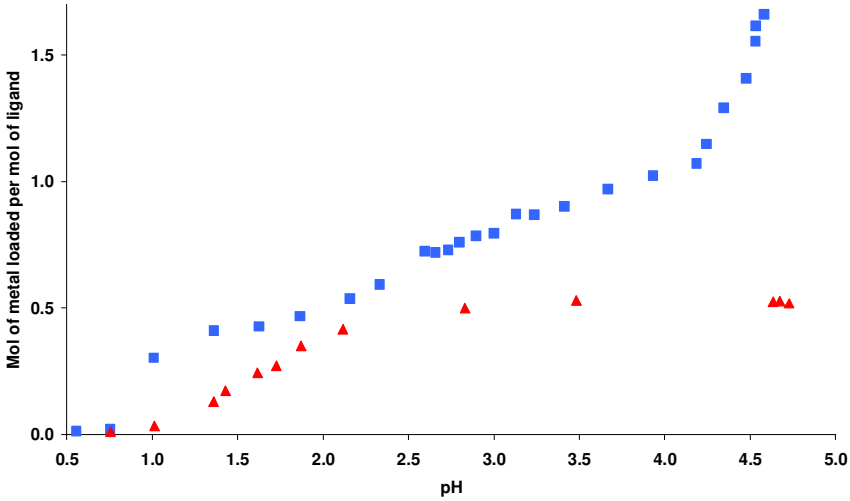

Figure 2.34: Comparison of the pH-dependence of copper loading by chloroform solutions of ligand **L7** (■) (0.0025 M) and *t*-octyl phenolic oxime **19** (▲) (0.0025 M) indicating **L7** is stronger than **P50**.

2.7 Speciation of Cu Complexes Formed by L4-L13

In order to define the mode of action of the trinucleating extractants and develop variants with improved strength and selectivity of copper-recovery it is necessary to understand the speciation of complexes in solution. This is not a trivial task. Sections 2.7.1 to 2.7.3 describe the use of UV/Visible spectroscopy, mass spectrometry and EPR to identify solution speciation. Section 2.8 describes the solid state structure of copper(II) complexes formed by **L4**-**L13**. Copper analysis by ICP-OES provides evidence for ligand to copper ratios which would be expected for *mono*-, *di*- and *tri*-nuclear copper complexes; $[Cu(L\text{-}H)_2]$, $[Cu_2(L\text{-}2H)_2]$ and $[Cu_3(L\text{-}3H)_2]$ supporting *empirical* formulae for these. Evidence for the molecular formulae was provided by electrospray ionisation mass spectrometry isotopic distribution patterns. Solution based characterisation data are provided in Appendix 7.2.1. X-ray data are provided in Appendix 7.2.3.

2.7.1 UV/Vis Spectroscopy of L7 Cu Complexes; $[Cu(L7\text{-}H)_2]$, $[Cu_2(L7\text{-}2H)_2]$ and $[Cu_3(L7\text{-}3H)_2]$

The extent of copper loading into the organic phase is visually apparent during the solvent extraction experiment. Figure 2.35 below shows the colour change of the organic phase in an extraction experiment for **L7** from almost colourless to; yellow, green and dark green as the equilibrium pH increases. These colour changes can be ascribed to the formation of the *mono*-, *di*- and *tri*-nuclear complexes $[Cu(\mathbf{L7}\text{-}H)_2]$, $[Cu_2(\mathbf{L7}\text{-}2H)_2]$ and $[Cu_3(\mathbf{L7}\text{-}3H)_2]$, based on the copper content in the organic extracts as determined by ICP-OES and evidence for the molecular formulae provided by mass spectrometry (see Section 2.7.2).

pH	0.52	0.78	1.44	2.29	2.51	2.80	3.00	4.49	4.70
% Cu	0.00	1.19	31.91	38.99	42.83	46.01	50.05	96.15	126.03*

Figure 2.35: Colours of the organic phases from pH-dependent copper(II) extraction by **L7** (see Section 2.6 for experimental details). (*copper content of the organic phase exceeds the loading capacity of the ligand as a result of precipitation and entrainment of copper).

The electronic spectra of the ligand, **L7**, and its presumed *mono*-, *di*- and *tri*-nuclear copper complexes were recorded using samples taken directly from solvent extraction experiments which generated the data in Figure 2.29. The spectra show evidence for four distinctly different species as seen in Figure 2.36.

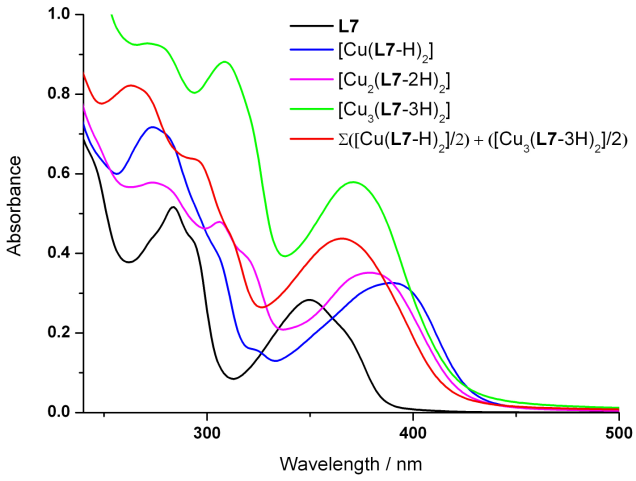

Figure 2.36: The UV/Vis spectrum of a (625 μM) chloroform solution of **L7** (black line) and the spectra of solutions containing *ca.* 33, 67 and 100%-loading of copper by **L7** (blue, magenta and green lines) corresponding to chloroform solutions (*ca.* 312.5 μM) presumed to contain the predominant species [Cu(**L7**-H)$_2$], [Cu$_2$(**L7**-2H)$_2$] and [Cu$_3$(**L7**-3H)$_2$] respectively. Measured using a 0.5 mm path-length cell between 500 and 245 nm (*ca.* cut-off for chloroform).[50]

The stock ligand solution (0.0025 M) and complex solutions (0.00125 M, assuming 2 mol of ligand are required to form each complex) had to be diluted by a factor of 4 to give 625 μM and 312.5 μM solutions respectively to obtain absorbance of < 1. The calculated molar extinction coefficients for the peaks of maximum absorbance for each species are given in Table 2.4.

Table 2.4: Wavelength of absorbance maxima and the corresponding molar extinction coefficients[#] for chloroform solutions of **L7**, [Cu(**L7**-H)$_2$], [Cu$_2$(**L7**-2H)$_2$] and [Cu$_3$(**L7**-3H)$_2$].

	Ligand **L7**		[Cu(**L7**-H)$_2$]		[Cu$_2$(**L7**-2H)$_2$]			[Cu$_3$(**L7**-3H)$_2$]		
Max Absorbance (nm)	284	350	274	390	274	306	379	271	309	371
ε x 10^3 ($mol^{-1}cm^{-1}$)	16.5	9.1	45.7	20.8	37.0	30.7	22.5	59.4	65.4	37.1

[#]Extinction coefficients (ε) were calculated using the equation A = ε[J]l , derived from the Beer-Lambert law.[51] Concentrations ([J]) of chloroform solutions of the extractant **L7** (625 μM) and copper complexes (312.5 μM) were defined by the masses of ligand taken to prepare the extractant solutions. Spectra were measured in a quartz cell of μM path-length (l) 0.5 mm. Values of absorbance of peaks were selected and recorded by the instrument software package UV WinLab 2.70.01.

The extinction coefficients of the major peaks in the spectra increase as the number of copper centres in the species increase.

Spectra of the copper extracts corresponding to 33, 67 and 100% loading all have prominent bands in the range 271-274 nm and 371-390 nm. Significantly, as the copper-loading increases beyond 33% the band at 390 nm shifts to 379 nm and a new band appears at 306 nm. This is consistent with the species originally formed, presumably [Cu(**L7**-H)$_2$], being converted to another complex, presumably [Cu$_2$(**L7**-2H)$_2$] at 67% Cu loading. At 67% Cu loading the spectrum (magenta line) does not correspond to one which would be expected (red line) by combining the spectra of the 33% and 100% loaded solutions. Consequently it can be concluded that at 67% loading the solution does not contain a 1:1 mixture of [Cu(**L7**-H)$_2$] and [Cu$_3$(**L7**-3H)$_2$]. This is supported by mass spectra analysis of the extracts at *ca*. 67% loading which shows the presence of [Cu$_2$(**L7**-2H)$_2$] (see Section 2.7.2).

At *ca*. 100% loading there is no plausible alternative to the formation of complexes other than $[Cu_3(\mathbf{L7}\text{-}3H)_2]$ or oligomers $[Cu_3(\mathbf{L7}\text{-}3H)_2]_n$, and mass spectral evidence was obtained for the presence of the former (see Section 2.7.2).

2.7.2 Mass Spectrometry

Mass spectrometry proved extremely useful for the identification of multinuclear copper complexes based on their isotopic distribution patterns. Samples were taken from solvent extraction experiments in which the equilibrium pH values were adjusted to those at which the *mono*-, *di*- and *tri*-nuclear complexes are assumed to be predominant (i.e. *ca*. 1.75, 3.5 and 5.0 respectively). The organic phases were dried and spectra measured by electrospray mass spectrometry of methanolic solutions. The spectra obtained for copper complexes of ligands **L5** (Figure 2.37) and **L7** (Figure 2.38) are in excellent agreement with the simulated spectra for the singly protonated molecular ion in positive mode.

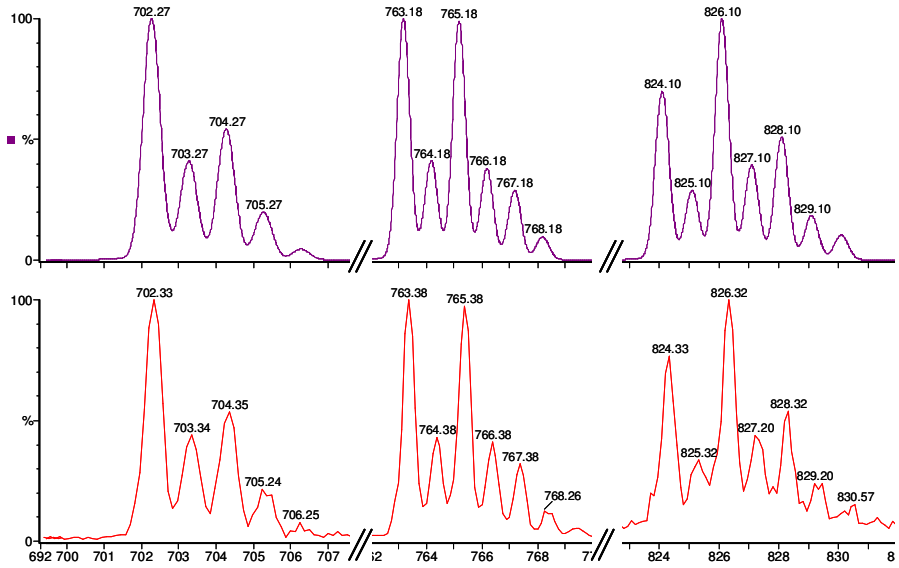

Figure 2.37: Collage of simulated (top) and experimental (bottom) electrospray mass spectra for MH^+ ions of the *mono*-, *di*- and *tri*-nuclear copper complexes of **L5**: $[Cu(\mathbf{L5}\text{-}H)_2]H^+$, $[Cu_2(\mathbf{L5}\text{-}2H)_2]H^+$ and $[Cu_3(\mathbf{L5}\text{-}3H)_2]H^+$ from left to right respectively.

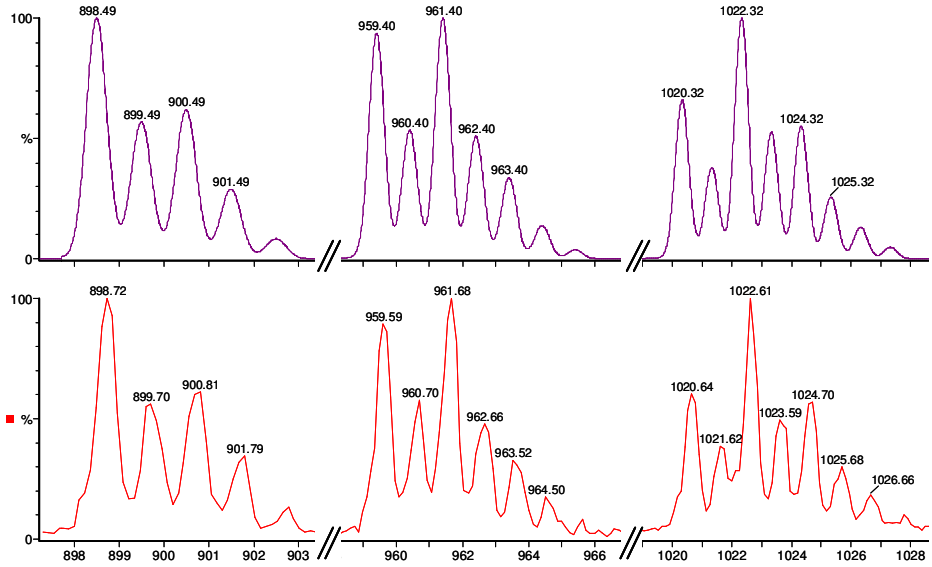

Figure 2.38: Collage of simulated (top) and experimental (bottom) electrospray mass spectra for MH^+ ions of the *mono*-, *di*- and *tri*-nuclear copper complexes of **L7:** $[Cu(\mathbf{L7}\text{-}H)_2]H^+$, $[Cu_2(\mathbf{L7}\text{-}2H)_2]H^+$ and $[Cu_3(\mathbf{L7}\text{-}3H)_2]H^+$ from left to right respectively.

2.7.3 Electron Paramagnetic Resonance

Copper(II) has an electronic configuration of d^9 and consequently is paramagnetic with one unpaired electron. This means that ^1H and ^{13}C NMR cannot be used easily to probe the environments of the atoms through excitation of their nuclear spins because the presence of paramagnetic nuclei broaden the spectra. This is observed when portions of the copper complexes of **L6** and **L7** are taken from extraction studies, dried and re-dissolved in deuterated chloroform. Presence of paramagnetic copper in the samples is supported by reappearance of the ligand ^1H spectra when copper is stripped from the organic phase when contacted with a concentrated sulfuric acid aqueous phase. Nevertheless, in principle, the spin of the unpaired electron can be observed *via* Electron Paramagnetic Resonance (EPR) and speciation information inferred from the *g*-factor and hyperfine coupling constant, A. Unpaired electrons in coordination complexes are usually delocalised and as a result are influenced by the electronic properties of the different atoms on which they reside to varying degrees. This results in deviation of the *g*-factor from that of a free electron (g_e). The magnitude of this deviation can be used to infer the symmetry of the

environment which the electron is in.[42] Hyperfine coupling, A, can arise when the unpaired electron interacts with the magnetic dipole of an atomic nucleus of non-zero nuclear spin.[51] The magnitude of A is related to the wavefunction of the molecular orbital containing the free electron, thus allowing the level of delocalisation from the metal centre onto these atoms to be determined. Simulation of the splitting pattern observed can provide information about the number of atoms the electron is influenced by and nature of their spin.

EPR has been used to determine the solution-based speciation of copper complexes formed by commercial solvent extractants[6] and the resulting ternary 5-coordinate copper adducts formed by nitrogen containing bases.[52, 53] As previously mentioned in Section 2.3.1, EPR has also been used in the Tasker group to follow quantitatively the extraction of copper into the organic phase by dinucleating ligands. As the equilibrium pH was raised, maximum signal intensity was reached indicating a predominance of the mononuclear species, thereafter the intensity decreased due to antiferromagnetic spin coupling as the dinuclear complex is formed.

It was anticipated that EPR would be useful for studying the speciation of the copper complexes formed by the trinucleating ligands **L4**-**L13** through the relationship between signal intensity and relative concentration of paramagnetic species in solution.[54] It might be possible to extend the observations for the dinucleating ligands, with the EPR signal intensity growing to a maximum when the mononuclear $[Cu(L\text{-}H)_2]$ complex predominates, decreasing to zero as the dinuclear $[Cu_2(L\text{-}2H)_2]$ complex becomes the major species and then increasing once more to a maximum when a third unpaired paramagnetic copper(II) is complexed to form $[Cu_3(L\text{-}3H)_2]$.

EPR spectra of fluid and frozen chloroform/toluene mixtures of $[Cu(\mathbf{L7}\text{-}H)_2]$, $[Cu_2(\mathbf{L7}\text{-}2H)_2]$ and $[Cu_3(\mathbf{L7}\text{-}3H)_2]$ were recorded at X-band frequency (9 GHz) between 5 and 300 K at the EPSRC National EPR service, Manchester by Daniel J. Stone and Professor Eric J. L. McInnes. X-band spectra displayed broad and unresolved peaks with g = 2.111, 2.106, 2.103, respectively (see Appendix 7.2.6). Higher frequency spectra were also broad and poorly resolved. Consequently, structural information could not be extrapolated from the data. These findings

suggest that there is coupling between copper centres, even though the extraction curves indicate that the *mono*-, *di*- and *tri*-nuclear species are stable within a well defined pH range. Although mass spectrometry data suggest these are the major species present in each case, the poor EPR spectra may be a result of paramagnetic impurities. Alternatively, they could be due to electronic dipole-dipole and exchange interactions or may be caused by slow tumbling of anisotropic molecules relative to the experimental time-scale.[54]

2.8 Solid State Structures of Cu Complexes of L4-L13

Although it was recognised that it is difficult to draw direct comparison between solution and solid phase structures due to solvent effects and crystal packing, attempts were made to isolate single crystals of each of the copper complexes for X-ray structure determination. The X-ray structures obtained (see below and Appendix 7.2.3) indicate that *intra*- and *inter*-molecular interactions as well as those with solvent and anion molecules greatly influence the solid state structures of these complexes. The following sections examine some of the crystal structures obtained and draws analogies between these and solution based experimental results.

When considering the predominant solution speciation for a mononuclear copper complex of ligands **L4**-**L13** it is necessary to consider the factors which influence the site in which the first metal cation will be complexed. The most influential parameter is the relative thermodynamic stability of the resulting copper(II) complex, which in turn is influenced by the coordination number of the metal centre. The most common coordination numbers found for copper complexes are 4, 5 or 6.[49] These are likely to exhibit square planar, square pyramidal and octahedral geometries respectively. The complexes formed are commonly tetragonally distorted as a result of the Jahn-Teller effect experienced by d^9 ions due to removal of degeneracy of the d_{z^2} and $d_{x^2-y^2}$ orbitals. Octahedral complexes are very susceptible as these have ligands coordinated in the d_{z^2} orbital dimension.[55]

The solvent extraction processes for which these ligands are designed to be used in are sulfuric acid based pH-swing processes. Adjustment of the aqueous phase pH controls the protonation level of the ligand and consequently the amount of copper extracted. Consequently, it is of interest to consider which proton is most readily ionised and how this will affect the mode by which the first copper will bind. The equilibria which occur in pH-swing solvent extraction systems are complicated by the dual phase nature of the processes. As a result one cannot simply record the acid dissociation constants (pK_a) in an aqueous solution and expect these to be transferable to the dual phase system as the acidity of protogenic species in non-aqueous solvents differ greatly from those in water.[43] This is demonstrated by the pK_a values calculated for deprotonation of the ionisable sites in the trinucleating ligand **L5** using the SPARC (SPARC Performs Automated Reasoning in Chemistry) program developed by the US environmental protection agency available online (Table 2.5). The predicted pK_a results for **L5** indicate that the carboxylic acid proton is most acidic in water, as one would expect, but the amino proton of the hydrazone is most acidic in chloroform.

Table 2.5: Acid dissociation constants (pK_a) calculated for **L5** by SPARC.

	Solvent dependent pK_a	
Ionisable proton	Water	Chloroform
COO***H***	2.92	17.44
PhO***H***	9.80	25.04
C=N-N***H***=COR	10.88	16.20

The following discussion considers the various species which may be present in solution for the *mono*-, *di*- and *tri*-nuclear complexes formed by the triacidic ligands **L4**-**L13**. Only four coordinate, square planar copper centres will be considered as both the commercial phenolic oxime reagents[5] and salicylaldehyde hydrazones discussed in the Section 2.3 form complexes which feature square planar Cu(II).

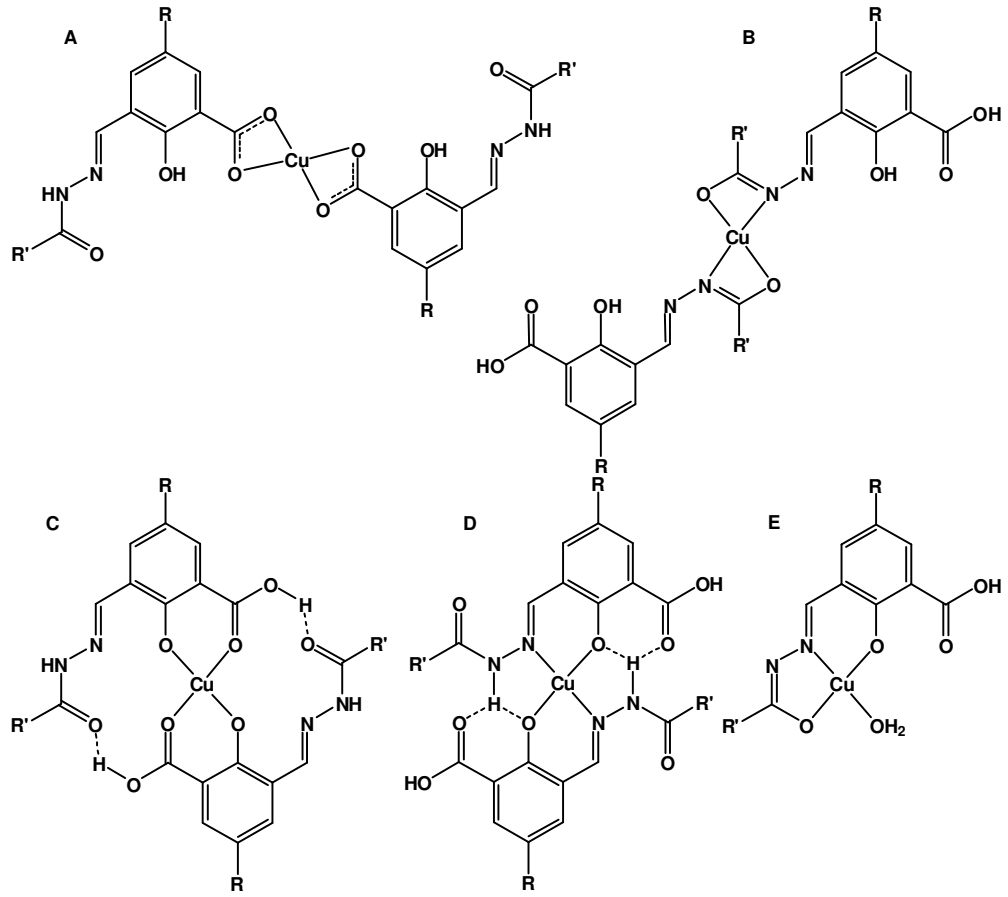

Figure 2.39: Possible structures of mononuclear copper complexes formed by the trinucleating ligands **L4**-**L13**.

Figure 2.39 shows plausible structures which could be adopted by the mononuclear copper complexes of **L4**-**L13**. If one considers the most easily ionised group to be the carboxylic acid, as predicted from the calculated aqueous phase pK_a values, a possible structure for the resulting complex could be **A**. Although complexes of this type exist, they are unlikely to be the most stable complex formed in this case because the resulting coordination geometry of the carboxylate oxygen atoms deviates from ideal. Also, the preferred structures for carboxylato copper(II) complexes is as the classic tetracarboxylate-bridged copper(II) dinuclear complex $[Cu_2(RCO_2)_4(H_2O)_2]$.[56] Similarly, if deprotonation of the amide occurs first, as predicted by the pK_a values calculated in chloroform, this could lead to structure **B**. However, once again the bond angles around the donors deviate from ideal. For deprotonation of the phenol two very plausible structures with geometry well suited to coordination of a square planar metal ion could be created as in **C** and **D**. Of these,

D is likely to be the more stable as a result of the mixed donor types and the intramolecular bifurcated hydrogen bonds. Another possibility is the formation of a ternary complex, if the ligand is doubly deprotonated as shown by **E** where the fourth coordination site is occupied by a neutral donor. Water or other neutral species present in industrial processes could form such structures. Work published which features dianionic species similar to those discussed in Section 2.3 where the carboxylic acid group of **L4**-**L13** is substituted with a bulkier *t*-butyl group suggests that the bulk sterically hinders dimerisation to produce the monomeric species (**E**).[30]

The three most plausible structures for dinuclear complexes formed by **L4**-**13** are shown in Figure 2.40. Because the complex has a 2Cu:2L stoichiometry, it is probable that one or more atoms will bridge the copper centres. **L4**-**L13** contain two chemically different oxygen atoms which can form a bridge.

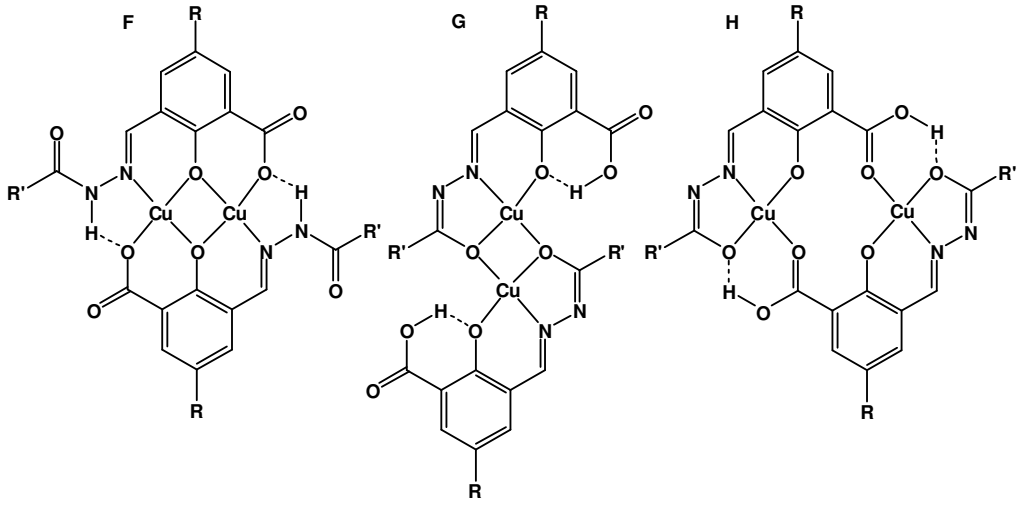

Figure 2.40: Possible bridging modes of the dinuclear copper complexes formed by Ligands **L4**-**L13**.

The phenolate could deprotonate and act as the bridge as in **F** or the amidate as in **G** if the acyl hydrazone amide is deprotonated. Although many examples of phenolate bridged (**F**) dinuclear copper complexes have been reported, few are planar with square planar copper centres. The X-ray structure of a complex similar to **F** has been published by the Andruh *et al*[57] is shown in Figure 2.41.

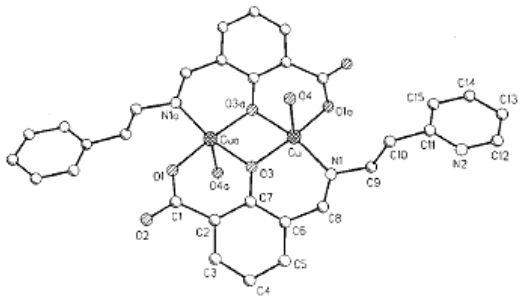

Figure 2.41: Dinuclear copper complex analogous to **F** (Figure 2.40) prepared from 3-[N-2-(pyridylethyl)forminidoyl]salicylic acid.[57] This ligand is also implicit in formation of a structure analogous to **H** (Figure 2.40).[58]

No X-ray structures have been reported for dinuclear amidate-bridged complexes (**G**)[21] but the structure has been inferred where bulky substituents replace the carboxylic acid group in dianionic ligands, for example *t*-butyl groups.[29, 30] An unusual alternative di-copper species (**H**), having much longer bridging distance between the copper centres is also possible. The only complex thought to have this conformation has also been reported by Andruh *et al*[58] using the same ligand as seen in Figure 2.41. It is used as a precursor to hexanuclear trivalent lanthanide clusters $[Ln_2Cu_4]$ where the lanthanide occupies the empty O_4^{2-} cavity, no structural evidence has been obtained by X-ray diffraction as supporting evidence.

Assuming copper(II) remains square planar upon complexation and the trinucleating ligand is deprotonated to form an NO_3^{3-} moiety, the planar, linear trinuclear copper complex shown in Figure 2.42 is the only plausible structure.

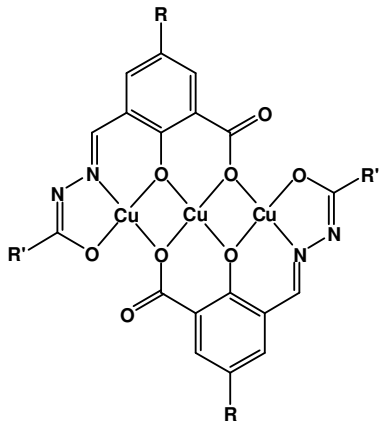

Figure 2.42: Probable solution phase trinuclear copper complex conformation for ligands **L4**-**L13.**

Attempts to isolate trinuclear complexes of **L4**-**L13** of the type shown in Figure 2.42 in a crystalline form suitable for X-ray structural determination failed. The results of X-ray diffraction determinations of *mono*-, *di*-, *hexa*- and *deca*-nuclear copper complexes formed by the triacidic ligands are discussed in the following sections. In general these structures indicate that the preferred binding sites for copper(II) are cavities provided by the imino and phenol groups. This suggests that the most stable mononuclear copper complex will contain an N-donor forming the structures **D** or **E** in Figure 2.39. The carboxylic acid is found to remain protonated in complexes formed by mono- and di-anionic forms of the ligands.

2.8.1 Mononuclear Cu Complex [Cu(L5-H)$_2$]

The mononuclear complex [Cu(**L5**-H)$_2$] was prepared by diffusion of nitromethane into a methanol solution of a powder sample of the mononuclear species obtained by evaporation of a chloroform extract with the aqueous phase adjusted to pH 2. The structure has two crystallographically independent molecules which create a four molecule unit cell in a triclinic crystal system with $P\bar{1}$ space group. The two halves of each crystallographically independent complex molecule have ligands "**A**" and "**B**" and "**C**" and "**D**" labelled in Figure 2.43. Of the crystallographically independent molecules, that containing Cu1 has the more regular structure with virtually planar ligands, see Table 2.6 for a comparison of the bond lengths and Table 2.7 for the bond angles. The maximum deviation from the least squares plane through the $CuNO_2$ complex unit of ligand **A** is 0.0568 Å and -0.0936 for O1A and Cu1 respectively with mean deviation of ±0.0565 Å. Similarly, maximum deviations of 0.0567 and -0.0281 Å are found for Cu1 and O1B respectively with a mean deviation of ±0.0277 Å in the **B** ligand. These planes are at almost right angles (91.7°) to each other. Whilst the **C** ligand of the second complex, containing Cu2 is even more closely planar with maximum displacements of 0.0175 and -0.0094 Å for Cu2 and O1C and mean of ±0.0094 Å, that of ligand **D** is least planar with maximum deviations for Cu2 and O65D of 0.1429 and 0.1008 Å respectively and mean of ±0.0995 Å. These planes are inclined at an angle of 86.4° to each other.

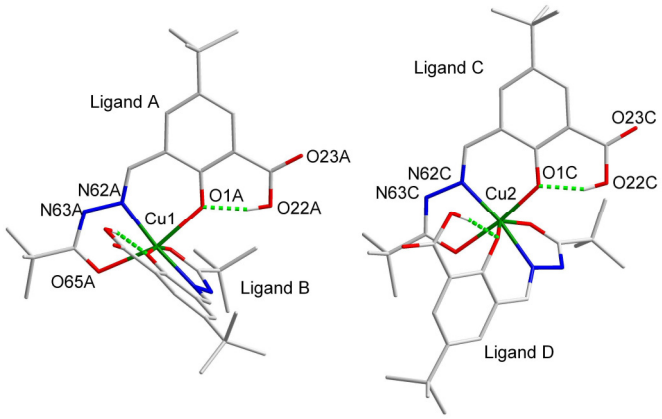

Figure 2.43: The two crystallographically independent molecules of [Cu(**L5**-H)$_2$] showing atoms labels used for the chemically related **A**- and **B**-halves and **C**- and **D**-halves of the complexes.

Table 2.6: Comparison of bond lengths and contact distances in the coordination spheres of the two crystallographically independent [Cu(**L5**-H)$_2$] complexes.

Lengths in Cu1 complex / Å		Lengths in Cu2 complex / Å	
Cu1-N62A	2.012(3)	Cu2-N62C	1.950(2)
Cu1-N62B	1.949(3)	Cu2-N62D	2.026(3)
Cu1-O1A	2.186(2)	Cu2-O1C	1.925(2)
Cu1-O1B	1.952(2)	Cu2-O1D	2.336(2)
Cu1-O65A	2.271(3)	Cu2-O65C	1.966(2)
Cu1-O65B	2.048(2)	Cu2-O65D	2.326(2)
O1A•••O22A	2.413(8)	O1C•••O22C	2.434(2)
O1B•••O22B	2.461(2)	O1D•••O22D	2.399(9)

Table 2.7: Comparison of the bond angles around the two crystallographically independent Cu1 and Cu2 centres of complex [Cu(**L5**-H)$_2$].

Angles /° about Cu1		Angles /° about Cu2	
O1A-Cu1-N62A	85.98(10)	O1C-Cu2-N62C	91.26(9)
O1A-Cu1-O65A	160.64(9)	O1C-Cu2-O65C	172.07(9)
O1A-Cu1-O1B	98.29(10)	O1C-Cu2-O1D	88.49(9)
O1A-Cu1-N62B	87.61(10)	O1C-Cu2-N62D	97.01(9)
O1A-Cu1-O65B	85.67(9)	O1C-Cu2-O65D	84.42(10)
O1B-Cu1-N62B	90.43(10)	O1D-Cu2-N62D	77.90(9)
O1B-Cu1-O65B	169.64(9)	O1D-Cu2-O65D	149.13(9)
O1B-Cu1-N62A	87.98(10)	O1D-Cu2-N62C	99.72(9)
O1B-Cu1-O65A	88.27(10)	O1D-Cu2-O65C	91.31(9)
N62B-Cu1-O65B	80.13(9)	N62D-Cu2-O65D	73.23(9)
N62B-Cu1-N62A	173.10(11)	N62D-Cu2-N62C	171.30(10)
N62B-Cu1-O65A	110.65(10)	N62D-Cu2-O65C	90.69(10)
O65B-Cu1-N62A	101.90(10)	O65D-Cu2-N62C	110.42(10)
O65B-Cu1-O65A	91.05(9)	O65D-Cu2-O65C	99.66(9)
N62A-Cu1-O65A	76.02(10)	N62C-Cu2-O65C	80.96(9)

Whilst the ligand structures are very similar in the complex containing Cu1, those in that containing Cu2 are not. Ligand **D** is significantly non-planar, so much so that no plane can be fitted through the ligand molecule. Comparison of ligands **B** and **D** from complexes containing Cu1 and Cu2, respectively, is seen in Figure 2.43. The bond lengths around the copper centres to imido nitrogen N62 and oxygen atoms O1 and O65 of the phenol and amidate respectively, are longer than the mean values reported[5] for C-N, 1.947(12), and C-O, 1.839(19) Å, in four-coordinate phenolic oxime complexes. This observation should be expected as a result of the higher coordination number and increased electron density on the copper(II) centre in the octahedral environment.

2.8.2 Mononuclear Cu Complex [Cu(L4-2H)(H$_2$O)]

The X-ray structure obtained for [Cu(**L4**-2H)(H$_2$O)] crystallised by slow evaporation of the filtrate of a reaction of **L4** with copper acetate in ethanol is shown in Figure 2.44. As with the structure just described in Section 2.8.1 there are two crystallographically independent molecules per asymmetric unit, but, in contrast the bond lengths and angles around the copper centres are almost identical, *i.e.* any differences are within three standard deviations of each other as shown in the comparison of bond lengths in Table 2.8 and angles in Table 2.9. The crystal system is monoclinic with 16 molecules per unit cell and has space group *C*2/*c*. With the exception of the methyl groups in the *t*-butyl substituents, the molecule is almost completely planar, with maximum deviations from the least squares planes of the molecule being 0.0829 and -0.0813 Å for O1T and O23B respectively and mean deviation of ±0.0308 Å.

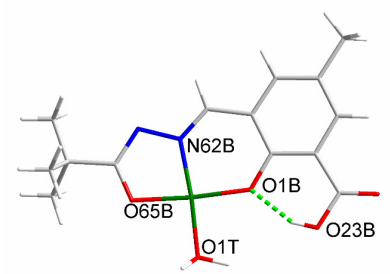

Figure 2.44: One of the two crystallographically independent mononuclear copper complexes, [Cu(**L4**-2H)(H$_2$O)], of doubly deprotonated **L4**.

Table 2.8: Comparison of bond lengths and contact distances in the coordination spheres of the two crystallographically independent [Cu(**L4**-2H)(H$_2$O)] complexes.

Lengths / Å in Cu1 complex		Lengths / Å in Cu2 complex	
Cu1-N62A	1.916(4)	Cu2-N62B	1.910(4)
Cu1-O65A	1.922(3)	Cu2-O65B	1.909(3)
Cu1-O1A	1.910(3)	Cu2-O1B	1.911(3)
Cu1-O1S	1.929(3)	Cu2-O1T	1.927(3)
O23A•••O1A	2.494(7)	O23B•••O1B	2.492(7)

Table 2.9: Comparison of the bond angles around the two crystallographically independent Cu1 and Cu2 centres of [Cu(**L4**-2H)(H_2O)].

Angles /° around Cu1		Angles /° around Cu2	
N62A-Cu1-O1A	94.02(14)	N62B-Cu2-O1B	94.07(15)
N62A-Cu1-O65A	81.50(15)	N62B-Cu2-O65B	81.50(14)
065A-Cu1-O1S	93.20(14)	065B-Cu2-O1T	93.28(14)
O1S-Cu1-O1A	91.28(14)	O1T-Cu2-O1B	91.32(14)
O1A•••N62A•••O65A	92.3(6)	O1B•••N62B•••O65B	92.20(15)

The monomeric copper unit [Cu(**L4**-2H)(H_2O)] assumes a geometry similar to a copper(II) complex of salicylaldehyde acetylhydrazone described in the literature[22] except this is protonated at the amide and charge balance is achieved by apical coordination of a chloride anion as shown in Figure 2.45.

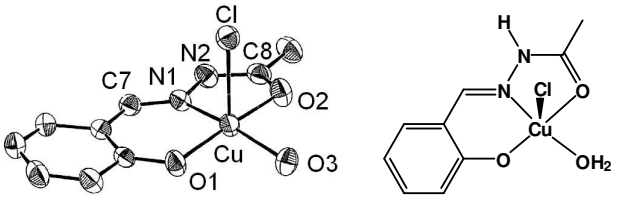

Figure 2.45: The crystal structure[22] and a graphical representation of the copper complex of the singly deprotonated (phenol) salicylaldehyde acetylhydrazone.

Table 2.10: Bond lengths and angles around the copper atom of the published copper complex of salicylaldehyde acetylhydrazone seen in Figure 2.45 above.[22]

Lengths / Å		Angles / °	
Cu-N1	1.940(2)	N1-Cu-O1	92.22(9)
Cu1-O1	1.907(2)	N1-Cu-O2	81.20(9)
Cu1-O2	1.992(2)	02-Cu-O3	91.08(9)
Cu1-O3	1.969(2)	O3-Cu-O1	93.25(9)
		O1•••N1•••O2	93.36(9)

The bond lengths around the copper centres of the complexes published[22] (Table 2.10) and discussed herein are very comparable. The amidato C-N bond lengths are also very similar, that measured in the published structure[22] of 1.339(4) Å for the C-N single bond is only slightly longer than the C=N double bond in [Cu(**L4**-2H)(H_2O)] of 1.330(6) Å. The geometry around the copper centres in the complexes of [Cu(**L4**-2H)(H_2O)] are distorted from ideal square planar with bond angles ranging from 81.50(14) to 94.07(15)°. The resulting contact angle of 92.20(15)° between the ONO coordinating unit also deviates from an absolute right angle. However this is in agreement with the ONO contact angle measured in the dinuclear complex [Cu_2(**L2**-2H)$_2$] of the structurally related diacidic ligand **L2** of 92.80(3)° but smaller than that of the published structure given in Figure 2.45 of 93.36(9)°.

An interesting feature which arises as a consequence of the molecular packing is the large rhombic channels perpendicular to the plane of the molecules as shown in Figure 2.46. These are alternately lipophilic (*ca*. 12.65 x 13.10 Å) and hydrophilic (*ca*. 11.34 x 11.99 Å) in character, like a chessboard, with one molecule on each edge. Cu1 form in the horizontal edges and Cu2 the vertical edges. The character of the rhombic cavities also alternates so that lipophilic layers stack on hydrophilic. These channels are occupied by the solvent molecules which were associated with the reaction conditions, ethanol and water. The solvent molecules are disordered, so were treated with van der Sluis[59] and Spek[60] methods in the structural determination by F. J. White.

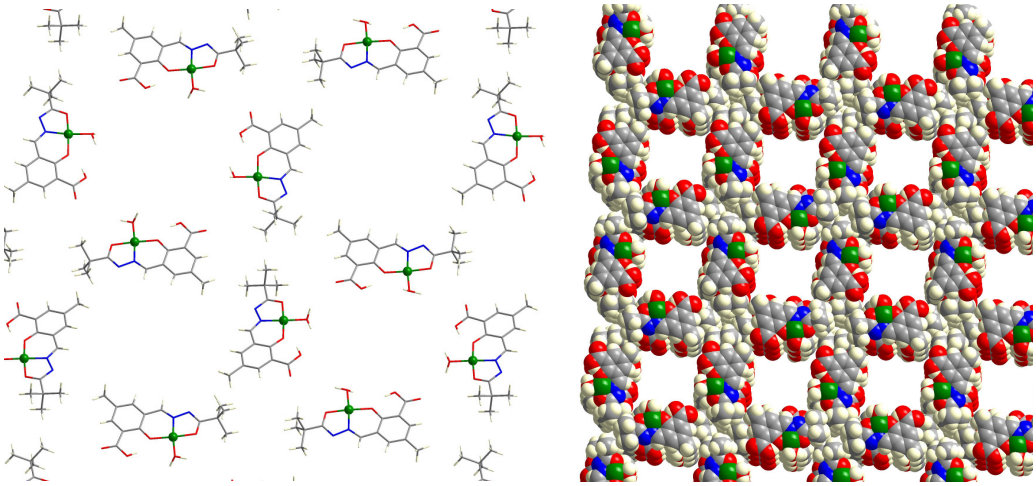

Figure 2.46: Packing diagrams for [Cu(**L4**-2H)(H_2O)].

2.8.3 Mononuclear Cu Complex [Cu(L5-H)(H_2O)][ClO_4]

Crystals of [Cu(**L5**-H)(H_2O)][ClO_4] were obtained by slow diffusion of nitromethane into an ethanol solution of **L5** and copper perchlorate over several days. The structure of [Cu(**L5**-H)(H_2O)][ClO_4], seen in Figure 2.47, has four molecular units per unit cell in the monoclinic crystal system $P2_1/n$. The copper atom is in a distorted square pyramidal geometry, equatorially coordinated by the O1•••N62•••O65 donor set of one **L5** molecule and the oxygen atom, O23, from the carbonyl group of the carboxylic acid of another molecule which acts as the polymeric link. A water molecule is present in the apical position, contributing to a displacement of the copper atom of -0.1489 Å from the least squares plane through Cu1, N62, O1, O65 and O23. The apical water binds only weakly to the copper centre. Each ligand molecule is singly deprotonated; the protons attached to N63 and O22 were found in the difference map. The charge is balanced by a perchlorate anion which is well separated from the copper coordination sphere, bound by hydrogen bonds to the water molecules.

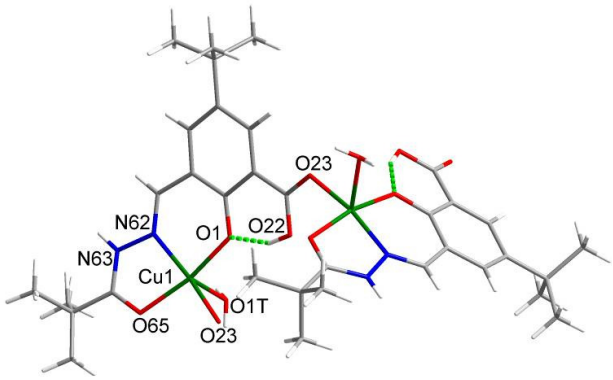

Figure 2.47: Part of the polymeric structure -[Cu(**L5**-H)(H_2O)]$^+$- formed by **L5.**

Table 2.11: Bond lengths, contact distances and angles for [Cu(**L5**-H)(H_2O)][ClO_4].

Lengths / Å		Angles /°	
Cu-O1	1.921(2)	O1-Cu-N62	90.41(7)
Cu-O23	1.973(2)	N62-Cu-O65	81.02(7)
Cu-O65	1.983(2)	O65-Cu-O23	97.05(6)
Cu-N62	1.939(2)	O23-Cu-O1	89.59(6)
Cu-O1T	2.204(2)	O1•••N62•••O65	94.53(7)
O1•••O22	2.438(2)		

Structural analogies can be drawn between [Cu(**L5**-H)(H_2O)][ClO_4] and that of [Cu(**L4**-2H)(H_2O)] described in Section 2.8.2 as the ligands only differ slightly in the nature of the alkyl substituent on the salicylic acid unit. The copper to ligand bond lengths are longer in [Cu(**L5**-H)(H_2O)][ClO_4]. This would be expected for a copper centre with higher coordination number due to the increased electron density on the copper atom. The deprotonation level of the ligand may also be a contributory factor as the amido N62 remains protonated in [Cu(**L5**-H)(H_2O)][ClO_4], therefore the amido oxygen O65 will not be as electron donating and consequently will not form as strong a bond. The O1•••N62•••O65 contact angle (Table 2.11) is also larger in [Cu(**L5**-H)(H_2O)][ClO_4] than [Cu(**L4**-2H)(H_2O)], *cf.* 94.53(7) and 92.20(15)° respectively, suggesting a weaker complex.

2.8.4 Dinuclear Cu Complex [Cu_2(L11-2H)$_2$]

The X-ray determination of [Cu_2(**L11**-2H)$_2$] reveals there are two molecules per unit cell with a triclinic crystal system and $P\bar{1}$ space group. The structure is centrosymmetric with phenolate oxygen O1 derived from the 2-hydroxyanil unit bridging the two copper centres. The copper centres are 3.056(2) Å apart, very close to the median of 3.061 Å calculated for 428 phenolate bridged dinuclear copper complexes in the CSD of range 2.788-3.575 Å. The Cu-O-Cu angle at the bridging phenolate is 103.0(3)°. This is greater than the median value of 100.2° but the range of angles reported is broad, 81.2-110.4°. The copper centres are distorted (see Table 2.12 for bond lengths and angles) square planar with short contacts above and below the molecular plane to the carboxylic acid oxygen atoms O14' (2.808(3) Å) and O15' (2.702(17) Å), see Figure 2.49. The $Cu_2N_2O_4$ complex unit is reasonably planar with maximum deviation from the least squares plane of ±0.0374 Å for the copper atoms and mean deviation of 0.0235 Å. The aromatic rings of the salicylic acid functionality are coplanar as are those of the 2-hydroxyanil unit but the planes of each are inclined at angle of 11.9° to each other.

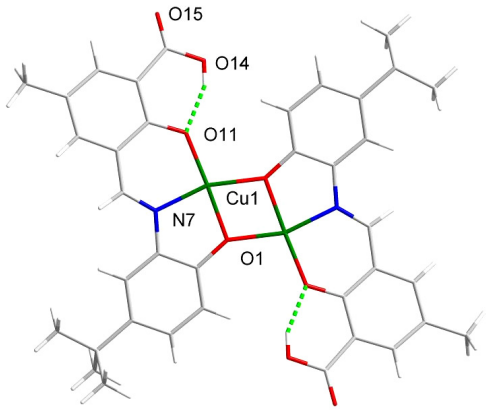

Figure 2.48: Dinuclear copper complex [Cu_2(**L11**-2H)$_2$] formed by **L11** omitting intermolecular bonds between O15 and Cu1 of neighbouring units.

Table 2.12: Bond lengths, contact distances and angles around the copper atom of [Cu_2(**L11**-2H)$_2$] (‘ denotes symmetry related atom).

Lengths / Å		Angles /°	
Cu1-Cu1	3.056(2)	Cu1-O1-Cu1’	103.0(3)
Cu1-O1	1.905(7)	O1-Cu1-O1’	77.0(3)
Cu1-O1’	1.955(6)	O1’-Cu1-O11	105.0(3)
Cu1-O11	1.902(7)	O1-Cu1-N7	83.9(3)
Cu1-N7	1.936(7)	N7-Cu1-O11	94.1(3)
O11•••O14	2.520(6)	O1•••N7•••O11	90.7(3)
Cu1•••O14	2.808(3)		
Cu1’•••O15	2.702(17)		

The structure of [Cu_2(**L11**-2H)$_2$] (Figure 2.48) corresponds to the isomer **G** shown in Figure 2.40 with the amidate oxygen atom replaced by a phenolate from the 2-hydroxyanil unit of **L11**. It is unlikely that **L11** could adopt the structural isomer type represented by **F** (Figure 2.40) as the non-bridging phenolate is coordinated to a copper atom and therefore would sterically clash with the carboxylic acid group as highlighted red in Figure 2.50.

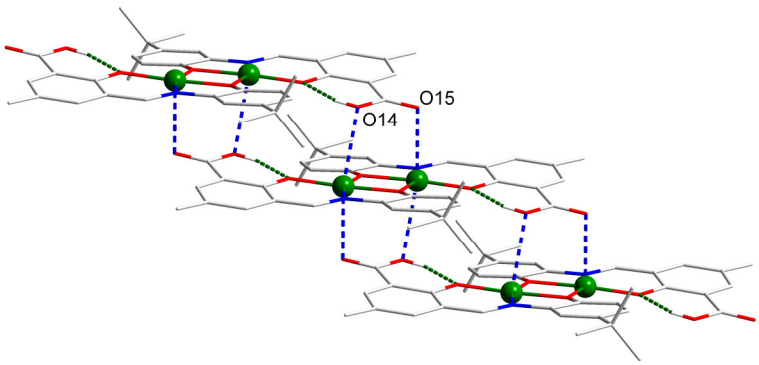

Figure 2.49: Structure of [Cu_2(**L11**-2H)$_2$] showing intermolecular contacts between the copper centres and the oxygen atoms O14 and O15 of the carboxylic acid groups of molecules stacked above and below.

The O1•••N7•••O11 contact angle of **L11** in the complex [Cu_2(**L11**-2H)$_2$] is larger than that in the free ligand and closer to a right angle (90.7(3)° *cf.* 88.8(4)°). Consequently the Cu-O1 (1.950(7)), Cu-O11 (1.902(7)) and Cu-N7 (1.936(7)) bond lengths (Å) are greater than those previously predicted from the structure of the free ligand in Section 2.5.3, assuming the copper atoms will lie on the midpoint of O11-O12 *cf.* 1.853(2) and 1.910(6) for Cu-N211 (Å). This can be attributed to the distorted square planar geometry around the copper centre which has angles varying from 77.0(3) to 105.0(3)° for O1-Cu-O1 and O1-Cu-O11 angles respectively. These distortion effects may be a result of the deviation of phenolate oxygen O1 from sp^2 geometry as imposed by the copper atom. The Jahn-Teller effect may also be contributing to this distortion, although to a lesser extent, as the copper centres are slightly displaced out of the $Cu_2N_2O_4$ plane (±0.0374 Å) through short contacts with oxygen atoms O14 and O15 of the carboxylic acid groups of neighbouring molecules above and below.

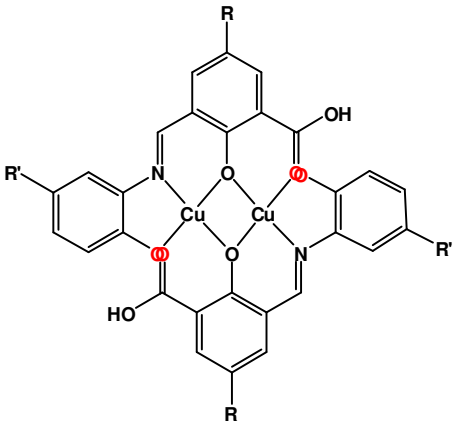

Figure 2.50: Illustration showing potential steric clash between the of the oxygen atoms of the hydroxyanil phenol and carboxylic acid groups.

2.8.5 Hexanuclear Cu Complex

$[Cu_6(L6\text{-}3H)_2(L6\text{-}2H)_2(MeO)_2(MeOH)_6 \bullet 6(MeOH)]$

$[Cu_6(\mathbf{L6}\text{-}3H)_2(\mathbf{L6}\text{-}2H)_2(MeO)_2(MeOH)_6 \bullet 6(MeOH)]$ was crystallised as green blocks from a deuterated methanol solution on cooling. It contains one molecule per unit cell which has a triclinic crystal system and $P\bar{1}$ space group. The complex is centrosymmetric (see Figure 2.51) with six square pyramidal copper atoms in three chemically different coordination environments, although all have NO_4 coordination spheres with apical methanol molecules. Cu3 also has a short contact to a second apical methanol molecule O1U which has resulted in a lengthening of the trans Cu2-O1V bond 2.483(4)Å relative to that of the other copper to apical methanol molecules (see Table 2.13). There are four **L6** molecules per discrete molecular unit giving a Cu to ligand stoichiometry of 3 : 2. The dinuclear phenolate/methoxide bridged unit contains Cu1 and Cu3 and is reasonably planar with largest deviations observed for O22B and N62B (0.6494 and -0.4662 Å respectively) with mean deviation of ±0.3314 Å for the plane through the complex unit defined by Cu1, Cu3, O65B, N62B, O1B, O2D, O22B and N63A. The unit containing Cu2 defined by Cu2, O21B, O1A, N62A and O65A lies at an angle of 70°. It is nearly planar with the largest displacement from the plane observed for O1A and Cu2 of 0.0385 and -0.0844 Å respectively and mean deviation of ±0.0338 Å.

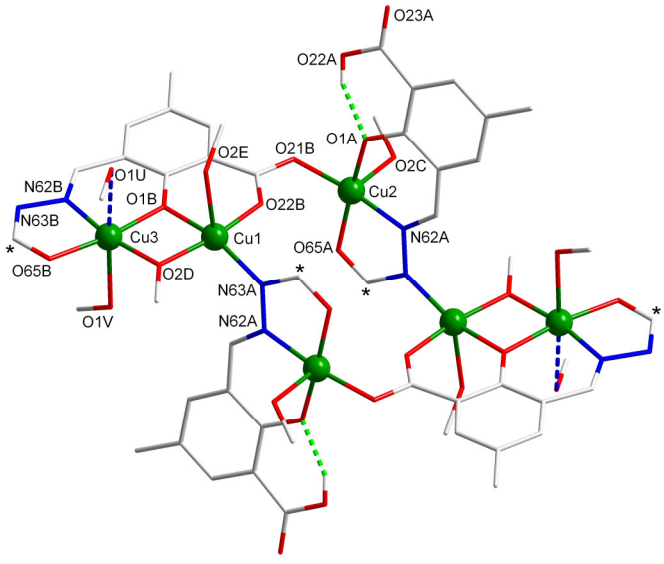

Figure 2.51: The hexanuclear copper complex $[Cu_6(\mathbf{L6}\text{-}3H)_2(\mathbf{L6}\text{-}2H)_2(MeO)_2(MeOH)_6 \bullet 6(MeOH)]$. Hydrogen atoms and heptyl chains (*) have been removed for clarity.

Table 2.13: Bond lengths, contact distances and angles for Cu1, Cu2 and Cu3 of [Cu_6(**L6**-3H)$_2$(**L6**-2H)$_2$(MeO)$_2$(MeOH)$_6$•6(MeOH)]. Atom labels are displayed in Figure 2.51.

Lengths / Å		Angles /°	
About Cu1			
Cu1-O1B	1.966(4)	O1B-Cu1-O2D	78.20(17)
Cu1-O2D	1.910(4)	O2D-Cu1-N63A	98.57(19)
Cu1-N63A	1.997(5)	N63A-Cu1-O22B	91.81(19)
Cu1-O22B	1.908(4)	O22B-Cu1-O1B	90.20(16)
Cu1-O2E	2.374(4)		
About Cu2			
Cu2-O21B	1.960(4)	O21B-Cu2-O1A	92.00(17)
Cu2-O65A	1.948(4)	O1A-Cu2-N62A	92.47(18)
Cu2-N62A	1.936(4)	N62A-Cu2-O65A	80.83(18)
Cu2-O2C	2.287(4)	O65A-Cu2-O21B	94.03(17)
Cu2-O1A	1.917(4)	O65A•••N62A•••O1A	93.04(19)
O1A•••O22A	2.481(7)		
About Cu3			
Cu3-N62B	1.920(5)	O1B-Cu3-N62B	91.70(18)
Cu3-O65B	1.940(4)	N62B-Cu3-O65B	81.81(18)
Cu3-O2D	1.904(4)	O65B-Cu3-O2D	107.65(17)
Cu3-O1B	1.955(4)	O2D-Cu3-O1B	78.61(16)
Cu3•••O1U	2.865(4)	O1B•••N62B•••O65B	94.02(2)
Cu3-O1V	2.483(4)	Cu3-O1B-Cu1	99.65(17)
Cu1•••Cu3	2.996(9)	Cu3-O2D-Cu1	103.54(18)

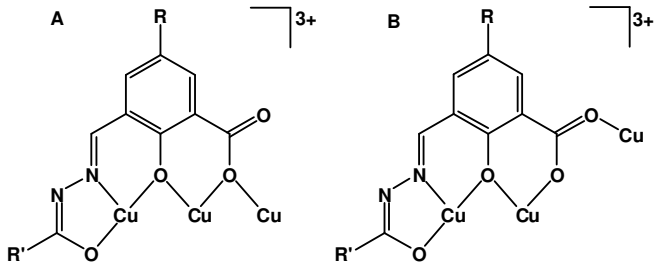

Figure 2.52: Trinuclear copper(II) assemblies formed by triacidic ligands **L4**-**L13**, with the pedant carboxylate forming a 120° μ_2 bridge in **A** and both the carboxylate and carbonyl forming a 120° bond in **B**.

This structure determination confirmed that the ligands of the type **L4**-**L13** can form trinuclear complexes. However, the ligand does not organise the three copper cations to be aligned in an approximately linear manner as in **A** in Figure 2.52. Instead, the *pendant* carbonyl oxygen atom, O21B, forms the bond to the third copper atom, Cu2. The structure of $[Cu_6(\mathbf{L6}\text{-}3H)_2(\mathbf{L6}\text{-}2H)_2(MeO)_2(MeOH)_6\bullet 6(MeOH)]$ confirms that the carboxylate group in the ligands **L4**-**L13** can be deprotonated and form a bond to copper and that the phenolate oxygen O1B from the salicylic acid unit of the triacidic ligands **L4**-**L13** can bridge two copper centres.

2.8.6 Decanuclear Cu Cluster $[Cu_{10}(L5\text{-}3H)_4(OH)_4(CH_3COO)_4(MeOH)_2\bullet 11(H_2O),3(MeOH)]$

The decanuclear copper cluster $[Cu_{10}(\mathbf{L5}\text{-}3H)_4(OH)_4(CH_3COO)_4(MeOH)_2\bullet 11(H_2O),$ 3(MeOH)] shown in Figure 2.53 separated as green blocks after several days from a methanolic solution of **L5** with 1.5 molar equivalents of copper(II) acetate and sodium hydroxide which had been refluxed for 3 hours. The unit cell contains a centrosymmetric molecule with five pairs of equivalent copper atoms. The crystal system is triclinic with space group $P\bar{1}$. There are two symmetry related pairs of **L5** molecules labelled **A** and **B** in Figure 2.53. Ligands **A** and **B** stack in a **BAAB** manner with 2, 3, 3 and 2 copper atoms in these planes; (Cu2 and Cu4) and (Cu1, Cu3 and Cu5). All Cu atoms are square pyramidal except Cu5 which is octahedral.

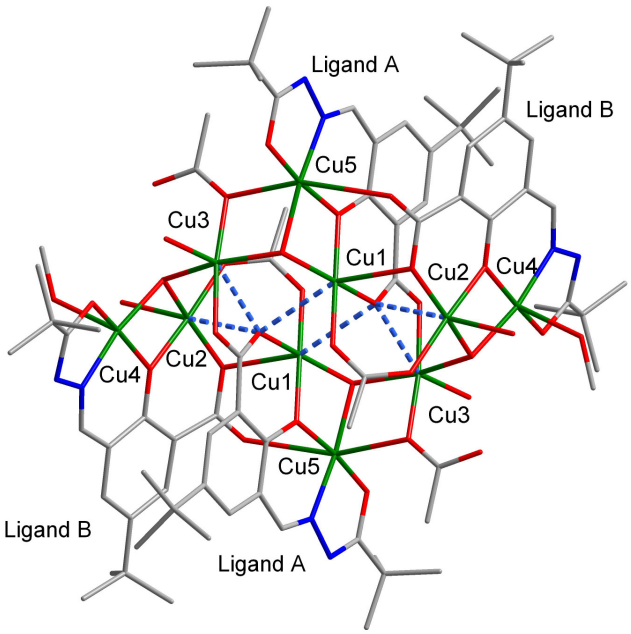

Figure 2.53: Decanuclear copper cluster $[Cu_{10}(\mathbf{L5}\text{-}3H)_4(OH)_4(CH_3COO)_4(MeOH)_2 \bullet 11(H_2O), 3(MeOH)]$ with hydrogen atoms removed for clarity.

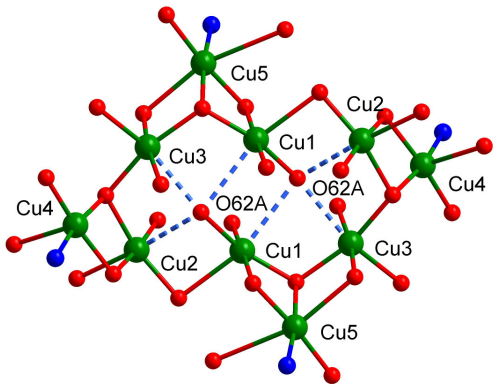

Figure 2.54: The copper, nitrogen and oxygen atoms in the core of decanuclear the copper cluster $[Cu_{10}(\mathbf{L5}\text{-}3H)_4(OH)_4(CH_3COO)_4(MeOH)_2 \bullet 11(H_2O), 3(MeOH)]$ showing carbonyl oxygen O62A.

The high nuclearity of this complex arises because both oxygen atoms of the carboxylic acid groups of **L5** are coordinated to copper atoms. An interesting feature of this complex which may cause debate is the coordination number of the carbonyl oxygen atom O62A shown in Figure 2.54. It is clearly formally bound to Cu1 (1.947(5) Å) but forms close contacts with Cu2, Cu3 and symmetry related Cu1'. The bond lengths and angles measured around O62A are given in Table 2.14. If the

longest of these O65A-Cu1', 2.740(5) Å, was to be classed as a bond this would be the first example of a 5-coordinate carbonyl oxygen atom bridging four transition metal centres. A published study[61] into the plasticity of copper(II) bound in CuO_6, CuO_5, CuN_6 and CuN_4O_2 based on empirical bond-valence theory suggests that Cu-O contacts below 3.07 Å should be considered as semicoordinated. Although all bond lengths in this complex are well within this limit, they have been designated short contacts because they are somewhat longer than those reported for the longest μ_4-OH^- oxygen atoms bound to copper centres of 2.592 Å.[62] There are four cases where a hydroxide oxygen atom bridges four transition metal centres in the CSD.[62-65]

Table 2.14: Bond lengths, contact distances and angles around carbonyl oxygen O62A from $[Cu_{10}(\mathbf{L5}\text{-}3H)_4(OH)_4(CH_3COO)_4(MeOH)_2 \bullet 11(H_2O), 3(MeOH)]$.

Lengths / Å		Angles /°	
O65A-Cu1	1.947(5)	Cu1-O65A•••Cu1'	93.5(2)
O65A•••Cu1'	2.740(5)	Cu1'•••O65A•••Cu3	76.6(16)
O65A•••Cu2	2.601(5)	Cu3•••O65A•••Cu2	82.0(19)
O65A•••Cu3	2.532(6)	Cu2•••O65A-Cu1	88.0(2)
O65A•••C61A	1.244(9)		

2.9 Significance of Observed Solid State Structures in Solvent Extraction Speciation

Although the conformation and nuclearity of the solid state complex structures isolated were not what was expected from the original ligand design, they do show that ligands **L4**-**L13** are capable of coordinating three copper centres. It could be that the speciation in solution is that which was intended, and was not observed in the solid state as a consequence of crystal packing forces which facilitate favourable intermolecular contacts. Formation of the observed structures may also be driven largely by the formation of strong interactions with anions and solvent molecules which are not present in the extraction experiments.

Of the structures isolated, the mononuclear species of the types [Cu(**L5**-H)$_2$] (Section 2.8.1) and [Cu(**L4**-2H)(H$_2$O)] (Section 2.8.2) are the most likely to cause concern in solvent extraction experiments. Octahedral complexes of the type [Cu(**L5**-H)$_2$] would cause concern if they were particularly thermodynamically stable species as this could inhibit formation of complexes of higher Cu:L stoichiometry. Complexes of the type [Cu(**L4**-2H)(H$_2$O)] could form in solvent extraction as all constituent species are available. However this type of species is not evident in mass spectra of methanol solutions of samples taken from solvent extraction experiments of **L5** and **L7.** Therefore it is unlikely to be the major species present. Nevertheless peaks are observed in mass spectra consistent with [Cu(L-H)(MeOH)]$^+$ molecular ions but these are expected to be a fragmentation product of the [Cu(L-H)$_2$] complexes rather than replacement of a water molecule from [Cu(L-H)(H$_2$O)] with that of methanol.

2.10 Increased Cu Mass Transport by Triacidic Ligands L4-L13

Ligands **L4**-**L13** have been shown above to form complexes of the type [Cu$_3$(L-3H)$_2$]. This is a three-fold enhancement of the copper to ligand stoichiometry relative to the current commercial copper solvent extractants. The mass transport efficiencies for the ligands are calculated and presented in Table 2.15.

Table 2.15: Masses of copper (g) transported per unit mass of extractant (kg) for the triacidic ligands **L4**-**L13** and the increases in mass transport efficiency relative to the commercial extractant, **P50**.

Ligand	M.W.	Cu : L	Cu (g) per L (kg)	Fold Increase
P50	263	1 : 2	121	0
L4	278	3 : 2	343	2.83
L5	320	3 : 2	298	2.46
L6	320	3 : 2	298	2.46
L7	419	3 : 2	228	1.88
L8	433	3 : 2	220	1.82
L9	354	3 : 2	269	2.23
L10	453	3 : 2	210	1.74
L11	327	3 : 2	292	2.41
L12	426	3 : 2	224	1.85
L13	440	3 : 2	217	1.79

The *tri*acidic ligands substantially increase the mass of copper transported per unit mass of extractant relative to the commercial extractant **P50**. As can be seen in Table 2.15 above 1.74 to 2.83 fold increases result. Unfortunately, none of the trinuclear complexes formed by the triacidic ligands studied had sufficient solubility in the water-immiscible hydrocarbon solvents used industrially. Consequently the next section considers using the triacidic ligands in 1 : 1 blends with phenolic oxime reagents in an attempt to improve the solubility of the resulting complexes in hydrocarbon solvents.

2.11 An Alternative Approach to Enhancing Mass Transport Efficiency Using Mixed Ligand Systems

It has been established in the previous sections of this chapter that acyl hydrazone ligands are selective copper extractants which demonstrate improved molar and mass transport efficiencies relative to the commercial phenolic oxime reagents and are of comparable strength for loading of the first copper as determined by the $pH_{½}$. This section considers the application of triacidic acyl hydrazone ligands in reagent blends with phenolic oxime reagents in an attempt to increase the molar transport capacity of the current copper-recovery technology. A successful system will require the two types of ligand to work synergistically to extract copper as a ternary dinuclear complex (Figure 2.55).

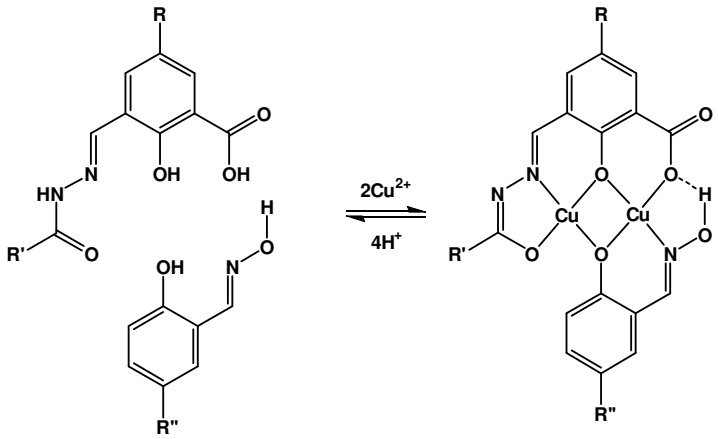

Figure 2.55: Possible structure of a ternary copper complex formed by an acyl hydrazone ligand and a phenolic oxime.

2.11.1 Solvent Extraction

To assess the ability of the ligand mixtures to extract copper, pH-dependent solvent extraction studies were carried out as described in Section 2.6. Chloroform solutions of a 1:1 mixture of **L6** and 5-nonylsalicylaldoxime, **P50**, were stirred with copper sulfate solutions at varying pH. These blends were formulated using half the molar quantity (5.0 ml, 0.00125 M) of each extractant used in previous extractions to give

an overall extractant solution of the same concentration (5.0 ml, 0.0025 M). The extraction curve obtained for the blend (●, in Figure 2.56) shows that the system loads to maximum capacity; 1 mol of copper is loaded per mol of ligand to form the dinuclear ternary complex [Cu_2(**L6**-3H)(**P50**-H)]. The $pH_{½}$ value at which the first copper is loaded for the mixed ligand extraction is similar to that of the component parts. The absence of well defined plateau in the loading profile for the **L6/P50** blend indicates that **L6** is not extracting copper as a binary system as previously observed (Figure 2.28). In the low pH-region of the loading curve (see ● Figure 2.56) there appears to be some synergism in Cu-loading with the blend giving higher loading than its components.

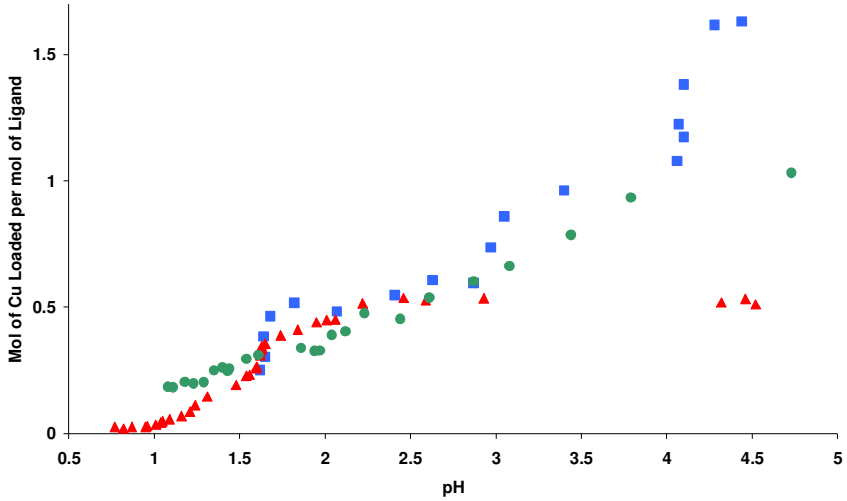

Figure 2.56: Comparison of the pH-dependent copper loading of a chloroform solution of **L6** (■) (0.0025 M), **P50** (▲) (0.0025 M) and a 1:1 mixture of **L6** and **P50** (●) (each present at 0.00125 M) for the formation of [Cu_3(**L6**-3H)$_2$], [Cu(**P50**-H)$_2$] and [Cu_2(**L6**-3H)(**P50**-H)] respectively.

A blend of **L7** and 5-*t*-octylsalicylaldoxime, **19**, (also in 1:1 molar ratio) was also studied (Figure 2.57). Again the blend loads copper to the maximum theoretical amount associated with the formation of a Cu : **L7** : **P50** ratio of 2 : 1 : 1 as in [Cu_2(**L6**-3H)(**P50**-H)]. The $pH_{½}$ is intermediate between the values expected for the extractants forming binary species.

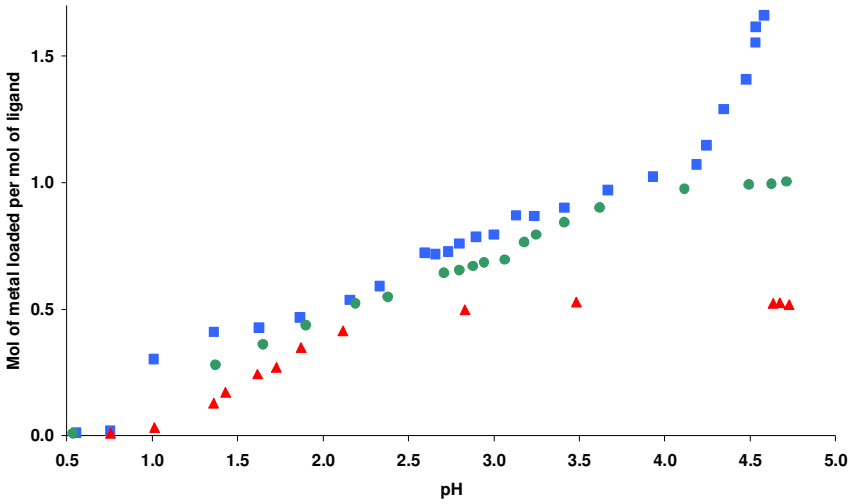

Figure 2.57: Comparison of the pH-dependent loading profiles for chloroform solutions of **L7** (■) (0.0025 M), **19** (▲) (0.0025 M) and a 1:1 mixture of **L7** and **19** (●) (each present at 0.00125 M) for the formation of $[Cu_3(\mathbf{L7}\text{-}3H)_2]$, [Cu (**19**-H)$_2$] and $[Cu_2(\mathbf{L7}\text{-}3H)(\mathbf{19}\text{-}H)]$ respectively.

2.11.2 Metal Selectivity

Having established that the reagent blends **P50** and **L6**, and, **19** and **L7** are capable of extracting copper to form ternary complexes, the selectivity of copper extraction was investigated. Although both types of reagent show selectivity for copper over other base metals when applied individually it may be possible to extract a heterometallic species when combined. Selectivity studies were carried out from a feed solution containing Co(II), Ni(II), Cu(II) and Zn(II). Iron(III) was omitted to allow the pH to be increased beyond 2.5, thus obtaining *ca.* 100% theoretical loading. The loading profile (Figure 2.58) indicates the mixed ligand extractant is very selective for copper over the other base metals.

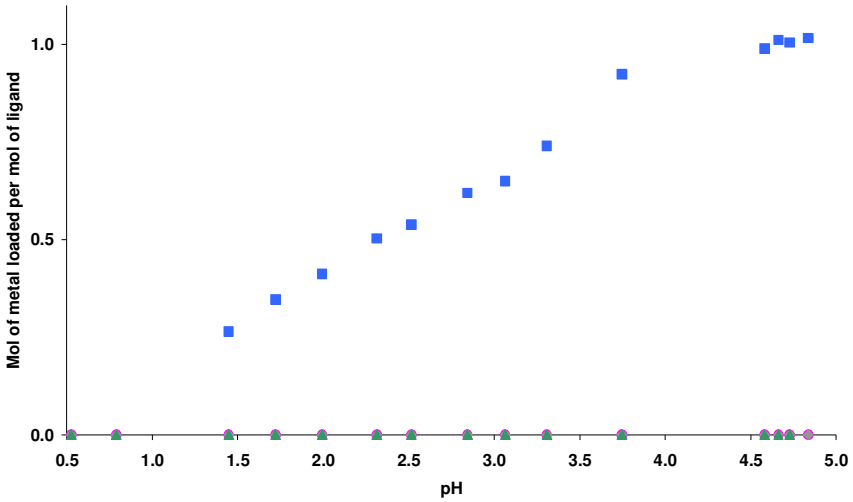

Figure 2.58: Metal selectivity study of a 1:1 mixture of **L7** and **19** in chloroform (each present at 0.00125 M) for the formation of the ternary complex [Cu_2(**L7**-3H)(**19**-H)] from a mixed metal feed solution (Cu(II), ■; Co(II), ●; Ni(II), ♦ and Zn(II), ▲).

To confirm the species extracted by the blends were the ternary complexes, e.g. [Cu_2(**L6**-3H)(**P50**-H)] and [Cu_2(**L7**-3H)(**19**-H)], rather than a mixture of the two binary complexes, samples were taken from solvent extraction experiments for analysis by electrospray mass spectrometry and UV/Vis spectroscopy.

2.11.3 Mass Spectrometry

Samples were prepared for mass spectrometric analysis by contacting a chloroform solution of the appropriate oxime and triacidic ligand, each present at a concentration of 0.00125 M with copper sulfate (0.02 M). The pH of the aqueous phase adjusted to *ca*. pH 5. Portions of the organic phase were taken, dried and made up in methanol for analysis. The spectra obtained for the mixtures of 5-*t*-butylsalicylaldoxime (**18**) and **L5** and 5-*t*-octylsalicylaldoxime (**19**) and **L7** are given in Figure 2.59. Good agreement between theoretical and experimental isotopic distributions for the single positively charged molecular ion peaks [Cu_2(**18**-H)(**L5**-3H)]H^+ and [Cu_2(**19**-H)(**L7**-3H)]H^+ were found.

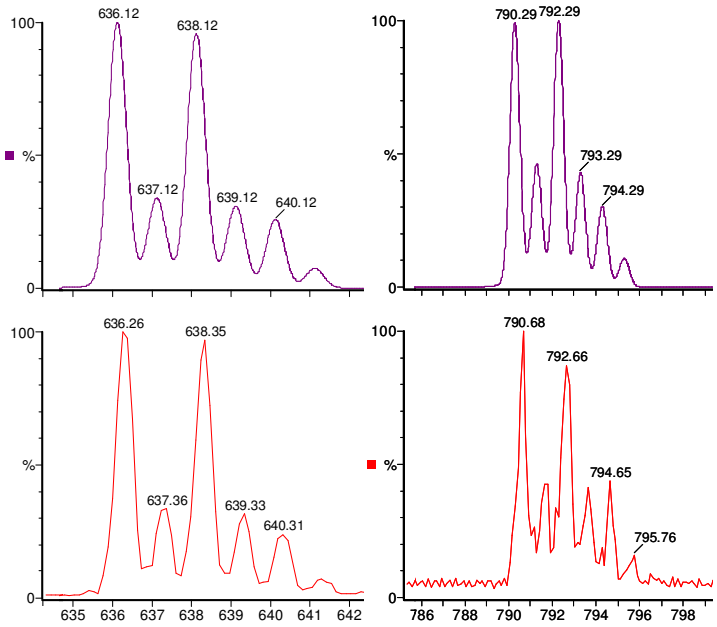

Figure 2.59: Simulated (top) and experimental (bottom) electrospray mass spectra of the ternary dinuclear copper complex formed by **L5** oxime and *p-t*-butylsalicylaloxime (**18**) $[Cu_2(\mathbf{18}\text{-H})(\mathbf{L5}\text{-3H})]H^+$, left and **L7** and **19** $[Cu_2(\mathbf{19}\text{-H})(\mathbf{L7}\text{-3H})]H^+$, right.

No other major cationic peaks were detected in the mass spectra consistent with the binary phenolic oxime or trinuclear complexes. The UV/Vis spectra were measured to ensure that the extracted species were the ternary complexes.

2.11.4 UV/Vis Spectroscopy

The electronic spectra of **L7**, **19** and a 1:1 mixture of **L7** and **19** at the same *total* concentration can be seen on the left of Figure 2.60. The spectra of the copper complexes, $[Cu_3(\mathbf{L7}\text{-3H})_2]$ and $[Cu(\mathbf{19}\text{-H})_2]$, and that of the presumed ternary complex $[Cu_2(\mathbf{19}\text{-H})(\mathbf{L7}\text{-3H})]$, each obtained after four-fold dilution of samples obtained directly from solvent extraction studies described in Section 2.11.1 are shown on the right. The peaks of maximum absorbance and their relative molar extinction coefficients are given in Table 2.16. Concentrations of extractants and complexes after dilution are 625 and 312.5 μM, respectively, the latter based on formation of $[Cu_n(L\text{-}nH)_2]$ complexes.

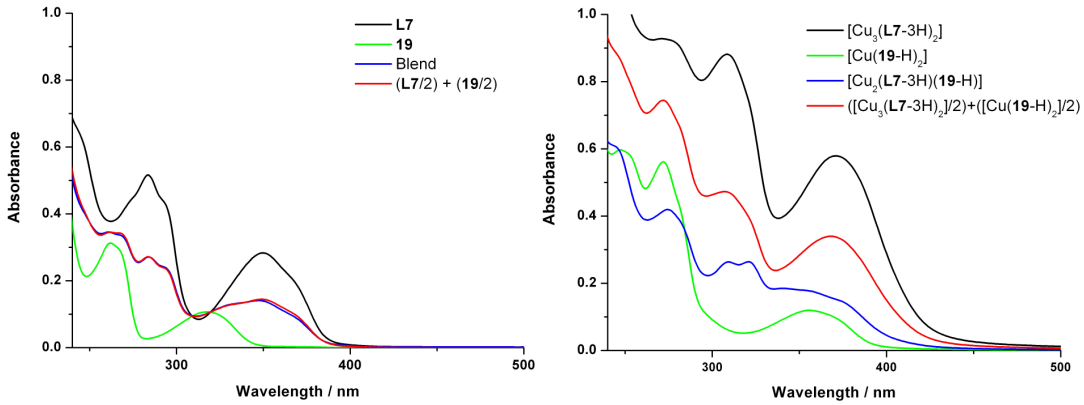

Figure 2.60: Electronic spectra of the 625 μM chloroform solutions of ligands **L7**, **19** and the 1:1 blend (left) and the 312.5 μM chloroform solutions of complexes formed by them (right).

Comparison of the wavelengths and absorbances of peaks in the spectra of the two reagents **L7**, **19** and the blend of **L7** + **19** are consistent with the blend being a simple mixture of the two ligands as the spectrum is the summation of the spectra of its components (the red line lies over the blue line). There is no evidence for formation of any adducts or assemblies.

The complexes $[Cu_3(\mathbf{L7}\text{-}3H)_2]$, $[Cu(\mathbf{19}\text{-}H)_2]$ and that presumed to be $[Cu_2(\mathbf{L7}\text{-}3H)(\mathbf{19}\text{-}H)]$ have bands in similar regions (Table 2.16) but, most significantly, the spectrum shown by the latter is not the summation of the spectra of $[Cu_3(\mathbf{L7}\text{-}3H)_2]$ and $[Cu(\mathbf{19}\text{-}H)_2]$. Characteristic peaks for $[Cu(\mathbf{19}\text{-}H)_2]$ at 272 and 356 nm and for $[Cu_3(\mathbf{L7}\text{-}3H)_2]$ at 271 and 371 are much less prominent (or shifted) in the spectrum of the extract formed by the blend of **L7** and **19** which is assumed to contain $[Cu_2(\mathbf{L7}\text{-}3H)(\mathbf{19}\text{-}H)]$. The latter also contains a peak at 321 nm which is not seen in the spectra of the binary complexes. Moreover, the absorbances recorded in the spectrum of the extract formed by the blend (blue line) are very different from those which would be predicted (red line) for the formation of a mixture of $Cu_3(\mathbf{L7}\text{-}3H)_2]$ and $[Cu(\mathbf{19}\text{-}H)_2]$. The results provide evidence that the principal complex formed by the blend is the ternary system $[Cu_2(\mathbf{L7}\text{-}3H)(\mathbf{19}\text{-}H)]$ and support the proposition that ligands of the type described in this chapter are well suited for forming bridged copper(II) complexes.

Table 2.16: Wavelengths and molar extinction coefficients[#] for peaks found in the electronic spectra of chloroform solutions of **L7**, **19** and their copper(II) complexes.

	L7		**19**		**L7** + **19** Blend		
Max Absorbance (nm)	284	350	262	318	261	284	347
$\varepsilon \times 10^3$ ($mol^{-1}cm^{-1}$)	16.5	9.1	10.0	3.4	11.1	8.7	4.5

	$[Cu_3(\mathbf{L7}\text{-}3H)_2]$		$[Cu(\mathbf{19}\text{-}H)_2]$		$[Cu_2(\mathbf{L7}\text{-}3H)(\mathbf{19}\text{-}H)]$				
Max Absorbance (nm)	271	309	371	247	272	356	274	309	321	341
$\varepsilon \times 10^3$ ($mol^{-1}cm^{-1}$)	59.4	65.4	37.1	38.2	35.9	7.6	26.8	16.9	16.9	11.8

[#]Extinction coefficients (ε) were calculated using the equation $A = \varepsilon[J]l$, derived from the Beer-Lambert law.[51] Concentrations ([J]) of chloroform solutions of the extractants **L7** and **19** (625 μM) and the 1 : 1 mixture of **L7** and **19**, each at a concentration of 312.5 μM, and that of the resulting copper complexes (312.5 μM) were defined by the masses of ligands taken to prepare the extractant solutions. Spectra were measured in a quartz cell of μM path-length (*l*) 0.5 mm. Values of absorbance of peaks were selected and recorded by the instrument software package UV WinLab 2.70.01.

2.12 Increased Cu Mass Transport by Blended Extractants

The *tri*nucleating ligands **L6** and **L7** have been demonstrated to form *di*nuclear complexes when used in an admixture with the commercial *mono*nucleating salicylaldoxime **P50** and an isomerically pure analogue of reagent, **19**, respectively. In general terms the resulting complexes $[Cu_2(L\text{-}3H)(L'\text{-}H)]$ which would be formed by phenolic oxime extractants, will double the molar transport of copper relative to commercial reagents. The corresponding mass of copper transported per unit mass of extractant is calculated in Table 2.17.

Table 2.17: Masses of copper (g) transported per unit mass of extractant (kg) for the blended ligand systems **L6+P50** and **L7+19** relative to the commercial reagent **P50**.

Ligand	M.W.	Cu : L	Cu (g) per L (kg)	Fold Increase
P50	263	1 : 2	121	0
L6 + P50	320 + 263	2 : 1 : 1	218	1.80
L7 + 19	419 + 249	2 : 1 : 1	190	1.57

The proof-of-concept established by using **L6** and **L7** in blends with **P50** and **19**, respectively, indicates that this could be used to increase copper mass transport efficiency. In principle it will be possible to assess this approach with blends involving **P50** and the other triacidic ligands and based on their molecular weights the resulting mass transport efficiency will be increased between 1.47 and 1.94 fold for ligands **L10** and **L4** respectively.

2.13 Conclusions and Future Work

This chapter dealt with increasing the molar and mass transport efficiencies of ligands for application in recovery of copper by pH-swing solvent extraction. The early part of this chapter involved the synthesis of less lipophilic dianionic ligands **L2** and **L3** structurally analogous to those investigated in previous work at the University of Edinburgh, **1**-**6**. Synthesis of **L2** allowed the solid state structure of the dinuclear copper complex $[Cu_2(\mathbf{L2}\text{-}2H)_2]$ to be determined by X-ray diffraction. The structure obtained confirmed that the dianionic hydrazone ligands (**1**-**6**, **L2** and **L3**) bridge the two copper centres through the phenolate oxygen rather than that of the amidate. This discovery is entirely consistent with finding for similar structures.[21, 23, 66] The Cu-Cu distance measured falls within the range expected for phenolate bridged di-copper complexes and the resulting Cu-O-Cu angle of 99.6° is expected to display antiferromagnetic behaviour. This was demonstrated through measurement of the variable temperature magnetic susceptibility, which indicted that the complex

was strongly antiferromagnetic and became essentially diamagnetic at temperatures of less than 160 K.

To complete the work related to the diacidic ligands and conclude the hypothesis for the coordination geometry of the copper complexes, it would be advantageous to synthesise analogues of the nitro-substituted ligands **2** and **4** with shorter alkyl chains in order to isolate single crystals for X-ray structure determination. The expected *mono*- and *di*-nuclear complexes are shown in Figure 2.61. To optimise the probability of isolating the dinuclear structure, it is recommended that R' should be methyl rather than *t*-butyl group to reduce inter-ligand steric repulsion be between R' and the nitro group of the *trans* ligand.

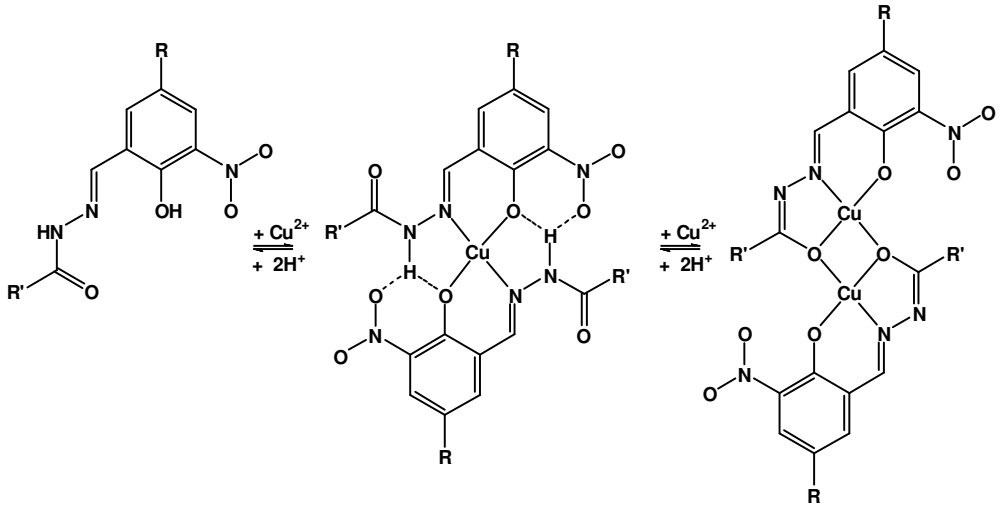

Figure 2.61: Predicted solid state *mono*- and *di*-nuclear copper complexes formed by less lipophilic structural analogues to **2** and **4**.

Confirmation of the mode of binding of the copper centres in the dianionic ligands allowed the fundamentals employed in the design of these ligands to be extended to a new class of potentially trinucleating, triacidic ligands **L4**-**L13**. The new reagents were shown to increase molar transport of copper to 3:2 from 1:2 and 2:2, observed for the commercial phenolic oxime reagents (e.g. **P50**) and the previously studied dianionic ligands (**1**-**7**, **L2** and **L3**). The mass transport efficiencies of the ligands were calculated by taking into consideration the mass of copper transported relative to the molecular mass of the ligands required. The results conclude that, not only has

the molar transport been increased 3 fold, but the mass transport can also be increased by up to 2.5 fold for **L6**.

To enhance the solubility of the triacidic ligands and the resulting complexes in water-immiscible hydrocarbon solvents as used industrially, it is suggested that a mixed isomer hydrazide, such as decanoic hydrazide, should be incorporated into **L8**. The increase in molecular weight to 461 amu does not significantly affect the mass transport as a resulting increase of 1.7 fold is calculated relative to **P50**, *c.f.* 1.9 fold for **L8** (Table 2.15).

The trianionic ligands were also demonstrated to double the molar transport of the phenolic oxime reagents and increase the mass transport by *ca.* 1.8 to 1.9 fold when mixed in 1:1 ratios through formation of a ternary 2:1:1, copper : triacidic ligand : phenolic oxime, complex. The resulting dinuclear complexes are expected to have greater solubility in organic solvent than the trinuclear complexes if mixed isomer alkyl substituents are incorporated into the ligands. Consequently, they have a greater potential for application as new commercial reagents.

Future work to improve the opportunities for application of the triacidic ligands in an industrial process should aim to reduce the pH range in which the ligands operate. Particularly when treating feed streams which contain iron, as the pH cannot be increased enough to allow the full loading potential of the ligands to be exploited due to precipitation of iron hydroxide. To achieve this one would initially assume a more acidic functional group which would be expected to deprotonate at a lower pH. However, the carboxylic acid is the most acidic functionality in these molecules and solid state structures indicate that it remains protonated until the third copper is extracted. Consequently, it is suggested that the carboxylic acid is replaced by a functional group with a higher pK_a value in water. Doing so may also provide an opportunity to enhance the solubility of the resulting complexes in industrial solvents. This, in contrast, may also increase the probability of isolating solid state structures with the geometries theorised for mono-, di- and tri-nuclear copper complexes. It is recommended that atoms with electron donor / acceptor properties are not used in place of the carbonyl of the carboxylic acid as it has been

demonstrated to be responsible for formation of complexes with higher nuclearity than desired. Nevertheless the current triacidic ligands may find application in non-conventional processes operating at higher pH.

2.14 References

1. J. Szymanowski, *Hydroxyoximes and Copper Hydrometallurgy*, CRC Press, London, 1993.
2. A. G. Smith, The University of Edinburgh, 2001, p. 44.
3. J. L. Wood, PhD Thesis, The University of Edinburgh, 2005.
4. D. C. R. Henry, PhD Thesis, The University of Edinburgh, 2007.
5. A. G. Smith, P. A. Tasker and D. J. White, *Coord. Chem. Rev.*, 2003, **241**, 61-85.
6. P. O'Brien, J. R. Thornback and J. Szymanowski, *J. Coord. Chem.*, 1983, **13**, 11-15.
7. G. A. Kordosky, Epomin 2000, International Conference on Clean Technologies for the Mining Industry, Santiago, Chile, 2000.
8. G. A. Kordosky, *J. South African Inst. Mining and Metall.*, 2002, **102**, 445-450.
9. V. Gasperov, S. G. Galbraith, L. F. Lindoy, B. R. Rumbel, B. W. Skelton, P. A. Tasker and A. H. White, *Dalton Trans.*, 2005, 139-145.
10. T. Matsushita, K. Takaishi, M. Fujiwara and T. Shono, *Polyhedron*, 1987, **6**, 289-293.
11. P. A. Vigato and S. Tamburini, *Coord. Chem. Rev.*, 2004, **248**, 1717-2128.
12. P. A. Vigato, S. Tamburini and L. Beltolo, *Coord. Chem. Rev.*, 2007, **251**, 1311-1492.
13. N. Kubota, M. Fujiwara, T. Matsushita and T. Shono, *Polyhedron*, 1985, **4**, 1051-1057.
14. K. Ikeda, M. Ohba and H. Okawa, *Dalton Trans.*, 2001, 3119-3124.
15. R. Aldred, R. Johnston, D. Levin and J. Neilan, *J. Chem. Soc., Perkin Trans. 1*, 1994, 1823-1831.
16. L. F. Lindoy, G. V. Meehan and N. Svenstrup, *Synthesis*, 1998, 1029-1032.
17. D. Stepniak-Biniakiewicz, *Pol. J. Chem.*, 1980, **54**, 1567-1571.
18. S. Owens, Cytec Industries, 1999, Private Communication.
19. F. H. Allen, *Acta Crystallogr. Sect. B*, 2002, **58**, 380-388.
20. N. R. Sangeetha, K. Baradi, R. Gupta, C. K. Pal, V. Manivannan and S. Pal, *Polyhedron*, 1999, **18**, 1425-1429.
21. M. F. Iskander, L. El-Sayed, N. M. H. Salem, W. Haase, H. J. Linder and S. Foro, *Polyhedron*, 2004, **23**, 23-31.
22. E. W. Ainscough, A. M. Brodie, A. J. Dobbs, J. D. Ranford and J. M. Waters, *Inorg. Chim. Acta*, 1998, **267**, 27-38.
23. L. L. Koh, O. L. Kon, K. W. Loh, Y. C. Long, J. D. Ranford, A. L. C. Tan and Y. Y. Tjan, *J. Inorg. Biochem.*, 1998, **72**, 155-162.

24. M. F. Iskander, T. E. Khalil, R. Werner, W. Haase, I. Svoboda and H. Fuess, *Polyhedron*, 2000, **19**, 1181-1191.

25. O. Kahn, *Molecular Magnetism*, VCH, New York, 1993.

26. R. S. Forgan, P. A. Wood, J. Campbell, D. K. Henderson, F. E. McAllister, S. Parsons, E. Pidcock, R. M. Swart and P. A. Tasker, *Chem. Commun.*, 2007, 4940-4942.

27. R. S. Forgan, PhD Thesis, The University of Edinburgh, 2008.

28. D. Cupertino, M. McPartlin and A. M. Zissimos, *Polyhedron*, 2001, **20**, 3239-3247.

29. V. V. Lukov, A. A. Knysh, S. N. Lyubchenko, Y. P. Tupolova and V. A. Kogan, *Russ. J. Coord. Chem.*, 2002, **28**, 874-876.

30. V. V. Lukov, Y. P. Tupolova, V. A. Kogan and L. A. Popov, *Russ. J. Coord. Chem.*, 2003, **29**, 335-338.

31. Z. B. Li, R. J. Bemish, D. R. Bill, S. Brenek, R. A. Buzon, C. K. F. Chiu and L. Newell, *American Chem. Soc.*, 2003, **226**, U133-U133.

32. V. H. Crawford, H. W. Richardson, J. R. Wasson, D. J. Hodgson and W. E. Hatfield, *Inorg. Chem.*, 1976, **15**, 2107-2110.

33. D. J. Hodgson, *Prog. Inorg. Chem.*, 1975, **19**, 173-241.

34. J. J. Borras-Almenar, J. M. Clemente-Juan, E. Coronado and B. S. Tsukerblat, *J. Comput. Chem.*, 2001, **22**, 985-991.

35. J. J. Borras-Almenar, J. M. Clemente-Juan, E. Coronado and B. S. Tsukerblat, *Inorg. Chem.*, 1999, **38**, 6081-6088.

36. O. Kahn, *Angew. Chem. Int. Ed.*, 1985, **24**, 834-850.

37. E. Ruiz, P. Alemany, S. Alvarez and J. Cano, *J. Am. Chem. Soc.*, 1997, **119**, 1297-1303.

38. M. Handa, N. Koga and S. Kida, *Bull. Chem. Soc. Jpn.*, 1988, **61**, 3853-3857.

39. J. S. Preston, *Hydromet.*, 1985, **14**, 171-188.

40. J. C. Duff, *J. Chem. Soc.*, 1941, 547-550.

41. Y. Ogata, A. Kawasaki and F. Sugiura, *Tetrahedron*, 1968, **24**, 5001-&.

42. D. F. Shriver and P. W. Atkins, *Inorganic Chemistry*, Third edn., Oxford University Press, Oxford, 1999.

43. H. S. Kim, T. D. Chung and H. Kim, *J. Electroanal. Chem.*, 2001, **498**, 209-215.

44. S. H. Hilal, S. W. Karickhoff and L. A. Carreira, US Environmental Protection Agency, 2003.

45. H. Irving and R. J. P. Williams, *J. Chem. Soc.*, 1953, 3192-3210.

46. S. F. A. Kettle, *Coordination Compounds*, 1st edn., Thomas Nelson and Sons Ltd, London, 1969.

47. R. G. Pearson, *J. Am. Chem. Soc.*, 1963, **85**, 3533.

48. J. Szymanowski and A. Borowiak-Resterna, *Crit. Rev. Anal. Chem.*, 1991, **22**, 519-566.

49. N. N. Greenwood and A. Earnshaw, *Chemistry of the Elements*, First edn., Butterworth-Heinemann, Oxford, 1995.

50. J. B. Lambert, H. F. Shurvell, D. Lightner and R. G. Cooks, *Organic Structural Spectroscopy*, 2nd edn., Prentice Hall, New Jersey, 2001.

51. P. W. Atkins, *Physical Chemistry*, 6th edn., Oxford University Press, Oxford, 1998.

52. B. McCudden, P. Obrien and J. R. Thornback, *Dalton Trans.*, 1983, 2043-2046.

53. P. O'Brien and J. R. Thornback, *Hydromet.*, 1982, **8**, 331-339.

54. F. E. Mabbs and D. Collison, *Electron Paramagnetic Resonance of d Transition Metal Compounds*, Elsevier, Amsterdam, 1992.

55. M. J. Winter, *d-Block Chemistry*, 2004 edn., Oxford University Press, Oxford, 1994.

56. J. N. Van Niekerk and F. R. L. Schoening, *Acta Cryst*, 1953, **6**, 227-232.

57. F. Tuna, L. Patron, Y. Journaux, M. Andruh, W. Plass and J. C. Trombe, *Dalton Trans.*, 1999, 539-545.

58. M. Andruh, I. Ramade, E. Codjovi, O. Guillou, O. Kahn and J. C. Trombe, *J. Am. Chem. Soc.*, 1993, **115**, 1822-1829.

59. P. V. d. Sluis, *Acta crystallogr., Sect. A*, 1990, **46**, 194-201.

60. A. L. Spek, *PLATON- A multipurpose Crystallographic Tool*, (2004) Utrecht University, Utrecht, The Netherlands.

61. F. Valach, *Polyhedron*, 1999, **18**, 699-706.

62. T. Sugiura, H. Yoshikawa and K. Awaga, *Inorg. Chem.*, 2006, **45**, 7584-7586.

63. B. F. Abrahams, M. G. Haywood and R. Robson, *Chem. Commun.*, 2004, 938-939.

64. V. McKee and S. S. Tandon, *Dalton Trans.*, 1991, 221-230.

65. V. McKee and S. S. Tandon, *Chem. Commun.*, 1988, 385-387.

66. S. C. Chan, L. L. Koh, P. H. Leung, J. D. Ranford and K. Y. Sim, *Inorg. Chim. Acta*, 1995, **236**, 101-108.

Chapter 3 Multiloading Copper Sulfate Extractants

The aim of this chapter is to extend the multiloading capabilities of the hydrazone-based metal extractants discussed in Chapter 2 to develop a novel class of zwitterionic multiloading reagents which transport metal *salts* into a water-immiscible solvent. New leach technologies which process copper sulfide ores to generate divalent metal sulfates[1] do not consume the equivalent amount of acid. Conventional metal *cation* reagents do not extract the sulfate anion and this results in a build up of acid at the front end of the circuit. Acid build up adversely affects the extraction process by sufficiently lowering the pH of the feed solution to a pH at which the conventional reagent can no longer deprotonate and extract the metal cation. In the case of bioleaching, acid build up inhibits further leachings as the organisms can die at low pH.[1, 2] Consequently, such processes require both the metal cation and attendant anion to be selectivity transported across the load/strip circuit.

In this chapter the synthesis of seven multiloading metal *salt* extractants is discussed and their ability to extract copper sulfate is examined. Their applicability as commercial reagents is investigated through experiments to evaluate their recyclability and selectivity using copper and mixed metal sulfate feed solutions.

3.1 Zwitterionic Metal Salt Extractants

Polytopic zwitterionic ligands[3] possess both positively and negatively charged binding sites and form overall charge-neutral complexes with metal *cations* and their attendant *anions* as shown in Scheme 3.1. This type of extractant can load metal cations *via* cation exchange, as for the conventional reagents, and attendant anions *via* anion exchange, in a similar manner to the pH-controllable processes using Alamine® reagents which are mentioned in Section 1.5 of Chapter 1. Ideally the protons liberated by deprotonation of the cation-binding site are used in protonation of the anion-binding sites and as a result, the process of *salt* extraction is then co-operative.[3]

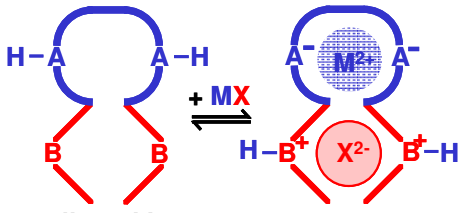

Scheme 3.1: Neutral complex formed by a ditopic zwitterionic ligand and divalent metal cation and anion.

Ligands of the type shown in Figure 3.1 for the extraction of metal salts in the form of diamino-[4-6] and diamino-diamido-[7] functionalised salen-type ligands have been studied by Tasker *et al.*

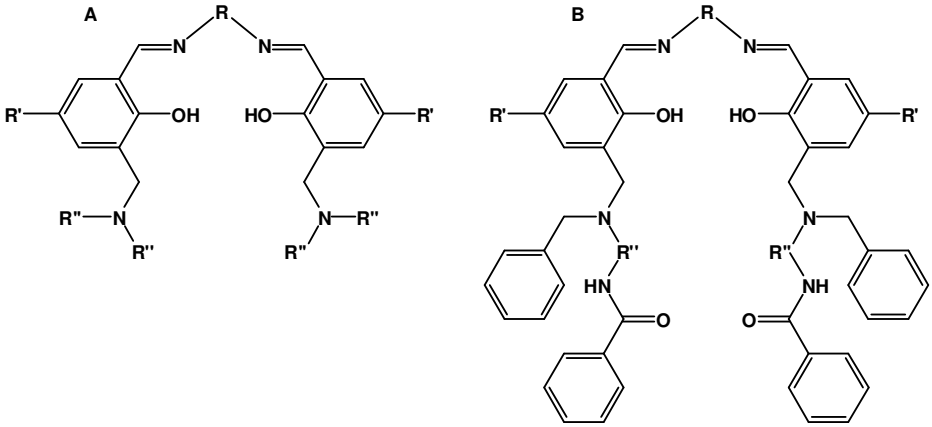

Figure 3.1: Salen-type amino- (A)[4-6] and amino-amido-*o*-substituted (B)[7] metal salt extractants.

The resulting complexes have been isolated and characterised by X-ray crystallography.[4, 7, 8] Of particular interest to the recovery of copper sulfate is the structure shown in Figure 3.2 where the protonated amine hydrogen bond donors are preorganised to provide an ideal cavity for accommodation of a sulfate anion.[9] The preorganisation occurs as a result of the geometry imposed by complexation of the copper cation.

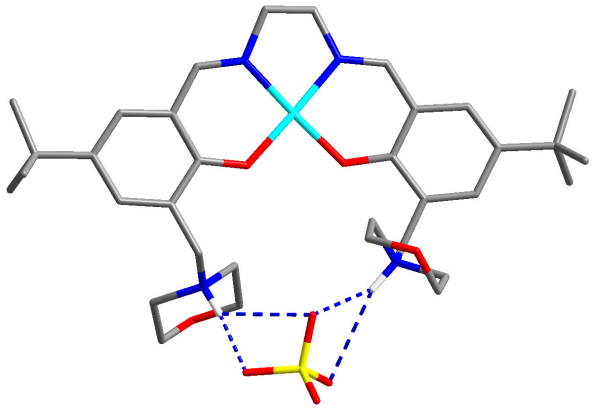

Figure 3.2: Compartmental complexation of $CuSO_4$ by 2,2'-[1,2-ethanediylbis(nitrilomethylidyne)]-bis[4-(*t*-butyl)-6-(4-morpholinylmethyl)-phenol.[9]

An alternative tactic to transport metal salts was inadvertently realised more recently by tethering amines in the 3-position of conventional salicylaldoximes as shown in Scheme 3.2. These were originally designed for recovery of base metal chlorides from chloride streams.[10] As these ligands are based on salicylaldoximes, they are inherently more hydrolytically stable[11] than the imine zwitterionic metal salt extractants previously studied.[12, 13] The resulting metal only complexes are *trans*-coordinated with square planar divalent cations, analogous to those of the unsubstituted salicylaldoxime ligands.[14, 15] The new ligands have been demonstrated to give copper(II) salt complexes containing nitrate, tetrafluoroborate and trifluoroacetate anions,[3] forming the tritopic assemblies shown in Scheme 3.2. The anions not only form hydrogen-bonded contact-ion pairs with the protonated amines but also make short contacts with the copper centres apical positions. Although experimental work has demonstrated the formation of $[Cu(L)_2(SO_4)]$ and $[Cu(L)_2(HSO_4)_2]$, the mode by which sulfate is bound is unknown.[16] Ligands with pendant amine arms in the 5-position were also studied but the resulting complexes were found to be less soluble than those aforementioned.[16]

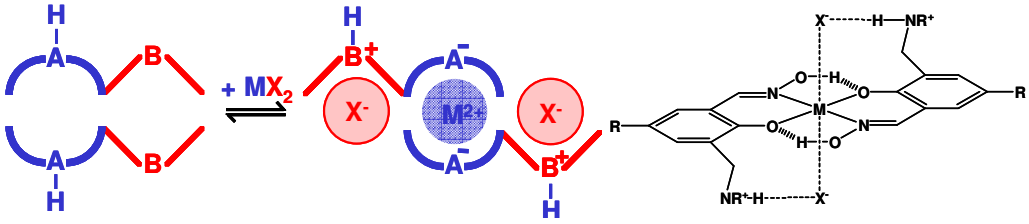

Scheme 3.2: Representations (centre and right) of the *trans* coordinated complexes having tritopic assemblies, as formed by 5-*t*-butyl-3-piperidin-1-ylmethyl-salicylaldoxime (R= *t*-butyl; M=Cu; X = NO_3, BF_4 and CF_3CO_2.[16]

Salicylaldoxime metal salt reagents of the type shown on the right of Scheme 3.2 with amine groups tethered in the 3-positions show high selectivity for chloride over sulfate.[14, 16] In the case of copper, they also transfer more chloride than would be expected by the formation of the tritopic binding motif illustrated in Scheme 3.2. X-ray structure determinations confirmed that 1 : 1 complexes of the type seen in Figure 3.3 were formed with $CuCl_2$ and $CuBr_2$.[14, 16] The ligand is in zwitterionic form with two hydrogen bonds from the piperidinium N-H to the phenolate oxygen atom and the halide. The oximic O-H group also forms a hydrogen bond with the *cis* halide atom.

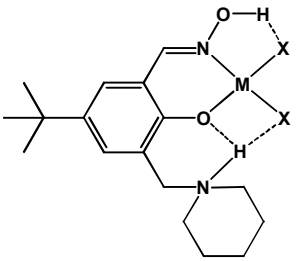

Figure 3.3: Illustration of the solid state copper halide (X = Cl, Br) structures isolated for 5-*t*-butyl-3-piperidin-1-ylmethyl-salicylaldoxime with $CuCl_2$ and $CuBr_2$.[14, 16]

3.2 Multiloading Zwitterionic Metal Salt Extractants

Simultaneous development of metal *salt* extractants[12] and multiloading metal extractants[17] in the Tasker group has led to efforts to develop multiloading *metal salt* extractants.[18] This new class of reagent will not only increase molar transport efficiency of cations relative to conventional reagents, but also facilitate transfer of attendant anions. Previous work[18] in this area has involved ligands which have the potential to transport two divalent cations and either a divalent anion[12] or two monovalent anions[17] to form $[Cu(II)_2(L\text{-}H)_2(X^-)_2]$ and $[Cu(II)_2(L)_2(X^{2-})_2]$ respectively as depicted in Scheme 3.3.[18] The extractants shown at the top and the bottom of Scheme 3.3 could find application in copper chloride or sulfate hydrometallurgical streams respectively.

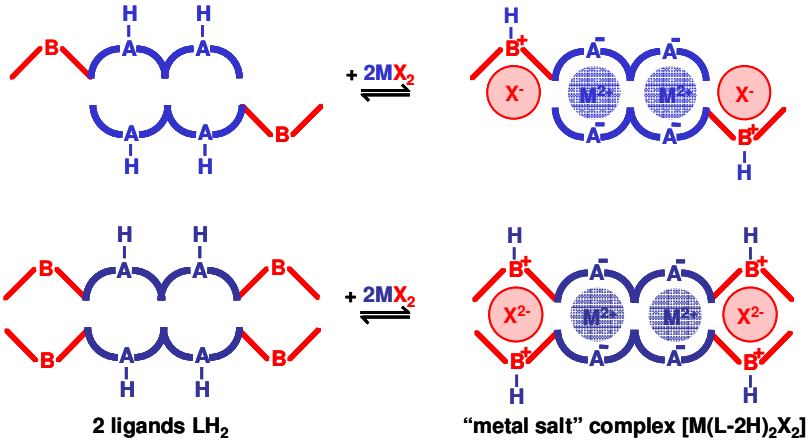

Scheme 3.3: Formation of dinuclear copper salt complexes with *mono-* and *di-* cationic zwitterionic ligands, top and bottom respectively.

The ligand systems previously studied[18] were *mono-* and *di*-amine functionalised hydroxyanil analogues of the dinucleating ligand **7** discussed in Section 2.3 of Chapter 2. The structures of the multiloading metal salt ligands synthesised in the previous work[18] are given in Figure 3.4.

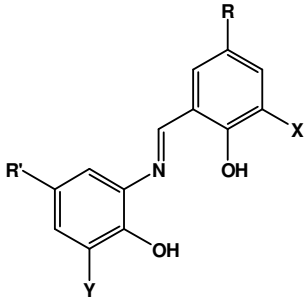

Ligand	20	21	22	23	24	25	26	27
R	*t*-Bu	*t*-Bu	*t*-Bu	*t*-Bu	*t*-Bu	*t*-Bu	Nonyl	Nonyl
R'	*t*-Bu	*t*-Bu	*t*-Bu	*t*-Bu	*t*-Bu	*t*-Bu	*t*-Bu	Nonyl
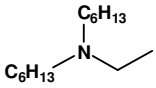	X	Y	X,Y	-	-	-	-	-
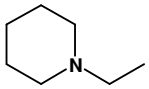	-	-	-	X	Y	X,Y	X	X
H	Y	X	-	Y	X	-	Y	Y

Figure 3.4: Multiloading amine functionalised hydroxyanil ligands previously studied.[18]

Solvent extraction experiments were only carried out for monoamino-substituted ligands **23** and **27**, largely because of the limited solubility of ligands **20**-**27** and the resulting metal salt complexes. Consequently, only complexes of the stoichiometry $[Cu_2(L\text{-}H)_2(SO_4)]$ were isolated.[18] The pH-dependent extraction profile for **27** is shown in Figure 3.5.

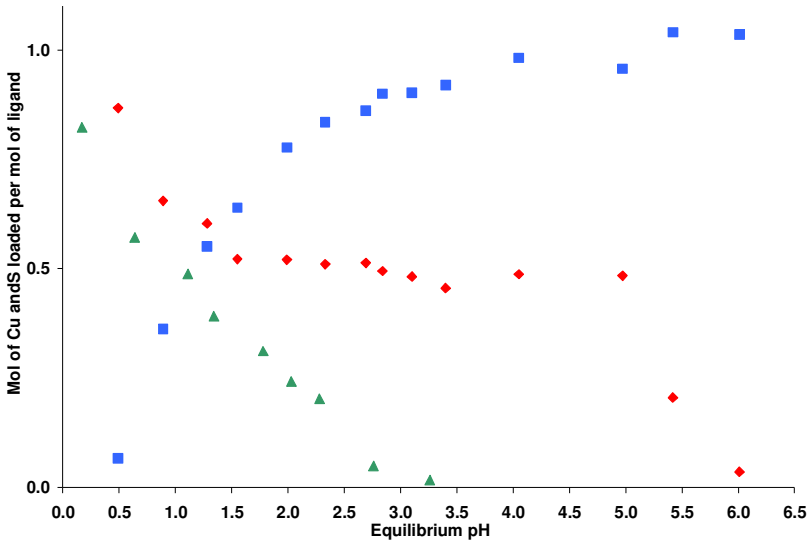

Figure 3.5: pH-dependent copper (■) and sulfate (♦) loading by chloroform solutions of **27** (0.0025 M) from copper sulfate (0.0025 M) and sulfate loading by **27** in the absence of copper (▲).

An interesting feature of the extraction results for **27** is the cooperative binding of copper and sulfate. In the absence of copper, the $pH_{½}$ for sulfate loading is *ca.* pH 1.75 and the plateau corresponding to formation of $[Cu_2(\mathbf{27}\text{-}H)_2(SO_4)]$ between 1.5 < pH < 5.0 is no longer observed. Below pH 1.0, the sulfate loading increases beyond 1:2 indicating double protonation of the system and formation of two $[(\mathbf{27}+H)(HSO_4)]$ contact-ion pairs. For these reasons, and based on the ratios of Cu:S loading of the organic phase, it was hypothesised[3, 18] that the speciation takes the form depicted on the left in Figure 3.6 at pH < 3.0 when copper loading begins to decrease, and that on the right at 5.0 < pH < 3.0 where sulfate is the dominant species.[19]

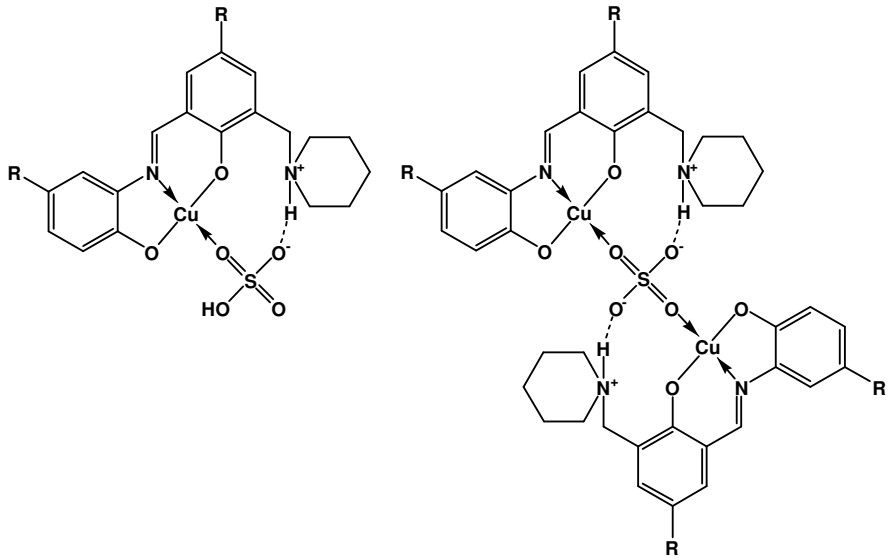

Figure 3.6: [Cu(L-H)(HSO_4)] (left) and [Cu_2(L-H)$_2$(SO_4)] (right) formed by **27** pH < 3.0 and 3.0 < pH < 5.0, respectively.

When the industrial viability of ligand **23** was examined in sequential load/strip cycles, it was found that it was hydrolysed when contacted with strong acid (150 g L^{-1}) and the constituent parts transferred to the aqueous phase. Increasing the alkyl chain bulk of R from *t*-butyl to *iso*-nonyl (**27**) improved the lifetime of the reagent significantly, but there were still losses on repeated load/strip cycles. Moreover, extraction from a mixed copper(II)/iron(III) feed solution showed that iron is preferentially extracted by this class of ligand. This is highly undesirable as transfer of iron to the electrolyte increases the current required to electro-deposit copper due to the oxidation and reduction of ferrous and ferric ions at the anode and cathode respectively.[20-22]

The high hydrolytic stability of hydrazones relative to imines[11] and the good selectivity for copper over iron, cobalt, nickel and zinc demonstrated by the "metal-only" hydrazone extractants discussed in Chapter 2 (see Section 2.6) identified them as good candidates for development of a new class of multiloading metal *salt* extractants.

3.2.1 Design of Hydrazone-Based Multiloading Copper Salt Extractants

The design of *tri*nucleating metal salt extractants using the ligand architecture shown in Figure 3.7 as discussed in Chapter 2 was considered unrealistic. Complexation of three Cu(II) cations from a copper sulfate stream would require three attendant SO_4^{2-} anions to be bound. To accommodate these, the assembly would need to have six easily protonated basic sites to form contact ion-pairs with the anions. If the structure of the metal binding site was retained, the protonatable sites could be integrated into the X, Y or Z positions of the structure shown in Figure 3.7.

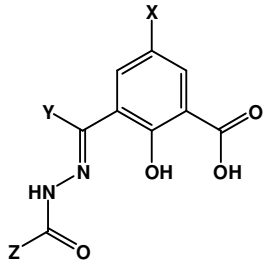

Figure 3.7: Sites (X, Y, and Z) available for incorporation of amines into the triacidic ligands discussed in Chapter 2.

A ligand of this nature is unlikely to meet some of the target S-criteria required in a commercially viable extractant as outlined in Section 1.5.1. The criteria which are expected to be most compromised include solubility and synthesis.

Solubility: the resulting tris-sulfato complex will contain a large number of polar groups. Consequently, it is expected to have very limited solubility in hydrocarbon solvents and may even be preferentially solvated in the aqueous phase. To ensure solubility in the organic phase, considerable lipophilic character will be required. Reasonable assumptions regarding the solubility of the possible tris-sulfato complexes can be made if lipophilic groups were placed in the X, Y, or Z positions. The findings for the trinucleating ligands and trinuclear complexes discussed in Chapter 2 and those of previous work in the area of metal salt extraction have been considered when arriving at these conclusions. The nature of the substituent in position Z was found to greatly influence the solubility of the triacidic ligands, *c.f.* **L6** and **L9**, therefore modification here should be avoided. Substitution of the alkyl

group 5-alkyl-salicylaldoximes with a dihexylaminomethyl group resulted in the formation of less soluble complexes[16] than those with the dihexylaminomethyl group in the 3-positon which are shown in Scheme 3.2. Consequently substitution of X and Z in Figure 3.7 were ruled out, leaving Y as the only remaining site available. Replacement of proton Y with an alkyl-amine group would be beneficial in terms of industrial applicability by improving resistance to hydrolysis. The increased hydrophobicity and steric bulk around the azomethine carbon atom should hinder acid attack and approach of hydroxonium ions and water molecules. Greater hydrolytic stability is displayed by 2-hydroxybenzophenone analogues of salicylaldoximes[23] and the amino-salen metal salt extractants[12] of type **A** shown in Figure 3.1. However, for this to be realised, a new class of ketone precursor would need to be synthesised which influences the synthesis S-criteria.

Synthesis: the practicability of synthesis must be considered when designing a viable commercial reagent to be produced on a large scale. Incorporation of additional protonatable sites will require additional reaction steps; these should be kept to a minimum, be high yielding, and use readily available inexpensive precursors. The addition of three amine groups and associated alkyl groups to aid solubility would not only increase the complexity of synthesis but add to the molecular weight and reduce the mass transport efficiency of the end product which already requires additional formylation and oxidation to introduce the carboxylic acid group.

As a result of the conclusions drawn above and the successful extraction of metal salts by the dinucleating salicylaldehyde-hydroxyanil ligands previously studied,[18] the new class of metal salt extractant selected for this study are capable of selectively extracting two copper cations and their attendant sulfate anions. The ligands discussed in this chapter were initially designed to carry two mol of sulfate by the mechanism shown in Scheme 3.4, rather than one mol achieved by the salicylaldehyde-hydroxyanil metal salt extractants.[18]

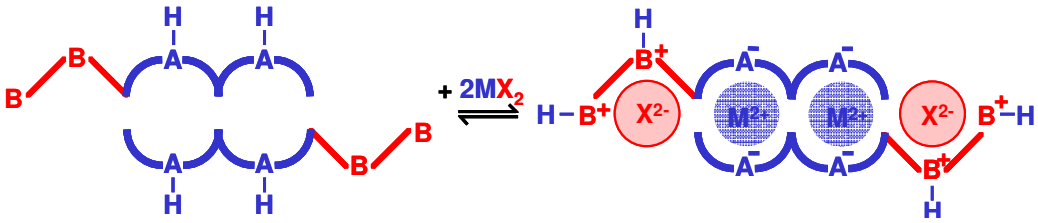

Scheme 3.4: Graphical representation of the $[Cu_2(L)_2(SO_4)_2]$ complexes formed by the ligands discussed in this chapter which are of dual zwitterionic nature.

Hydrazones demonstrate greater hydrolytic stability than imines.[11] Accordingly, the diacidic salicylaldehyde-hydrazones which were found to form phenolate bridged dinuclear copper complexes of the type discussed in Sections 2.3.2 and 2.3.3 were selected as the basic building block rather than the salicylaldehyde-hydroxyanil analogues. The salicylaldehyde precursors to these ligands are generally alkylated in the 5-position to impart solubility in water-immiscible organic solvents. Therefore, the only easily accessible site available for substitution is the 3-position, X on left of Figure 3.8.

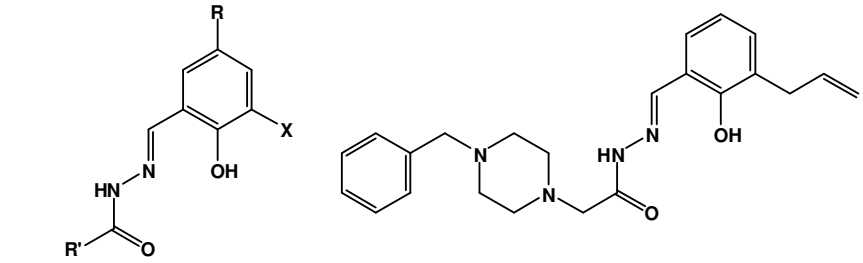

Figure 3.8: Generic structure of the dinucleating salicylaldehyde-acylhydrazones (X = H) discussed in Section 2.3 and a piperazino derivative (SAC-1) patented for its anticancer activity.[24]

The $pH_{½}$ values of copper loading for 5-alkyl-salicylaldehyde-acyl-hydrazone extractants have been found[17] to be between pH 2 and 3. Therefore, when the ligand is fully loaded with copper the predominant sulfate species present in the aqueous phase will be sulfate.[6, 19] As a result, the anion receptors chosen for application here were piperazine groups because these are capable of being doubly protonated to give reagents of the type shown in Scheme 3.4. The piperazine unit can be tethered[25] in

the 3-position (Z) of the 5-alkylsalicylaldehyde-acylhydrazone or, alternatively, to the hydrazone precursor,[24, 26] as illustrated in Figure 3.8.

The piperazine functionalised salicylaldehyde hydrazone (SAC-1) shown in Figure 3.8 has demonstrated potential as an anticancer compound against colon cancer cells through the activation of a protein central to cell death.[24, 26] The pendant benzylpiperazine group in SAC-1, the dihexylaminomethyl and piperidinomethyl groups used in the metal salt extractants previously studied in the Tasker group and benzhydrylpiperazine were incorporated into the design of the ligands studied in this thesis: these are listed in Figure 3.10.

To quantitatively transfer copper sulfate, the piperazine units in **L14**-**L17** must be doubly protonated to accommodate a sulfate anion. These protons would be provided by phenol and acylhydrazone groups to generate a dianionic unit to bind to three sites of a "square" planar Cu(II) ion. Effective binding of sulfate requires the piperazine to adopt a chair conformation as shown in Figure 3.9 for examples where the piperazine is tethered *via* the hydrazone function (**L14** and **L15**) or in the 3-position (**L16** and **L17**) or, Z and Y in Figure 3.10.

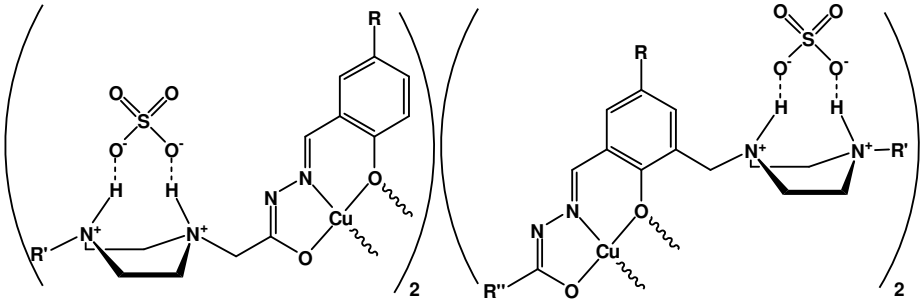

Figure 3.9: Proposed structures of the metal salt complexes $[Cu_2(L)_2(SO_4)_2]$ formed by **L14** or **L15** (left) or **L16** or **L17** (right).

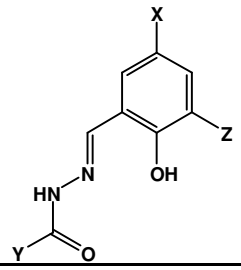

	X	Y	Z
L14	*t*-Bu	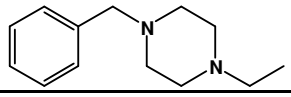	H
L15	Nonyl	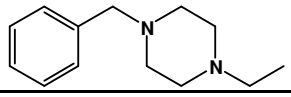	H
L16	*t*-Bu	C_7H_{15}	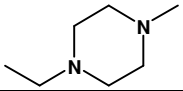
L17	Nonyl	C_7H_{15}	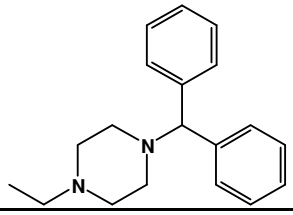
L18	*t*-Bu	C_7H_{15}	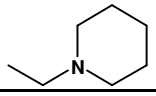
L19	*t*-Oct	C_7H_{15}	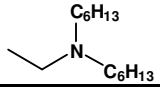
L20	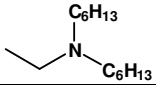	C_7H_{15}	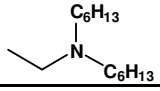

Figure 3.10: The mono- and di-amino functionalised salicylaldehyde-hydrazone ligands prepared for evaluation as metal salt extractants in this thesis.

3.3 Ligand Synthesis

3.3.1 Piperazinomethyl Ligands L14-L17

L14 and **L16** were designed to compare the efficacy of having the piperazino group tethered in the 3-position of the benzene ring or in the acyl group of the hydrazone.

Ligand **L14** was synthesised by Schiff base condensation of 5-*t*-butylsalicylaldehyde (**30**) and 4-benzylpiperazinoacetic acid hydrazide (**32**). The latter was prepared by the method of Putt *et al.*[26] from 1-benzylpiperazine and hydrazine hydrate *via* the ester intermediate ethyl-(4-benzylpiperazino)acetate. It was expected that the *t*-butyl group of **L14** would increase the probability of obtaining a single crystal of any resulting copper sulfate complexes for X-ray structure determination. The low solubility of the resulting complexes in solvent extraction processes led to the synthesis of **L15** where *t*-butyl group in **L14** is replaced by a mixed isomer nonyl group.

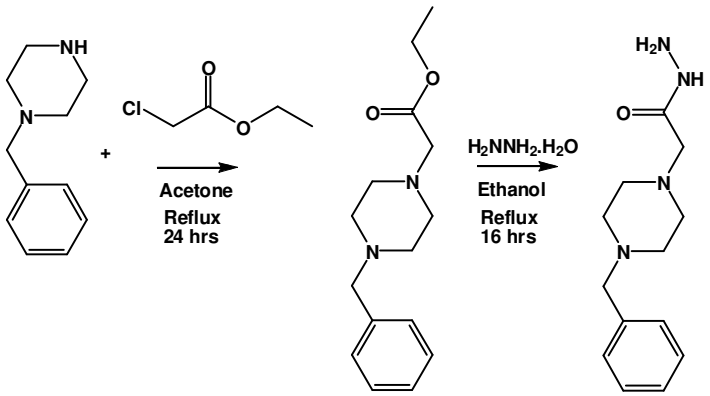

Scheme 3.5: Preparative route to 4-benzylpiperazinoacetic acid hydrazide.[26]

L15 was synthesised by the same procedure as **L14** using 5-nonylsalicylaldehyde. Unfortunately, solubility of the resulting complex was insufficient to allow effective solvent extraction experiments to be performed.

L16 was prepared from 3-bromomethyl-5-*t*-butylsalicylaldehyde (**33**), *via* treatment with 1-methylpiperazine in the presence of potassium carbonate desiccant as described by Wang *et al.*[25] The resulting piperazino-functionalised salicylaldehyde, 5-*t*-butyl-3-(4-methylpiperazinomethyl)salicylaldehyde (**34**), was treated by Schiff

base condensation with octanoic hydrazide to generate **L16**. Again, it was anticipated that incorporation of the *t*-butyl group would provide samples for characterisation by X-ray crystallography.

L17 was created in a similar manner to **L16** from 3-bromomethyl-5-nonylsalicylaldehyde (**35**), 1-benzhydrylpiperazine and octanoic hydrazide. Incorporation of the 1-benzhydrylpiperazino group into **L17** resulted in sufficient solubility of the ligand and its complexes to allow extraction experiments to be performed over a wide range of pH (see Section 3.4.1).

3.3.2 Piperidinomethyl Ligand L18

Ligand **L18** was prepared and tested as a consequence of the poor extractive properties of **L14**-**L17** (see Section 3.4.1) in a bid to establish whether incorporation of previously tried and tested[12, 16, 18] piperidinomethyl groups would lead to effective extractants. **L18** was synthesised by Schiff base condensation of octanoic hydrazide using a sample of 3-piperidinyl-5-*t*-butylsalicylaldehyde previously prepared by Henry.[18]

3.3.3 Dihexylaminomethyl Ligands L19 and L20

The dihexylaminomethyl group was incorporated into the salicylaldehyde precursors for these new ligands because it has previously been found to impart high solubility in metal salt extractants and their resulting complexes in chloroform.[12]

L19 and **L20** were prepared by Schiff base condensation of octanoic hydrazide with 3-((dihexylamino)methyl)-5-*t*-octyl-salicylaldehyde (**36**) and 3,5-bis((dihexylamino)methyl)-salicylaldehyde (**37**), respectively. Precursors **36** and **37** were prepared by reaction of samples of the Mannich base, N-ethoxymethyldihexylamine, previously prepared by Forgan[16] and Henry,[18] with *t*-octyl-salicylaldehyde and salicylaldehyde respectively.

3.4 Solvent Extraction

A key objective for metal salt extractants is to obtain maximum loading of both cations and attendant anions within the same pH-range. An idealised loading graph for the ligands studied in this chapter is plotted in Figure 3.11, where the shaded area represents the formation of $[Cu_2(L)_2(SO_4)_2]$.

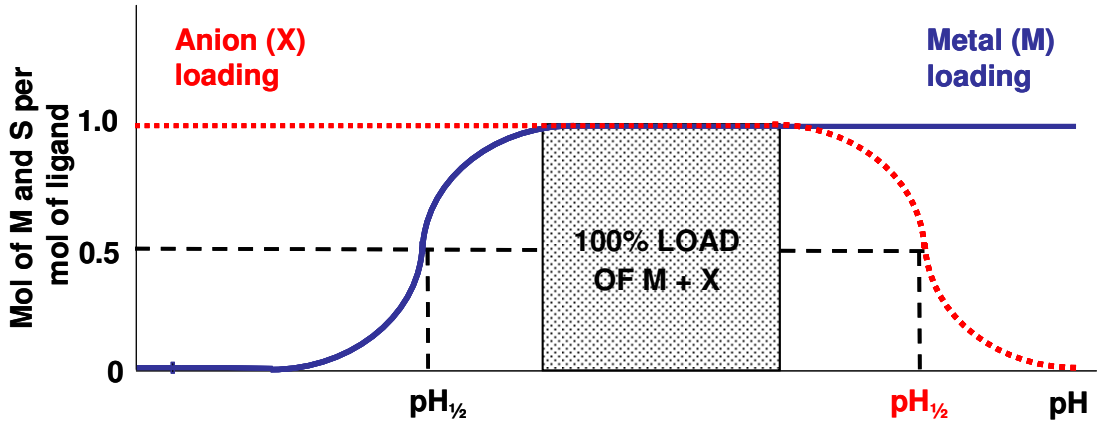

Figure 3.11: Idealised metal cation (blue) and attendant anion (red) binding profiles as a function of pH of the aqueous phase for the dinucleating ligands in this chapter. For **L18** and **L19**, containing only one pendant amino group, the anion loading will be halved.

Solvent extraction experiments were carried out by contacting chloroform solutions of the ligands (5 ml, 0.0025 M) with aqueous copper sulfate solutions (5 ml, 0.0120 M) of varying pH, adjusted by addition of sulfuric acid or sodium hydroxide. The phases were stirred for 16 hrs and separated. The "equilibrium pH" of the aqueous phase was recorded and the copper and sulfate content of the organic phase measured by ICP-OES. The copper and sulfate loading, recorded as a fraction of the maximum loading capacity expected for formation of $[Cu_2(L)_2(SO_4)_2]$, were plotted against the the equilibrium pH of the aqueous phase.

3.4.1 Copper Sulfate Extraction by Piperazinomethyl Ligands L14-L17

Unfortunately, the piperazine functionalised ligands, **L14**-**L17**, proved to be unsuitable for solvent extraction studies as the resulting copper sulfate complexes were of either limited solubility in chloroform (**L14** and **L15**) or in the case of **L16**, were found to be soluble in the aqueous phase. Replacement of the methylpiperazine and *t*-butyl groups of **L16** with benzhydrylpiperazine and nonyl groups respectively (**L17**) did yield complexes which were soluble in the organic phase. However, the maximum sulfate loading was *ca.* 20% of the theoretical maximum based on formation of $[Cu_2(L)_2(SO_4)_2]$. This could be a result of steric hindrance of the piperazine protons caused by the bulky phenyl groups of the benzhydrylpiperazine.

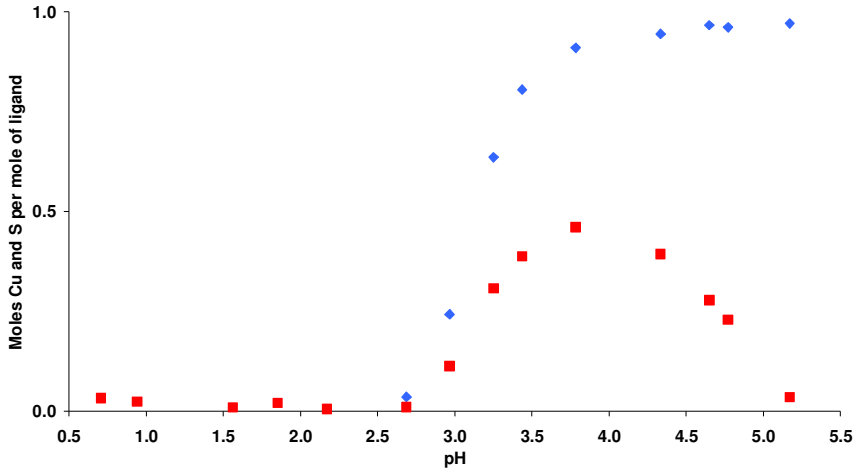

Figure 3.12: The pH-dependence of copper (♦) and sulfate (■) loading by a chloroform solution of **L16** (0.0025 M) from copper sulfate (0.0120 M).

Figure 3.12 shows the S-curves obtained for copper sulfate loading by **L16**. These plots appear to provide a good example of cooperative extraction of copper and sulfate, although only 50% of the ligand's potential sulfate-capacity is achieved. Unfortunately, below pH 3.25, the complex transfers to the aqueous phase, evident by the appearance of a green coloured complex in the aqueous phase. Consequently no $pH_{½}$ value for sulfate-loading can be extrapolated. The data presented in Figure 3.12 suggest that the complex formed in the organic phase is $[Cu_2(L\text{-}H)_2(SO_4)]$ at *ca.* pH 3.75. Below this pH the transfer of the complex to the aqueous phase is consistent with the formation of $[Cu_2(L)_2(SO_4)_2]$.

The hydrophilic complex formed by **L16** may be preferentially soluble in the aqueous phase as a result of the large number of polar functional groups present when two sulfates are bound in $[Cu_2(L)_2(SO_4)_2]$. To investigate whether aqueous solubility of the complex formed by **L16** is caused by two sulfate groups being bound in the complex, the pendant *piperaz*inomethyl group was replaced with a *piperid*inomethyl group in **L18**. This will adversely affect the ligand's sulfate-carrying capacity, cutting it by half because there are only two pendant ammonium groups in the dinuclear assembly. A possible structure for an assembly, $[Cu_2(\mathbf{L}\text{-}H)_2(SO_4)]$, formed by **L18** is shown in Figure 3.13.

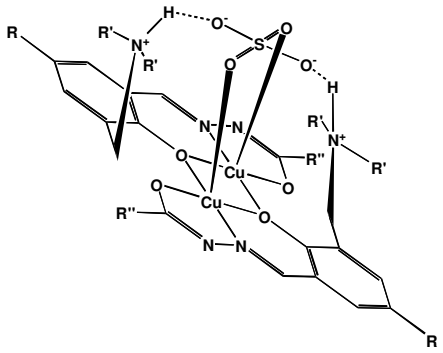

Figure 3.13: A possible sulfate-binding mode in dinuclear complexes of the mono-amino functionalised ligands **L18** and **L19**.

Although the reduced number of polar groups in **L18** did reduce solubility in the aqueous phase, the resulting copper sulfate complex was not suitably soluble in chloroform to permit extraction studies. It is therefore possible that the complex formed by **L16** was of limited solubility in chloroform as a result of the combined effects caused by the hydrophilicity of the polar sulfate groups and a lack of lipophilicity in the ligand. The piperidinomethyl group of **L18** was replaced with a dihexylaminomethyl group and the *t*-butyl group in the 5-position was replaced with a *t*-octyl in **L19** to increase the lipophilicity of the mono-amino ligand.

3.4.2 Copper Sulfate Loading by Dihexylaminomethyl Ligand L19

Organic solubility was vastly improved by increasing the lipophilicity of **L18** to give **L19**. The copper-loading S-curve for **L19** (Figure 3.14) indicates the ligand extracts one mol of copper per mol of ligand and has a $pH_{½}$ value of *ca*. 0.75 in chloroform. This suggests that the ligand is not only significantly stronger than the analogous *di*- and *tri*-nucleating hydrazone ligands **3** and **L7** without pendant amine groups ($pH_{½}$ *ca*. 2-3), but also stronger than the commercial salicylaldoxime extractants ($pH_{½}$ *ca*. 1.5 in chloroform).

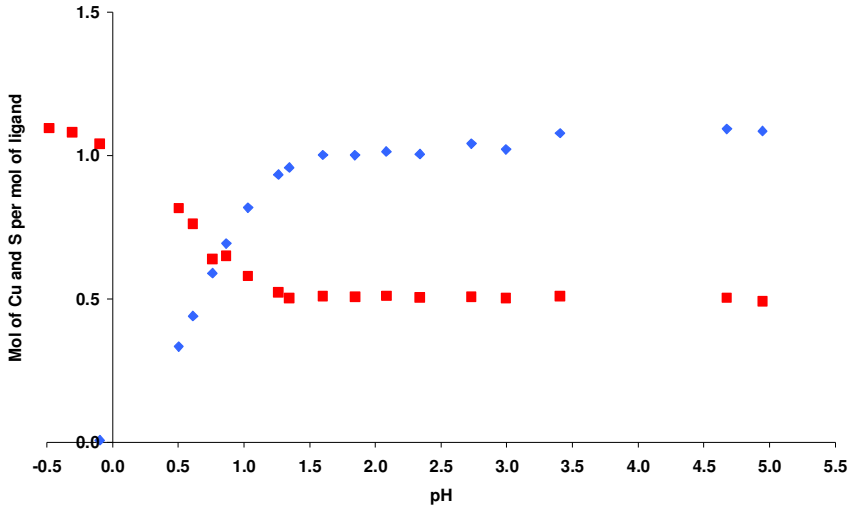

Figure 3.14: The pH-dependence of copper (♦) and sulfate (■) loading by a chloroform solution of **L19** (0.0025 M) from copper sulfate (0.012 M).

Figure 3.14 also shows that the ligand is capable of extracting sulfate; one mol of sulfate is extracted per two mol of ligand between pH 1.5 and 5.5 and is consistent with the formation of a $[Cu_2(L\text{-}H)_2(SO_4)]$ complex structure similar to that suggested in Figure 3.13. The very wide pH-range which this complex prevails over suggests it is particularly stable. An alternative structure to that shown in Figure 3.13 corresponding to 2:2:1 Cu:L:S stoichiometry $[Cu_2(L\text{-}H)_2(SO_4)]$ was suggested[18] for the previously studied hydroxyanil multiloading metal salt extractants. This is shown in Figure 3.15.

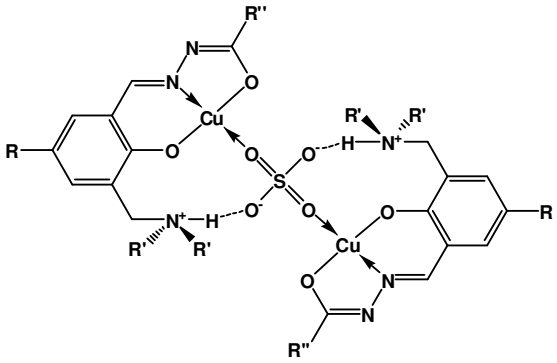

Figure 3.15: Alternative structure to that proposed in Figure 3.13 for the $[Cu_2(\mathbf{L19}\text{-}H)_2(SO_4)]$ species extracted into chloroform solution, based on related anil systems.[18]

Once copper begins to be stripped from the complex as the pH is lowered below 1.5, the amount of sulfate in the organic phase increases and plateaus at 1 mol per mol of ligand at *ca*. pH -0.5. This corresponds with one hydrogensulfate per ligand as would be expected when the amine in the free ligand is protonated to give $[(\mathbf{L19}\text{+}H)(HSO_4)]$ and occurs at pH 1.75 where hydrogensulfate becomes the principal species in the aqueous sulfate solution.[19] This behaviour also supports the proposition that the loading of copper and sulfate by **L19** is cooperative and that the resulting complex $[Cu_2(L\text{-}H)_2(SO_4)]$ is stable over a wider pH-range than expected. It may also be concluded that within this pH-range the ligand is selective for sulfate over hydrogensulfate. The loading and extraction equilibria at pH > 1.5 and < 0.5 respectively are given below.

Load: $\quad 2Cu(II) + SO_4 + 2\mathbf{L19} \rightleftharpoons [Cu_2(\mathbf{L19}\text{-}H)_2(SO_4)] + 2H^+$

Strip: $[Cu_2(\mathbf{L19}\text{-}H)_2(SO_4)] + 4H^+ + H_2SO_4 \rightleftharpoons 2Cu(II) + 2[(\mathbf{L19}\text{+}H)(HSO_4)]$

Having demonstrated that the dihexylaminomethyl pendant arm can increase the solubility of the metal salt complexes relative to the piperidinomethyl group, a second dihexylaminomethyl group was incorporated into the basic salicylaldehyde substructure to increase both the solubility and the sulfate-carrying capacity of **L19** in **L20**.

3.4.3 Copper Sulfate Loading by L20

Ligand **L20** was designed to permit the loading of two mol of copper sulfate to form $[Cu_2(\mathbf{L20})_2(SO_4)_2]$, as originally intended at the outset of this work through incorporation of two dihexylaminomethyl groups in the 3- and 5-positions of the salicylaldehyde precursor. Each molecule of **L20** has two protonatable amine sites, allowing it to form a charge-neutral complex $[Cu_2(\mathbf{L20})_2(SO_4)_2]$ if **L20** is in a 2+/2- zwitterionic form. This should increase the Cu:L:S stoichiometry to 2:2:2, enabling quantitative transfer of copper sulfate. The extraction data for **L20** are shown in Figure 3.16. These indicate that **L20** extracts the desired Cu:L:S species of stoichiometry 2:2:2 within a relatively narrow pH range of *ca.* 2.0 < pH < 2.5 which could have the structure shown in Figure 3.17. The $pH_{½}$ value for copper-loading is approximately 1 pH unit higher (1.75) than that of **L19** and, like **L19**, is a significantly stronger extractant than the "copper-only" hydrazone analogues, **3** and **L7**, and is very similar to that of the commercial salicylaldoximes. It could therefore potentially find application in copper recovery circuits working within the conventional pH ranges.

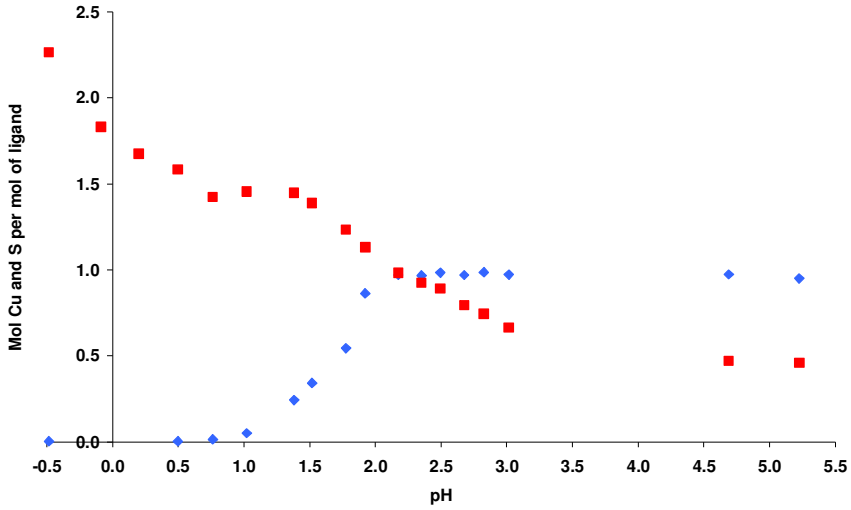

Figure 3.16: The pH-dependence of copper (♦) and sulfate (■) loading by a chloroform solution of **L20** (0.0025 M) from copper sulfate (0.012 M).

Comparison of S-curves measured for **L19** and **L20** between 3.5 < pH < 5.5 indicates that both form species with Cu:L:S stoichiometry, 2:2:1, within this range. This is an

unexpected result as **L20** has twice as many protonatable amine sites and therefore the ability to carry twice the number of mol of sulfate. This may suggest that both ligands form a similar type of complex within this pH range, and the structures postulated for the **L19** complex $[Cu_2(\mathbf{L19}\text{-}H)_2(SO_4)]$ shown in Figure 3.13 and in Figure 3.15 can also be applied to the mono-deprotonated form of **L20** as in $[Cu_2(\mathbf{L20}\text{-}H)_2(SO_4)]$. This monosulfonato complex appears to have an especially stable structure and protonation of the dihexylaminomethyl group in the 5-position to form a species similar to that in the middle of Figure 3.18 only occurs at lower pH (< 2.0).

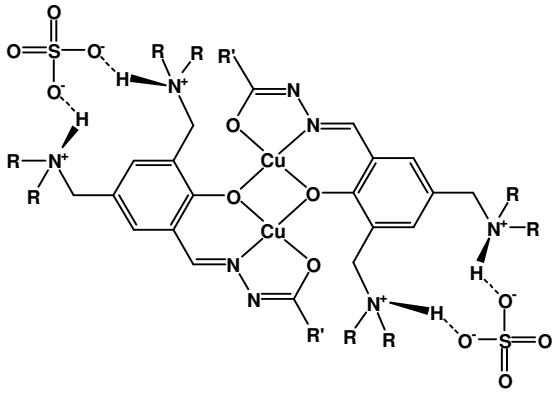

Figure 3.17: A possible structure of the copper sulfate complex $[Cu_2(\mathbf{L20})_2(SO_4)_2]$ formed by **L20**.

Below pH 2.0 copper loading decreases to zero at pH 0.75 and sulfate loading increases to a plateau between 0.5 < pH < 1.5 which corresponds 1.5 mol of sulfate per mol of ligand. The complex formed here is more likely to have a 2:3 stoichiometry, consistent with reprotonation of the phenol and amidate and protonation of the dihexylaminomethyl groups in the 5-position. A $[(\mathbf{L20})_2(SO_4)(HSO_4)_2]$ complex with a sulfate anion bridging two **L20** molecules can be proposed as shown in Figure 3.18 (middle), assuming the copper complexes form the structures shown in Figure 3.13 and in Figure 3.15.

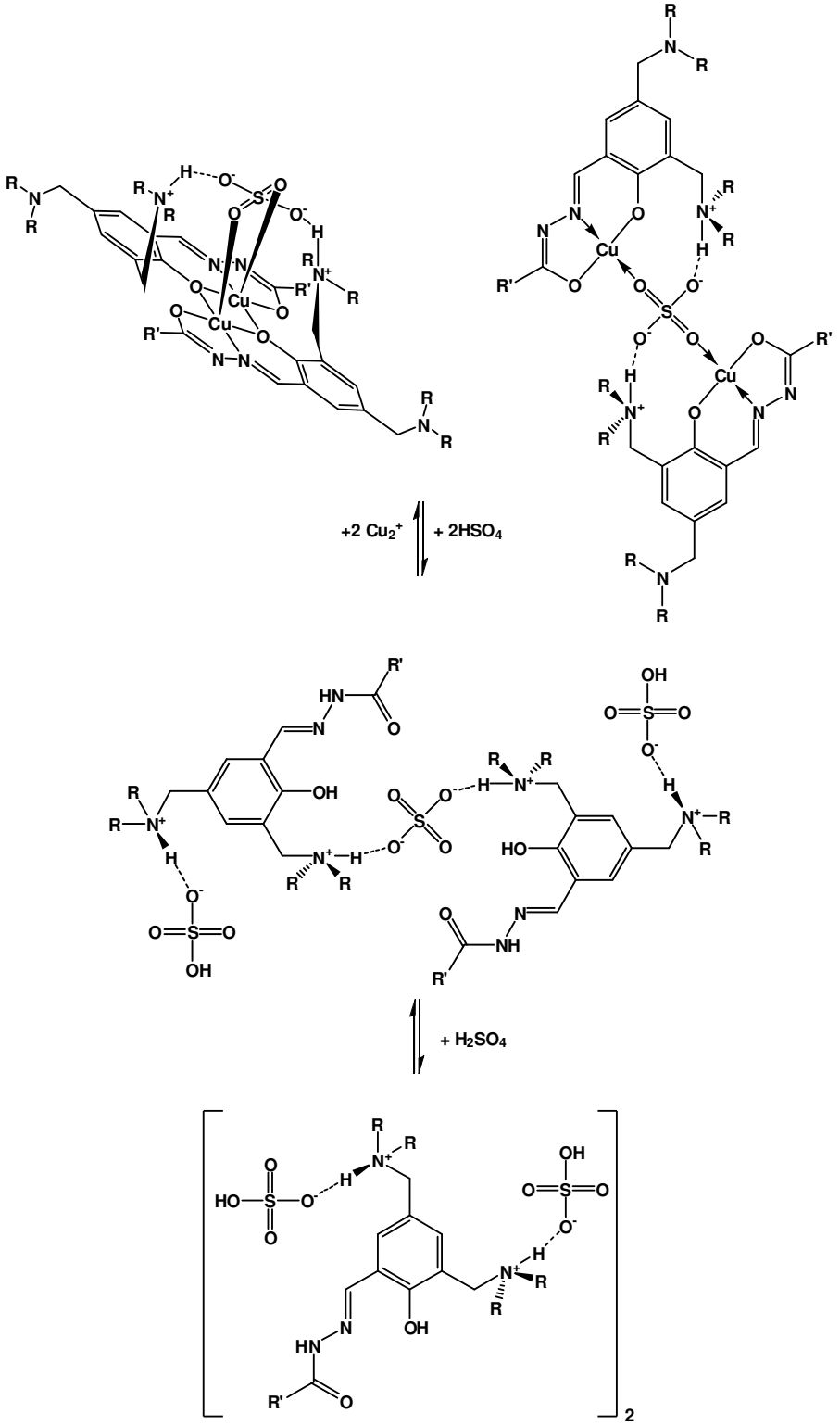

Figure 3.18: Conversion of $[Cu_2(\mathbf{L20}\text{-}H)_2(SO_4)]$ to $[(\mathbf{L20}+2H)_2(SO_4)(HSO_4)_2]$ as the pH is lowered from pH 3.5 to 0.5, resulting in displacement of copper and uptake of two hydrogensulfate ions followed by protonation of the bridging sulfate anion and incorporation of an additional sulfate anion to form two $[(\mathbf{L20}+2H)(HSO_4)_2]$ contact-ion pairs.

This theory is supported by the observed increase in sulfate content of the organic phase as the pH is decreased below 0.5, which would result in an increase in hydrogensulfate concentration and subsequent break-up of the $[(\mathbf{L20}+2)_2(SO_4)(HSO_4)_2]$ structure to form two $[(\mathbf{L20}+2)(HSO_4)_2]$ units. The increase of sulfate concentration in the organic phase to greater than the ligand's carrying capacity (2S : 1**L20**) below *ca*. pH -0.25 could arise from protonation of the hydrazone group but this has not been observed with this class of ligands previously.

The resulting loading and stripping equilibria for **L20** at pH > 2.5 and < 1.5 respectively are:

Load: $2Cu(II) + SO_4 + 2\mathbf{L20} \rightleftharpoons [Cu_2(\mathbf{L20}\text{-}H)_2(SO_4)] + 2H^+$

Strip: $[Cu_2(\mathbf{L20}\text{-}H)_2(SO_4)] + 4H^+ + 3H_2SO_4 \rightleftharpoons 2Cu(II) + 2[(\mathbf{L20}+2H)(HSO_4)_2]$

It is clear that the novel extractants **L19** and **L20** can transfer copper(II) ions and sulfate to a water-immiscible solvent from an aqueous feed solution. Electrospray mass spectrometry evidence for the composition of assemblies formed in the extraction experiments described above is presented in Section 3.4.4. To explore their industrial applicability, the hydrolytic stability and selectivity for copper over other metal cations were investigated under conditions similar to those in a commercial plant (see Section 3.5).

3.4.4 Characterisation of Metal Salt Complexes by Electrospray Mass Spectrometry

Mass spectrometry proved useful in establishing the speciation of the metal salt complexes formed in extraction experiments due to the distinctive isotope patterns obtained for multinuclear copper complexes. The spectra obtained for the complexes formed by ligands **L14**-**L20** are given in Table 3.1 below. The extracts from solvent extraction experiments were evaporated to dryness and analysed as methanolic solutions. The samples selected correspond to those with the highest simultaneous loading of copper and sulfate. In all cases, the spectra suggest that the extracted species are dinuclear copper complexes. In some cases (**L16**, **L18** and **L20**) the

attendant anion was also observed and characterised as sulfate. The simulated and experimental spectra observed for **L18**, **L19** and **L20** are shown in Figure 3.19. The relative abundances of the isotopic distribution pattern of the complex formed by **L20** do not match the simulated values as well as for the other complexes: this is due in part to the poorer resolution at high molecular mass.

Table 3.1: Species detected in electrospray mass spectra of organic extracts from aqueous copper(II) sulfate solutions formed by **L14**-**L20**.

Ligand	*m/z*	Complex Cation
L14	941.59	$[Cu_2(L\text{-}2H)_2]H^+$
L15	1081.88	$[Cu_2(L\text{-}2H)_2]H^+$
L16	1083.24	$[Cu_2(L\text{-}H)_2SO_4]H^+$
L17	1429.54	$[Cu_2(L\text{-}2H)_2]H^+$
L18	1053.23	$[Cu_2(L\text{-}H)_2SO_4]H^+$
L19	1267.68	$[Cu_2(L\text{-}2H)_2]H^+$
L20	1535.80	$[Cu_2(L\text{-}H)_2)SO_4]H^+$

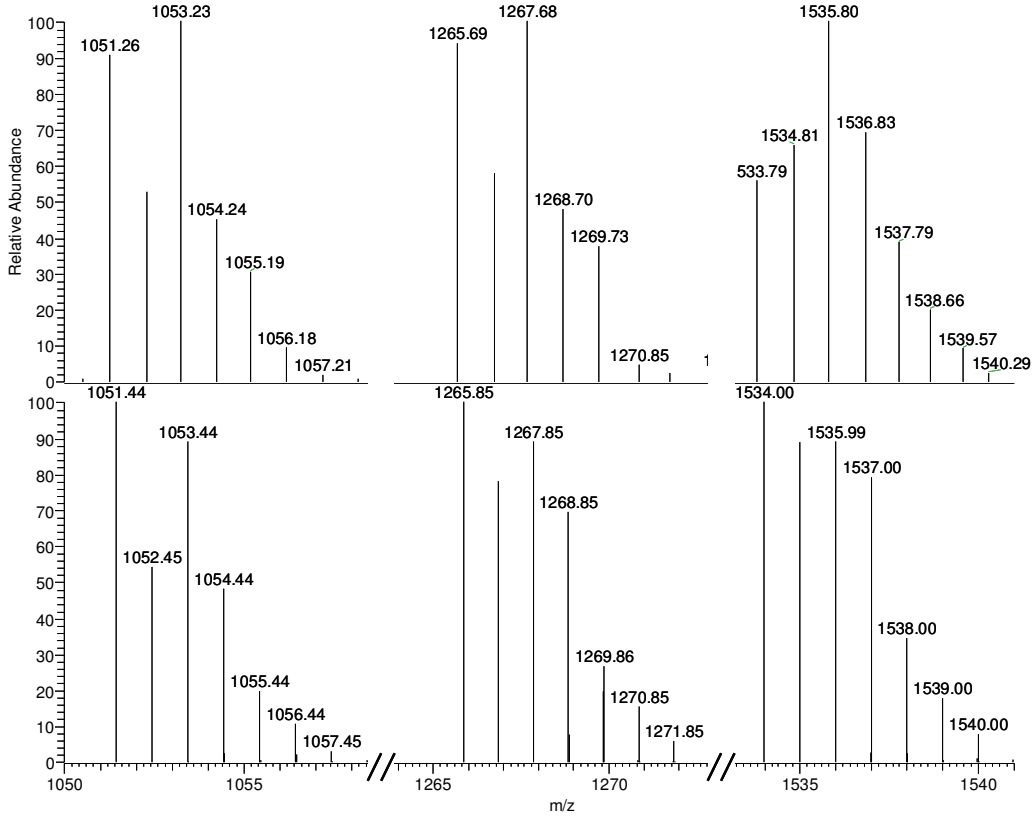

Figure 3.19: Collage of the simulated (bottom) and experimental (top) electrospray mass spectra for complex ions $[Cu_2(\mathbf{L18}\text{-}H)_2SO_4]H^+$, $[Cu_2(\mathbf{L19}\text{-}2H)_2]H^+$, $[Cu_2(\mathbf{L20}\text{-}H)_2)SO_4]H^+$ from left to right respectively.

3.5 The Industrial Viability of L19 and L20 as $CuSO_4$ Extractants.

3.5.1 Hydrolytic Stability.

The hydrolytic stability of the *di*nucleating hydrazone ligands was not previously studied by Wood.[17] Consequently a portion of one of the ligands (**4**, Section 2.3)[17] was dissolved in chloroform (0.0025 M) and subjected to acid stripping conditions (H_2SO_4, 150 g L^{-1}) similar to those present in conventional electrolytic tankhouse for 16 hrs. The acid-treated organic phase was evaporated to dryness and ^1H and ^{13}C NMR recorded. These demonstrated that the ligand was still intact, through presence of the imine proton (8.15 ppm) and carbon (138.37 ppm) signals and absence of the peaks representative of aldehyde formation *via* hydrolysis (9.87 and 197.12 ppm for proton and carbon respectively).

3.5.2 Ligand Regeneration from Copper Sulfate

Having demonstrated the hydrolytic stability of the azomethine bond in the hydrazone ligands, the performance of **L19** in four load/strip cycles was tested. These were carried out by contacting a chloroform solution of **L19** with copper sulfate (1.0 M) and sulfuric acid (150 g L^{-1}) alternately for periods of 1 hr. Portions of the organic phase were taken after the 1-hr contacts and the copper and sulfate content analysed by ICP-OES. The results are plotted as a bar chart in Figure 3.20.

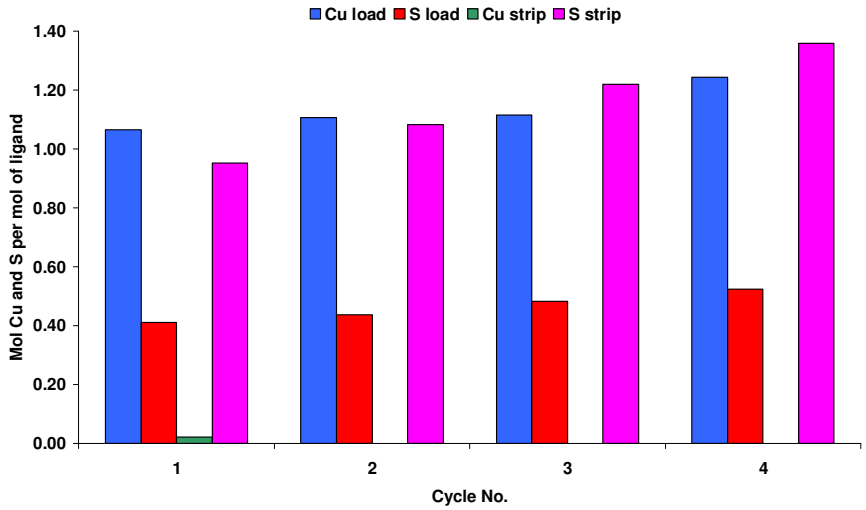

Figure 3.20: Copper and sulfate loading from $CuSO_4$ (1.0 M) and stripping by H_2SO_4 (150 g L^{-1}) by chloroform solutions of **L19** (0.0025 M).

The ligand loads copper to its full capacity after each load/strip cycle, although, curiously, in all instances, the copper content measured was *ca*. 5-25% greater than theoretically possible. This anomaly could be due to entrainment of aqueous copper sulfate in the organic phase, but is assigned to evaporation of chloroform as the copper and sulfate loading increases on each cycle. The sulfate content of the organic phase after loading and stripping is consistent with formation of $[Cu_2(\mathbf{L19}\text{-}H)_2(SO_4)]$ and two $[(\mathbf{L19}+H)(HSO_4)]$ respectively. The sulfate content of the organic phase also increases after each successive strip. These preliminary results indicate that the dinucleating metal salt extractants are robust enough to merit further investigations into their industrial viability. The metal selectivity is considered in Section 3.5.3.

3.5.3 Metal Selectivity

Although the *tri*-nucleating hydrazone ligands discussed in Chapter 2 were demonstrated to be selective for copper over iron, cobalt, nickel and zinc; the *di*-nucleating "metal-only" extractants developed by Wood[17] were not previously tested for copper selectivity from mixed metal feed solutions. Figure 3.21 shows that ligand **4** is selective for copper from a mixed metal feed solution in the absence of iron. This experiment was performed using a sample of the ligand prepared by Wood.[17] Iron(III) was omitted from the test as it precipitates from solution at the pH values needed to get high copper loading. No transfer of cobalt, nickel or zinc to the organic phase was detected in the pH range studied (see Figure 3.21).

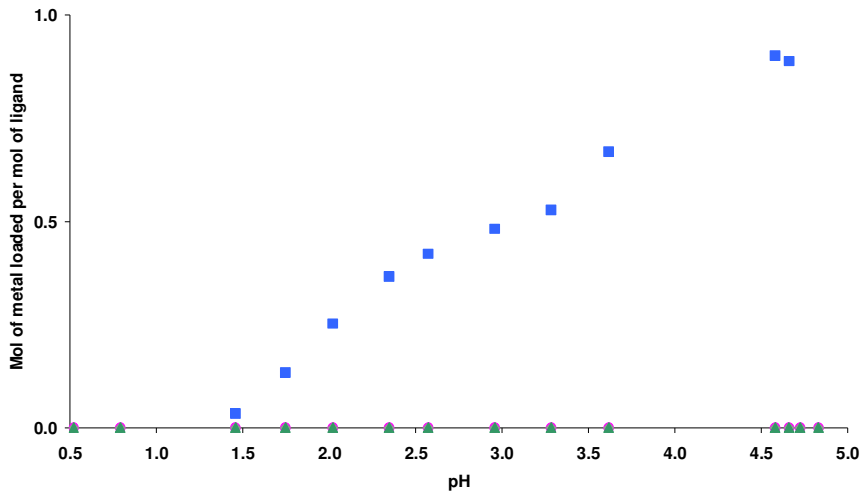

Figure 3.21: The pH-dependence of metal-loading by a 0.0025 M chloroform solution of ligand **4** from a mixed metal feed solution containing Co(II), ●; Ni(II), ♦; Cu(II), ■; and Zn(II), ▲; sulfate (0.0120 M of each).

As both *di*- and *tri*-nucleating "metal-only" hydrazone ligands are selective for copper over Co(II), Fe(III), Ni(II) and Zn(II) it is possible that the structurally related metal salt reagents would also be selective for copper. However, the inclusion of additional nitrogen functionality creates new potential binding sites which may result in favourable complex formation with cations other than copper. The extraction

results for **L19** from a mixed metal sulfate solution containing iron are given in Figure 3.22.

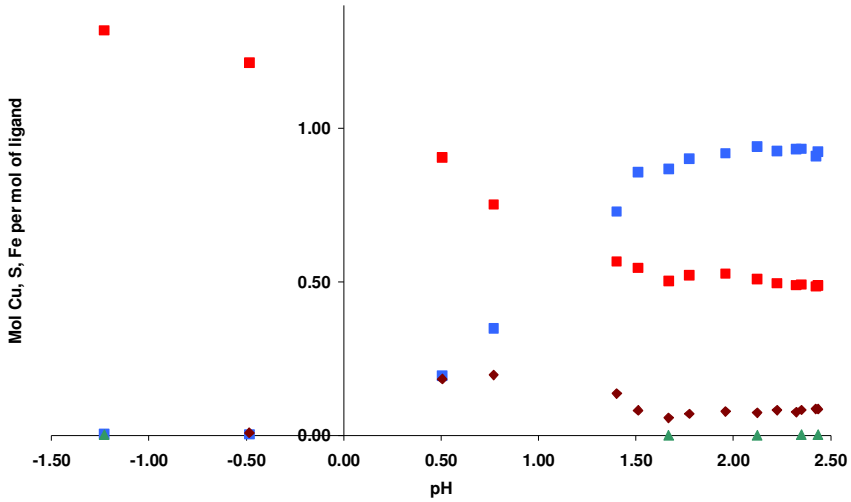

Figure 3.22: The pH-dependence of metal loading by 0.0025 M chloroform solutions of ligand **L19** from a mixed metal feed solution containing; Fe(III), ♦; Co(II), ●; Ni(II), ♦; Cu(II), ■; and Zn(II), ▲; sulfate S, ■. (0.012 M of each).

Although the ligand is selective for copper over Co(II), Ni(II) and Zn(II) metals, it does extract *ca*. 0.1 - 0.2 molar equivalents of iron. In the pH-range for high copper-loading (> 1.5) there is a corresponding 10% decrease in copper loading. The iron-loading is higher at low pH and extraction of iron does not affect the ligand's ability to load sulfate. Consequently, it appears that the iron- and sulfate-loading are co-operative and may involve species similar to those postulated for copper and sulfate loading in Section 3.4.

3.5.4 Ligand Regeneration after Mixed Metal Loading

The ability to regenerate **L19** after loading from a mixed metal feed solution was investigated to assess whether the ligand's affinity for iron adversely affected its recyclability. Four successive load/strip cycles were performed as defined previously in Section 3.5.2 using a mixed metal sulfate solution containing Fe(III), Co(II), Ni(II), Cu(II) and Zn(II) (0.012 M of each), see Figure 3.23.

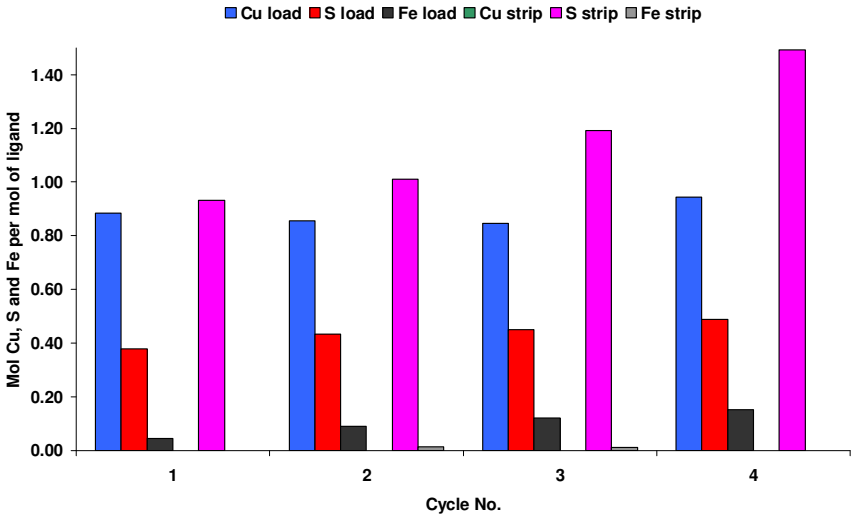

Figure 3.23: Copper and sulfate loading from solution containing Fe(III), Co(II), Ni(II), Cu(II) and Zn(II) sulfate (0.0120 M of each) and stripping by H_2SO_4 (150 g L^{-1}) by chloroform solutions of **L19** (0.0025 M).

As observed in the extraction curves in Figure 3.22, copper-loading is inhibited by the extraction of iron by *ca.* 10% and one mol of sulfate or hydrogensulfate is extracted per two mol of ligand. The sulfate content of the strip solution increases each time the solution is contacted with sulfuric acid as was observed in Section 3.5.2. Another curious feature is that the amount of iron loaded increases on each successive cycle. It is difficult to explain this behaviour as both copper and iron are fully stripped after each cycle. If it were a result of solvent evaporation then both the copper and the sulfate loadings would increase from cycle to cycle but copper loading remains fairly constant.

3.5.5 Solubility

For industrial application ligands **L19** and **L20** will need to have solubilities in hydrocarbon-based solvents on a par with the commercial salicylaldoxime reagent **P50** which is used at concentrations of *ca.* 0.1-0.3 M.[23] Both were found to be soluble in kerosene at a concentration of 0.1 M. However, although the resulting copper sulfate complex of **L19** was found to be soluble, that formed by **L20** was not. This is possibly due to the 5-dihexylaminomethyl group which has previously been found to be less soluble than the 3-substituted analogue.[16] Nevertheless a few volume percent of decanol added to the solvent enhanced solubility. This formulation approach to improving solubility, viscosity and enhancing phase transfer and phase disengagement kinetics common in commercial applications and is discussed further in Chapter 4. There is always a concern that addition of such molecules will have an adverse effect on the selectivity of extraction.

3.6 Conclusions

The work described in this chapter has demonstrated that hydrazone-based multiloading metal salt extractants are potential candidates for application in commercial systems as they can transport both metal cations and attendant anions and are stable towards hydrolysis.

The complexes of ligands which incorporate piperazine functional groups (**L14**-**L17**) as anion receptors were found to display low solubility in chloroform, and in some cases, notably the copper sulfate complex of **L16**, had greater solubility in the aqueous phase. Consequently, it is extremely unlikely that the piperazine-based ligands could have potential industrial applications.

Incorporation of an additional dihexylaminomethyl functionality to generate ligands **L19** and **L20** successfully addressed these problems. These show the greatest potential for industrial application due to their high solubility and that of their complexes in kerosene-based solvents. Both exhibit unexpectedly high selectivity for extraction of copper and sulfate to form $[Cu_2(\mathbf{L}\text{-}H)_2(SO_4)]$ from a copper sulfate feed

solution. In particular, **L19**, extracts both copper and sulfate over a wider pH range than other metal *salt* reagents studied previously. The extraction of iron from a mixed metal feed solution is undesirable and requires further investigation, as does the extent of sulfate extraction at very low pH.

3.7 Future Work

Whilst proof-of-concept that the potentially dinucleating ligands **L19** and **L20** can be used to transport *both* copper and sulfate ions has been established, a more exhaustive study of their hydrolytic stability, selectivity and extraction kinetics is required before their commercial potential can be evaluated. The ability to regenerate the ligands *via* an acid strip stage also requires investigation. Such development work falls beyond the remit of this thesis and may be undertaken by the industrial sponsor. **L20** has not been subjected to any tests of this kind. It would be particularly interesting to discover whether it exhibits a similar, undesired, ability to transport iron.

Experiments should also be carried out to establish the anion selectivity of these reagents to assess their ability to selectively extract sulfate over chloride anions. If the reagents were found to be selective for chloride over sulfate, they may yet find application in chloride hydrometallurgy. However, the favourable performance of **L19** on the co-operativity of copper and sulfate binding may not be the case for copper(II) chloride transport.

3.8 References

1. D. Dreisinger, *Hydromet.*, 2006, **83**, 10-20.
2. M. E. Clark, J. D. Batty, C. B. van Buuren, D. W. Dew and M. A. Eamon, *Hydromet.*, 2006, **83**, 3-9.
3. P. A. Tasker, C. C. Tong and A. N. Westra, *Coord. Chem. Rev.*, 2007, **251**, 1868-1877.
4. D. J. White, N. Laing, H. Miller, S. Parsons, S. Coles and P. A. Tasker, *Chem. Commun.*, 1999, 2077-2078.
5. H. A. Miller, N. Laing, S. Parsons, A. Parkin, P. A. Tasker and D. J. White, *Dalton Trans.*, 2000, 3773-3782.
6. S. G. Galbraith, P. G. Plieger and P. A. Tasker, *Chem. Commun.*, 2002, 2662-2663.
7. S. G. Galbraith, Q. Wang, L. Li, A. J. Blake, C. Wilson, S. R. Collinson, L. F. Lindoy, P. G. Plieger, M. Schroder and P. A. Tasker, *Chem. Eur. J.,* 2007, **13**, 6091-6107.
8. P. G. Plieger, P. A. Tasker and S. G. Galbraith, *Dalton Trans.*, 2004, 313-318.
9. R. A. Coxall, L. F. Lindoy, H. A. Miller, A. Parkin, S. Parsons, P. A. Tasker and D. J. White, *Dalton Trans.*, 2003, 55-64.
10. D. K. Henderson and P. A. Tasker, Unpublished work, 2008.
11. J. Kalia and R. T. Raines, *Angew. Chem., Int. Ed. Int.*, 2008, **47**, 7523-7526.
12. S. G. Galbraith, PhD Thesis, The University of Edinburgh, 2004.
13. N. Akkus, J. C. Campbell, J. Davidson, D. K. Henderson, H. A. Miller, A. Parkin, S. Parsons, P. G. Plieger, R. M. Swart, P. A. Tasker and L. C. West, *Dalton Trans.*, 2003, 1932-1940.
14. R. S. Forgan, J. E. Davidson, S. G. Galbraith, D. K. Henderson, S. Parsons, P. A. Tasker and F. J. White, *J. Chem. Soc., Chem. Commun.*, 2008, 4049-4051.
15. A. G. Smith, P. A. Tasker and D. J. White, *Coord. Chem. Rev.*, 2003, **241**, 61-85.
16. R. S. Forgan, PhD Thesis, The University of Edinburgh, 2008.
17. J. L. Wood, PhD Thesis, The University of Edinburgh, 2005.
18. D. C. R. Henry, PhD Thesis, The University of Edinburgh, 2007.
19. J. M. Casas, F. Alvarez and L. Cifuentes, *Chem. Eng. Sci.*, 2000, **55**, 6223-6234.
20. V. Gerald and I. Jergensen, *Copper Leaching, Solvent Extraction, and Electrowinning Technology*, Society for Mining, Metallurgy, and Exploration, Colorado, 1999.
21. M. J. Nicol, C. A. Fleming and J. S. Preston, *Comprehensive Coordination Chemistry*, 1987, **6**, 779-942.

22. S. G. Galbraith, L. F. Lindoy, P. A. Tasker and P. G. Plieger, *Dalton Trans.*, 2006, 1134-1136.

23. J. Szymanowski, *Hydroxyoximes and Copper Hydrometallurgy*, CRC Press, London, 1993.

24. P. J. Hergenrother, K. S. Putt, G. W. Chen and J. M. Pearson, *WO2006128173*, 2006, 132pp.

25. Q. Wang, C. Wilson, A. J. Blake, S. R. Collinson, P. A. Tasker and M. Schroder, *Tetrahedron Lett.*, 2006, **47**, 8983-8987.

26. K. S. Putt, G. W. Chen, J. M. Pearson, J. S. Sandhorst, M. S. Hoagland, J. T. Kwon, S. K. Hwang, H. Jin, M. I. Churchwell, M. H. Cho, D. R. Doerge, W. G. Helferich and P. J. Hergenrother, *Nature Chem. Bio.*, 2006, **2**, 543-550.

Chapter 4 : Modifier–Ligand and Modifier–Complex Interactions

This chapter considers the chemistry of "equilibrium modifiers" which are commonly used in extractive metallurgy to improve recovery efficiency by displacing the equilibrium under stripping conditions. The mode of action of these modifiers at a molecular level is poorly understood. The literature (see Section 4.2) makes reference to displacement of the phase distribution of copper by formation of adducts with the extractants (L) and/or the copper complexes ($[Cu(L\text{-}H)_2]$) (see Scheme 4.1).

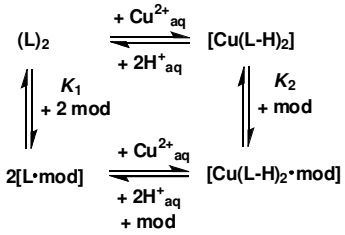

Scheme 4.1: Equilibria involving the formation of adducts of an equilibrium modifier (mod) with an extractant dimer (L_2) or with a copper complex ($[Cu(L\text{-}H)_2]$) in a water immiscible solvent.

The important practical requirement is that the modifier assists stripping and reduces the concentration of acid required. This can occur by formation of adducts which either destabilise the copper-extractant bonds in $[Cu(L\text{-}H)_2]$ or stabilise the ligand L. Simplistically it must be the latter.

The chelating salicylaldoxime reagent **P50**, type A in Figure 4.1 where R = 5-C_9H_{19}, is used extensively in commercial solvent extraction processes for copper recovery. This reagent is extremely selective for copper in a conventional sulfuric acid heap leach circuit, see Section 1.6 of Chapter 1. Its $pH_{½}$ value for copper extraction is *ca.* 0.5 in aliphatic hydrocarbon solvents. Stripping the copper from the organic phase to generate a sulfate electrolyte requires[1] a sulfuric acid solution of concentration 250-300 g L^{-1}. However, most plants[2] operate with sulfuric acid strip solutions of concentrations up to 250 g L^{-1} within the pH range 1.5 and 2.3 because higher electrolyte acidities diminish the purity of the copper cathode.[1] Because copper cannot be efficiently stripped under the desired operating conditions, "equilibrium modifiers" are added to extractants at 5-10% concentration relative to that to that of the extractant to facilitate copper stripping in a more suitable pH range.[3]

Equilibrium modifiers enhance the mass transfer of copper in sulfate based solvent extraction circuits which employ salicylaldoxime reagents.[1, 3] Although they decrease the extraction capacity of the reagent, the overall mass transfer is greater than unmodified systems.[4] Extraction modifiers are hydrogen bond donors and/or acceptors and have been shown[5, 6] to interact with the extractant molecules (see Section 4.2.2). This intermolecular interaction lowers the concentration of the active extractant at the hydrocarbon/water interface and also affects the interfacial behaviour of the system and phase transfer kinteics.[3, 7-9] However, the mode by which they interact with the copper complex is not fully understood.[9]

A recent study commissioned[10] by Cytec Industries Inc. employed molecular dynamic simulations and Density Functional Theory (DFT) calculations to investigate the hydrogen bonding stabilisation between free and complexed salicylaldoxime and known extraction modifiers. The computational study indicated that the interactions between modifiers and free salicylaldoximes were favourable, giving negative overall free energy values after adduct formation. Modifier interactions with the copper complex were unfavourable, resulting in an overall positive free energy. The strength of the interactions were found to be dependent on the type of modifier used.

The aim of the work discussed herein is to investigate the findings of the theoretical study using experimental methods. Particular efforts are made to establish whether a modifier-complex adduct is formed.

4.1 Hydroxyoximes

The term “hydroxyoxime” encompasses four classes of reagent; salicylaldoximes (A), 2-hydroxybenzoketoximes (B), 2-hydroxybenzophenone oximes (C) and aliphatic α-hydroxyketone oximes (D). Their structures can be seen in Figure 4.1.

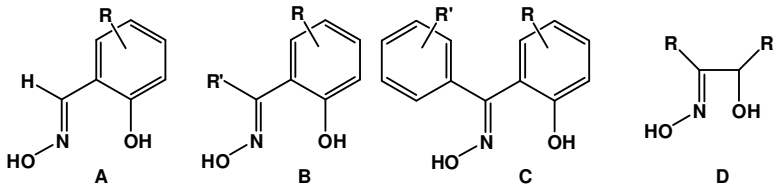

Figure 4.1: Structures of the different hydroxyoximes developed for application in hydrometallurgy.

Reagents of type D are unsuitable for use in conventional sulfuric acid streams as they do not extract copper within the operating pH-range 1.5-2.00, nor do they selectively extract copper in the presence of iron.[1] They are also particularly susceptible to hydrolysis. The hydrolytic stability of the commercially viable hydroxyoxime reagents increases in the order A < B < C.[1] The acidity of the phenolic proton of these extractants is inverse to their hydrolytic stability, following the order C (*E*-isomer) < B < A < C (*Z*-isomer). Although the *Z*-isomer of 2-hydroxybenzophenone oximes (seen in Figure 4.2) contains the most acidic proton as a result of anion stabilisation by the intramolecular hydrogen bond with the oximic hydroxyl group,[11] it is inactive in copper solvent extraction because the oximic hydroxyl group blocks approach of the metal to the phenolate binding site, and thus will be disregarded in the following discussion. Salicylaldoximes form the active *E*-isomer exclusively.[8]

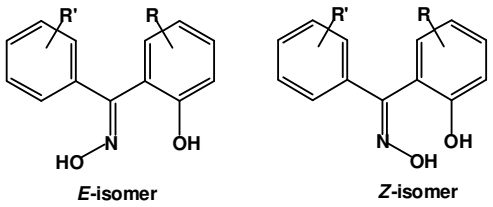

Figure 4.2: Active *E*- and inactive *Z*- isomers formed by 2-hydroxybenzophenone oximes.

The extractive properties of phenolic oximes can be tuned by substituents in the 3- and 5-positions. Electron withdrawing groups in these positions decrease the electron density on the aromatic ring and phenolate oxygen, weakening the O-H bond and increasing the acidity of the phenolic proton.[1] The decrease in electron density on the phenolic oxygen also results in decreased copper complex stability as a result of less σ-bond donation to the metal (although in some cases, the opposite effect has been

reported).[12] Conversely, the ligand's π-accepting ability is increased.[13] Increased alkyl chain length in the 5-position also decreases copper complex stability.[14, 15] It is necessary in industrial applications to have long alkyl chains in the 5-position to ensure solubility of the ligand and copper complex in the hydrocarbon solvents used. Consequently it is unrealistic to substitute in the 5-position to tune complex stability. Recently[16] in the Tasker group, bifurcated H-bond buttressing[17] has been demonstrated to influence the strength of 3-substituted-salicylaldoxime copper complexes (see Figure 4.3). Hydrogen bond acceptor groups (e.g., X = NO_2, Br) favour complex formation by both enhancing intra-complex H-bonding and by increasing the acidity of the phenolic group. The importance of the H-bond buttressing is underlined by the methoxy-substituted ligand (X = OMe) also being one of the stronger extractants despite its electronic properties lowering the acidity of the phenol.

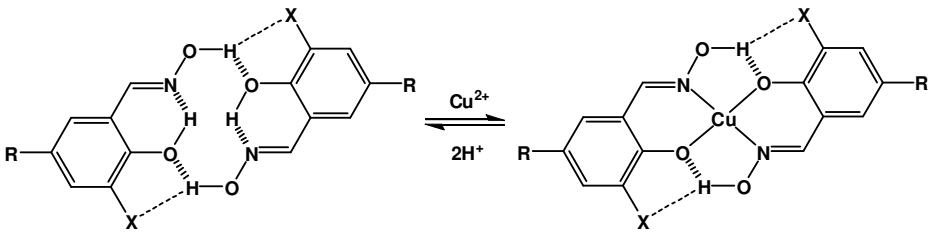

Figure 4.3: Stabilisation of the 3-substituted-5-alkylsailcylaldoxime dimer and copper complex as a result of bifurcated hydrogen bond buttressing between X and trans-oximic hydroxyl groups.

Although current phenolic oximes can be tuned to decrease their extractive strength by increasing the acidity of the phenolic proton, this approach would require a new extractant to be developed to suit individual ores and their process streams. A much more cost effective alternative is to use the strongest reagent and optimise its extraction properties for individual applications through the addition of equilibrium modifiers.[9] As a result, modified salicylaldoximes blends are the most widely used copper extractants.

4.1.1 5-Nonylsalicylaldoxime and its Blends

5-Nonylsalicyaldoxime (**P50**, formerly P1) was marketed as P5100, P5200 and P5300 blends, containing 1, 2 and 3 molar equivalents of 4-nonylphenol respectively.[1] These were inexpensive to produce as 4-nonylphenol is the starting material for **P50**, and is carried through the manufacturing process to the formulated products where it is present in significant quantities.[1] Initially some problems arose when applied in commercial plants as 4-nonylphenol caused swelling of the rubber linings and fittings.[1, 12]

Consequently, 4-nonylphenol was replaced with a new aliphatic modifier, tridecanol (TDA). Because TDA is a stronger modifier than 4-nonylphenol;[4, 9] less is required to increase the mass transfer by the same amount, and is used in a 1 : 2 , TDA : **P50** blend as P5050. This reagent has similar extraction properties to P5100.[4] The third generation of ACORGA reagents from CYTEC employ hydrophobic esters blended with **P50** in the M and OPT series.

The LIX series of reagents which are marketed by Cognis (previously Henkel) generally consist of mixtures of salicylaldoximes with ketoximes or 2-hydroxybenzophenone oximes, although LIX622 is a mixture of 5-dodecylsalicyaldoxime and TDA.[4]

4.1.2 Self-Association of Extractants

Hydroxyoxime reagents can dimerise through intermolecular hydrogen bonds in non-aromatic hydrocarbon solvents. The resulting “pseudomacrocylic” structure is preorganised for *trans* chelatation of square planar copper(II) cations, as shown in Figure 4.3. Consequently, the free energy of complex formation should be considerably less. Hydroxyoximes of type D have been reported[18] to form polymeric two-dimensional copper complex arrays, these will not be discussed as they are not relevant to the systems under investigation.

X-ray diffraction studies have confirmed the formation of salicylaldoxime dimers in the solid state.[19, 20] More recently,[16, 21] the strength of the intermolecular bonding in

these pseudomacrocylic dimers has been related to the hydrogen bond buttressing ability of substituents in the 3-position, see also Section 4.1 above. All of these structures have been obtained for salicylaldoximes with relatively small alkyl substituents in the 5-position. Introduction of bulkier groups, as used in industrial applications, leads to oligomeric solid state structures.[19] This effect is expected to be due to inefficient intermolecular stacking as a result of the removal of planarity.[19]

It must be realised that solid state structures are obtained as a result of favourable hydrogen bonding and crystal packing forces which are often governed by solvate molecules. Consequently the structures obtained are highly dependent on the solvent systems that the crystals are obtained from. As a result it is very difficult to draw comparisons between a series of analogous structures unless the same crystallisation solvent is used and no solvates are present within the crystal obtained. Although solid state structures may be indicative of intra- and inter-molecular interactions, they cannot be used to definitively assign the predominant interactions and species present in solution.

Infrared spectroscopy has been widely used to investigate the speciation of hydroxyoximes in solution.[11, 12, 22-25] There are three assignable bands in the hydroxyl fingerprint region, 3000-4000 cm^{-1}. These absorbances are assigned to the "free" oximic hydroxyl (*ca.* 3600 cm^{-1}), intermolecularly hydrogen-bonded oximic hydroxyl group (*ca.* 3400 cm^{-1}) (see Figure 4.3) and the intramolecularly bound phenolic group (*ca.* 3200 cm^{-1}).[24] Of these bands, only the last is observed as a broad band between 3350-3250 $cm^{-1}$when measured as a KBr disc.[26]

The detection of intermolecular hydrogen bonding by IR in solutions of hydroxyoximes can only indicate the presence of associated molecules; it cannot distinguish between dimers and higher aggregates.[26] However, solution based IR studies can been used to monitor monomer-aggregate equilibria as a function of concentration and association constants can be calculated from these.[27] Association constants for pure salicylaldoximes increase with the length[25] and degree of branching in the 5-alkyl substituent.[28] The study[15] of hydrogen bond buttressing between the 3-substituent and the oximic OH hydrogen found no direct relationship

between the extractant strength and association enthalpies calculated from IR spectra measured in 0.05 M chloroform solution.[15] It has been suggested that hydroxyoxime association can be ignored below concentrations of 0.1 M and 0.01 M in aromatic and aliphatic hydrocarbon solvents respectively.[1] Under such conditions more than 90% of the extractant is in its monomeric form.[4, 8]

4.1.3 Solvent Dependence of Extractant Self-Association

Hydroxyoxime self-association constants are different in aromatic and aliphatic hydrocarbons. This is due to favourable interactions between the solvent and extractant which also determine their solubility and degree of solvation. The strength of these interactions generally increases with increasing dipole moment and dielectric constant of the solvent.[29]

Previous work at Edinburgh University[26] involved monitoring the chemical shift of protons on 5-*t*-butylsalicylaldoxime by ^{1}H NMR as a function of the dielectric constant of solvent. The experiments were carried out at room temperature, with a solution concentration of 0.12 M.

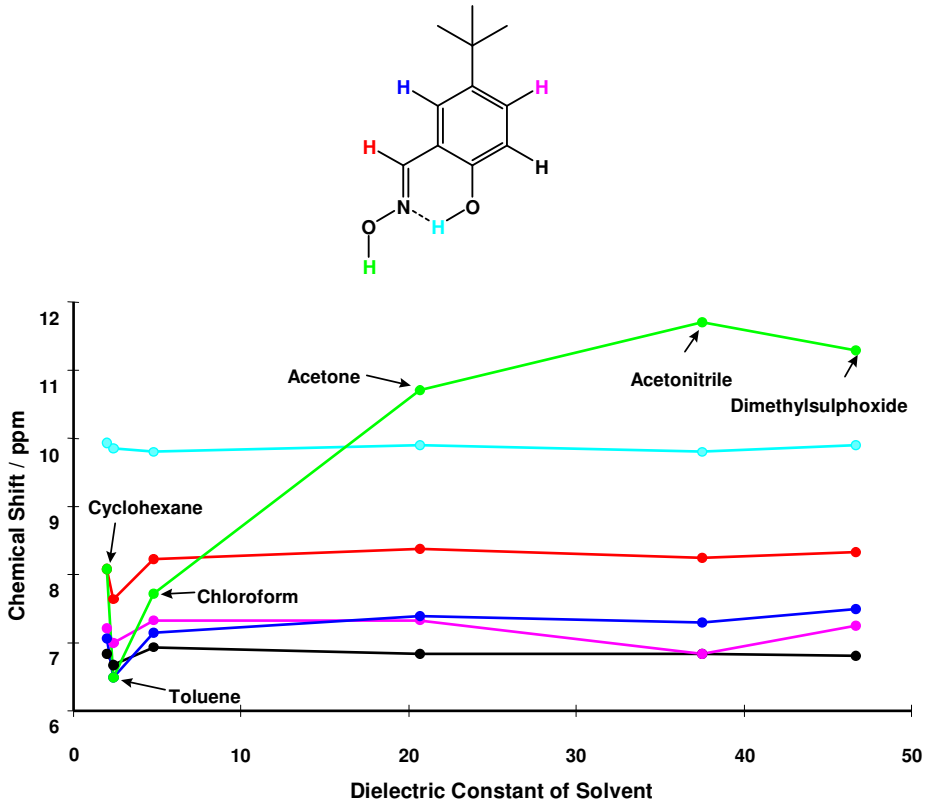

Figure 4.4: Solvent dependence of ^{1}H NMR chemical shifts of 5-*t*-butylsalicylaldoxime (**18**) as a function of the dielectric constant of NMR solvents.[26]

The results shown in Figure 4.4 indicate that the oximic proton is most affected by the change in solvent with shifts measured at *ca*. 6.5 and 11.7 ppm for toluene and acetonitrile respectively. All other protons are essentially uninfluenced. Nuclear Overhauser Effect (NOE) experiments provide evidence for the association of salicylaldoxime in chloroform (0.37 M) and cyclohexane (0.1 M). Selective irradiation of the oximic proton resulted in an equivalent irradiation of the phenolic proton indicating fast exchange relative to the NMR timescale.[26] However this evidence was qualitative and provides no information on the speciation of the aggregate.

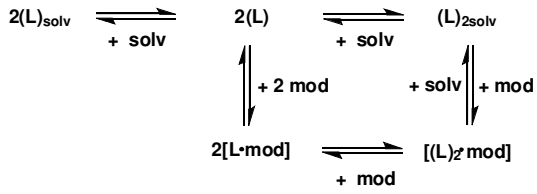

Scheme 4.2: Possible equilibrium processes between extractant (L), modifier (mod) and solvent (solv).

Formation of extractant adducts with modifiers results in an effective decrease in the concentration of the active extractant. Scheme 4.2 shows some of the equilibria between modifier, solvent and extractant. The interactions noted between aromatic extractants and solvating aromatic hydrocarbons is attributed to their ability to form hydrogen bonds (and possibly act as hydrogen bond acceptors to form T-shaped hydrogen bonds) and act as π-donors to form intermolecular π-complexes.[4] Consequently, extractant strengths are lower and extraction rates are slower in aromatic solvents than they are in aliphatic solvents.[29] Aromatic solvents also have higher dielectric constants and dipole moments therefore interact more favourably with water.[29] This could result in the entrainment of water and other species which may be present in the pregnant leach solution to form a third phase. For similar reasons branched and cyclic aliphatic hydrocarbons are the preferred[29] method of improving the solubility of the extractants and their complexes because these are less likely to form stable micelles.[4] However, using aliphatic hydrocarbons also means a more acidic sulfuric acid solution is required to strip the metal because the $pH_{½}$ is lowered relative to that in aromatic solvents.[1, 4] To this end extractant modifiers are added to increase the solubility of extractants and their complexes, preventing formation of a third phase and enhancing mass transport.[9]

4.2 Modifiers

Extraction modifiers are oxygen containing hydrogen bond donor and/or acceptors. They are added to improve mass transfer by decreasing the strength of an extractant and increasing its $pH_{½}$ value under strip conditions.[3, 9] Those which are routinely used in blends with 5-alkyl-salicylaldoximes fall into three categories; 4-alkylphenols, alcohols and esters.[9] 4-Alkylphenols and branched alcohols have the ability to act as hydrogen bond donors and acceptors through the hydroxyl hydrogen and oxygen respectively. Consequently, they can self-aggregate in non-polar solvents.[30, 31]

Strong self-aggregation of hydroxyl containing modifiers has lead to the introduction of ester modifiers which predominantly act as hydrogen bond acceptors.[9] This minimises self-aggregation and optimises their ability to interact with the extractant.[9] Esters are the primary examples of hydrogen bond-acceptor only modifiers used in reagent blends.[9] Another class which will be discussed in this chapter are phosphine oxides. These are not widely used in copper solvent extraction processes but are used as synergists in other hydrometallurgy applications, particularly in lanthanide solvent extraction[32] by phosphoric and phosphinic acids.[33] Phosphine oxides are also used for extraction of mineral[34-36] and organic acids from aqueous effluents.

4.2.1 Self-Association of Modifiers

Self-association of alkylphenols and alcohols reduces their efficiency as extraction modifiers. 4-Alkylphenols form only linear associates[6] and larger aggregates than alcohols.[37] Polymerisation constants calculated[38] for 4-ethylphenol (83) > 4-*i*-propylphenol (69) ≈ 4-*n*-propylphenol (70) > 4-*t*-butylphenol (51) (units are not defined as degree of association is not stated) in cyclohexane at 298 K decrease with alkyl chain length. Infrared studies[31] have shown that straight-chain alcohols, 1-butanol and 1-octanol, are present in non-polar solvents such as *n*-decane as monomers at low concentration and linear or cyclic tetramers at higher concentration, these are depicted in Figure 4.5. The equilibrium constants calculated

for 1-butanol and 1-octanol tetramers in *n*-decane at 303 K, K = 430 and 490 M^{-3} respectively, are an order of magnitude greater than those reported above for 4-alkylphenols and also for phenol (70) and ethanol (45) in carbon tetrachloride at 298 K.[31]

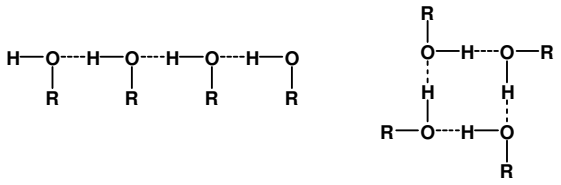

Figure 4.5: Linear and cyclic tetramers formed by aliphatic alcohols in non-polar solvents.

Semiempirical PM3 molecular modelling of C_4H_9OH alcohols found[5] dimers to be always linear and cyclic tetramers slightly more energetically favourable than linear tetramers. The definition of the speciation of trimers is less well pronounced as the heat of formation of linear and cyclic trimers are very similar. However, the modes by which they associate are determined by their structure. Of the four alcohols modelled;[5] primary alcohols, *n*-butanol and 2-methylpropanol form linear trimers whilst more sterically hindered secondary alcohols, 1-methylpropanol and *t*-butanol, form cyclic trimers. Conversely, an IR study[6] found the primary alcohol, *n*-tridecanol to trimerise in *n*-heptane within the 0.017-0.2 M concentration range (K = 1995 M^{-2} at 293 K). In the same work, no significant aggregation was observed for the highly branched primary alcohol, 2-(1,3,3-trimethylbutyl)-5,7,7-trimethyloctanol. This is in agreement with the finding that the self-association constants of sterically hindered 2,2,4,4-tetramethyl-pentan-3-ols decrease with the bulk of the 3-substituent.[30]

5-Alkyl-salicylaloxime reagents have hydrogen-bond donor and acceptor groups, both of which are responsible for their excellent copper extraction capability (see Section 1.6). Therefore structural alteration is only applicable to the modifier. This is the reason that a range of alcohols are used in extraction modification. Aliphatic alcohols have greater electron density on the oxygen than phenols,[9] consequently form stronger hydrogen bonds and have greater tendency to self-aggregate. Introduction of steric bulk in aliphatic alcohols reduces their ability to self-aggregate without a significant adverse effect on their ability to interact with other species.[6, 8, 30]

Self-aggregation of modifiers is significantly diminished when alcohols are replaced by esters as these have only hydrogen bond accepting capabilities.[9] An analogous class of hydrogen bond acceptors which were used in this thesis are phosphine oxides. Although these are only hydrogen bond acceptors they have been found to self-associate due to the polar nature of the P=O bond.[39] Dimers[40] or higher aggregates form in aliphatic hydrocarbons as their concentration increases beyond 10 mM and above ~170 mM reverse micelles predominate[41] as shown in Figure 4.6. Most of these studies have been conducted using tri-*n*-butylphosphate (TBP)[42] but can be applied to tri-*n*-octylphosphine oxide (TOPO) which is discussed in this work. Such behaviour must also be true for esters as they are structurally analogous, but to a lesser extent if one simply considers the difference in Pauling electronegativities,[43] *cf*. 0.89 and 1.25 for C=O and P=O bonds respectively, without consideration of other substituents. Dimerisation constants for TBP are in general an order of magnitude lower than phenols and two to three orders of magnitude lower than aliphatic alcohols. They have been experimentally calculated[44] to be 2.5, 2.6 and 2.9 (M^{-1}) in cyclohexane, *n*-dodecane and *n*-hexane respectively.

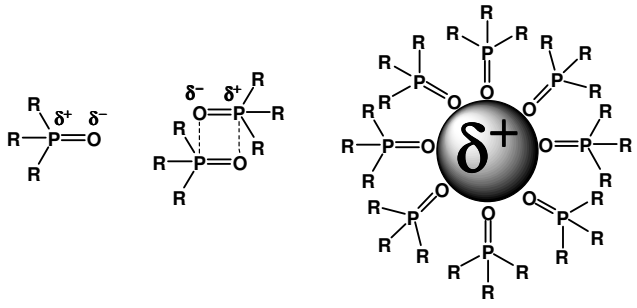

Figure 4.6: Depiction of the dipole moment in phosphine esters and resulting dimers and reversed micelles (showing the polarity on the surface of the water core) formed as a result electronic attraction.

It can be concluded from the discussion above that the self-association constants of the modifiers decrease in the order *n*-alcohol > phenol > sterically hindered *i*-alcohol > phosphine oxide > ketone > ester > ether. The aim of extraction modification is to adjust the extractant strength by addition of non-innocent molecules which interact with the diluent, extractant or complex. The association constants for these hetero-interactions should be greater than those of self-aggregation. However the strength of

the interactions between diluent and extractant should not be too favourable as this would result in diminished extractive ability. Similarly, the interaction between diluent and complex should not be too favourable as a stabilised complex which is more difficult to strip may result. Also, the effects of modification should be more prevalent under strip than load conditions.

4.2.2 Association of Modifiers with Extractants

The association of modifiers with extractants lowers the effective concentration of active extractant molecules.[4, 5, 9] Phenolic oxime extractants have an intramolecular bond between the phenolic proton and the oximic nitrogen (see B Figure 4.7). If this remains intact throughout interaction with modifiers, the two oxygen atoms of the phenolic group and an oximino group can act as hydrogen bond acceptors and the oximic proton acts as a hydrogen bond donor. As a result, extractants can interact with both hydrogen-bond donor and acceptor type modifiers.

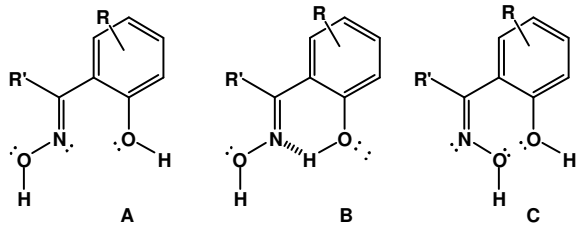

Figure 4.7: Possible isomers of hydroxyoxime extractants with 3, 2 and 1 lone pairs, from left to right, available to act as hydrogen bond acceptors.

Theoretically the lone pairs on the oxygen atoms of the phenolic and oximic groups and the lone pair on the imino nitrogen can form hydrogen bonds if the intramolecular hydrogen bond is not present (see A Figure 4.7). This may occur if a more favourable interaction is formed between the phenolic proton and the modifier than is formed between the phenolic proton and oximic nitrogen atom and would result in a total of five potentially hydrogen-bonding sites. Molecular modelling has indicated that one or two modifier molecules can be associated per phenolic oxime.[5, 8] This seems to be a reasonable prediction as modifiers are generally bulky to impart solubility in water-immiscible hydrocarbons. However, only hydrogen bond donors

will be able to form 2:1 associates[5] because phenolic oximes have one free hydrogen bond donor group available to acceptors when the phenolic hydrogen is involved in intramolecular hydrogen bonding (B, Figure 4.7). The phenolate proton will form only very weak interactions with H-bond acceptors because its acidity is greatly reduced by the interaction with the imino nitrogen.[1] Consequently esters[5] and phosphine oxides are likely only to form 1:1 assemblies *via* the oximic hydrogen.

Association constants calculated for the interaction between **P50** and alcohols *n*-tridecanol and 2-(1,3,3-trimethylbutyl)-5,7,7-trimethyloctanol in *n*-heptane by IR were found[6] to be 1700 and 1300 M^{-2}. These are in agreement with the conclusion that branched alcohols form weaker associates than straight chain alcohols.[30] However this publication also reported that the ester, pentyl acetate, also formed 2:1 associates with **P50** where K = 580 M^{-2}. The only explanation for this is that the interaction between the ester and **P50** oximic group resulted in destabilisation of the intramolecular hydrogen bond (A, Figure 4.7) to form two more favourable intermolecular hydrogen bonds. Another anomalous result reported in this paper is that the **P50** analogue dodecylsalicylaldoxime only formed 1:1 associates with 2-(1,3,3-trimethylbutyl)-5,7,7-trimethyloctanol. However, comparison of results for association of **P50** analogue dodecylsalicylaldoxime with *n*-tridecanol, 2951 and 1738 M^{-2} are in agreement with the finding[45] that increasing alkyl chain length of the 5-substituent results in increased electron density on the phenolic oxygen, therefore making the OH bond more polarised and more susceptible to hydrogen bond donation.[17] Similarly, phenols are presumed to form weaker associates with phenolic oximes as they have lower electron density on the phenolic oxygen atom.[4]

The association of phenolic oxime extractants with alcohol and ester modifiers has been extensively studied,[4-6, 8] as have their effect on the interfacial tension of the hydrocarbon/water interface,[3, 40, 46-48] and the interfacial activity of extractants and the consequences these effects have on the extraction rates and mass transfer capabilities.[7, 46, 49-51] However, to the best of our knowledge interactions between phenolic oximes and phosphine oxides have not been reported.

4.2.3 Modifier-Complex Interactions

It is not a simple task to investigate modifier-complex interactions in copper solvent extraction systems. Consequently all studies to date have indirectly investigated such interactions through the effect they have on extraction rates and equilibria. Under equilibrium conditions, the favourable interaction between modifiers and free extractant molecules lowers the concentration of metal complex available for binding to the modifier.[4, 9] Ideally all organic and aqueous phase species need to be identified and the extent of the interactions between modifier, solvent, free extractant molecules and metal complexes should be known. Only when the concentrations of all species are known can association constants be calculated.

It is not feasible to do this by assimilation of the available data reported in the literature. Not only have different association constants been quoted for the same system[1, 4] but in most cases, the solvent systems differ and the concentrations of components and temperatures have not been reported. Moreover in all cases, even single phase studies of the interaction between modifier and diluent or extractant, the water content has not measured. The comprehensive study[31] of association constants of *t*-octanol in *n*-decane as a function of temperature demonstrates the affect temperature has on association constants with values ranging from 2 to 6920 M^{-3} at 373 K and 278 K respectively and illustrates why it must be reported for comparisons to be drawn. In addition, conflict between results obtained for very similar systems are likely to arise as a result of insufficient or unknown sample purity.[1, 4]

Commercial phenolic oximes are supplied as mixed isomers to enhance solubility of extractants and their copper complexes and to reduce viscocities[1] in kerosene based solvents. One study[28] has reported as many as 50 different hydrocarbons are present within the nonyl chain of a commercial sample of **P50**. Another author has suggested[4] that thorough purification of commercial samples by standard methods including; distillation, crystallisation, column chromatography and gas-liquid chromatography may not be sufficient for accurate comparisons of interfacial tension data to be made. Industrial grade samples are routinely used without purification for

determination of association constants.[1] Consequently, appreciable quantities of impurities of unknown structure are often present with quantities of modifiers when investigated in modification studies.[1, 4, 28] In the present study (see Section 4.4) attempts have been made to use high purity, single isomer materials throughout.

4.2.4 Molecular Modelling

The effects of modifiers on the hydrogen bond stabilisation of free and copper complexed phenolic oximes were investigated using computational molecular modelling by Dr. Daniel Tackley of Intertek ASG,[10] data are provided in Appendix 7.4.4. These studies were undertaken to define the energy-minimised structures in the gas phase and do not account for any desolvation processes. The molecules chosen for study were geometry optimised using the DFT method BPW91/6-31G(d,p) to give the lowest energy conformation. The electrostatic potential of the molecules were mapped using CHelpG charges. Molecular dynamic simulations were carried out to find the overall lowest energy structure and most favourable energy interaction between the two components. To achieve this, the oxime molecules and that of the copper complex were restrained, thereafter the lowest energy adducts were subject to full DFT optimisations to determine the effects of these interactions on the structural geometry of the ligand and complex.[10]

To minimise the size of the calculations, single isomer systems where used, these include; phenolic oxime 5-*t*-butylsalicylaldoxime (**18**), *iso*-alcohol TDA and the sterically hindered diester TXIB, see Figure 4.8. The latter are the major components of the commercial modifiers.

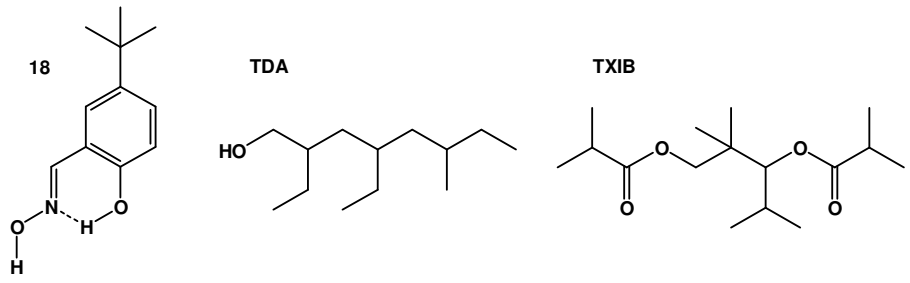

Figure 4.8: Extractant and modifiers selected for study by computational molecular modelling.[10]

The results indicate a favourable hydrogen bond interaction between the oximic hydrogen atom of **18** and the hydroxyl oxygen atom of TDA with stabilisation energy of 21 kJ mol^{-1}. This enthalpy of association is very close to the free energy of reaction measured[6] by IR for **P50** and 1-tridecanol in *n*-heptane of 18 kJ mol^{-1} (converted using $\Delta G_{bind} = (-\ln K)RT$, T = 293 K). TXIB forms a more favourable, 27 kJ mol^{-1}, hydrogen bond with the oximic proton and the more sterically hindered carbonyl oxygen atom shown on the right in Figure 4.8. This is unexpected as alcohols are predicted to interact more strongly with phenolic oximes than esters.[9]

The dynamic simulations of interactions between the copper complex and TDA indicated that the hydroxyl oxygen atom of the alcohol interacted with the apical position of the copper atom. There were additional hydrogen bonds formed between the alcohol's hydroxyl hydrogen atom and various nitrogen and oxygen atoms on the phenolic oxime ligands in the complex during the molecular dynamic simulations.[10] However, when the modifier-copper complex adduct was energy minimised, the difference in energy between this and the sum of its constituent parts gave an overall positive energy, 116 kJ mol^{-1}, indicating that the association process TDA + [Cu(**P50**-H)$_2$] → [Cu(**P50**-H)$_2$•TDA] is unfavourable. A DFT optimisation of the lowest energy structure determined by molecular dynamics, produced the structure shown on the left of Figure 4.9. This structure indicates that the Cu-O and Cu-N bond lengths to the phenol and oxime, respectively, were longer in the presence of the modifier. The intracomplex O•••H hydrogen bonds between the oximic proton and phenolic oxygen atom of the mutually *trans* molecules were shorter as a result of distortion towards square pyramidal geometry of the copper centre which will allow the extractants to approach each other more closely than in a planar arrangement.

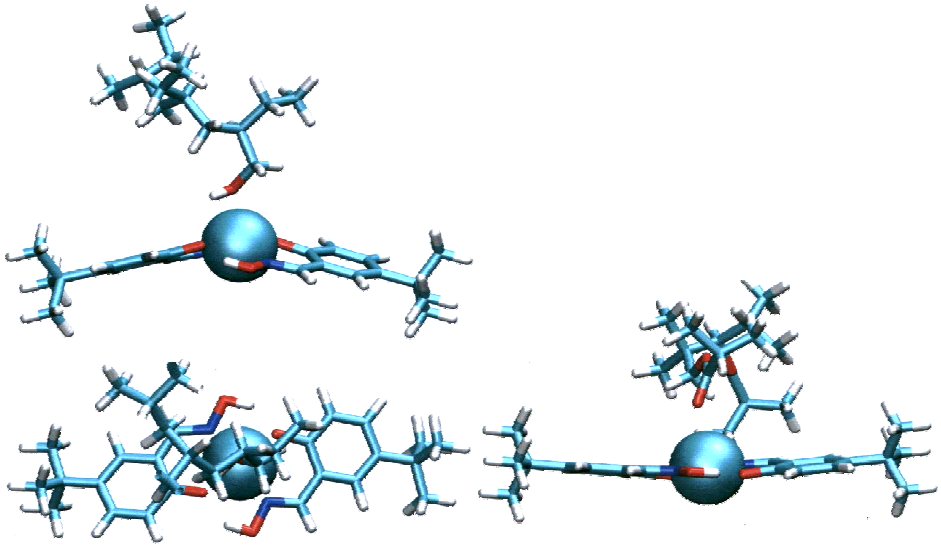

Figure 4.9: Energy minimised structures of the adducts predicted to form between the copper complex of 5-*t*-butylsalicylaldoxime (**18**) and the modifiers TDA and TXIB, left and right respectively.

Similar observations were made for the TXIB-complex system, although to a lesser extent. Formation of the [Cu(**18**-H)$_2$•TXIB] adduct is associated with an energy increase of 38 kJ mol^{-1}. The Cu-N and Cu-O bond lengths were increased to a lesser extent than in the formation of the TDA adduct. Deviation of the [Cu(**18**-H)$_2$•TXIB] adduct from planarity was also less pronounced, see Figure 4.9.

The molecular modelling studies indicate that formation of phenolic oxime copper complex-modifier adducts [Cu(L-H)$_2$•mod] is unfavourable. In contrast, formation of adducts with the free ligands is energetically favourable. These observations are consistent with the modifier stabilising the free ligand to form [L•mod] relative to the copper complex and consequently favouring the stripping process, ie. $K_1 > K_2$ in Scheme 4.3.

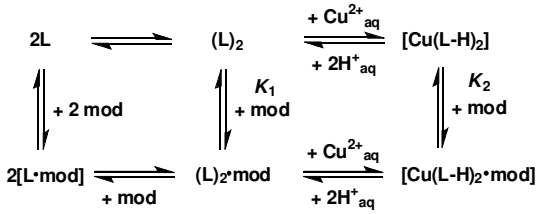

Scheme 4.3: Equilibria involving the formation of adducts of an equilibrium modifier (mod) with an extractant molecule (L), extractant dimer (L_2) or with a copper complex [Cu(L-H)$_2$] in a water-immiscible solvent.

The calculations indicate that, when 1:1 assemblies of the modifier and [Cu(**18**-H)$_2$] are energy minimised they have a higher energy than the parent complex. Consequently they will not be present in significant concentrations in an equilibrium controlled system. However they could provide models for intermediates in which the modifier acts as a "kinetic booster", enhancing the rates of copper stripping by destabilising the planar geometry.

Although no adducts of modifiers have been reported for Cu(II) complexes of phenolic oximes, interactions have been reported between metal complexes of β-diketonates and phosphorus esters, amides, alcohols and ketones.[52, 53] Of particular relevance to this study is the formation of phosphine oxide-copper β-diketonate adducts which is discussed below.[54]

4.3 Bis-β-diketonato Copper(II)-Phosphine Oxide Adducts

Phosphine esters such as trioctylphosphine oxide (TOPO) have been demonstrated to enhance the extraction of di-, tri- and tetra-valent metal cations by β-diketonate chelating reagents.[52, 53, 55, 56] Copper β-diketonate complexes show some solubility in the aqueous phase and formation of the adduct with TOPO enhances it solubility in water-immiscible solvents. In the resulting phase transfer of copper, TOPO acts as a solvating reagent.[54, 57] The formation of the organic soluble adducts [Cu(diketonate-H)$_2$•(TOPO)] arises from the favourable electronic interaction between the Lewis acidic copper complex and the strongly Lewis basic oxygen atom of the phosphine oxide.[58] A square pyramidal complex is formed with the oxygen atom of the

phosphine oxide in the apical position.[59] The strength of this interaction can be increased by introducing electronegative atoms into the *β*-diketonate, e.g. fluorine as in thenoyltrifluoroacetone.[60] Although introduction of electron withdrawing groups decreases the electron density on the keto/enol oxygen atoms and destabilises the *β*-diketonate copper complexes,[60] it has the opposite affect on the interaction with TOPO as it increases the Lewis acidity of the copper complex. Conversely, introducing electron withdrawing substituents onto the phosphine oxide, as in triphenylphosphine oxide or phosphate esters, results in less electron density on the oxygen of the phosphorus ester, reducing its Lewis basicity and weakening the interaction with the copper complex.[54, 60]

Analogous *β*-diketonate adducts have been reported[61] with heterocyclic nitrogenous bases in the apical position. Although the bases studied were less basic and form less stable adducts as a consequence, they have been characterised. Of greater importance to this thesis is the isolation and characterisation of nitrogen-base adducts of copper oxime complexes.[18, 62-65] Isolation of nitrogen adducts with both phenolic oxime and *β*-diketonate copper complexes and phosphine oxide adducts of the latter provides support for the possible formation of similar phosphine oxide adducts with phenolic oxime copper complexes. For the copper complex-modifier adduct to be stabilised relative to the extractant-modifier adduct, K_2 in Scheme 4.3 would need to be greater than K_1.

4.4 Experimental Investigations into Copper Complex-Modifier Adducts

To investigate whether modifier-complex adducts are present in solution, experiments were carried out using pure single isomer analogues of the commercial extractant blends (see Figure 4.10). *n*-Heptane was selected as the solvent because it has very low water-miscibility and is non-polar, therefore should not disrupt the hydrogen-bonding interactions under investigation. The phenolic oxime selected was *t*-octyl-salicylaldoxime (**19**) to ensure single isomer purity and maintain sufficient solubility in *n*-heptane. Two modifiers were investigated in this study. Firstly, an

alcohol because of its strong modifying ability in commercial systems. Initial results from this study proved inconclusive, consequently the alcohol modifier was replaced with a phosphine oxide as a result of observations made by John Campbell[66] at CYTEC Industries Inc. which indicated that phosphine oxides are much stronger modifiers than alcohols or esters. Other observations made by John Campbell[66] are discussed in Section 4.5.

4.4.1 2-Ethylhexanol as Modifier

2-Ethylhexanol (2-EH) was selected to mimic TDA which had been investigated[10] by molecular modelling because it is also β-branched (see Figure 4.10).

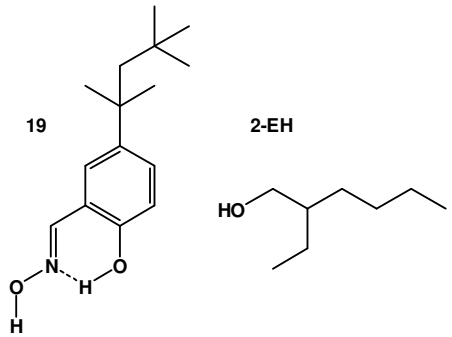

Figure 4.10: The phenolic oxime, 5-*t*-octyl-salicylaldoxime (**19**) and alcohol 2-ethylhexanol (2-EH) chosen to probe interactions between modifiers and extracted copper complexes.

Solvent extraction experiments were carried out to investigate whether the chosen system would behave in a similar manner to those of the commercial extractant-modifier blends.

4.4.2 Effects of 2-Ethylhexanol on Copper Loading

The copper extraction S-curve for **19** in *n*-heptane was defined (Figure 4.11). Solutions of **19** (5 ml, 0.01 M) were contacted with copper sulfate (4 ml, 0.02 M) and the pH adjusted by addition of sulfuric acid or potassium hydroxide to yield an overall aqueous copper sulfate solution (5 ml, 0.016 M). The phases were stirred for 16 hrs to allow the system to equilibrate fully. The S-curve obtained is shown in

Figure 4.11 where 100% Cu loading corresponds to formation of [Cu(**19**-H)$_2$]. The $pH_{½}$ of the system is *ca*. 0.8.

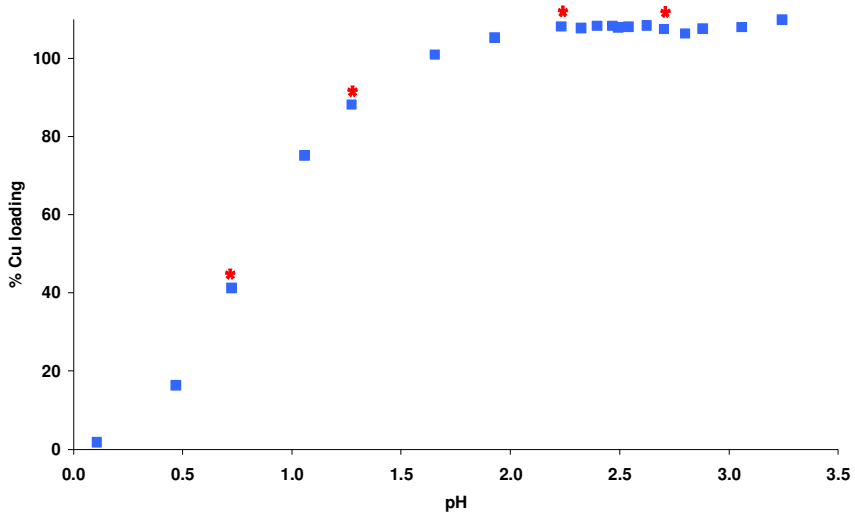

Figure 4.11: pH-dependent Cu loading by a 0.01 M *n*-heptane solution of **19** from aqueous copper sulfate (0.016 M). The effect of addition of 2-EH were subsequently studied for mixtures which generated the points marked ✱.

To determine the effects of 2-EH on copper loading, aqueous copper sulfate solutions with compositions which generated the four points marked (✱) in Figure 4.11 were contacted with 0.01 M *n*-heptane solutions of **19** containing increasing molar quantities of modifier. Aqueous feed solutions which gave the points with equilibrium pH values of *ca*. pH 0.7, 1.3 and 2.7 were selected for study as they represent less than 50%, between 50 and 100% and 100% Cu loading respectively. The point at pH 2.2 represents the system where only copper sulfate is present in the aqueous phase, i.e. no acid or base had been added to adjust the pH.

Solutions of **19** (0.01 M) containing either zero, 0.2, 0.5, 1.0, 2.0 or 10.0 molar equivalents of 2-EH were added to each sample of the aqueous feed solutions which had given the extraction loadings marked ✱ in Figure 4.11. The organic solutions were prepared by mixing *n*-heptane solutions of **19** (2.5ml, 0.02 M) with *n*-heptane solutions of 2-EH (2.5 ml; 0.4, 1.0, 2.0, 4.0, 20.0 molar equivalents) to give the overall modifier to copper ratios of 0.2, 0.5, 1.0, 2.0 and 10.0 to 1. The percentage of

theoretical copper loading by **19** is plotted as function of the molar ratio of 2-EH to [Cu(**19**-H)$_2$] in Figure 4.12.

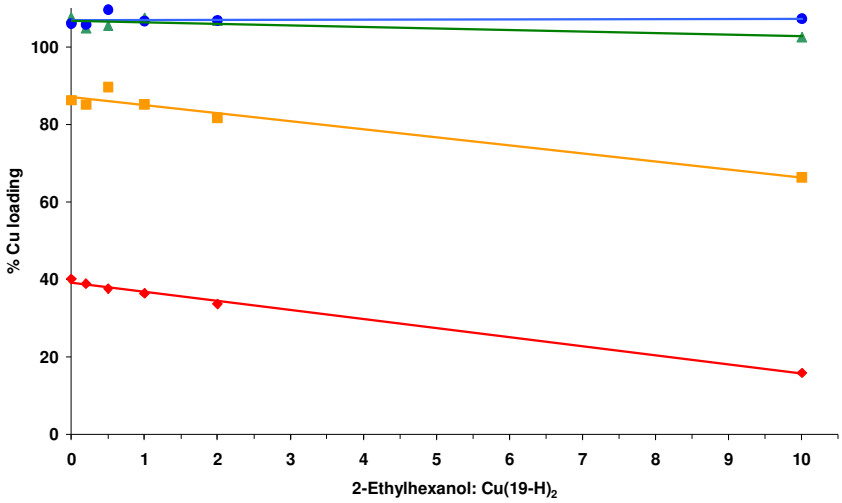

Figure 4.12: The effect of increasing concentration of 2-ethylhexanol in *n*-heptane solutions of **19** on the %Cu loading from the aqueous solutions which, in the absence of modifier give equilibrium pH values of 0.7 (♦), 1.3 (■), 2.2 (▲) and 2.7 (●).

Addition of 2-EH to solutions of **19** influences copper loading to varying extents depending on the initial and equilibrium pH of the aqueous phase. When the ligand is fully loaded, i.e. pH > 2.0 there is little or no effect on the %Cu loading. However at pH 1.3 and 0.7 there is a 20 and 25% decrease in copper loading, respectively, when 10 molar equivalents of modifier are added. In practice modifiers are usually added at 5-10% of the concentration of the extractant.[3] In the above case, only *ca.* 1% decrease in copper content of the organic phase is measured when 20% modifier is used. Even though a 10 fold excess of modifier was added to the system which is fully loaded (●), relative to the copper complex [Cu(**19**-H)$_2$], no change in copper content was detected. These findings are in agreement with the general observation that modifiers influence the system differently under load and strip conditions.

Release of copper into the aqueous phase requires protonation of the extractant. As these protons must be sourced from the aqueous phase, experiments in which the modifier has promoted release of copper might be expected to show higher

equilibrium pH values. For the experiments with 2-ethylhexanol no increases were evident (Figure 4.13).

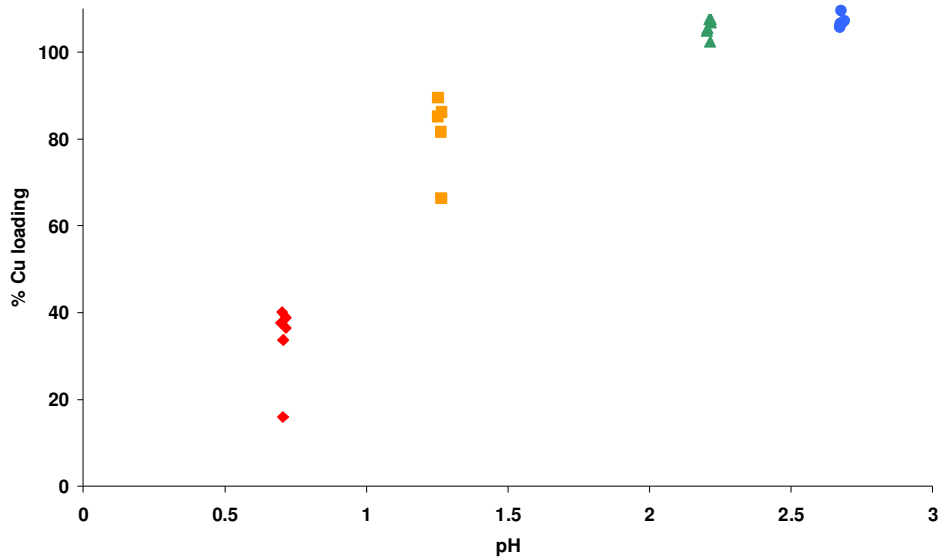

Figure 4.13: The effect of increased concentrations of 2-ethylhexanol (0, 0.2, 0.5, 1.0, 2.0, 10.0 molar equivalents relative to the formation of [Cu(**19**-H)$_2$]) in *n*-heptane solutions of **19** (0.01 M) on the equilibrium pH of the aqueous phase for mixtures with pH values of 0.7 (♦), 1.3 (■), 2.2 (▲) and 2.7 (●) with no added 2-ethylhexanol.

The reason no change in equilibrium pH of the aqueous phase solution is detected is because very few protons are being transferred into the organic phase relative to the concentration of protons present at these low pH values. The concentration of protons transferred to the organic phase would be 0.002 M for a 20% decrease in copper loading. This would result in a pH increase of 0.004 and 0.02 at pH 0.70 and 1.30 respectively. Although the latter is within the limits (±0.002) of the pH electrode used in this study, sulfate/bisulfate buffering in this pH range will make differences in pH very small.

4.4.3 IR

IR analysis was performed using samples from the solvent extraction experiments above. Spectra were recorded on neat samples and the *n*-heptane background subtracted. The spectra measured for the samples replicated at pH 2.2 (▲) are given in Figure 4.14. Only the regions of the spectra where changes are observed are plotted in Figure 4.14 which records the addition of 2-EH to [Cu(**19**-H)$_2$] at pH 2.2 (▲). Unfortunately, the only changes detected correspond to the peaks present in 2-EH.

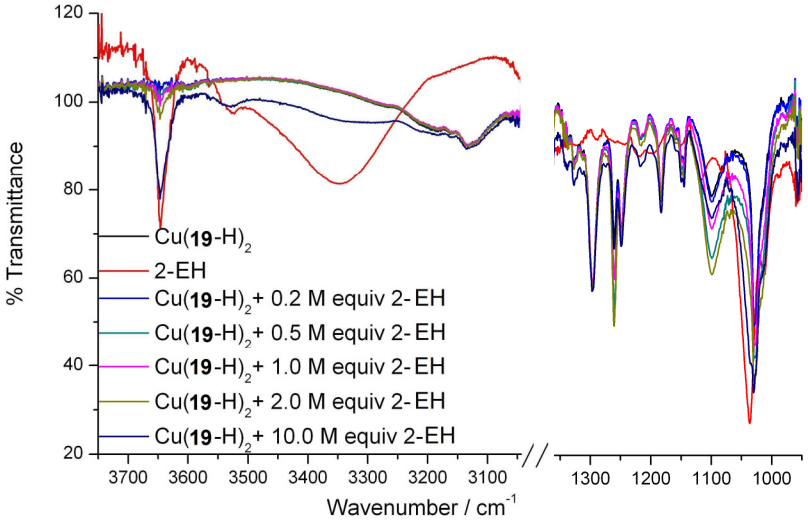

Figure 4.14: IR spectra of the samples of [Cu(**19**-H)$_2$] replicated at pH 2.2 as a function of 2-ethylhexanol (2-EH) added.

The C-O band of 2-EH overlies that of the phenol[24] C-O at *ca.* 1030 cm^{-1} causing an apparent shift but this is most likely to be due to broadening of the alcohol C-O as a result of aggregation effects as the 2-EH molecules self-associate. Interestingly, the intensity of the band at *ca.* 1100 cm^{-1}, present in [Cu(**19**-H)$_2$] varies but not as a function of modifier concentration. This band is tentatively assigned as an aromatic vibration. The sharp band at *ca.* 3645 cm^{-1} was initially assigned to the alcohol O-H stretching frequency, but was also observed in the TOPO system (see Section 4.5.2) and is assigned to free monomeric water[67, 68] in the organic phase in reversed micelles.[69]

4.4.4 UV/Vis

The electronic spectra of the fully loaded samples of [Cu(**19**-H)$_2$] were recorded on the samples from the extractions in which no modifier was present. Formation of a modifier-[Cu(**19**-H)$_2$] adduct as shown in Figure 4.9 and Scheme 4.3 should result in a change in the electronic transitions of the compound. Spectra of the 5 mM solutions of [Cu(**19**-H)$_2$] do not display any distinct absorbance above 400 nm. To measure the spectra below 300 nm, a 10-fold dilution was necessary. These spectra are shown in Figure 4.15 for the extract which has an equilibrium pH of 2.2 (▲) in the absence of the modifier.

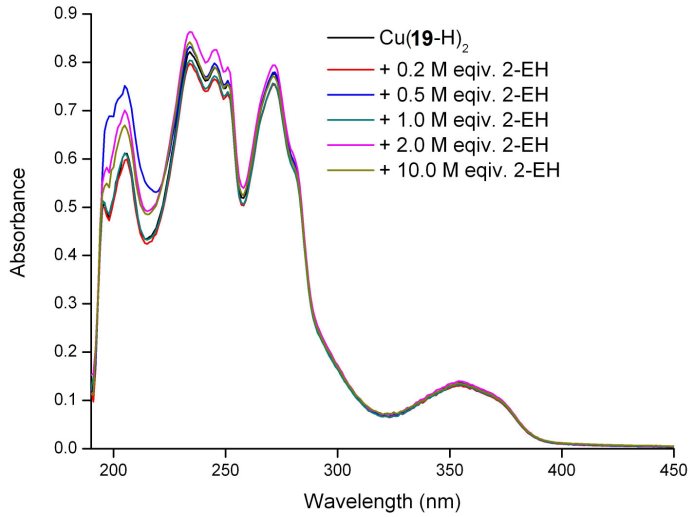

Figure 4.15: Electronic spectra of the replicated samples of [Cu(**19**-H)$_2$] at pH 2.2 (▲) with increasing molar equivalents of 2-ethylhexanol.

Above 225 nm very little change is observed in the spectrum of [Cu(**19**-H)$_2$] as 2-EH concentration is increased. The intensity of the peak observed at *ca.* 206 nm does vary, but not with concentration of 2-EH. The maximum intensity is measured when the molar ratio of [Cu(**19**-H)$_2$] to 2-EH is 2:1. This is anomalous and no trend in maxima and minima are observed to indicate isobestic points. To probe further the electronic characteristics of the copper centre, EPR was used.

4.4.5 EPR

Measurement of the EPR spectra of the organic extracts from the solvent extraction experiment described above (equilibrium pH = 2.2 (▲) in the absence of modifier) should allow the environment of the copper centre's unpaired electron to be probed, providing information about any changes in its coordination sphere. If the Cu-N bonds are lengthened by interaction with the alcohol modifier, as suggested by the computational molecular modelling,[10] a decrease in copper-nitrogen coupling constants should be observed.[70] The spectra obtained for the neat samples of the organic phase from the solvent extraction experiment carried out in Section 4.4.2 are displayed in Figure 4.16.

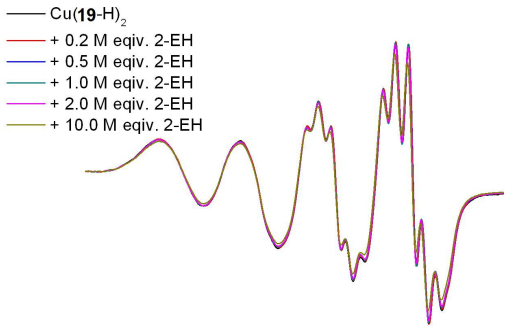

Figure 4.16: EPR spectra of the extractions containing [Cu(**19**-H)$_2$] at an equilibrium pH 2.2 (▲) with increasing molar equivalents of 2-ethylhexanol in the organic phase.

There is no change in hyperfine coupling in the experimental spectra, although slight differences in intensity are observed. These are attributed to the very slight variations in the copper concentration of the samples as recorded by ICP-OES (Section 4.4.2) and are also observed by UV/Vis (Section 4.4.4). When simulated, the *g*-value and copper and nitrogen hyperfine coupling were extrapolated; the results are given in Table 4.2. No trend is observed in the data.

Table 4.1: Hyperfine coupling (A) and *g*-values calculated for the EPR spectra of [Cu(**19**-H)$_2$] at pH 2.2 with increasing molar equivalents of 2-ethylhexanol.

	A^{Cu}	A^{N}	*g*
[Cu(**19**-H)$_2$]	89.991	14.608	2.097
[Cu(**19**-H)$_2$] + 0.2 M equiv 2-EH	90.335	14.638	2.097
[Cu(**19**-H)$_2$] + 0.5 M equiv 2-EH	90.162	14.624	2.097
[Cu(**19**-H)$_2$] + 2.0 M equiv 2-EH	90.434	14.832	2.096
[Cu(**19**-H)$_2$] + 5.0 M equiv 2-EH	90.220	14.763	2.096
[Cu(**19**-H)$_2$] + 10.0 M equiv 2-EH	90.142	14.663	2.097

Of the experimental data collected in Section 4.4, investigating the interaction between 2-ethylhexanol and [Cu(**19**-H)$_2$], none provide evidence to support the formation of an adduct between 2-EH and [Cu(**19**-H)$_2$] over the concentration range studied (0.2-10 molar equivalents). This supports the results obtained from the molecular modelling study which suggest that the interaction between modifier and extractant is stronger than that with the copper complex, i.e. $K_1 > K_2$ in Scheme 4.3.

4.5 Trioctylphosphine Oxide as Modifier

Trioctylphosphine oxide (TOPO, CYANEX 921) was investigated as a modifier as a result of findings by John Campbell at Cytec Industries Inc.[66] These indicate that TOPO is a much stronger modifier than 4-nonylphenol or tridecanol. Further studies[66] were carried out on a liquid analogue, CYANEX 923 which is a mixture of four different phosphine oxides; $R_3P{=}O$, $R_2R'P{=}O$, $RR'_2P{=}O$ and $R'_3P{=}O$ where R and R' are *n*-octyl and *n*-hexyl respectively. These investigations analysed the extraction of sulfuric acid into the organic phase. Results are given in Table 4.2.

Table 4.2: Sulfuric acid extraction by CYANEX 923 under load/strip conditions in the presence and absence of **P50**.[66]

Sample	1 Control	2 Load	3 Strip	4 Control	5 Load	6 Strip
Cyanex 923 (M)	0.1	0.1	0.1	0.1	0.1	0.1
P50 (M)	-	-	-	0.19	0.19	0.19
$Cu_{(aq)}$ (g L^{-1})	-	6	30	-	6	30
$H_2SO_{4(aq)}$ (g L^{-1})	-	-	180	-	-	180
pH	-	2	-	-	2	-
$H_2SO_{4(org)}$ (M)	0	0	0.314	0	0	0

Comparison of the results from experiments 1-3 indicate that the under strip conditions (experiment 3) sulfuric acid is extracted into the organic phase which is entirely in agreement with TOPO being an acid extractant.[36] However, when **P50** is present in the organic phase (experiment 6), sulfuric acid is no longer extracted. This suggests that the interaction between **P50** and TOPO is more favourable than that between sulfuric acid and TOPO.

4.5.1 Solvent Extraction

Solutions of **19** (5 ml, 0.01 M) containing either zero, 0.1, 0.5, 1.0, 2.0 and 10.0 molar equivalents of TOPO were added to samples of the aqueous feed solutions which had given the extraction loadings marked ✱ in Figure 4.11. The equilibrium pH of the sample marked ✱ in Figure 4.11 at pH 2.7 (●) is now pH 3.1 because a new stock solution of base was prepared for use in this experiment. The organic solutions were prepared by mixing *n*-heptane solutions of **19** (2.5 ml, 0.02 M) with *n*-heptane solutions of TOPO (2.5 ml; 0.2, 1.0, 2.0, 4.0, 20.0 molar equivalents) to give the overall modifier to copper ratios of 0.1, 0.5, 1.0, 2.0, 10.0 to 1. The percentage of theoretical copper loading by **19** is plotted as function of the molar ratio of TOPO to [Cu(**19**-H)$_2$] in Figure 4.17.

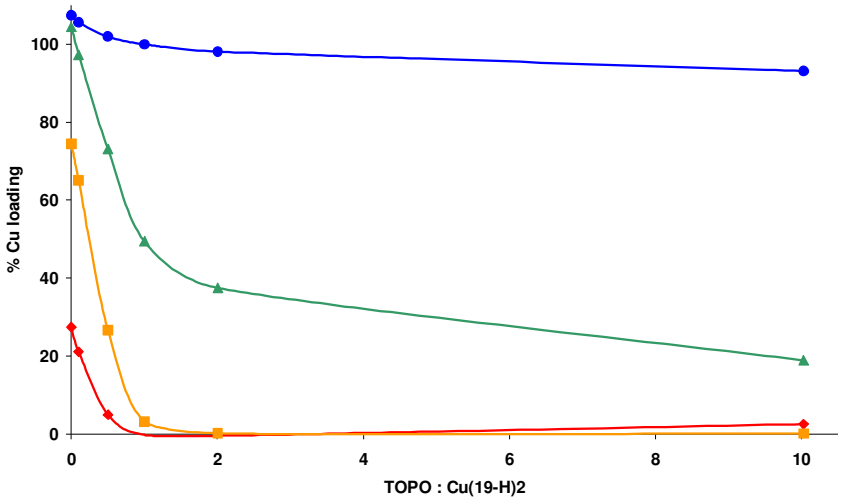

Figure 4.17: The effect of increasing the concentration of TOPO in *n*-heptane solutions of **19** on the Cu loading initial equilibrium pH's of 0.7 (♦), 1.3 (■), 2.2 (▲) and 3.1 (●).

It can be seen that TOPO depresses copper extraction significantly more than 2-EH at all pH values. Comparison of the copper loadings measured for samples with equimolar equivalents of TOPO and 2-EH at initial equilibrium pH of 1.3 (■) show a decrease in copper loading of *ca.* 71 and 1% respectively. TOPO also has a significant effect on the copper loading at pH 2.2 (▲), with *ca.* 80% decrease. Almost no depression was observed when 10 molar equivalents of 2-EH was added at this pH. The lower copper loadings in the presence of added TOPO for the extractions under conditions which would have given an equilibrium pH of 2.2 (▲) and pH 3.1 (●) were accompanied by a significant increase in equilibrium pH values, Figure 4.18. This is to be expected because, as the copper content of the organic phase decreases, twice as many protons are required to transfer to the organic phase to reprotonate the ligand.

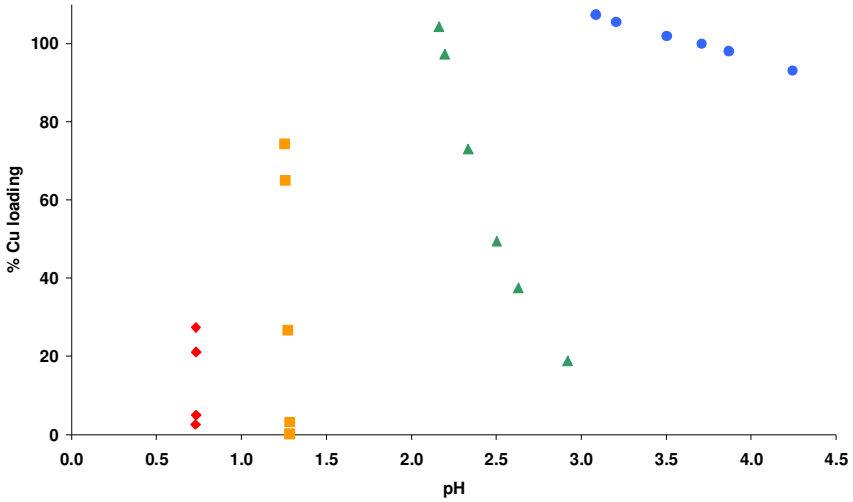

Figure 4.18: The effect of increasing the concentration of TOPO in *n*-heptane solutions of **19** on the pH of the aqueous phase at initial equilibrium pH's of 0.7 (♦), 1.3 (■), 2.2 (▲) and 3.1 (●).

4.5.2 IR

The IR spectra shown in Figure 4.19 were recorded on neat samples obtained from the solvent extraction experiments in Section 4.5.1. Only those spectra measured for solvent extraction experiments at initial equilibrium pH 3.1 (●) are considered suitable to investigate complex-adduct interactions because significant new bands and shifts will be observed in the spectra of the samples measured at lower pH due to the increasing concentrations of free extractant molecules because copper is stripped from the complex.

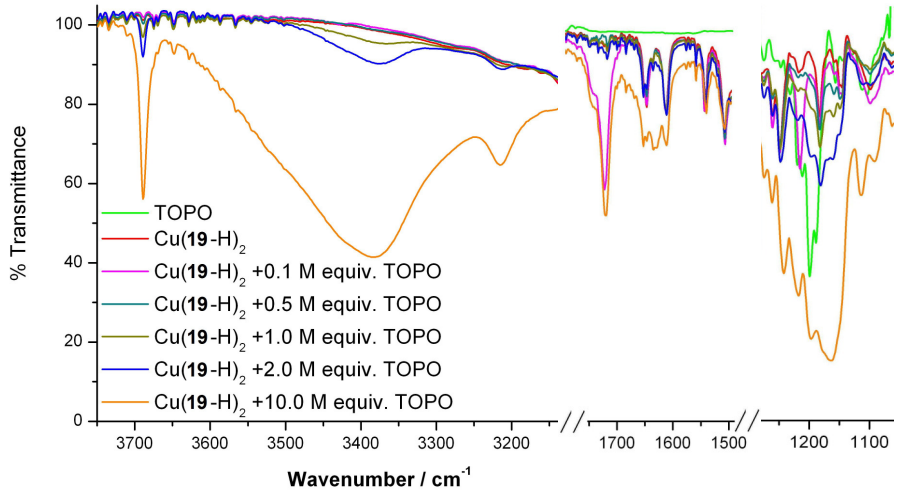

Figure 4.19: Infrared spectra of the solvent extraction samples replicated at equilibrium pH 3.1 shown in Figure 4.17 displaying regions which feature changes.

Between 3750 and 3050 cm^{-1} the spectra show very little change until > 1.0 M equivalents of TOPO are added, beyond this a sharp band grows in intensity at 3689 cm^{-1}. This band shows a striking resemblance to that observed at 3650 cm^{-1} in the 2-EH system and is best assigned to free monomeric water[67, 68] in the organic phase in reversed micelles.[69] Broad bands also appear at *ca.* 3384 and 3215 cm^{-1}, these are attributed to hydrogen bonded water but are within the regions expected for phenolic oxime intermolecular oximic- and intramolecular phenolic- hydrogen bonds.

A peak at 1722 cm^{-1} appears when 0.1 molar equivalent of TOPO is added. The only other spectrum containing this peak is that with 10 molar equivalents of TOPO, 1720 cm^{-1}. This is very anomalous as it occurs in the fingerprint regions of C=O bonds and none are present in the compounds analysed.

Peaks at 1612 and 1543 cm^{-1}, attributed to coupled C=N and C=C stretches, shift to 1611 and 1540 cm^{-1} respectively as the concentration of TOPO is increased. Similarly, the peak at 1183 assigned to the oxime N-O shifts to lower frequency 1181 cm^{-1}, as does that of the phenol C-O, 1028 shifts to 1024 cm^{-1}. Unfortunately the P=O stretching frequencies observed for monomer and aggregate, 1198 and 1178 cm^{-1}, are masked by the oxime N-O. To monitor the behaviour of the P=O bond upon adduct formation, a titration of copper oxime complex to a standard solution of

TOPO would be required. A decrease in P=O vibration frequency is expected as a result of delocalisation of electrons upon coordination as previously reported for copper β-diketonate-TOPO adducts.[56, 71]

4.5.3 UV/Vis

Upon addition of TOPO to solutions of [Cu(**19**-H)$_2$] the colour of the *n*-heptane phase turned from pale yellow to lime green, indicating a change in the environment of the copper centre. The colour of the adduct formed is similar to that of the phosphine oxide adduct of the thenoyltrifluoroacetone copper complex.[54]

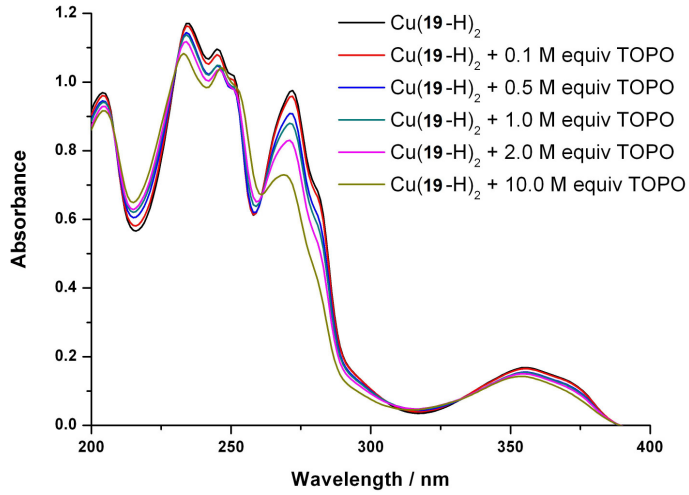

Figure 4.20: Electronic spectra of the solvent extraction samples replicated at equilibrium pH 3.1 (●) shown in Figure 4.17 displaying regions which feature changes.

The electronic spectra measured for the solvent extraction samples with initial equilibrium pH 3.1 (●) can be seen in Figure 4.20. A 10-fold dilution was required to obtain absorbances in the range 0 to 1.2. The spectra of the solvent extraction experiments carried out at lower pH values were not recorded due to the decrease in copper content which will result in a change of absorbances, regardless of adduct formation. The electronic spectra recorded show evidence for the formation of a single 5-coordinate species due to the presence of isobestic points.

4.5.4 EPR

The electronic spectra reported in Section 4.5.3 indicate that a new 5-coordinate species is formed, consequently the EPR spectra were measured to confirm that the colour change was due to a change in the coordination environment of the copper atom. The room temperature, liquid phase experimental spectra shown in Figure 4.21 were recorded directly on neat samples of the organic phase extracts at initial equilibrium pH 3.1 (●) taken from the solvent extraction experiment described in Section 4.5.1.

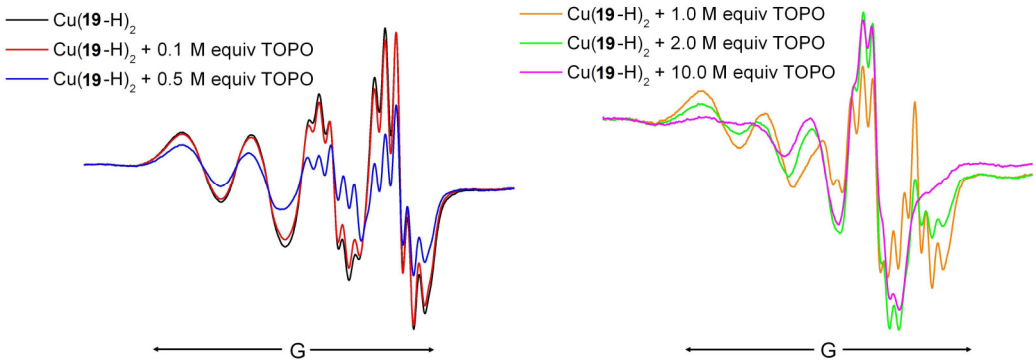

Figure 4.21: EPR spectra of the solvent extraction samples of [Cu(**19**-H)$_2$] replicated at equilibrium pH 3.1 (●) as shown in Figure 4.17.

The intensity of the spectra changes significantly upon addition of 0.5 molar equivalents of TOPO (blue line Figure 4.21, left) which may indicate a decrease in copper concentration due to transfer to the aqueous phase rather than formation of an EPR silent copper containing material in the organic phase but is not consistent with copper content of the organic phase measured by ICP-OES. When a 1.0 molar equivalent of TOPO or greater is added (right, Figure 4.21), the hyperfine coupling of the spectra changes and signal intensity increases. This indicates the formation of a new species where the unpaired electron is in a different environment.

The hyperfine coupling constants and *g*-value were determined by computational simulation for the experimental spectra of [Cu(**19**-H)$_2$] and that presumed to be [Cu(**19**-H)$_2$•TOPO] when 10 molar equivalents of TOPO are added. The copper (A^{Cu}) and nitrogen (A^{N}) coupling constants were reduced from 90 and 14 to 76 and 13 G respectively. A decrease in coupling constant corresponds to a change in the

environment of the unpaired electron[70] to one where it is less influenced by the copper and nitrogen. This result may be indicative of a lengthening of the copper-nitrogen bond and redistribution of electron density on the copper centre and is consistent with the findings of the DFT energy minimised structure of the lowest energy molecular dynamic simulations carried out for TDA and [Cu(**18**-H)$_2$] in 4.2.4. The *g*-value increases from 2.097 to 2.118 indicting coupling to filled orbitals. Resolution is also lost upon addition of TOPO and linewidths increase from 10.5 to 13.5 which are most likely to be indicative of slower tumbling caused by an increase in molecular bulk.[72] These findings agree with those measured for the analogous pyridine adduct of the copper complex of **P50**: copper (A^{Cu}) and nitrogen (A^{N}) coupling reduce from 93 and 17 to 74 and 15 G respectively.[62] The *g*-value also increases from 2.098 to 2.115. It can be concluded that the results obtained are consistent with the formation of a TOPO adduct [Cu(**19**-H)$_2$•TOPO].

4.5.5 Mass Spectrometry

The mass spectrum of a methanolic solution of equimolar [Cu(**19**-H)$_2$] and TOPO (*ca*. 14 μM) was obtained *via* sonic-spray ionisation[73, 74] mass spectrometry by Ben Roach at the University of Edinburgh. The species identified are given in Table 4.3.

Table 4.3: Major species identified in the sonic-spray mass spectrum of [Cu(**19**-H)] containing equimolar quantities of TOPO.

Species	*m/z*
[(TOPO)$_2$]H$^+$	773.47
[(TOPO)$_2$]Na$^+$	795.47
[(TOPO)$_2$]K$^+$	811.20
[Cu(**19**-H)$_2$TOPO]Na$^+$	968.07
[Cu(**19**-H)$_2$TOPO]K$^+$	983.67
[(TOPO)$_3$]Na$^+$	1181.27
[Cu(**19**-H)$_2$(TOPO)$_2$]Na$^+$	1353.40
[(TOPO)$_4$]Na$^+$	1566.53

Isotopic distribution patterns consistent with 1:1 and 1:2 TOPO adducts of [Cu(**19**-H)$_2$] were isolated. The most intense peaks are assigned to TOPO and its aggregates, suggesting that these are major species or have the greatest propensity to ionise due to the large electron density on the oxygen atom of the phosphine oxide. Identification of the [Cu(**19**-H)$_2$TOPO] adduct *via* sonic-spray mass spectrometry provides further evidence for its formation in solution.

4.6 Determination of Association Constants

Identification of adduct formation between phenolic oxime copper complex [Cu(**19**-H)$_2$] and TOPO when present in at least equimolar quantities indicates the formation of a 1:1 complex. To support this suggestion, a continuous variation Job plot[75, 76] was carried out on the [Cu(**19**-H)$_2$]:TOPO system in *n*-heptane (0.4 mM) by UV/Vis spectroscopy following the intensity of the absorbance at 234nm, this is plotted in Figure 4.22. The maximum in the graph at 0.5 corresponds to the formation of a 1:1 species.

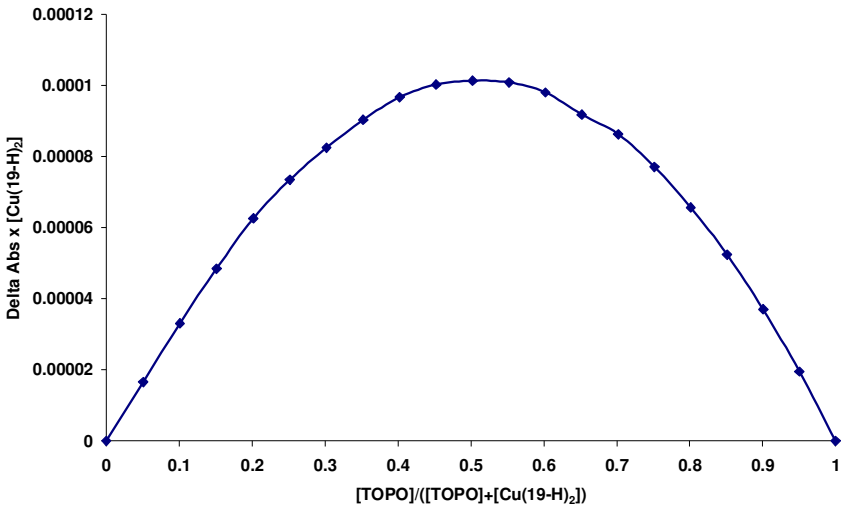

Figure 4.22: Continuous variation Job plot for TOPO interaction with [Cu(**19**-H)$_2$] following the intensity of the absorbance at 234 nm.

4.6.1 TOPO + Cu(19-H)$_2$ in *n*-Heptane

Having established that a 1:1 adduct is formed between TOPO and [Cu(**19**-H)$_2$], the binding constant was determined *via* UV/Vis titration. This titration was carried out as a single phase to ensure that the "modifier properties" of TOPO did not result in reduction of copper concentration by transfer to the aqueous phase (see equilibrium in Scheme 4.3). A standard solution (0.4 mM) of [Cu(**19**-H)$_2$] was prepared and used as diluent to dissolve and make solutions of TOPO to volume. TOPO concentration was varied between 0.2[Cu(**19**-H)$_2$] to 50[Cu(**19**-H)$_2$]. The spectra are shown in Figure 4.23.

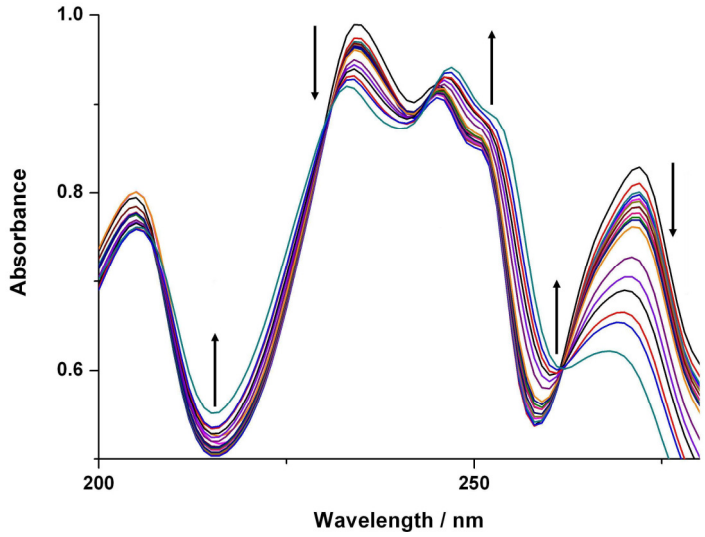

Figure 4.23: Electronic spectra of [Cu(**19**-H)$_2$] showing changes in absorbance with increasing molar equivalents of TOPO.

The intensity of the absorbance at 271 nm was used to calculate the binding constant *via* the method previously reported.[77] The concentrations of [Cu(**19**-H)$_2$], [TOPO] and the 1:1 adduct ([Cu(**19**-H)$_2$]-[TOPO]) are assumed to be sufficiently low for the respective activity coefficients to be equal to unity. The total concentration of [Cu(**19**-H)$_2$] is denoted by [Cu(**19**-H)$_2$]$_0$, the mole fraction of 'free' [Cu(**19**-H)$_2$] molecules by χ_{free} and the total TOPO concentration by [TOPO]$_0$ then [TOPO-Cu(**19**-H)$_2$] = [TOPO-Cu(**19**-H)$_2$]$_0$(1-χ_{free}) and inserting these relations into the mass-action law gives χ_{free}:

$$K = \frac{[TOPO - \mathrm{Cu}(\mathbf{19}\text{-}\mathrm{H})_2]c^{\phi}}{[TOPO][\mathrm{Cu}(\mathbf{19}\text{-}\mathrm{H})_2]} \qquad \text{where} \quad c^{\phi} = 1 \text{ mol dm}^{-3}$$

$$\chi_{free} = \frac{-(1+K\Delta)+\sqrt{(1+K\Delta)^2+4K[\mathrm{Cu}(\mathbf{19}\text{-}\mathrm{H})_2]_0/c^{\phi}}}{2K[\mathrm{Cu}(\mathbf{19}\text{-}\mathrm{H})_2]_0/c^{\phi}}$$

where $\Delta = ([\mathrm{TOPO}]_0 - [\mathrm{Cu}(\mathbf{19}\text{-}\mathrm{H})_2]_0)/c^{\phi}$. The measured absorption coefficient of [Cu(**19**-H)$_2$] at fixed wavelength λ is a weighted sum of the free and adduct absorption coefficients: $\varepsilon([\mathrm{Cu}(\mathbf{19}\text{-}\mathrm{H})_2]_0\,\lambda) = \chi_{free}\varepsilon_{free}(\lambda) + (1-\chi_{free})\varepsilon_{complex}(\lambda)$. The binding constant was determined to be: K = 378 ± 28 M^{-1}, ΔG_{free} = -15 ± 1 kJ mol^{-1}, reduced χ^2 = 1.38 x 10^{-5} (see Appendix 7.4.3 for fitted curve).

4.6.2 TOPO + 19 in *n*-Heptane

The binding constant TOPO + **19** $\rightleftharpoons$ [TOPO•**19**] was determined to establish whether TOPO interacts more strongly with the **19** than the copper complex [Cu(**19**-H)$_2$]. Increasing molar equivalents of **19** (0.1-2.0[TOPO]) were dissolved in and made to volume with a standard solution of TOPO (5 mM) in *n*-heptane. The ^{31}P NMR shifts were measured in non-deuterated *n*-heptane and referenced to 85% H_3PO_4 at 0 ppm.[78] A capillary containing 85% H_3PO_4 was used in *d*-chloroform (0.5 ml) to lock the NMR instrument. As the molar concentration of **19** is increased, the ^{31}P signal of TOPO is shifted downfield as seen in Figure 4.24.

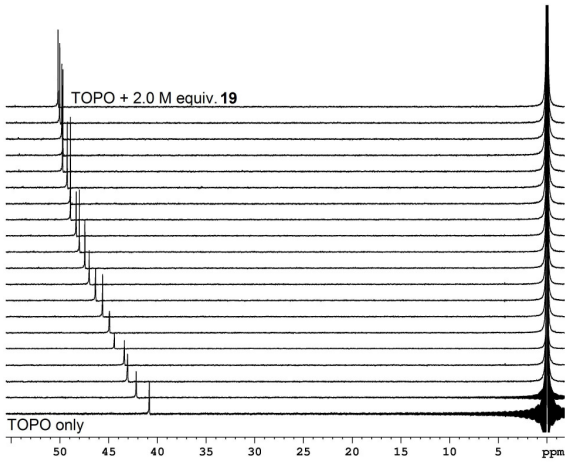

Figure 4.24: Downfield ^{31}P chemical shift measured for stock solutions of TOPO as increasing molar equivalents of **19** are added.

The results of the ^{31}P NMR titration were treated in the same manner to those from the electronic spectra using the chemical shift (δ). Because the concentration of TOPO is constant and that of **19** varies, [TOPO] replaces [Cu(**19**-H)$_2$] in the equations previously used and [**19**] replaces [TOPO] to give $\delta([\mathrm{T}OPO]_0) = \chi_{free}\delta_{free} + (1-\chi_{free})\delta_{complex}$. K = 403 ± 56 M^{-1}, ΔG_{free} = -15 ± 2 kJ mol^{-1}, reduced χ^2 = 0.0155 (see Appendix 7.4.3 for fitted curve).

Although the association constant calculated for formation of [**19**•TOPO] is greater than that for formation of the copper complex adduct [Cu(**19**-H)$_2$•TOPO], the values are within the calculated error of each other. This result would suggest that K_1 and K_2 in Scheme 4.3 are essentially equal and that the equilibrium is pH-controlled. To investigate the effect of pH on the formation of the **19**•TOPO adduct, an *n*-heptane solution of TOPO was saturated with sulfuric acid.

4.6.3 Acidified TOPO + 19 in *n*-Heptane

Modifiers are found have a greater affect when stripping copper from the complex at low pH in conventional circuits. Consequently it is important to know how TOPO interacts with free extractant at low pH. If this interaction is more favourable than

formation of the copper complex it may the driving force behind the shifting equilibria and decrease in extractant strength determined by $pH_{½}$.

A solution of TOPO in *n*-heptane (5 mM) was contacted with sulfuric acid (1.0 M) several times until back-titration of the equilibrated aqueous phase indicated no further acid was extracted into the organic phase. The organic phase was filtered through phase separating papers to remove any entrained aqueous phase. Samples were prepared and treated as Section 4.6.2 for analysis by ^{31}P NMR. A similar downfield shift is observed, as seen in Figure 4.25, and the calculated binding constant, although very similar to that for TOPO is slightly smaller, K = 341 ± 53 M^{-1}, ΔG_{free} = -15 ± 2 kJ mol^{-1}, reduced χ^2 = 0.0189 (see Appendix 7.4.3 for fitted curve) indicating a weaker interaction.

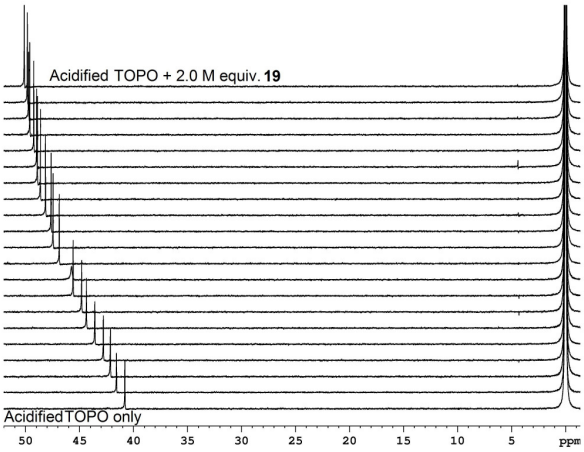

Figure 4.25: Downfield ^{31}P chemical shift measured for stock solutions of an acidified *n*-heptane solutions of TOPO as increasing molar equivalents of **19** are added.

Titration of a sulfuric acid saturated *n*-heptane solution of TOPO with **19** gave a weaker binding constant for the formation of [**19**•TOPO] than the analogous titration **19** of the with the TOPO solution which had not been in contact with sulfuric acid (Section 4.6.2). Although the two binding constants are within experimental error of each other, the lower result obtained when sulfuric acid is present would be expected due to some competitive binding as TOPO is a known acid extractant.[34, 36, 79]

It is reported[36] that 3 mol of TOPO are required to extract each mol of sulfuric acid and the association constant was calculated to be 266 M^{-3} in *n*-heptane. This supports the results obtained in this the current section and Section 4.6.2, that the interaction between TOPO and **19** is greater than that between TOPO and sulfuric acid, hence does not significantly affect the value of the association constant calculated. This evidence supports the finding[66] that CYANEX 923 does not extract sulfuric acid into the organic phase when a **P50** is present as discussed in the introduction to Section 4.5.

4.6.4 TOPO + 19 in Toluene

Commercial solvent extraction diluents are complex mixtures of hydrocarbons and have significant quantities of aromatic components.[1] This experiment was carried out to understand the extent to which solvent influences the interaction between modifiers and extractants.

The influence of toluene on the interaction between TOPO and **19** was determined. Varying molar quantities of **19** were dissolved in portions of a standard solution of TOPO. ^{31}P NMR spectra were measured and data were treated as above. Calculation of the association constant; $K = 122 \pm 31$ M^{-1}, $\Delta G_{free} = -12 \pm 3$ kJ mol^{-1}, reduced $\chi^2 =$ 0.136 (see Appendix 7.4.3 for fitted curve), indicates a significantly weaker interaction than measured in *n*-heptane and suggests competitive interactions with the solvent molecules.

In industrial applications the association constants between TOPO and **19** are expected to be somewhere between those calculated in *n*-heptane and toluene, but closer to that in *n*-heptane because there are generally more aliphatic and non-aromatic cyclic components present in the diluents used in industrial solvent extraction processes.[1]

4.7 Conclusions

At the outset of this work it was hoped that determining the relative sizes of the equilibrium constants for the formation of modifier adducts with **19** or its copper complex would clarify the mode of action of an "equilibrium modifier". In the event these equilibrium constants were found to be almost the same within experimental error. Experimental results obtained from EPR, IR, MS and UV/Vis spectra support formation of [Cu(**19**-H)$_2$•TOPO] adducts. The binding constants calculated in *n*-heptane indicate the interaction between TOPO and [Cu(**19**-H)$_2$] is slightly less favourable than that with free **19**; *c.f.* $K = 378 \pm 28$ M^{-1}, $\Delta G_{free} = -15 \pm 1$ kJ mol^{-1}, $K = 403 \pm 56$ M^{-1}, $\Delta G_{free} = -15 \pm 2$ kJ mol^{-1}, respectively. However, the binding constant to TOPO in an *n*-heptane solution which was saturated with sulfuric acid is weaker than both; $K = 341 \pm 53$ M^{-1}, $\Delta G_{free} = -15 \pm 2$ kJ mol^{-1}. These results are very similar and each is within the calculated error of the fit of the data for the others. Consequently it is difficult to make judgments as to the reason modifiers behave differently under load and strip conditions.

Experimental results provide evidence for adduct formation between [Cu(**19**-H)$_2$] and TOPO. This interaction is favourable as it involves an interaction between a Lewis acid and base. If TOPO was protonated when contacted with sulfuric acid, it too would be a Lewis acid. Therefore, the interaction with [Cu(**19**-H)$_2$] will be unfavourable, but protonated TOPO could make two favourable interactions with the two hydrogen bond acceptor sites on the free phenolic oxime ligand. This could be the reason why modifiers behave differently under loading and stripping. However, there is no evidence to suggest TOPO is protonated when contacted with sulfuric acid,[34] only that it extracts sulfuric into the organic phase.[36]

No evidence was found for formation of adducts between [Cu(**19**-H)$_2$] and 2-ethylhexanol and molecular modelling[10] suggested that adduct formation between the copper complex and the alcohol TDA was less favourable than with the ester TXIB. This difference in behaviour could be a result of the different hydrogen bonding properties of the two systems. Alcohols are hydrogen bond donors and/or acceptors and esters are predominantly hydrogen bond acceptors. The electron density on the

ester oxygen atom is greater than that on the alcohol oxygen atom. Therefore the ester will be more susceptible to association with the Lewis acidic copper atom of [Cu(**19**-H)$_2$]. Alcohols also form strong self-associates and competition for self aggregation will lead to less copper complex adduct forming.

The formation of TOPO adducts with phenolic oximes such as **19** or their copper complexes could indicate that adduct formation might be possible with esters as they feature similar oxygen atoms. However, the electronegativity of the ester oxygen will be less than that of the phosphine oxide oxygen atom, therefore the association constants are expected to be lower for the ester. Association constants for modifier-extractant adducts are an order of magnitude greater for alcohols than those with TOPO which are expected to be greater than those with esters. However, esters such as TXIB have been claimed to show greater modifying abilities than alcohols when used with phenolic oximes in industrial applications.[9]

Taking these points into consideration it is proposed that esters and phosphine oxides modify extraction properties *via* a different route to alcohols. It is suggested that alcohols perturb the equilibrium in favour of forming strong associates with free extractant molecules while esters and phosphine oxides interact with both the extractant and the copper complex. Interaction with the copper complex weakens the C-N and Cu-O bonds, making them more kinetically labile and once copper is stripped they interact with the free ligand. Because this process is dependent on protonation of the phenolate, it is pH dependent. This type of behaviour has been demonstrated for TOPO (see Section 4.5.1) because when base was present in the aqueous phase (pH 3.1) TOPO had very little effect on copper loading relative to when the aqueous phase only contained copper sulfate where free protons are available (pH 2.2).

4.8 Future Work

The aim of this work was to find evidence for the formation of adducts between copper complexes of commercial phenolic oximes and oxygen containing modifiers. Adduct formation was detected for [Cu(**19**-H)$_2$] when TOPO was used as a modifier but not for 2-ethylhexanol. To relate the experimental results using TOPO as a modifier with those obtained computationally for the alcohol TDA and ester TXIB, molecular modelling should be repeated using a simple phosphine oxide. Similarly ^{13}C NMR titrations of **19** with an alcohol and carbon ester following the shifts their α-C would be very useful to rank their association constants with **19** to that of TOPO and relate this to their modifying ability.

The association constants determined in this work were done so using organic solvents of unknown water content. This was reasonable as the titration of **19** with sulfuric acid saturated TOPO required contact with aqueous sulfuric acid. Although, results suggest that protonation has little effect on the binding constant, water is a hydrogen bond donor and acceptor. Therefore, it will interact with modifier and extractant and decrease the association constants measured between **19** and TOPO. Consequently, all solvents used in future studies should be anhydrous or of consistent water content.

Association constants were not determined for 2-ethylhexanol adduct formation as UV/Vis was not applicable because no isobestic points were observed. However it may be that a long path-length cell could be used to observe wavelength and intensity changes of the copper *d-d* transitions which were not of sufficient intensity for the maximum concentration (5 mM) and cell of longest path-length (1 cm, all other studies used 0.5 mm) used in this study.

Collision Induced Mass Spectrometry (CIDMS) has been used previously by the Tasker group in collaboration with Bridgette Duncombe at the University of Edinburgh to probe the strength of 3-substituted phenolic oxime copper complexes.[15] As discussed earlier the strength of the copper complexes has been demonstrated to be related to the hydrogen bond buttressing effect between the 3-substituent and the

oximic hydrogen. The strength of the copper complex is also related to the acidity of the phenolic proton which is influenced by the inductive properties of the 3- and 5-substituents. This also influences the Lewis acidity of the copper atom of the complex.[58] Moreover, the Lewis acidities of β-diketonate copper complexes have been demonstrated to affect the stability of their adducts with nitrogen and oxygen containing molecules. Consequently, CIDMS may have the potential not only to rank the strength of interaction between phenolic oximes and a range of oxygen containing modifier but also to investigate how the Lewis acidity of the copper complex influences its interaction with different classes of modifiers.

4.9 References

1. J. Szymanowski, *Hydroxyoximes and Copper Hydrometallurgy*, CRC Press, London, 1993.
2. J. M. Casas, F. Alvarez and L. Cifuentes, *Chem. Eng. Sci.*, 2000, **55**, 6223-6234.
3. K. Prochaska and K. Staszak, *J. Colloid Interface Sci.*, 2005, **285**, 1-8.
4. J. Szymanowski, *Crit. Rev. Anal. Chem.*, 1995, **25**, 143-194.
5. M. B. Bogacki and J. Szymanowski, *Solv. Extr. R&D, Japan*, 1996, **3**, 10-22.
6. M. Majdan, R. P. Sperline, W. G. Gu, W. H. Yu and H. Freiser, *Solvent Extr. Ion Exch.*, 1989, **7**, 987-1005.
7. J. Szymanowski, *Solvent Extr. Ion Exch.*, 2000, **18**, 729-751.
8. M. B. Bogacki, *Solvent Extr. Ion Exch.*, 1997, **15**, 731-755.
9. A. M. Sastre, Szymanowski, J., *Solvent Extr. Ion Exch.*, 2004, **22**, 737-759.
10. D. Tackley, Intertek ASG, 2006, Confidential Communication.
11. A. W. Ashbrook, *Hydromet.*, 1975, **1**, 5-24.
12. J. Szymanowski and A. Borowiak-Resterna, *Crit. Rev. Anal. Chem.*, 1991, **22**, 519-566.
13. J. R. Parrish, *J. South African Chem. Inst.*, 1970, **23**, 129-135.
14. D. Stepniak-Biniakiewicz and J. Szymanowski, *Hydromet.*, 1981, **7**, 299-313.
15. R. S. Forgan, PhD Thesis, The University of Edinburgh, 2008.
16. R. S. Forgan, P. A. Wood, J. Campbell, D. K. Henderson, F. E. McAllister, S. Parsons, E. Pidcock, R. M. Swart and P. A. Tasker, *Chem. Commun.*, 2007, 4940-4942.
17. T. Steiner, *Angew. Chem. Int. Ed.*, 2002, **41**, 48-76.
18. P. O'Brien, J. R. Thornback and J. Szymanowski, *J. Coord. Chem.*, 1983, **13**, 11-15.
19. A. G. Smith, P. A. Tasker and D. J. White, *Coord. Chem. Rev.*, 2003, **241**, 61-85.
20. P. A. Tasker, P. G. Plieger and L. C. West, *Comprehensive Coordination Chemistry II*, 2004, **9**, 759-808.
21. R. S. Forgan, D. K. Henderson, F. E. McAllister, P. A. Tasker, F. J. White, J. Campbell and R. M. Swart, *Can. Metall.l Quart.*, 2008, **47**, 293-300.
22. K. Burger, F. Ruff, I. Ruff and I. Egyed, *Acta Chimica Academiae Scientarium Hungaricae*, 1965, **46**, 1-&.
23. R. L. Atwood and J. D. Miller, *Trans. Soc. Mining Engin. AIME*, 1973, **254**, 319-323.
24. Ramaswam.Kk, C. I. Jose and D. N. Sen, *Indian. J. Chem.*, 1967, **5**, 156.
25. D. Stepniak-Biniakiewicz, *Pol. J. Chem.*, 1987, **61**, 433-441.

26. L. C. Emeleus, PhD Thesis, University of Edinburgh, 1999.
27. J. T. Harris and M. E. Hobbs, *J. Am. Chem. Soc.*, 1954, **76**, 1419-1422.
28. T. A. Ainscow, I. Aldalur, A. E. Beezer, J. A. Connor, N. C. Garbett, J. C. Mitchell, A. L. Page, N. Tindale, K. A. Turner and R. J. Willson, *J. Colloid Interface Sci.*, 1999, **213**, 87-91.
29. P. K. Kuipa and M. A. Hughes, *Sep. Sci. Technol.*, 2002, **37**, 1135-1152.
30. J. S. Lomas, *J. Phys. Org. Chem.*, 2005, **18**, 1001-1012.
31. A. N. Fletcher and C. A. Heller, *J. Phys. Chem.*, 1967, **71**, 3742-&.
32. K. Prochaska, M. Walczak and K. Staszak, *J. Colloid Interface Sci.*, 2002, **248**, 143-148.
33. A. VasilescuSaidel, C. N. Turcanu and R. Grosescu, *J. Radioanal. Nucl. Chem.* 1996, **203**, 177-187.
34. F. J. Alguacil and F. A. Lopez, *Hydromet.*, 1996, **42**, 245-255.
35. D. M. Petkovic, M. M. Kopecni and A. A. Mitrovic, *Solvent Extr. Ion Exch.*, 1992, **10**, 685-696.
36. S. Y. Xue, Y. H. Yang, Y. Z. Yang, S. X. Sun and B. R. Bao, *J. Radioanal. Nucl. Chem.*, 1998, **229**, 161-163.
37. K. Staszak and K. Prochaska, *Hydromet.*, 2008, **90**, 75-84.
38. R. Barela and H. Buchowski, *Fluid Phase Equilib.*, 1990, **59**, 99-107.
39. R. C. Miller, C. D. Miller, W. Rogers, Jr. and L. A. Hamilton, *J. Am. Chem. Soc.*, 1957, **79**, 424-427.
40. S. Kamila, V. Chakravortty and S. Jena, *J. Solution Chem.*, 2004, **33**, 363-378.
41. J. K. Lorenz and A. B. Ellis, *J. Am. Chem. Soc.*, 1998, **120**, 10970-10975.
42. K. Osseo-Asare, *Adv. Colloid Interface Sci.*, 1991, **37**, 123-173.
43. P. W. Atkins and D. F. Shriver, *Inorganic Chemistry*, 3rd edn., Oxford University Press, Oxford, 1999.
44. D. M. Petkovic, *J. Inorg. Nucl. Chem.*, 1968, **30**, 603-609.
45. D. Stepniak-Biniakiewicz, *Pol. J. Chem.*, 1986, **60**, 725-729.
46. J. Szymanowski and R. Cierpiszewski, *Solvent Extr. Ion Exch.*, 1992, **10**, 663-683.
47. K. Staszak and K. Prochaska, *J. Colloid Interface Sci.*, 2004, **280**, 184-191.
48. K. Staszak and K. Prochaska, *J. Colloid Interface Sci.*, 2006, **294**, 411-417.
49. J. H. Russell and R. L. Rickel, *Solvent Extr. Ion Exch.*, 1990, **8**, 855-873.
50. M. B. Bogacki, *Industrial & Engineering Chemistry Research*, 1999, **38**, 1611-1617.
51. J. A. Connor, N. Tindale and R. F. Dalton, *Hydromet.*, 1991, **26**, 265-280.
52. T. V. Healy, *J. Inorg. Nucl. Chem.*, 1961, **19**, 314-327,328-339.
53. T. V. Healy and J. R. Ferraro, *J. Inorg. Nucl. Chem.*, 1962, **24**, 1449-1461.

54. W. R. Walker and N. C. Li, *J. Inorg. Nucl. Chem.*, 1965, **27**, 411-&.
55. T. V. Healy, D. F. Peppard and G. W. Mason, *J. Inorg. Nucl. Chem.*, 1962, **24**, 1429-1448.
56. J. R. Ferraro and T. V. Healy, *J. Inorg. Nucl. Chem.*, 1962, **24**, 1463-1474.
57. J. W. Mitchell and R. Ganges, *Anal. Chem.*, 1974, **46**, 503-508.
58. D. P. Graddon, *Coord. Chem. Rev.*, 1969, **4**, 1-28.
59. D. P. Graddon and E. C. Watton, *Nature*, 1960, **187**, 1021-1022.
60. C. H. Ke and N. C. Li, *J. Inorg. Nucl. Chem.*, 1966, **28**, 2255-&.
61. D. P. Graddon and E. C. Watton, *J. Inorg. Nucl. Chem.*, 1961, **21**, 49-57.
62. P. Obrien and J. R. Thornback, *Inorg. Chim. Acta*, 1982, **64**, L35-L37.
63. B. McCudden, P. Obrien and J. R. Thornback, *Dalton Trans.*, 1983, 2043-2046.
64. P. O'Brien and J. R. Thornback, *Hydromet.*, 1982, **8**, 331-339.
65. I. Rani, K. B. Pandeya and R. P. Singh, *J. Inorg. Nucl. Chem.*, 1981, **43**, 2743-2745.
66. J. Campbell, Manchester, Private Communication, 2007.
67. M. S. Johnson, K. T. Kuwata, C.-K. Wong and M. Okumura, *Chem. Phys. Lett.*, 1996, **260**, 551-557.
68. A. Loewenschuss, A. Givan and C. J. Nielsen, *J. Mol. Struct.*, 1997, **408**-**409**, 533-537.
69. X. Jiang, Y. Yang, S. Sun, Z. Yin, X. Wang and M. Bao, *J. Phys. Chem. B*, 1999, **103**, 8657-8662.
70. P. W. Atkins, *Physical Chemistry*, 6th edn., Oxford University Press, Oxford, 1998.
71. N. C. Li, S. M. Wang and W. R. Walker, *J. Inorg. Nucl. Chem.*, 1965, **27**, 2263-&.
72. F. E. Mabbs and D. Collison, *Electron Paramagnetic Resonance of d Transition Metal Compounds*, Elsevier, Amsterdam, 1992.
73. A. Hirabayashi, M. Sakairi and H. Koizumi, *Anal. Chem.*, 1995, **67**, 2878-2882.
74. Y. Hirabayashi, A. Hirabayashi, Y. Takada, M. Sakairi and H. Koizumi, *Anal. Chem.*, 1998, **70**, 1882-1884.
75. P. Job, *Ann. Chim. Appl.*, 1928, **9**, 113-203.
76. J. L. Cook, C. A. Hunter, C. M. R. Low, A. Perez-Velasco and J. G. Vinter, *Angew. Chem. Int. Ed.*, 2007, **46**, 3706-3709.
77. R. J. Cooper, P. J. Camp, R. J. Gordon, D. K. Henderson, D. C. R. Henry, H. McNab, S. S. De Silva, D. Tackley, P. A. Tasker and P. Wight, *Dalton Trans.*, 2006, 2785-2793.
78. N. Muller, P. C. Lauterbur and J. Goldenson, *J. Am. Chem. Soc.*, 1956, **78**, 3557-3561.

79. V. V. Sharutin, I. V. Egorova, T. K. Ivanenko, O. K. Sharutina and A. V. Gerasimenko, *Russ. J. Coord. Chem.*, 2003, **29**, 297-299.

Chapter 5 : Experimental

Instrumentation

All solvents and reagents were used as received from Acros, Fisher, Merck, Rathburn, Sigma-Aldrich, TCI Europe or VWR, except 5-nonylsalicylaldehyde which was obtained from CYTEC Industries Inc. and purified by wet silica column chromatography (10% ethyl acetate in hexane eluent) before use. Water used in solvent extraction experiments was obtained from a Milli-Q purification system.

^{1}H and ^{13}C NMR were recorded at 298 K (unless stated otherwise) obtained using a Bruker; ARX250, ADVANCE DPX360 or ADVANCE DMX500 Fourier transform instruments. Chemical shifts (δ) are reported in parts per million (ppm) relative to internal standards. ^{31}P NMR spectra were collected the Bruker ADVANCE DMX500 instrument for the non-deuterated *n*-heptane samples and the Bruker ADVANCE DPX360 for the titration in deuterated toluene. Spectra were referenced relative to the external standard H_3PO_4 ($\delta = 0$) in a capillary.

Fast atom bombardment mass spectrometry was carried out using a Kratos MS50TC spectrometer with a 3-nitrobenzyl alcohol (NOBA) or thioglycerol matrix. Electrospray ionisation mass spectra (ESI-MS) were obtained on a Micromass ZMD mass spectrometer or a Thermo-Fisher LCQ mass spectrometer. Methanol solutions were infused directly at a rate of 5-30 μL/min. The capillary voltage was 3.5 kV on the ZMD and 4.5 kV on the LCQ. The cone voltage and source temperature were varied depending on sensitivity. Data acquisition was obtained using MassLynx (Version 2.5) on the ZMD and Xcalibur (Version 2.0) software on the LCQ.

Inductively coupled plasma optical emission spectroscopy (ICP-OES) analysis was carried out using a Perkin Elmer Optima 5300DV spectrometer. Data was processed using WinLab32 for ICP-OES, version 3.0.0.0103.

Ultraviolet-visible (UV/Vis) spectroscopy was carried out on a Perkin-Elmer Lambda-9 UV/Vis spectrophotometer using 0.5 mm path-length quartz cuvettes. Data was processed using UV WinLab, version 2.70.01.

IR spectra were collected on a JASCO FT/IR 410 spectrometer as KBr discs, nujol mulls or as chloroform or heptane solutions in a 0.5 mm path-length sodium chloride

cell. Data was processed using JASCO Spectra Manager, version 1.53.00 (Build 1). The wavelengths of maximum absorbance (ν_{max}) are quoted in cm^{-1}.

Elemental analysis was carried out on a Carlo Erba CHNS analyser at the University of St. Andrews. In some instances the correlation between calculated and theoretical values fall out with the recognised limit for publication of ±0.3%. This is particularly true for samples which have not been isolated as a solid and for metal complexes, where residual solvent and incomplete combustion, respectively, are expected to be the cause of the reported deviation from the expected results.

pH measurement was carried out using a Sartorius Professional PP-50 pH meter and a Sartorius PY-P11 pH electrode.

EPR data were recorded on an X-band Bruker ER 200-D SRC spectrometer connected to a datalink 486DX desktop PC running EPR acquisition system version 2.42. A quartz flat cell was used. Data was interpreted and simulated using WINEPR SimFonia, version 1.25.

Variable temperature (5-300 K), solid-state direct current (dc) magnetic susceptibility measurements were collected on a 7 Tesla Quantum Design MPMS SQUID Physical Properties Measurement Systems magnetometer (QD PPMS-7). Data were interpreted and simulated using MAGPACK.

A Sartorius Ultramicro balance (d = 0.0001 mg) was used to weigh samples for NMR titrations.

5.1 Ligand Synthesis

5-*t*-Octylsalicylaldehyde (**31**)

Preparation follows the method of Aldred *et al.*[1] Magnesium turnings (20.0 g, 0.8 mol) were stirred in a solution of methanol (373 ml) and toluene (160 ml). A few drops of magnesium methoxide (8% w/w solution in methanol) were added and the mixture stirred vigorously under reflux until all magnesium had dissolved and hydrogen evolution ceased. To this 4-*t*-octylphenol (268.2 g, 1.3 mol) was added and stirred under reflux for 1 h, during which toluene (250 ml) was added to allow the slurry formed to mix and redissolve. The mixture was distilled to near dryness, removing the methanol-toluene azeotrope. A slurry of paraformaldehyde (120.0 g, 4.0 mol) in toluene (200 ml) was added dropwise with vigorous stirring over a period of 1 h. Distillation was continued over this period and for a further 2 h after addition was complete. This gave an extremely viscous bright yellow oil which solidified upon cooling to room temperature. To this aqueous sulfuric acid (800 ml, 20% v/v) and toluene (400 ml) was added. The mixture was stirred for 30 min at 50°C before cooling to RT, during which a colour change was observed from bright yellow to beige. The aqueous phase was extracted with toluene (2 x 200 ml). Organic extracts were combined, washed with aqueous sulfuric acid (2 x 150 ml, 10% v/v), water (150 ml) and dried over anhydrous magnesium sulfate. Solvent was evaporated then dried further *in vacuo* to give a pale yellow oil. A portion (45 g) was purified by column chromatography using 2% ethyl acetate in hexane eluent. Solvent was removed by rotary evaporation and the product crystallised upon cooling to RT. This was dried *in vacuo* to yield 5-*t*-octylsalicylaldehyde (29 g, 64.5%). (Anal. Calc. for $C_{15}H_{22}O_2$: C, 76.88; H, 9.46. Found: C, 77.19; H, 9.91%). ^{1}H NMR (250 MHz, $CDCl_3$): δ_H (ppm) 10.86 (s, 1H, Ar-O*H*), 9.87 (s, 1H, C*H*O), 7.54 (dd , 1H, Ar-*H*), 7.46 (d , 1H, Ar-*H*), 6.91 (d, 1H, Ar-*H*), 1.71 (s, 2H, CH_2), 1.35 (s, 6H, C(CH_3)$_3$), 0.71 (s, 9H, C(CH_3)$_3$). ^{13}C NMR (63 MHz, $CDCl_3$): δ_C (ppm) 197.1 (1C, *C*HO), 159.6 (1C, Ar-*C*-OH), 142.0 (1C, Ar-*C*), 135.7 (1C, Ar-*C*H), 130.7 (1C, Ar-*C*H), 120.2 (1C, Ar-*C*), 117.2 (1C, Ar-*C*H), 56.9 (1C, *C*H_2), 38.2 (1C, *C*(CH_3)$_2$), 32.6 (1C, *C*(CH_3)$_3$), 32.0 (3C, (*C*H_3)$_3$), 31.7 (2C, (*C*H_3)$_2$). *m/z* 235 $(MH)^+$.

5-*t*-Octylsalicyclic acid (**11**)

Silver nitrate (17.56 g, 103 mmol) in water (300 ml) was stirred vigorously at room temperature while a solution of sodium hydroxide (4.51 g, 115 mmol) in water (150 ml) was added dropwise over a period of *ca*. 1.5 h to afford a grey-green precipitate. Further sodium hydroxide (19.22 g, 475 mmol) in water (50 ml) was added at the same rate. After addition was complete the reaction mixture was heated to 60°C and 5-*t*-octylsalicylaldehyde (**31**) (11.75 g, 50 mmol) added. The reaction temperature was raised to 85°C and stirred overnight. The precipitate was filtered and washed with water. The filtrate was acidified by addition of hydrochloric acid (conc.) to afford an off-white precipitate; addition was continued until no further precipitation occurred. The precipitate was filtered, washed with cold water, dried *in vacuo* in the presence of P_2O_5 to give 5-*t*-octylsalicylic acid (9.75 g, 78%). (Anal. Calc. for $C_{15}H_{22}O_3$: C, 71.97; H, 8.86. Found: C, 71.62; H, 8.95%). ^{1}H NMR (250 MHz, $CDCl_3$): δ_H (ppm) 10.24 (s, 1H, COO*H*), 7.86 (d, 1H, Ar-*H*), 7.54 (dd, 1H, Ar-*H*), 6.93 (d, 1H, Ar-*H*), 1.70 (s, 2H, CH_2), 1.34 (s, 6H, (CH_3)$_2$), 0.71(s, 9H, (CH_3)$_3$). ^{13}C NMR (63 MHz, $CDCl_3$): δ_C 175.6 (1C, *C*OOH), 160.2 (1C, Ar-*C*-OH), 141.7 (1C, Ar-*C*), 135.7 (1C, Ar-*C*H), 127.9 (1C, Ar-*C*H), 117.4 (1C, Ar-*C*H), 110.6 (1C, Ar-*C*), 56.9 (1C, *C*H_2), 38.2 (1C, *C*(CH$_3$)$_2$), 32.6 (1C, *C*(CH$_3$)$_3$), 32.1 (3C, (*C*H$_3$)$_3$), 31.7 (2C, (*C*H$_3$)$_2$). *m/z* 251 $(MH)^+$.

3-Formyl-5-*t*-octylsalicylic acid (**14**)

Preparation followed the method of Ruell *et al*.[2] 5-*t*-Octylsalicylic acid (**11**) (10.42 g, 42 mmol) was stirred in trifluoroacetic acid (50 ml). Hexamethylenetetramine (15.5 g, 110 mmol) was added and the resultant mixture heated to 100°C overnight. The solution was then poured without cooling into an aqueous solution of hydrochloric acid (1 M, 150 ml) and stirred overnight to yield a brown emulsion. This was extracted with ethyl acetate (3 x 150 ml). Extracts were combined and washed with water (150 ml), then dried over anhydrous magnesium sulfate. Solvent was removed by rotary evaporation then *in vacuo*. The resulting material was purified by silica-60 wet flash column chromatography (2% methanol in chloroform eluent) (9.59 g,

82.1%). (Anal. Calc. for $C_{16}H_{22}O_4$: C, 69.04; H, 7.97. Found: C, 69.40; H, 8.26. ^{1}H NMR (250 MHz, $CDCl_3$): δ_H (ppm) 11.55 (s (br), 1H, COO*H*), 10.32 (s, 1H, Ar-C*H*O), 8.27 (d, 1H, Ar-*H*), 8.00 (d, 1H, Ar-*H*), 1.75 (s, 2H, CH_2), 1.38 (s, 6H, (CH_3)$_2$), 0.71 (s, 9H, (CH_3)$_3$). ^{13}C NMR (63 MHz, $CDCl_3$): δ_C 191.4 (1C, *C*HO), 172.3 (1C, *C*OOH), 162.0 (1C, Ar-*C*-OH), 142.1 (1C, Ar-*C*), 136.0 (1C, Ar-*C*H), 133.8 (1C, Ar-*C*H), 123.2 (1C, Ar-*C*), 113.7 (1C, Ar-*C*), 56.7 (1C, *C*H_2), 38.4 (1C, *C*(CH_3)$_2$), 32.6 (1C, *C*(CH_3)$_3$), 32.1 (3C, (*C*H_3)$_3$), 31.5 (2C, (*C*H_3)$_2$). *m/z* 279 $(MH)^+$.

3-((Hydroxyimino)methyl)-5-*t*-octylsalicylic acid (**L1**)

Solutions of potassium hydroxide (0.38 g, 6.7 mmol) in ethanol (20 ml) and hydroxylamine hydrochloride (0.46 g, 6.7 mmol) in ethanol (20 ml) were mixed and stirred overnight. The resulting precipitate was filtered and the filtrate transferred to a round bottom flask containing 3-formyl-5-*t*-octylsalicylic acid (**14**) (1.39 g, 5.0 mmol). The mixture was stirred under reflux for 3 hrs and evaporated to dryness to yield a pale brown solid. This was purified by silica-60 wet flash column chromatography (DCM diluent gradient to 50% acetone) to yield a pale white solid on drying (0.67 g, 45.5%). (Anal. Calc. for $C_{16}H_{23}NO_4$: C, 65.51; H, 7.90; N, 4.77. Found C, 63.38; H, 8.02; N, 4.61%). ν_{max}/cm^{-1} (KBr): 3377 (PhO-H), 2954 (CH), 2544, 1668 (C=O), 1610 (C=N), 1471, 1388, 1365, 1246, 1192, 1151, 1111, 989. ^{1}H NMR (250 MHz, CD_3OD): δ_H (ppm) 8.45 (s, 1H, C*H*N), 7.97 (d, 1H, Ar-*H*), 7.91 (d, 1H, Ar-*H*), 1.74 (s, 2H, CH_2), 1.35 (s, 6H, (CH_3)$_2$), 0.72 (s, 9H, (CH_3)$_3$). ^{13}C NMR (63 MHz, CD_3OD): δ_C (ppm) 175.1 (1C, *C*OOH), 158.9 (1C, Ar-*C*-OH), 146.4 (1C, Ar-*C*), 141.1 (1C, *C*HN), 131.0 (1C, Ar-*C*H), 129.9 (1C, Ar-*C*H), 120.8 (1C, Ar-*C*), 116.5 (1C, Ar-*C*), 57.9 (1C, CH_2), 39.1 (1C, *C*(CH_3)$_2$), 33.3 (1C, *C*(CH_3)$_3$), 32.5 (3C, C(*C*H_3)$_3$), 32.3 (2C, C(*C*H_3)$_2$). ESI *m/z* 294 $(MH)^+$.

2,2-Dimethyl-propanoic hydrazide (**8**)

Sodium hydroxide (12.90 g, 323 mmol) was dissolved in water (400 ml). Hydrazine monohydrate (20.81 g, 400 mmol) was added and the mixture cooled (*ca.* 0 to -5°C). Trimethylacetylchloride (38.6 ml, 320 mmol) was added drop wise and the temperature maintained over the duration *ca.* 1 hr. The mixture was concentrated (ca. 100 ml) by rotary evaporation (**Caution!** Hydrazine, potentially explosive) and resultant solution filtered. The filtrate was collected and toluene added (100 ml). Water was removed using Dean-Stark apparatus and volume of the resultant solution reduced (*ca.* 40 ml) and hot filtered, the product precipitated as a white microcrystalline solid on cooling (7.78 g, 21.0%). (Anal. Calc. for $C_5H_{12}N_2O$: C, 51.70; H, 10.41; N, 24.12. Found: C, 51.94; H, 10.84; N, 23.74%). ^{1}H NMR (250 MHz, $CDCl_3$): δ_H (ppm) 7.43(s (br), 1H, N*H*), 3.85 (s (br), 2H, NH_2), 1.14 (s, 9H, C(CH_3)$_3$). ^{13}C NMR (63 MHz, $CDCl_3$): δ_C (ppm) 179.3 (1C, *C*O), 38.1 (1C, *C*(CH$_3$)$_3$), 27.4 (3C, C(*C*H$_3$)$_3$). ESI *m/z* 117.1 $(MH)^+$.

5-Methylsalicylaldehyde-pivaloylhydrazide (**L2**)

5-Methylsalicylaldehyde (1.36 g, 10 mmol) and 2,2-dimethylpropanoic hydrazide (**8**) (1.16 g, 10 mmol) were dissolved in dichloromethane (100 ml). The mixture was heated under reflux for 3 hrs. The resulting solution was reduced in volume (*ca.* 30 ml) and the product crystallised as a white crystalline solid upon cooling (1.53 g, 65%). (Anal. Calc. for $C_{13}H_{18}N_2O_2$: C, 66.64; H, 7.74; N, 11.96%; Found: C, 66.41; H, 7.91; N, 11.65). ν_{max}/cm^{-1} (KBr): 3446 (PhO-H), 3317vs (N-H), 3062, 2976 (CH), 2933 (CH), 2871w (CH), 1670vs (C=O), 1630 (C=N), 1614, 1585, 1543vs (N-H), 1469, 1358s, 1279s, 1194s.^{1}H NMR (250 MHz, DMSO-d_6): δ_H (ppm) 11.18 (s (br), 1H, COO*H*), 8.49 (s, 1H, C*H*N), 7.23 (s , 1H, Ar-*H*), 7.05 (dd, 1H, Ar-*H*), 6.79 (d, 1H, Ar-*H*), 2.22 (s, 3H, CH_3), 1.26 (s, 9H, (CH_3)$_3$). ^{13}C NMR (63 MHz, DMSO-d_6): δ_C (ppm) 173.7 (1C, *C*OOH), 155.4 (1C, Ar-*C*-OH), 147.5 (1C, *C*HN), 131.8 (1C, Ar-*C*H), 129.5 (1C, Ar-*C*H), 127.7 (1C, Ar-*C*), 118.3 (1C, Ar-*C*), 116.3 (1C, Ar-*C*H), 37.7 (1C, *C*(CH$_3$)$_3$), 27.1 (3C, C(*C*H$_3$)$_3$), 20.0 (1C, *C*H$_3$). ESI *m/z* 235 $(MH)^+$.

5-*t*-Butylsalicylaldehyde (**30**)

Procedure followed that of (**31**), using 4-*t*-Butylphenol (200 g, 1.33 mol). Purification by vacuum distillation (1 mm Hg, 120°C) and silica-60 wet column chromatography (2% ethyl acetate in hexane eluent) yielded a bright yellow oil (133.99g, 56.6%). (Anal. Calc. for $C_{11}H_{14}O_2$: C, 74.1; H, 7.9. Found: C, 73.4; H, 8.3%). ^{1}H NMR (360 MHz, DMSO-d_6): δ_H (ppm) 10.54 (s, 1H, O*H*), 10.23 (s, 1H, C*H*O), 7.64 (d, 1H, Ar*H*), 7.55 (dd, 1H, Ar*H*), 6.94 (d, 1H, Ar*H*), 1.23 (s, 9H C(C*H*$_3$)$_3$). ^{13}C NMR (90 MHz, DMSO-d_6): δ_C (ppm) 192.2 (1C, *C*HO), 158.8 (1C, Ar-*C*), 141.6 (1C, Ar-*C*), 133.9 (1C, Ar-*C*H), 125.2 (1C, Ar-*C*H), 121.4 (1C, Ar-*C*), 117.0 (1C, Ar-*C*H), 33.8 (1C, *C*(CH$_3$)$_3$), 31.0 (3C, C(*C*H$_3$)$_3$). *m/z* 179 $(MH)^+$.

5-*t*-Butylsalicylaldehyde-pivaloylhydrazide (**L3**)

5-*t*-Butylsalicylaldehyde (**31**) (0.89 g, 5.0 mmol) and 2,2-dimethylpropanoic hydrazide (**8**) (0.58 g, 5.0 mmol) were dissolved in ethanol (50 ml) and heated under reflux for 16 hrs. The resulting solution was evaporated to dryness and partially purified by silica-60 wet flash column chromatography (DCM eluent) (0.94 g, 68.1%). ν_{max}/cm^{-1} (KBr): 3276br (PhO-H), 2974s (CH), 2873w (CH), 1651s (C=O), 1631s (C=N), 1500s (N-H), 1400w, 1367w, 1188br. ^{1}H NMR (250 MHz, $CDCl_3$): δ_H (ppm) 10.94 (s (br), 1H, COO*H*), 9.30 (s (br), 1H, N*H*), 8.49 (s, 1H, C*H*N), 7.26 (dd, 1H, Ar-*H*), 7.09 (d, 1H, Ar-*H*), 6.85 (d, 1H, Ar-*H*), 1.27 (s, 9H, (C*H*$_3$)$_3$), 1.21 (s, 9H, (C*H*$_3$)$_3$). ^{13}C NMR (63 MHz, $CDCl_3$): δ_C (ppm) 174.7 (1C, *C*OOH), 156.4 (1C, Ar-*C*-OH), 151.9 (1C, *C*HN), 142.1 (1C, Ar-*C*H), 129.3 (1C, Ar-*C*H), 127.6 (1C, Ar-*C*), 117.0 (1C, Ar-*C*), 116.8 (1C, Ar-*C*H), 38.7 (1C, *C*(CH$_3$)$_3$), 34.1 (1C, *C*(CH$_3$)$_3$), 27.6 (3C, C(*C*H$_3$)$_3$), 27.3 (3C, C(*C*H$_3$)$_3$). ESI *m/z* 277 $(MH)^+$.

3-Formyl-5-methylsalicylic acid (**9**)

Preparation followed the method (**14**) using 5-methylsalicylic acid (5.5 g, 36 mmol) The resulting yellow precipitate was washed with cold water and dried *in vacuo*, recrystallised in water by addition of minimum ethanol to yield an off-white powder (4.09 g, 63%). (Anal. Calc. for $C_9H_8O_4$: C, 60.00; H, 4.48. Found: C, 59.96; H, 4.31%). ^{1}H NMR (250 MHz, $CDCl_3$): δ_H (ppm) (250 MHz, DMSO-d_6) 10.30 (s, 1H, C*H*O), 7.85 (d, 1H, Ar-*H*), 7.67 (d, 1H, Ar-*H*), 2.25 (s, 3H, Ar-CH_3). ^{13}C NMR (63 MHz, DMSO-d_6): δ_C (ppm) 188.4 (1C, *C*HO), 171.6 (1C, *C*OOH), 161.5 (1C, Ar-*C*-OH), 137.0 (1C, Ar-*C*H), 133.8 (1C, Ar-*C*H), 128.2 (1C, Ar-*C*), 123.5 (1C, Ar-*C*), 114.1 (1C, Ar-*C*), 19.7 (1C, *C*H_3). FAB *m/z* 179 $(M-H)^+$.

5-Methyl-3-((2,2-dimethylpropanoylhydrazono)methyl)salicylic acid (**L4**)

3-Formyl-5-methylsalicylic acid (**9**) (1.80 g, 10 mmol) and 2,2-Dimethyl-propanoic hydrazide (**8**) (1.16 g, 10 mmol) were dissolved separately in chloroform (75 ml) and mixed to give an immediate yellow/green solution. This was heated under reflux for 3 hrs. An off-white precipitate formed on cooling. This was filtered and recrystallised from chloroform (2.06 g, 74.1%). (Anal. Calc. for $C_{14}H_{18}N_2O_4$: C, 60.42; H, 6.52; N, 10.07. Found: C, 60.20; H, 6.52; N, 10.04%). ν_{max}/cm^{-1} (KBr): 3261br (PhO-H), 3045br (NH), 2974 (CH), 2875w (CH), 1682s (C=O), 1622s (C=N), 1614s, 1556s (COOH), 1456, 1423, 1373, 1234s, 1196vs. ^{1}H NMR (250 MHz, DMSO-d_6): δ_H (ppm) 11.03 (s, 1H, COO*H*), 8.68 (s, 1H, C*H*N), 7.78 (d, 1H, Ar*H*), 7.64 (dd, 1H, Ar*H*), 2.26 (s, 3H, (CH_3)), 1.18 (s, 9H, (CH_3)$_3$). ^{13}C NMR (63 MHz, $CDCl_3$): δ_C (ppm) 173.8 (1C, *C*O), 171.7 (1C, *C*OOH), 157.6 (1C, Ar-*C*OH), 141.6 (1C, *C*HN), 131.9 (1C, Ar-*C*H), 131.8 (1C, Ar-*C*H), 127.8 (1C, Ar-*C*), 121.9 (1C, Ar-*C*), 113.9 (1C, Ar-*C*), 37.8 (1C, *C*(CH$_3$)$_3$), 27.1 (3C, C(*C*H$_3$)$_3$) 19.9 (1C, (*C*H$_3$)). ESI *m/z* 279.1 $(MH)^+$.

5-*t*-Butylsalicylic acid (**10**)

Preparation follows the method of (**11**) using 5-*t*-butylsalicylaldehyde (**30**) (8.90 g, 50 mmol). The filtrate was acidified by addition of hydrochloric acid (conc.) to afford an off-white precipitate; addition was continued until no further precipitation occurred. The precipitate was filtered, washed with cold water, dried *in vacuo* over P_2O_5 to (9.41 g, 97%). (Anal. Calc. for $C_{11}H_{14}O_3$: C, 68.02; H, 7.27. Found: C, 67.24; H, 7.01%). ^{1}H NMR (360 MHz, DMSO-d_6): δ_H (ppm) 7.75 (d, 1H, Ar-*H*), 7.57 (dd, 1H, Ar-*H*), 6.89 (dd, 1H, Ar-*H*), 1.26 (s, 9H, (C*H*$_3$)$_3$). ^{13}C NMR (90 MHz, DMSO-d_6): δ_C (ppm) 172.0 (1C, *C*OOH), 159.0 (1C, Ar-*C*OH), 141.3 (1C, Ar-*C*), 133.1 (1C, Ar-*C*H), 125.9 (1C, Ar-*C*H), 116.8 (1C, Ar-*C*H), 112.0 (1C, Ar-*C*), 33.8 (1C, *C*(CH$_3$)$_3$), 31.1 (3C, C(*C*H$_3$)$_3$). FAB *m/z* 193 (M-H)$^-$.

5-*t*-Butyl-3-formyl-salicylic acid (**13**)

Method follows that of (**14**) using 5-*t*-butyl-salicylic acid (**10**) (4.32 g, 21 mmol) Upon cooling the solution was poured into aqueous hydrochloric acid (150 ml, 1 M) and stirred to yield a yellow semi solid. This was dried *in vacuo* and recrystallised from a minimum of ethanol in water to yield a white powder (2.87 g, 62%). (Anal. Calc. for $C_{12}H_{14}O_4$: C, 64.85; H, 6.35. Found: C, 64.82; H, 6.58%). ^{1}H NMR (360 MHz, DMSO-d_6): δ_H (ppm) 10.36 (s, 1H, C*H*O), 8.10 (d, 1H, Ar-*H*), 7.93 (d, 1H, Ar-*H*), 1.28 (s, 9H, (C*H*$_3$)$_3$). ^{13}C NMR (90 MHz, DMSO-d_6): δ_C (ppm) 188.7 (1C, *C*HO), 171.5 (1C, *C*OOH), 161.5 (1C, Ar-*C*OH), 141.2 (1C, Ar-*C*), 133.3 (1C, Ar-*C*H), 130.2 (1C, Ar-*C*H), 123.3 (1C, Ar-*C*-CHO), 114.5 (1C, Ar-*C*), 33.9 (1C, *C*(CH$_3$)$_3$), 30.8 (3C, C(*C*H$_3$)$_3$). FAB *m/z* 221 (M-H)$^-$.

5-*t*-Butyl-3-((2,2-dimethylpropanoylhydrazono)methyl)salicylic acid (**L5**)

5-*t*-Butyl-3-formylsalicylic acid (**13**) (2.22 g, 10 mmol) and 2,2-dimethyl-propanoic hydrazide (**8**) (1.16 g, 10 mmol) were stirred in methanol (50 ml) under reflux. An immediate white precipitate formed on cooling. This was filtered and recrystallised from methanol to yield colourless crystals (2.41 g, 75.3%). (Anal. Calc. for $C_{17}H_{24}N_2O_4 \bullet CH_3OH$: C, 61.34; H, 8.01; N, 7.95. Found: C, 61.20; H, 8.31; N, 7.89%). ν_{max}/cm^{-1} (KBr): 3653s, 3398br, 3273 (PhO-H), 3062w (NH), 2964 (CH), 2910w (CH), 2871w (CH), 1680s (C=O), 1633s (C=N), 1614s, 1543, 1479, 1458, 1400, 1365, 1196. ^{1}H NMR (360 MHz, DMSO-d_6): δ_H (ppm) 11.02 (s, 1H, COO*H*), 8.74 (s, 1H, C*H*N), 8.00 (d, 1H, Ar*H*), 7.84 (d, 1H, Ar*H*), 1.28 (s, 9H, ArC(CH_3)$_3$), 1.19 (s, 9H, COC(CH_3)$_3$). ^{13}C NMR (90 MHz, DMSO-d_6): δ_C (ppm) 173.8 (1C, *C*O), 171.7 (1C, *C*OOH), 157.6 (1C, Ar-*C*OH), 142.0 (1C, *C*HN), 141.1 (1C, Ar-*C*), 128.2 (1C, Ar-*C*H), 128.1 (1C, Ar-*C*H), 121.6 (1C, Ar-*C*), 113.6 (1C, Ar-*C*), 37.8 (1C, *C*(CH$_3$)$_3$), 33.9 (1C, *C*(CH$_3$)$_3$) 31.0 (3C, C(*C*H$_3$)$_3$), 27.1 (3C, C(*C*H$_3$)$_3$). *m/z* 319.3 $(M-H)^-$.

5-Methyl-3-octanoylhydrazonosalicylic acid (**L6**)

A suspension of 3-formyl-5-methylsalicylic acid (**9**) (1.80 g, 10 mmol), octanoic hydrazide (1.58 g, 10 mmol) and anhydrous magnesium sulfate in chloroform (50 ml) was warmed to 40°C and stirred overnight. The mixture was filtered to remove unreacted starting material and magnesium sulfate, and washed with cold chloroform. The filtrate was evaporated to dryness then in vacuo to yield a white power (2.91 g, 91%). (Anal. Calc. for $C_{17}H_{24}N_2O_4$: C, 63.73; H, 7.55; N, 8.74. Found: C, 63.42; H, 7.94; N, 8.65%). ν_{max}/cm^{-1} (KBr): 3168w (Ph-OH), 3064w (NH), 2956 (CH), 2925 (CH), 2856 (CH), 1666s (C=O), 1593 (C=N), 1429. ^{1}H NMR (250 MHz, $CDCl_3$): δ_H (ppm) 11.36 (s (br), 1H, COO*H*), 11.05 (s, 1H , Ar-O*H*), 7.95 (s, 1H, C*H*N), 7.54 (d, 1H, Ar-*H*), 7.42 (d , 1H, Ar-*H*), 2.58 (t, 2H, C=OCH_2), 2.19 (s, 3H, Ar-CH_3), 1.63 (t, 2H, CH_2), 1.37-1.23 (m, 8H, (CH_2)$_4$), 0.94-0.83 (m, 3H, CH_3). ^{13}C NMR (63 MHz, $CDCl_3$): δ_C (ppm) 178.5 (1C, *C*OOH), 174.5 (1C, *C*O),

159.1 (1C, Ar-*C*-OH), 140.8 (1C, *C*HN), 133.1 (1C, Ar-*C*H), 131.7 (1C, Ar-*C*H), 127.8 (1C, Ar-*C*), 121.3 (1C, Ar-*C*), 112.3 (1C, Ar-*C*), 32.0 (2C, *C*H_2), 29.7 (1C, *C*H_2), 29.4 (1C, *C*H_2), 24.5 (1C, *C*H_2), 22.9 (1C, *C*H_2), 20.7 (1C, Ar-*C*H_3), 14.4 (1C, *C*H_3). FAB *m/z* 321 $(MH)^+$.

Initial attempts to synthesise (**L6**) by reflux of 3-formyl-5-methylsalicylic acid (**9**) and octanoic hydrazone in various solvents at >40°C yielded 3,3'-(azinodimethylidyne)bis(5-methylsalicylic acid) (**16**) and *di*-(octan-1-one)azine (**17**).

3,3'-(Azinodimethylidyne)bis(5-methylsalicylic acid) (**16**)

3-Formyl-5-methylsalicylic acid (**9**) (1.82g, 10 mmol) and octanoic hydrazide (2.42 g, 15 mmol) were dissolved in propan-1-ol (50 ml) and stirred under reflux for 24 hrs and allowed to cool to RT. The resulting bright orange precipitate was filtered and washed with propan-1-ol (1.18 g, 66.3%). (Anal. Calc. for $C_{18}H_{16}N_2O_6$•2DMSO: C, 51.55; H, 5.51; N, 5.47. Found: C, 51.51; H, 5.13; N, 5.36%). ν_{max}/cm^{-1} (KBr): 3413br (PhO-H), 2924br (CH), 2472, 1855w, 1678 (C=O), 1618s (C=N-N=C), 1454s, 1354, 1327, 1279, 1255s. ^{1}H NMR (360 MHz, DMSO-d_6 at 60°C): δ_H (ppm) 8.93 (s, 2H, 2 x C*H*O), 7.98 (d, 2H, 2 x Ar-*H*), 7.77 (d, 2H, 2 x Ar-*H*), 2.32 (s, 6H, 2 x Ar-C*H*$_3$). (90 MHz, DMSO-d_6 at 60°C): δ_C (ppm) 171.0 (2C, 2 x *C*OOH), 158.4 (2C, 2 x Ar-*C*-OH), 156.4 (2C, 2 x *C*HN), 133.6 (2C, 2 x Ar-*C*H), 132.9 (2C, 2 x Ar-*C*H), 127.8 (2C, 2 x Ar-*C*), 120.7 (2C, 2 x Ar-*C*), 114.1 (2C, 2 x Ar-*C*), 19.6 (2C, 2 x *C*H_3). ESI *m/z* 355 $(M-H)^-$.

di-(Octan-1-one)azine (**17**)

di-(Octan-1one)azine was recovered as colourless crystals by reduction in the volume of the filtrate of the above reaction. These were filtered and washed with hexane (1.44 g, 50.7%). (Anal. Calc. for $C_{16}H_{32}N_2O_2$: C, 67.56; H, 11.34; N, 9.85. Found: C, 67.85; H, 12.22; N, 9.86%).^{1}H NMR (250 MHz, $CDCl_3$): δ_H (ppm) 9.46 (s (br), 2H, 2 x N*H*), 2.09 (t, 4H, 2 x C=OC*H*$_2$), 1.52 (t, 4H, 2 x C*H*$_2$), 1.34-1.21 (m, 16H, 2 x (C*H*$_2$)$_4$), 0.87 (t, 6H, 2 x C*H*$_3$). ^{13}C NMR (63 MHz, $CDCl_3$): δ_C (ppm) 170.7 (2C, 2 x *C*O), 33.0 (2C, 2 x *C*H$_2$), 30.8 (2C, 2 x *C*H$_2$), 28.2 (2C, 2 x *C*H$_2$), 28.1 (2C, 2 x *C*H$_2$), 24.7 (2C, 2 x *C*H$_2$), 21.7 (2C, 2 x *C*H$_2$), 13.5 (2C, 2 x *C*H$_3$). FAB *m/z* 285 $(MH)^+$.

3-((2-octanoylhydrazono)methyl)-5-*t*-octylsalicylic acid (**L7**)

3-Formyl-5-*t*-octylsalicylic acid (**14**) (2.78 g, 10 mmol) and octanoic hydrazide (1.58 g, 10 mmol) were stirred in ethanol (200 ml) under reflux for 16 hrs. The resultant solution was evaporated to dryness and recrystallised in water from a minimum of acetonitrile to yield a white powder (2.61 g, 62%). (Anal. Calc. for $C_{24}H_{38}N_2O_4$: C, 68.87; H, 9.15; N, 6.69. Found: C, 69.05; H, 9.47; N, 6.86%). ν_{max}/cm^{-1} (KBr): 3215w (PhO-H), 3066w (NH), 2954 (CH), 2929 (CH), 2862 (CH), 1668s (C=O), 1614 (C=N), 1456. ^{1}H NMR (250 MHz, $CDCl_3$): δ_H (ppm) 11.67 (s, 1H, COO*H*), 11.49 (s (br), 1H, Ar-O*H*), 8.43 (s, 1H, C*H*N), 8.12 (d, 1H, Ar-*H*), 8.01 (d , 1H, Ar-*H*), 2.81 (t, 2H, C=OC*H*$_2$), 1.83-1.65 (m, 4H, (C*H*$_2$)$_2$), 1.45-1.25 (m, 14H, (C*H*$_2$)$_4$ and (C*H*$_3$)$_2$), 0.87 (t, 3H, C*H*$_3$), 0.74 (s, 9H (C*H*$_3$)$_3$). ^{13}C NMR (63 MHz, $CDCl_3$): δ_C 179.2 (1C, *C*OOH), 175.3 (1C, *C*O), 159.1 (1C, Ar-*C*-OH), 141.9 (1C, *C*HN), 141.11 (1C, Ar-*C*), 131.1 (1C, Ar-*C*H), 129.8 (1C, Ar-*C*H), 120.8 (1C, Ar-*C*), 112.8 (1C, Ar-*C*), 56.9 (1C, *C*H$_2$), 38.3 (1C, *C*(CH$_3$)$_2$), 34.4 (1C, *C*H$_2$), 32.6 (1C, *C*(CH$_3$)$_3$), 32.2 (3C, C(*C*H$_3$)$_3$), 31.7 (2C, C(*C*H$_3$)$_2$), 29.6 (1C, *C*H$_2$), 29.3 (1C, *C*H$_2$), 25.6 (1C, *C*H$_2$), 25.1 (1C, *C*H$_2$), 22.8 (1C, *C*H$_2$), 14.3 (1C, *C*H$_3$). *m/z* 419 $(MH)^+$.

5-Nonylsalicylic acid (**12**)

Procedure was followed as (**11**) using 5-nonylsalicylaldehyde (12.45 g, 50 mmol). Hydrochloric acid (conc.) was added until precipitation ceased. The resulting brown oil was extracted with hexane (400 ml, 2 x 200 ml), extracts washed with water (2 x 200 ml) and dried over $MgSO_4$, filtered and evaporated to dryness (12.43 g, 94.2%). ^{1}H NMR (250 MHz, $CDCl_3$): δ_H (ppm) 10.22 (s, 1H, O*H*), 7.85-7.75 (m, 1H, Ar-*H*), 7.52-7.42 (m, 1H, Ar-*H*), 6.95-6.91 (d, 1H, Ar-*H*), 1.64-0.65 (m, 19H, C_9H_{19}). ^{13}C NMR (63 MHz, CD_3OD): δ_C (ppm) 175.7 (1C, *C*OOH), 160.1 (1C, Ar-*C*-OH), 139.5 (1C, Ar-*C*), 136.1 (m, 1C, Ar-*C*H), 128.7 (m, 1C, Ar-*C*H), 117.5 (1C, Ar-*C*H), 110.6 (1C, Ar-*C*), 51.7-8.7 (9C, $(CH_2)_8CH_3$). ESI *m/z* 263 $(M-H)^-$.

3-Formyl-5-nonylsalicylic acid (**15**)

Preparation followed that of (**14**) using 5-nonylsalicylic acid (**12**) (0.81 g, 3.07 mmol). The resulting brown oil was extracted with diethyl ether (30 ml) and ethyl acetate (2 x 30 ml). the extracts were combined washed with water (2 x 30 ml), dried over $MgSO_4$ and evaporated to dryness (0.67 g, 74.7%). ^{1}H NMR (250 MHz, $CDCl_3$): δ_H (ppm) 11.47 (s, 1H, O*H*), 10.36 (s, 1H, O*H*), 10.23 (s, 1H, C*H*O), 8.22-8.11 (m, 1H, Ar-*H*), 7.98-7.83 (m, 1H, Ar-*H*), 1.64-0.65 (m, 19H, C_9H_{19}).

5-Nonyl-3-((2-octanoylhydrazono)methyl)salicylic acid (**L8**)

3-Formyl-5-nonylsalicylic acid (**15**) (0.51 g, 1.75 mmol) and octanoic hydrazide (0.28 g, 1.77 mmol) were stirred in acetonitrile (25 ml) under reflux for 16 hrs. The resulting suspension was hot filtered. A white powder precipitated, this was filtered, washed and recrystallised from a minimum volume of acetonitrile (0.67 g, 88.6%). (Anal. Calc. for $C_{25}H_{40}N_2O_4$: C, 69.41; H, 9.32; N, 6.48. Found: C, 69.19; H, 10.03; N, 7.44%). ν_{max}/cm^{-1} (KBr): 3224 (PhO-H), 3068br (NH), 2956 (CH), 2925 (CH), 2856 (CH), 1670s (C=O), 1599vs (C=N), 1458, 1377, 1248. ^{1}H NMR (250 MHz, $CDCl_3$): δ_H (ppm) 11.60 (s (br), 1H, Ar-O*H*), 11.51 (s , 1H, COO*H*), 8.43 (s, 1H,

C*H*N), 8.10-7.90 (m, 2H, Ar-*H*), 2.80 (t, 2H, CH_2), 2.24 (t, 2H, CH_2), 1.79-1.59 (m, 4H, CH_2), 1.31-1.23 (m, 16H, CH_2), 0.89-0.068 (m, 10H, (CH_2)$_2$ and (CH_3)$_2$. ^{13}C NMR (63 MHz, DMSO-d$_6$): δ_C 179.1 (1C, *C*OOH), 174.3 (1C, *C*=O), 171.0 (1C, Ar-*C*OH), 157.3 (1C, Ar-C), 141.1 (1C, *C*HN), 137.1 (1C, Ar-*C*H), 128.6 (1C, Ar-*C*H), 121.6 (1C, Ar-*C*), 112.8 (1C, Ar-*C*), 34.2-22.0 (14C, *C*H$_2$), 13.9 (2C, *C*H$_3$). *m/z* 431.12 $(M-H)^-$.

3-((2-(4-*t*-Butylbenzoyl)hydrazono)methyl)-5-methylsalicylic acid (**L9**)

3-Formyl-5-methylsalicylic acid (**9**) (2.43 g, 13.61 mmol) and 4-*t*-butylbenzoic hydrazide (2.61g, 13.61 mmol) were stirred in DCM (200 ml) under reflux for 3 hrs. The resulting precipitate was recrystallised from a minimum volume of DCM to yield a white powder (4.76 g, 99%). (Anal. Calc. for $C_{20}H_{22}N_2O_4$: C, 67.78; H, 6.26; N, 7.90. Found C, 67.64; H, 6.09; N, 7.65%). ν_{max}/cm^{-1} (KBr): 3194br (PhO-H), 3041 (NH), 2964 (CH), 2870 (CH), 1658s (C=O), 1610s (C=N), 1554, 1464, 1419, 1356, 1265.^{1}H NMR (250 MHz, DMSO-d$_6$): δ_H (ppm) 11.90 (s, 1H, COO*H*), 8.78 (s, 1H, C*H*N), 7.87 (d, 3H, Ar-*H*), 7.69 (d, 1H, Ar-*H*), 7.53 (d (br), 2H, Ar-*H*), 2.30 (s, 3H, CH_3), 1.31 (s, 9H, (CH_3)$_3$). ^{13}C NMR (63 MHz, DMSO-d$_6$): δ_C (ppm) 171.7 (1C, *C*OOH), 162.9 (1C, *C*O), 157.7 (1C, Ar-*C*-OH), 154.7 (1C, Ar-*C*), 142.3 (1C, *C*HN), 132.2 (1C, Ar-*C*H), 131.8 (1C, Ar-*C*H), 130.5 (1C, Ar-*C*), 128.0 (1C, Ar-*C*), 127.5 (2C, Ar-*C*H), 125.5 (2C, Ar-*C*H), 121.8 (1C, Ar-*C*), 113.7 (1C, Ar-*C*H), 34.7 (1C, *C*(CH$_3$)$_3$), 30.9 (3C, C(*C*H$_3$)$_3$), 19.9 (1C, *C*H$_3$). FAB *m/z* 355 $(MH)^+$.

3-((2-(4-*t*-Butylbenzoyl)hydrazono)methyl)-5-*t*-octylsalicylic acid (**L10**)

3-Formyl-5-*t*-octylsalicylic acid (**14**) (0.61 g, 2.19 mmol) and 4-*t*-butylbenzoic hydrazide (0.42 g, 2.19 mmol) were stirred in DCM (50 ml) under reflux for 16 hrs. The resulting yellow solution was evaporated to dryness to give a yellow solid. This was recrystallised from a minimum of chloroform on cooling at 5°C to yield an off-white solid which was filtered and washed with a minimum of cold chloroform (0.81 g, 81.8%). (Anal. Calc. for $C_{27}H_{36}N_2O_4$: C, 71.65; H, 8.02; N, 6.19. Found C, 70.76;

H, 8.53; N, 6.20%). ν_{max}/cm^{-1} (KBr): 3222br (PhO-H), 2958s (CH), 2904 (CH), 2870 (CH), 1657s (C=O), 1612s (C=N), 1552, 1462, 1365, 1267, 1242, 1186, 1157. ^{1}H NMR (250 MHz, CD_3OD): δ_H (ppm) 8.87 (s, 1H, C*H*N), 8.41 (d, 1H, Ar-*H*), 7.95 (d, 1H, Ar-*H*), 7.90 (d, 2H, Ar-*H*), 7.47 (d, 2H, Ar-*H*), 1.75 (s, 2H, CH_2), 1.36 (s, 6H, (CH_3)$_2$), 1.29 (s, 9H, (CH_3)$_3$), 0.70 (s, 9H, (CH_3)$_3$). ^{13}C NMR (63 MHz, CD_3OD): δ_C (ppm) 173.5 (1C, *C*OOH), 167.0 (1C, *C*O), 160.8 (1C, Ar-*C*-OH), 157.0 (1C, Ar-*C*), 146.0 (1C, *C*HN), 142.1 (1C, Ar-*C*), 131.8 (1C, Ar-*C*H), 131.5 (1C, Ar-*C*H), 131.2 (1C, Ar-*C*), 128.9 (2C, Ar-*C*H), 126.7 (2C, Ar-*C*H), 122.5 (1C, Ar-*C*), 114.0 (1C, Ar-*C*), 57.7 (1C, CH_2), 39.3 (1C, *C*(CH$_3$)$_2$), 35.9 (1C, *C*(CH$_3$)$_3$), 33.3 (1C, *C*(CH$_3$)$_3$), 32.6 (3C, C(*C*H$_3$)$_3$), 32.2 (2C, C(*C*H$_3$)$_2$), 31.7 (3C, C(*C*H$_3$)$_3$). FAB *m/z* 453 (MH)$^+$.

3-((5-*t*-Butyl-2-hydroxyphenylamino)methyl)-5-methylsalicylic acid (**L11**)

3-Formyl-5-methylsalicylic acid (**9**) (1.80 g, 0.01 mol) and 2-amino-4-*t*-butyl-phenol (1.65 g, 0.01 mol) were stirred in methanol (100 ml) for 1 h. A deep red precipitate formed on contact. This was filtered and washed with cold methanol and dried *in vacuo* (3.26 g, 99.7%). (Anal. Calc. for $C_{19}H_{21}NO_4$: C, 69.71; H, 6.47; N, 4.28. Found C, 69.19; H, 5.99; N, 4.09%). ν_{max}/cm^{-1} (KBr): 3132br (PhO-H), 2960 (CH), 2868 (CH), 1682 (C=O), 1637s (C=N), 1608w, 1522, 1466, 1282, 1240s.^{1}H NMR (250 MHz, DMSO-d_6): δ_H (ppm) 10.77 (s, 1H, COO*H*), 9.43 (s, 1H, C*H*N), 7.98 (d , 1H, Ar-*H*), 7.82 (d, 1H, Ar-*H*), 7.64 (d, 1H, Ar-*H*), 7.30 (dd, 1H, Ar-*H*), 6.99 (dd, 1H, Ar-*H*), 2.56 (s, 3H, CH_3), 1.31 (s, 9H, (CH_3)$_3$). ^{13}C NMR (63 MHz, DMSO-d_6): δ_C (ppm) 173.5 (1C, *C*OOH), 167.5 (1C, Ar-*C*-OH), 158.4 (1C, *C*HN), 146.8 (1C, Ar-*C*-OH), 142.9 (1C, Ar-*C*), 141.0 (1C, Ar-*C*H), 139.6 (1C, Ar-*C*H), 126.7 (1C, Ar-*C*H), 124.3 (1C, Ar-*C*), 130.1 (1C, Ar-*C*), 118.9 (1C, AR-*C*), 116.2 (1C, Ar-*C*), 116.1 (1C, Ar-*C*H), 114.7 (1C, Ar-*C*H), 34.3 (1C, *C*(CH$_3$)$_3$), 31.2 (3C, C(*C*H$_3$)$_3$), 19.6 (1C, *C*H$_3$). FAB *m/z* 328 (MH)$^+$.

3-((5-*t*-Butyl-2-hydroxyphenylimino)methyl)-5-*t*-octylsalicylic acid (**L12**)

3-Formyl-5-*t*-octylsalicylic acid (**14**) (0.50 g, 1.80 mmol) and 2-amino-4-*t*-butylphenol (0.30 g, 1.81 mmol) were stirred in methanol (25 ml). An immediate orange precipitate formed. This was filtered, washed with cold methanol and dried *in vacuo* (0.57g, 74.5%). (Anal. Calc. for $C_{26}H_{35}NO_4$: C, 73.38; H, 8.29; N, 3.29. Found: C, 73.08; H, 8.69; N, 3.28%). ν_{max}/cm^{-1} (KBr): 3155br (PhO-H), 2954s (CH), 2902 (CH), 2871w (CH), 1637s (C=O), 1595 (C=N), 1522s, 1462, 1365, 1250s. ^{1}H NMR (250 MHz, DMSO-d_6): δ_H (ppm) 10.77 (s, 1H, COO*H*), 9.53 (d, 1H, C*H*N), 8.20 (m, 2H, Ar-*H*), 7.86 (d, 1H, Ar-*H*), 7.31 (dd, 1H, Ar-*H*), 7.00 (d , 1H, Ar-*H*), 1.72 (s, 2H, CH_2), 1.37 (s, 6H, (CH_3)$_2$), 1.33 (s, 9H, C(CH_3)$_3$), 0.74 (s, 9H, C(CH_3)$_3$). ^{13}C NMR (63 MHz, DMSO-d_6): δ_C 173.6 (1C, *C*OOH), 167.7 (1C, Ar-*C*-OH), 158.8 (1C, *C*HN), 146.7 (1C, Ar-*C*), 142.9 (1C, Ar-*C*), 138.3 (1C, Ar-*C*H), 137.2 (1C, Ar-*C*H), 135.3 (1C, Ar-*C*), 126.7 (1C, Ar-*C*H), 124.2 (1C, Ar-*C*), 118.4 (1C, Ar-*C*), 116.0 (1C, Ar-*C*), 115.8 (1C, Ar-*C*H), 114.5 (1C, Ar-*C*H), 55.9 (1C, *C*H$_2$), 37.4 (1C, *C*(CH$_3$)$_2$), 34.3 (1C, *C*(CH$_3$)$_3$), 32.1 (1C, *C*(CH$_3$)$_3$), 31.6 (3C, C(*C*H$_3$)$_3$), 31.3 (3C, C(*C*H$_3$)$_3$), 31.1 (2C, C(*C*H$_3$)$_2$). ESI *m/z* 426 $(MH)^+$.

3-((5-*t*-Butyl-2-hydroxyphenylimino)methyl)-5-nonylsalicylic acid (**L13**)

3-Formyl-5-nonylsalicylic acid (**15**) (1.14 g, 3.90 mmol) and 2-amino-4-*t*-butyl-phenol (0.65 g, 3.94 mmol) were stirred in methanol (50 ml) for 4 hrs. A deep red precipitate formed on addition of water. This was filtered and washed with cold 50:50 methanol-water mixture and dried *in vacuo* over P_2O_5 (1.17 g, 68.3%). (Anal. Calc. for $C_{27}H_{37}NO_4$: C, 73.77; H, 8.48; N, 3.19; Found: C, 71.48; H, 8.11; N, 3.00%). ν_{max}/cm^{-1} (KBr): 3167br (PhO-H), 2962s (CH), 2933 (CH), 2871 (CH), 1676 (C=O), 1637vs (C=N), 1520s, 1464, 1379, 1365, 1282, 1242s. ^{1}H NMR (250 MHz, DMSO-d_6): δ_H (ppm) 10.88 (s (br), 1H, COO*H*), 9.54 (s (br), 1H, C*H*N), 8.15-8.10 (m , 1H, Ar-*H*), 7.86 (d, 1H, Ar-*H*), 7.80-7.75 (m, 1H, Ar-*H*), 7.30 (dd, 1H, Ar-*H*), 7.02 (d, 1H, Ar-*H*), 1.56-0.56 (m, 28H, (CH_2)$_8$,CH_3, (CH_3)$_3$). ^{13}C NMR (63 MHz, DMSO-d_6): δ_C (ppm) 179.1 (1C, *C*OOH), 173.5 (1C, Ar-*C*-OH), 167.8 (1C, Ar-*C*-

OH), 158.6 (1C, *C*HN), 146.7 (1C, Ar-*C*), 142.9 (1C, Ar-*C*), 138.1 (C, Ar-*C*H), 137.8 (1C, Ar-*C*H), 126.7 (1C, Ar-*C*H), 124.2 (1C, Ar-*C*), 118.5 (1C, Ar-*C*), 116.0 (1C, Ar-*C*H), 115.9 (1C, Ar-*C*), 114.6 (1C, Ar-*C*H), 34.3 (1C, $C(CH_3)_3$), 31.2 (3C, $C(CH_3)_3$), 28.7-8.4 (9C, $(CH_2)_8CH_3$). ESI m/z 440 $(MH)^+$.

5-*t*-Butylsalicylaldoxime (**18**)

Potassium hydroxide (1.35 g, 20 mmol) dissolved in ethanol (50 ml) was added to a solution of hydroxylamine hydrochloride (1.40 g, 20 mmol) in ethanol (50 ml). the resulting white precipitate was filtered and the filtrate transferred into a round bottomed flask containing 5-*t*-butylsalicylaldehyde (3.00 g, 15 mmol). The resulting mixture was stirred under reflux for 3 hrs then evaporated to dryness and the resulting solid was recrystallised from a minimum of hexane to yield colourless needles (2.85 g, 98%). (Anal. Calc. for $C_{11}H_{15}NO_2$: C, 68.37; H, 7.82; N, 7.25%; Found: C, 68.40; H, 7.84; N, 7.11). ^{1}H NMR (250 MHz, $CDCl_3$): δ_H (ppm) 8.23 (s, 1H, Ar-C*H*N), 7.32 (dd, 1H, Ar-*H*), 7.15 (d, 1H, Ar-*H*), 6.93 (d, 1H, Ar-*H*), 1.29 (s, 9H, $(CH_3)_3$). ^{13}C NMR (63 MHz, $CDCl_3$): δ_C (ppm) 154.9 (1C, Ar-*C*OOH), 153.6 (1C, Ar-*C*HN), 142.8 (1C, Ar-*C*), 128.8 (1C, Ar-*C*H), 127.5 (1C, Ar-*C*H), 116.4 (1C, Ar-*C*H), 115.9 (1C, Ar-*C*), 34.2 (1C, $C(CH_3)_2$), 31.6 (3C, $C(CH_3)_3$),. FAB *m/z* 194 $(MH)^+$.

5-*t*-Octylsalicylaldoxime (**19**)

Procedure was followed as for **18** using 5-*t*-octylsalicylaldehyde (3.51 g, 15 mmol) to yield a yellow/brown solid. This was recrystallised from a minimum of hexane to yield a pale yellow flaky solid (2.97 g, 79.5%). (Anal. Calc. for $C_{15}H_{23}NO_2$: C, 72.25; H, 9.30; N, 5.62%; Found: C, 72.53; H, 9.76; N, 5.79). ^{1}H NMR (250 MHz, $CDCl_3$): δ_H (ppm) 9.79 (s, 1H, Ar-CO*H*), 8.22 (s, 1H, Ar-C*H*N), 7.86 (s, 1H, NOH), 7.29 (dd, 1H, Ar-*H*), 7.11 (d, 1H, Ar-*H*), 6.90 (d, 1H, Ar-*H*), 1.68 (s, 2H, (CH_2), 1.33 (s, 6H, $(CH_3)_2$), 0.70 (s, 9H, $(CH_3)_3$). ^{13}C NMR (63 MHz, $CDCl_3$): δ_C (ppm) 154.9 (1C, Ar-*C*OOH), 153.8 (1C, Ar-*C*HN), 141.8 (1C, Ar-*C*), 129.7 (1C, Ar-*C*H), 128.4

(1C, Ar-*C*H), 116.2 (1C, Ar-*C*H), 115.7 (1C, Ar-*C*), 57.1 (1C, *C*H_2), 38.1 (1C, *C*$(CH_3)_2$), 32.5 (1C, *C*$(CH_3)_3$), 32.0 (3C, C(*C*$H_3)_3$), 31.8 (2C, C(*C*$H_3)_2$). FAB *m/z* 250 $(MH)^+$.

4-Benzylpiperazinoacetic acid hydrazide (**32**)

Two step preparation follows that of K.S.Putt *et al.*[3] 1-Benzylpiperazine (7.92 g, 45.0 mmol) and $NaHCO_3$ (4.74 g, 56.4 mmol) were stirred in acetone (90 ml). To this mixture ethyl chloroacetate (6.08 g, 50.0 mmol) was added dropwise over a period of *ca*. 5 mins. The resulting mixture was stirred under reflux for 24 hrs. Upon cooling the mixture was filtered and salts washed with acetone. The filtrate and washings were combined and evaporated to yield yellow oil. This was purified by chromatography on a silica column (5% MeOH, 0.5% ammonia in DCM eluent) to yield ethyl(4-benzylpiperazino)acetate as a pale yellow solution upon drying (11.86 g, 95%). ^{1}H NMR (250 MHz, $CDCl_3$): δ_H (ppm) 7.31-7.12 (m, 5H, Ar-*H*), 4.10 (q, 2H, C*H*$_2$), 3.45 (s, 2H, C*H*$_2$), 3.13 (s, 2H, C*H*$_2$), 2.52 (m (br), 4H, (C*H*$_2)_2$), 2.47 (m (br), 4H, (C*H*$_2)_2$), 1.19 (t, 3H, C*H*$_3$).

Ethyl-(4-benzylpiperazino)acetate (9.50 g, 36.3 mmol) was dissolved in ethanol (50 ml). To this hydrazine monohydrate (5.55 g, 111 mmol) was added dropwise over a period of *ca*. 5 min. The resulting solution was stirred under reflux for 16 hrs then evaporated to dryness. A solution of saturated NaCl : H_2O, 1:1 (40 ml), pH >14 (by addition of KOH) was added. The product was extracted into DCM (3 x 30 ml) and EtOAc (30 ml). Organic extracts were combined, dried over $MgSO_4$, evaporated to dryness to yield a white crystalline solid upon cooling. This was dissolved in a minimum of ethanol under reflux, once dissolved diethyl ether (75 ml) was added slowly. 4-Benzylpiperazino acetic acid hydrazide crystallised upon standing overnight (4.94 g, 55%). (Anal. Calc. for $C_{15}H_{20}N_4O$: C, 62.88; H, 8.12; N, 22.56. Found: C, 62.85; H, 8.49; N, 22.41%). ^{1}H NMR (250 MHz, CD_3OD): δ_H (ppm) 7.44-7.32 (m, 5H, Ar-*H*), 3.63 (s, 2H, C*H*$_2$), 3.13 (s, 2H, C*H*$_2$), 2.63 (s, 8H, (C*H*$_2)_4$). ^{13}C NMR (63 MHz, CD_3OD): δ_C (ppm) 171.5 (1C, *C*O), 138.5 (1C, Ar-*C*), 130.8 (2C,

Ar-*C*H), 129.4 (2C, Ar-*C*H), 128.5 (1C, Ar-*C*H), 63.9 (1C, *C*H_2), 61.2 (1C, *C*H_2), 54.2 (2C, (*C*H_2)$_2$), 53.9 (2C, (*C*H_2)$_2$). *m/z* 249 $(MH)^+$.

2-(4-Benzylpiperazine-5-*t*-butyl-2-hydroxybenzylidene)acetohydrazide (**L14**)

t-Butylsalicylaldehyde (**30**) (1.78 g, 10 mmol), 4-benzylpiperazinoacetic acid hydrazide (**32**) (2.49 g, 10 mmol) and HCl (0.5 ml, conc.) were stirred in ethanol for 48 hrs. The resulting mixture was evaporated to dryness and recrystallised in hexane by addition of a minimum ethanol. Colourless thin plates crystallised on cooling, these were washed with cold hexane (3.67 g, 90.0%). (Anal. Calc. for $C_{24}H_{32}N_4O_2$: C, 70.56; H, 7.90; N, 13.71. Found: C, 70.61; H, 8.41; N, 13.69%). ν_{max}/cm^{-1} (KBr): 3278 (PhOH), 2952 (CH), 2935 (CH), 2808, 2765, 1672 (NH), 1612 (C=N), 1523 (C=O). ^{1}H NMR (250 MHz, $CDCl_3$): δ_H (ppm) 10.72 (s, 1H, Ar-O*H*), 9.99 (s, 1H, N*H*), 8.50 (s, 1H, C*H*N), 7.85-7.26 (m, 6H, Ar-*H*), 7.18 (d, 1H, Ar-*H*), 6.92 (d, 1H, Ar-*H*), 3.53 (s, 2H, CH_2), 3.17 (s, 2H, CH_2), 2.61 (br, 4H, (CH_2)$_2$), 2.52 (br, 4H, (CH_2)$_2$), 1.28 (s, 3H, (CH_3)$_3$). ^{13}C NMR (63 MHz, $CDCl_3$): δ_C (ppm) 166.1 (1C, *C*O), 156.5 (1C, Ar-*C*-OH), 152.2 (1C, *C*HN), 142.2 (1C, Ar-*C*), 138.0 (1C, Ar-*C*), 129.5 (1C, Ar-*C*), 129.3 (2C, Ar-*C*H), 128.5 (2C, Ar-*C*H), 127.7 (1C, Ar-*C*H), 127.4 (1C, Ar-*C*H), 116.9 (1C, Ar-*C*H), 116.8 (1C, Ar-*C*H), 63.1 (1C, *C*H_2), 61.2 (1C, *C*H_2), 53.9 (2C, (*C*H_2)$_2$), 53.2 (2C, (*C*H_2)$_2$), 34.2 (1C, *C*(CH_3)$_3$), 31.6 (3C, C(*C*H_3)$_3$). *m/z* 409 $(MH)^+$.

2-(4-Benzylpiperazine-5-nonyl-2-hydroxybenzylidene)acetohydrazide (**L15**)

4-Benzylpiperazinoacetic acid hydrazone (**32**) (1.25 g, 5 mmol) was suspended in ethanol (50 ml) to this a solution of 5-nonyl-salicylaldehyde (1.25 g, 5 mmol) in ethanol (50 ml) was added. The resulting mixture was stirred under reflux for 16 hrs. The resulting pale yellow solution was evaporated to yield a yellow oil/semi-solid. This was purified by column chromatography on silica by removing unreacted 5-nonyl-salicylaldehyde starting material using 5% ethyl acetate in hexane. The desired product was collected using chloroform, evaporated to dryness to yield a pale brown

semi solid (2.09 g, 87%). (Anal. Calc. for $C_{29}H_{42}N_4O_2$: C, 72.77; H, 8.84; N, 11.70. Found: C, 71.48; H, 9.08; N, 11.60%). ν_{max}/cm^{-1} (KBr): 3222 (PhOH), 2958 (CH), 2871 (CH), 2816, 1680 (NH), 1624 (C=N), 1579 (C=O), 1493. ^{1}H NMR (250 MHz, $CDCl_3$): δ_H (ppm) 10.03 (s, 1H, Ar-O*H*), 8.39 (s, 1H, C*H*N), 7.25-6.99 (m, 7H, Ar-*H*), 6.85 (d, 1H, Ar-*H*), 3.47 (s, 2H, CH_2), 3.11 (s, 2H, CH_2), 2.55 (br, 4H, (CH_2)$_2$), 2.46 (br, 4H, (CH_2)$_2$), 1.74-0.39 (m, 19H, (CH_2)$_8$CH_3). ^{13}C NMR (63 MHz, $CDCl_3$): δ_C (ppm) 166.0 (1C, *C*O), 156.2 (1C, Ar-*C*-OH), 152.0 (1C, *C*HN), 141.5 (1C, Ar-*C*), 138.8 (1C, Ar-*C*), 137.7 (1C, Ar-*C*), 130.7 (1C, Ar-*C*), 130.1 (1C, Ar-*C*H), 129.2 (2C, Ar-*C*H), 128.4 (2C, Ar-*C*H), 127.3 (1C, Ar-*C*H), 116.7 (1C, Ar-*C*H), 62.9 (1C, *C*H$_2$), 61.0 (1C, *C*H$_2$), 53.7 (2C, (*C*H$_2$)$_2$), 53.0 (2C, (*C*H$_2$)$_2$), 43.8-8.6 (9C, (*C*H$_2$)$_8$*C*H$_3$). ESI *m/z* 479 $(MH)^+$.

3-Bromomethyl-5-*t*-butylsalicylaldehyde (**33**)

Preparation carried out as Q. Wang *et al.*[4] HBr 48% in water (13.68 g, 81.07 mmol) was added to a mixture of 5-*t*-butylsalicylaldehyde (**30**) (2.00 g, 10.90 mmol) and paraformaldehyde (0.49 g, 16.4 mmol). A few drops (catalytic) of H_2SO_4 conc. were added. The resulting mixture was stirred and heated to 70°C for 20 hrs. This was then allowed to cool to room temperature before water (20 ml) was added and the product extracted into dichloromethane (20 ml). The organic phase was separated and dried over anhydrous Na_2SO_4, dried by rotary evaporation, then in vacuo to yield a yellow/brown oil (2.67 g, 97%). (Anal. Calc. for $C_{12}H_{15}BrO_2$: C, 53.15; H, 5.58. Found: C, 53.17; H, 5.58%). ^{1}H NMR (250 MHz, $CDCl_3$): δ_H (ppm) 11.30 (s, 1H, Ar-O*H*), 9.88 (s, 1H, C*H*O), 7.62 (d, 1H, Ar-*H*), 7.50 (d , 1H, Ar-*H*), 4.57 (s, 2H, CH_2), 1.31 (s, 9H, (CH_3)$_3$). ^{13}C NMR (63 MHz, $CDCl_3$): δ_C (ppm) 196.8 (1C, *C*HO), 157.6 (1C, Ar-*C*-OH), 143.1 (1C, Ar-*C*), 135.8 (1C, Ar-*C*H), 130.9 (1C, Ar-*C*H), 126.0 (1C, Ar-*C*), 120.4 (1C, Ar-*C*), 34.4 (1C, *C*(CH$_3$)$_3$), 31.4 (3C, C(*C*H$_3$)$_3$), 27.3 (1C, *C*H$_2$). ESI *m/z* 291 $(M)Na^+$.

5-*t*-Butyl-3-(4-methylpiperazinomethyl)salicylaldehyde (**34**)

1-Methylpiperazine (0.50 g, 5 mmol) was dissolved in anhydrous acetonitrile (55 cm^3). To this 3-bromomethyl-5-*t*-butylsalicylaldehyde (**33**) (1.36 g, 5 mmol) and K_2CO_3 (1.05g, 7.60 mmol) were added. The mixture was stirred and heated to reflux under N_2 for 6 hrs. Thereafter was allowed to cool to RT and filtered. The filtrate was evaporated by rotary evaporator to yield a yellow oil which solidified on cooling. This was redissolved in DCM, filtered and the filtrate taken to dryness to yield a yellow oil. This was purified by silica-60 wet flash column chromatography (5% MeOH in DCM eluent) to yield a yellow oil (1.33g, 96%). ^{1}H NMR (250 MHz, $CDCl_3$): δ_H (ppm) 10.30 (s, 1H, C*H*O), 7.60 (d, 1H, Ar-*H*), 7.27 (d, 1H, Ar-*H*), 3.70 (s, 2H, Ar-CH_2N), 2.58 (br, 8H, N(CH_2)$_2$(CH_2)$_2$N), 2.28 (s, 3H, NCH_3), 1.25 (s, 9H, (CH_3)$_3$). ^{13}C NMR (63 MHz, $CDCl_3$): δ_C (ppm) 191.9 (1C, *C*HO), 159.4 (1C, Ar-*C*-OH), 142.0 (1C, Ar-*C*), 133.0 (1C, Ar-*C*H), 124.9 (1C, Ar-*C*H), 123.0 (1C, Ar-*C*), 122.3 (1C, Ar-*C*), 60.1 (1C, *C*H_2), 55.0 (2C, CH_2N-(*C*H_2)$_2$), 52.8 (2C, CH_3N-(*C*H_2)$_2$), 46.1 (1C, *C*H_3), 34.3 (1C, *C*(CH_3)$_3$), 31.5 (3C, C(*C*H_3)$_3$).

5-*t*-Butyl-2-hydroxy-3-((4-methylpiperazin-1-yl)methyl)benzylidene octanehydrazide (**L16**)

5-*t*-Butyl-3-(4-methylpiperazinomethyl)salicylaldehyde (**34**) (1.52 g, 5.2 mmol) was dissolved in ethanol (50 ml). To this a solution of octanoic hydrazide (0.90 g, 5.7 mmol) in ethanol (50 ml) was added. The resulting solution was stirred under reflux for 24 hrs. The resulting solution was taken to dryness to yield yellow semi-solid. This was purified by silica-60 wet flash column chromatography (5% MeOH in DCM eluent) to yield a yellow semi-solid (1.58 g, 70.7%). (Anal. Calc. for $C_{25}H_{42}N_4O_2$•H_2O: C, 66.93; H, 9.89; N, 12.49. Found: C, 67.37; H, 9.82; N, 12.47%). ^{1}H NMR (250 MHz, $CDCl_3$): δ_H (ppm) 9.18 (s, 1H, Ar-O*H*), 8.44 (s, 1H, C*H*N), 7.65 (d, 1H, Ar-*H*), 7.05 (d, 1H, Ar-*H*), 3.68 (s, 2H, Ar-CH_2N), 2.54 (br, 8H, N(CH_2)$_2$(CH_2)$_2$N), 2.17 (s, 3H, NCH_3), 1.69-1.18 (m, 21H, (CH_2)$_6$ and (CH_3)$_3$), 0.84 (t, 3H, CH_3). ν_{max}/cm^{-1} (KBr): 3180 (PhOH), 2954 (CH), 2927 (CH), 2856, 2798,

1670 (NH), 1612 (C=N), 1560 (C=O). ^{13}C NMR (63 MHz, $CDCl_3$): δ_C (ppm) 176.1 (1C, *C*O), 154.8 (1C, Ar-*C*-OH), 142.1 (1C, Ar-*C*), 141.1 (1C, *C*HN), 128.3 (1C, Ar-*C*H), 122.3 (1C, Ar-*C*H), 121.8 (1C, Ar-*C*), 119.6 (1C, Ar-*C*), 60.8 (1C, *C*H_2), 55.1 (2C, CH_2N-(*C*H_2)$_2$), 52.7 (2C, CH_3N-(*C*H_2)$_2$), 46.0 (1C, *C*H_3), 34.2 (1C, *C*$(CH_3)_3$), 33.2 (1C, *C*H_2), 31.9 (1C, *C*H_2), 31.6 (3C, C(*C*H_3)$_3$), 29.7 (1C, *C*H_2), 29.2 (1C, *C*H_2), 25.1 (1C, *C*H_2), 22.8 (1C, *C*H_2), 14.3 (1C, *C*H_3). *m/z* 431 $(MH)^+$.

3-Bromomethyl-5-nonylsalicylaldehyde (**35**)

Reaction was carried out as for (**33**) using 5-nonylsalicylaldehyde (2.72 g, 10.97 mmol). The resulting mixture was stirred and heated to 70°C for 9 days. The resulting brown/black oil was partially purified by silica column chromatography using 5% methanol in chloroform eluent (2.54 g, 68%). ^{1}H NMR (250 MHz, $CDCl_3$): δ_H (ppm) 11.31 (s, 1H, Ar-O*H*), 9.87 (s, 1H, C*H*O), 7.58 (m, 1H, Ar-*H*), 7.35 (m , 1H, Ar-*H*), 4.57 (s, 2H, C*H*$_2$), 1.99-0.65 (m, 19H, (C*H*$_2$)$_8$C*H*$_3$). ^{13}C NMR (63 MHz, $CDCl_3$): δ_C (ppm) 197.0 (1C, *C*H=O), 159.5 (1C, Ar-*C*-OH), 157.3 (1C, Ar-*C*), 135.8 (m, 1C, Ar-*C*H), 130.8 (m, 1C, Ar-*C*H), 126.2 (1C, Ar-*C*), 119.8 (1C, Ar-*C*), 50.8-8.8 (m, 10C, *C*H_2, (*C*H_2)$_8$*C*H_3). ESI *m/z* 361 $(M)Na^+$.

3-((4-benzhydrylpiperazin-1-yl)methyl)-2-hydroxy-5-nonylbenzylidene)octanehydrazide (**L17**)

1-Diphenyl-methylpiperazine (1.26 g, 5.0 mmol) was dissolved in acetonitrile (55 ml, anhydrous). To this, $NaCO_3$ (1.05 g, 10 mmol) and 3-bromomethyl-5-nonylsalicylaldehyde (**35**) (2.00 g, 5.9 mmol) were added. The mixture was stirred under reflux for 6 hrs. The mixture was cooled, filtered and evaporated to dryness. Attempts to purify the resulting viscous black oil failed and the next step of the synthesis was carried out on the crude intermediate. This was re-dissolved in acetonitrile (50 ml) and octanoic hydrazide (0.79 g, 5.0 mmol) added. The resulting mixture was stirred under reflux for 16 hrs, evaporated to dryness and purified by silica-60 wet flash column chromatography (10% acetone in DCM eluent) to yield a

brown toffee-like solid on cooling (0.92 g, 29.8%). (Anal. Calc. for $C_{42}H_{60}N_4O_2$: C, 77.26; H, 9.26; N, 8.58. Found: C, 76.41; H, 9.58; N, 8.19%). ν_{max}/cm^{-1} (KBr): 2956 (CH), 2927 (CH), 2856, 1662 (NH), 1614 (C=N), 1556 (C=O). ^{1}H NMR (250 MHz, $CDCl_3$): δ_H (ppm) 9.31 (s, 1H, Ar-O*H*), 8.11 (s, 1H, C*H*N), 7.60-6.89 (m, 12H, Ar-*H*), 4.23 (s, 1H, C*H*), 3.68 (s, 2H, Ar-CH_2-N), 2.75-2.23 (m, 8H, N-(CH_2)$_2$(CH_2)$_2$N-), 1.79-0.47 (m, 34H, 14 x CH_2 and 2 x CH_3). ^{13}C NMR (126 MHz, $CDCl_3$): δ_C (ppm) 176.4 (1C, *C*O), 154.6 (1C, Ar-*C*-OH), 148.1 (1C, Ar-*C*HN), 142.6 (1C, Ar-*C*H), 138.7 (2C, 2 x Ar-*C*), 132.6 (1C, Ar-*C*), 128.7 (4C, 4 x Ar-*C*H), 128.0 (4C, 4 x Ar-*C*H), 127.2 (2C, 2 x Ar-*C*H), 121.9 (1C, Ar-*C*), 119.1 (1C, Ar-*C*), 116.3 (1C, Ar-*C*H), 76.2 (1C, *C*H), 60.5 (1C, Ar-*C*H_2-N), 53.0 (2C, 2 x N-(*C*H_2CH_2)-N), 51.9 (2C, 2 x N-(CH$_2$*C*H$_2$)-N), 41.6-14.3 (16C, (CH$_2$)$_6$CH$_3$ and (CH$_2$)$_8$CH$_3$). ESI m/z 653 $(MH)^+$.

5-*t*-Butyl-2-hydroxy-3-(piperidin-1-ylmethyl)benzylidene)octanehydrazide (**L18**)

5-*t*-Butyl-2-hydroxy-3-(piperidine-1-ylmethyl)-benzaldehyde, previously by Henry[5] (1.39 g, 5.05 mmol) was dissolved in methanol, to this a methanol solution (25 ml) of octanoic hydrazide (0.80 g, 5.05 mmol) was added. The mixture was stirred under reflux for 16 hrs, evaporated to dryness and dried *in vacuo* to yield a viscous yellow oil. The desired material was obtained as a white solid by trituration from hexane (1.30 g, 62.0%). (Anal. Calc. for $C_{25}H_{41}N_3O_2$: C, 72.25; H, 9.94; N, 10.11. Found: C, 72.49; H, 10.62; N, 10.21%). ν_{max}/cm^{-1} (KBr): 3195 (PhOH), 2925 (CH), 2856, 2806, 1674 (NH), 1614 (C=N), 1556 (C=O).^{1}H NMR (250 MHz, $CDCl_3$): δ_H (ppm) 10.85 (s, 1H, Ar-O*H*), 8.94 (s, 1H, N*H*), 8.14 (s, 1H, C*H*N), 7.69 (d, 1H, Ar-*H*), 7.00 (d, 1H, Ar-*H*), 3.64 (s, 2H, NCH_2), 2.73 (t, 2H, COCH_2), 2.49 (s (br), 4H, (CH_2)$_2$), 1.75-1.34 (m, 6H, (CH_2)$_3$), 1.27-1.10 (m, 19H, (CH_2)$_5$, (CH_3)$_3$), 0.85 (t, 3H, CH_3). ^{13}C NMR (63 MHz, $CDCl_3$): δ_C (ppm) 75.9 (1C, *C*O), 155.4 (1C, Ar-*C*-OH), 141.8 (1C, *C*HN), 140.5 (1C, Ar-*C*), 127.9 (1C, Ar-*C*), 122.1 (1C, Ar-*C*), 121.5 (1C, Ar-*C*), 119.7 (1C, Ar-*C*H), 62.1 (1C, Ar-*C*H$_2$N), 54.1 (2C, N(*C*H$_2$)$_2$), 34.2 (1C, *C*H$_2$), 33.3 (1C, *C*H$_2$), 32.0 (1C, *C*(CH$_3$)$_3$), 31.6 (3C, (*C*H$_3$)$_3$), 29.7 (1C, *C*H$_2$), 29.3 (1C, *C*H$_2$),

26.0 (2C, (CH_2)$_2$), 25.2 (1C, CH_2), 24.1 (1C, CH_2), 22.8 (1C, CH_2), 14.3 (3C, CH_3). ESI *m/z* 414 $(M-H)^-$.

5-*t*-Octyl-3-((dihexylamino)methyl)salicylaldehyde (**36**)

5-*t*-Octyl-salicylaldehyde (**31**) (2.35 g, 10.0 mmol) and ethyoxymethyldihexylamine previously prepared by Henry[5] (2.74 g, 11.3 mmol) were stirred in acetonitrile (40 ml) under reflux and nitrogen for 6 days. The resulting red solution was evaporated to yield a viscous red oil. The desired product was purified by silica-60 wet flash column chromatography (5% ethyl acetate in hexane eluent) as a pale yellow oil (1.63 g, 37.9%). (Anal. Calc. for $C_{28}H_{49}NO_2$: C, 77.90; H, 11.44; N, 3.24. Found: C, 77.90; H, 12.14; N, 3.51%). ^{1}H NMR (250 MHz, $CDCl_3$): δ_H (ppm) 11.45 (s, 1H, Ar-O*H*), 10.39 (s, 1H, C*H*O), 7.59 (d, 1H, Ar-*H*), 7.22 (d, 1H, Ar-*H*), 3.56 (s, 2H, Ar-CH_2N), 2.49 (t, 4H, 2 x NCH_2), 1.65 (s, 2H, CH_2), 1.51 (m, 4H, 2 x CH_2), 1.31-1.23 (m, 18H, 6 x CH_2, C((CH_3)$_2$), 0.84 (t, 6H, 2 x CH_3), 0.66 (s, 9H, (CH_3)$_3$). ^{13}C NMR (63 MHz, $CDCl_3$): δ_C (ppm) 191.4 (1C, *C*HO), 160.2 (1C, Ar-*C*-OH), 140.5 (1C, Ar-*C*), 133.3 (1C, Ar-*C*H), 124.6 (1C, Ar-*C*H), 123.7 (1C, Ar-*C*), 122.5 (1C, Ar-*C*), 57.5 (1C, CH_2), 57.0 (1C, CH_2), 53.7 (1C, (CH_2)$_2$), 38.1 (1C, $C(CH_3)_2$), 32.5 (1C, $C(CH_3)_3$), 32.0 (3C, C(CH_3)$_3$), 31.8 (2C, 2 x CH_3), 31.7 (2C, 2 x CH_2), 27.2 (2C, 2 x CH_2), 26.3 (2C, 2 x CH_2), 22.7 (2C, 2 x CH_2), 14.2 (2C, 2 x CH_3). ESI *m/z* 432 $(MH)^+$.

(5-*t*-Octyl-3-((dihexylamino)methyl)-2-hydroxybenzylidene)octanehydrazide (**L19**)

5-*t*-Octyl-3-((dihexylamino)methyl)salicylaldehyde (**36**) (0.70 g, 1.62 mmol) and octanoic hydrazide (0.26 g, 1.65 mmol) were stirred in methanol (40 ml) under reflux for 16 hrs. The resulting yellow solution was evaporated and purified by silica-60 wet flash column chromatography (diethyl ether eluent) to yield the desired product as a pale yellow oil (0.73 g, 78.7%). (Anal. Calc. for $C_{36}H_{65}N_3O_2$: C, 75.60; H, 11.40; N, 7.35. Found: C, 75.84; H, 11.55; N, 7.35%). ν_{max}/cm^{-1} (nujol): 3201s (PhOH), 3065s (CH), 1670vs (NH), 1614 (C=N), 1591, 1556 (C=O). ^{1}H NMR (250 MHz,

$CDCl_3$): δ_H (ppm) 9.09 (s, 1H, Ar-O*H*), 8.14 (s, 1H, C*H*N), 7.66 (d, 1H, Ar-*H*), 7.00 (d, 1H, Ar-*H*), 3.71 (s, 2H, Ar-CH_2N), 2.72 (t, 2H, COCH_2), 2.46 (t, 4H, 2 x NCH_2), 1.76-1.64 (m, 2H, CH_2), 1.61 (s, 2H, CH_2), 1.49 (m, 4H, 2 x CH_2), 1.32-1.23 (m, 26H, 10 x CH_2, 2 x CH_3), 0.84 (m, 9H, 3 x CH_3), 0.69 (s, 9H, (CH_3)$_3$). ^{13}C NMR (63 MHz, $CDCl_3$): δ_C (ppm) 176.1 (1C, *C*O), 155.3 (1C, Ar-*C*-OH), 140.8 (1C, *C*HN), 140.4 (1C, Ar-*C*), 128.8 (1C, Ar-*C*H), 122.7 (1C, Ar-*C*), 122.5 (1C, Ar-*C*H), 119.5 (1C, Ar-*C*), 57.9 (1C, *C*H_2), 57.1 (1C, *C*H_2), 53.6 (2C, 2 x *C*H_2), 38.1 (1C, *C*(CH$_3$)$_2$), 33.3 (1C, CH$_2$), 32.6 (1C, *C*(CH$_3$)$_3$), 32.0 (3C, C(*C*H$_3$)$_3$), 32.0 (2C, 2 x *C*H_2), 31.8 (2C, C(*C*H$_3$)$_2$), 29.9 (1C, *C*H_2), 29.7 (1C, *C*H_2), 29.3 (1C, *C*H_2), 27.2 (2C, 2 x *C*H_2), 26.3 (2C, 2 x *C*H_2), 25.2 (1C, *C*H_2), 22.8 (1C, *C*H_2), 22.8 (2C, 2 x *C*H_2), 14.3 (1C, *C*H$_3$), 14.2 (2C, 2 x *C*H$_3$). ESI *m/z* 572 $(MH)^+$.

3,5-Bis((dihexylamino)methyl)-salicylaldehyde (**37**)

Salicylaldehyde (6.10 g, 50 mmol) and 1-ethyoxymethyldihexylamine, previously prepared by Forgan[6] (25.50 g , 105 mmol) were stirred in dry acetonitrile (250 ml) under nitrogen at reflux for 6 days. The resulting orange solution was evaporated to dryness to yield a red oil. This was purified by silica-60 wet flash column chromatography (DCM to remove unreacted salicylaldehyde followed by 1:1 hexane:ethyl acetate) as a yellow oil (13.28 g, 51.5%). (Anal. Calc. for $C_{33}H_{60}N_2O_2$: C, 76.69; H, 11.70; N, 5.42. Found: C, 76.73; H, 11.82; N, 7.75%). ^{1}H NMR (360 MHz, $CDCl_3$): δ_H (ppm) 11.78 (s (br, 1H, Ar-O*H*), 10.39 (s, 1H, C*H*O), 7.51 (d, 1H, Ar-*H*), 7.23 (d, 1H, Ar-*H*), 3.72 (s, 2H, Ar-CH_2N), 3.41 (s, 2H, Ar-CH_2N), 2.48 (t, 4H, 2 x NCH_2), 2.34 (t, 4H, 2 x NCH_2), 1.49 (m, 4H, 2 x NCH$_2$CH_2), 1.40 (m, 4H, 2 x NCH$_2$CH_2), 1.28-1.16 (m, 24H, 12 x CH_2), 0.85 (m, 12H, 4 x CH_3). ^{13}C NMR (90 MHz, $CDCl_3$): δ_C (ppm) 190.0 (1C, *C*HO), 161.4 (1C, Ar-*C*-OH), 135.5 (1C, Ar-*C*H), 130.6 (1C, Ar-*C*), 127.6 (1C, Ar-*C*H), 124.1 (1C, Ar-*C*), 122.7 (1C, Ar-*C*), 57.9 (1C, Ar-*C*H_2), 57.3 (1C, Ar-*C*H_2), 53.9 (2C, 2 x *C*H_2), 53.7 (2C, 2 x *C*H_2), 32.0 (1C, 2 x *C*H_2), 31.9 (2C, 2 x *C*H_2), 27.3 (2C, 2 x *C*H_2), 27.2 (2C, 2 x *C*H_2), 27.1 (2C, 2 x *C*H_2), 26.8 (2C, 2 x *C*H_2), 22.8 (2C, 2 x *C*H_2), 22.7 (2C, 2 x *C*H_2), 14.2 (2C, 2 x *C*H$_3$), 14.1 (2C, 2 x *C*H$_3$). ESI *m/z* 517 $(MH)^+$.

3,5-Bis((dihexylamino)methyl)-2-hydroxybenzylidene)octanehydrazide (**L20**)

3,5-Bis((dihexylamino)methyl)-salicylaldehyde (**37**) (2.00 g, 3.86 mmol) and octanoic hydrazide (0.61 g, 3.86 mmol) were stirred in methanol (50 ml) under reflux for 16 hrs, evaporated to dryness to yield a yellow oil. This was purified by silica-60 wet flash column chromatography (5% methanol in DCM eluent) to a pale yellow oil (2.50 g, 98.6%). (Anal. Calc. for $C_{41}H_{77}N_4O_2$: C, 74.94; H, 11.66; N, 8.53. Found: C, 74.29; H, 12.65; N, 8.68%). ν_{max}/cm^{-1} (nujol): 3195s (PhOH), 3057s (CH), 1672s (NH), 1614 (C=N), 1591, 1556 (C=O). ^{1}H NMR (360 MHz, $CDCl_3$): δ_H (ppm) 8.65 (s (br, 1H, Ar-O*H*), 8.10 (s, 1H, C*H*O), 7.57 (d, 1H, Ar-*H*), 7.23 (d, 1H, Ar-*H*), 3.71 (s, 2H, Ar-CH_2N), 3.42 (s, 2H, Ar-CH_2N), 2.72 (t, 2H, COCH_2), 2.48 (t, 4H, 2 x NCH_2), 2.36 (t, 4H, 2 x NCH_2), 1.70 (m, 2H, $COCH_2CH_2$), 1.50-1.23 (m, 40H, 20 x CH_2), 0.85 (m, 15H, 5 x CH_3). ^{13}C NMR (90 MHz, $CDCl_3$): δ_C (ppm) 175.7 (1C, *C*O), 156.6 (1C, Ar-*C*-OH), 140.1 (1C, *C*HN), 131.1 (1C, Ar-*C*H), 130.7 (1C, Ar-*C*), 125.2 (1C, Ar-*C*H), 123.0 (1C, Ar-*C*), 119.9 (1C, Ar-*C*), 58.2 (1C, Ar-*C*H_2), 58.0 (1C, Ar-*C*H_2), 53.9 (2C, 2 x *C*H_2), 53.7 (2C, 2 x *C*H_2), 33.0 (1C, *C*H_2), 32.0 (2C, 2 x *C*H_2), 32.0 (2C, 2 x *C*H_2), 31.8 (1C, *C*H_2), 29.6 (1C, *C*H_2), 29.3 (1C, *C*H_2), 27.4-27.1 (8C, 8 x *C*H_2), 26.4 (1C, *C*H_2), 25.0 (1C, *C*H_2), 22.9 (2C, 2 x *C*H_2), 22.8 (2C, 2 x *C*H_2), 14.2 (3C, 3 x *C*H_3), 14.1 (2C, 2 x *C*H_3). ESI *m/z* 657 $(MH)^+$.

5.2 Metal Complex Synthesis

$[Cu_2(\mathbf{L2}\text{-}2H)_2]$

5-Methylsalicylaldehyde-pivaloylhydrazide (**L2**) (0.24 g, 1.0 mmol) and copper acetate (0.27 g, 1.1 mmol) were stirred in ethanol for 6 h. The resultant green precipitate was filtered and washed with water and ethanol, dried *in vacuo* and recrystallised from a minimum of chloroform to yield the dinuclear copper complex (0.27 g, 91.5%). (Anal. Calc. for $C_{26}H_{32}Cu_2N_4O_4$: C, 52.78; H, 5.45; N, 9.47%; Found: C, 52.41; H, 4.83; N, 9.07). *m/z* 591 $(MH)^+$.

$[Cu(\mathbf{19}\text{-}H)_2]$

5-*t*-Octylsalicylaldoxime (19) and $Cu(OAc)_2 \bullet H_2O$ were stirred in methanol (50 ml) for 24 hrs. The resulting brown solid was filtered and washed with water and methanol and recrystallised from a minimum of hexane to yield very fine brown needles (0.41 g, 73.3%). (Anal. Calc. for $C_{30}H_{44}CuN_2O_4$: C, 64.32; H, 7.92; N, 5.00%; Found: C, 64.64; H, 8.13; N, 5.30). ν_{max}/cm^{-1} (KBr): 3132br (NOH), 2952 (CH), 2900 (CH), 1647, 1612 (C=N). ESI *m/z* 840 $(MH)^+$.

5.3 Liquid : Liquid Extraction Experiments

5.3.1 Metal Loading by L6 and L7

Initial loading experiments were carried out for **L6**. Experiments were carried out in 50 ml glass jars, all other solvent extraction experiments were carried out in 14 ml screw-cap vials. A solution of **L6** in chloroform (5ml, 0.01 M) was contacted with a copper sulfate aqueous phase (5ml, 0.015 M). The aqueous phase contained copper sulfate (3 ml, 0.025 M) and varying quantities of aqueous solutions of sodium hydroxide or sulfuric acid to adjust the pH and water to make the solution to volume (5 ml). The solutions were stirred to equilibrium for 16 hrs and a portion of the organic phase (0.5 ml) taken, evaporated to dryness and redissolved and made to volume (10 ml) using butan-1-ol. The copper content was analysed by ICP-OES and the pH of the aqueous phase measured. Data are provided in Appendix 7.2.2.

Future experiments were carried out using **L7**. A solution of **L7** in chloroform (5 ml, 0.0025 M) were contacted with metal sulfate solutions containing either Fe(III), Co(II), Ni(II), Cu(II) or Zn(II) sulfate salts (5 ml, 0.012 M). The aqueous phases were prepared from the appropriate metal salt solution (3 ml, 0.020 M) and pH adjusted by addition of aqueous sulfuric acid or sodium/potassium hydroxide. The samples were equilibrated and analysed as above. Data are provided in Appendix 7.2.2.

5.3.2 Metal Selectivity of L7

Metal selectivity was probed using **L7**. The procedure follows that of single metal loading by **L7** (5 ml, 0.0025 M) detailed in Section 5.3.1 using a mixed metal feed solution containing Fe(III), Co(II), Ni(II), Cu(II) or Zn(II) sulfate salts, each present at 0.02M. Data are provided in Appendix 7.2.2.

To enable maximum loading, iron was omitted from the mixed metal feed solution which permitted the pH being increased beyond 2.5 which was inhibited by precipitation of iron (oxy)hydroxides. Data are provided in Appendix 7.2.2.

5.3.3 Copper Loading by Blended Extractants (L6+P50) and (L7+19)

Portions of the *mono*acidic ligands **P50** and **19** were mixed with portions of the *tri*acidic ligands **L6** and **L7**, respectively, in chloroform. Each was present at (0.00125 M) to yield an overall extractant concentration of (0.0025 M). Solvent extraction experiments were carried out as for **L7** (5 ml, 0.0025 M) detailed in Section 5.3.1. Data are provided in Appendix 7.2.2.

5.3.4 Metal Selectivity by Blended Extractants (L6+P50) and (L7+19)

Metal selectivity studies for the blended extractant systems were carried out using organic solutions prepared as detailed in Section 5.3.3 following the solvent extraction procedure as for **L7** detailed in Section 5.3.2 without iron(III) present in solution. Data are provided in Appendix 7.2.2.

5.3.5 Metal Sulfate Loading by L14-L20

Solvent extraction experiments using chloroform solutions of **L14**-**L20** (5 ml, 0.0025 M) were carried out as detailed for **L7** in Section 5.3.2. Copper and sulfur content were measured by ICP-OES. Data are provided in Appendix 7.3.2.

5.3.6 Metal Selectivity by L14-L20 from a Sulfate Aqueous Phase

Metal selectivity experiments for chloroform solutions of **L14**-**L20** (5 ml, 0.0025 M) were carried out as detailed for **L7** in Section 5.3.2 with Fe(III) present in the mixed metal feed solution. Data are provided in Appendix 7.3.2.

5.3.7 Copper Sulfate Load/Strip Cycles by L19

Load: A solution of **L19** (0.0025 M) in chloroform was contacted with an aqueous solution of $CuSO_4$ (1.0 M). The system was stirred for 1hr then separated. An aliquot (1.0 ml) of the organic phase was taken from the organic phase, evaporated to dryness and redissolved in butan-1-ol. Copper and sulfate content were analysed by ICP-OES.

Strip: The remaining organic phase, separated from the aqueous copper sulfate solution was contacted with sulfuric acid (150 g L^{-1}) and stirred for 1 hr. the layers were separated and analysed as for the load samples.

This procedure was repeated four times. Data are provided in Appendix 7.3.2.

5.3.8 Mixed Metal Sulfate Load/Strip Cycles by L19

Procedure was repeated as Section 5.3.7 using mixed metal sulfate aqueous phase (0.012 M) prepared as detailed in Section 5.3.2 using a solution containing Fe(III). Data are provided in Appendix 7.3.2.

5.4 Modifier Titrations

5.4.1 Copper Loading by 19

Before the effect of modifiers on the extractive abilities of **19** could be established, the copper loading profile was obtained for **19**. Experiments were carried out in 14 ml screw-cap vials. A solution of **19** in *n*-heptane (5 ml, 0.01 M) was contacted with copper sulfate (5 ml, 0.016 M). The aqueous phase was prepared from copper sulfate (4 ml, 0.020 M) and pH adjusted by addition of aqueous sulfuric acid or potassium/sodium hydroxide and made to volume with water. The solutions were stirred to equilibrium over 16 hours. The phases were separated and an aliquot (1.0 ml) of the organic phase was taken, evaporated to dryness and redissolved in butan-1-ol and copper content measured by ICP-OES. The aqueous phase pH was measured. Data are provided in Appendix 7.4.1.

5.4.2 The Effect of 2-Ethylhexanol on Copper Loading by 19

Solutions of **19** in *n*-heptane (2.5 ml, 0.02 M) were mixed with solutions of 2-ethylhexanol (2.5 ml; 0.4, 1.0, 2.0, 4.0, 20.0 molar equivalents) to give solutions of **19** (5 ml, 0.01 M) with overall 2-ethylhexanol to copper ratios in the resulting complex of 0.2, 0.5, 1.0, 2.0 and 10.0 to 1. The resulting solutions were treated using the procedure as detailed in Section 5.4.1. Data are provided in Appendix 7.4.1.

The IR, UV/Vis and EPR spectra were recorded and are provided in Appendix 7.4.2.

5.4.3 The Effect of Trioctylphosphine Oxide on Copper Loading by 19

Experiments were repeated as detailed in Section 5.4.2 except solutions of trioctylphosphine oxide (2.5 ml; 0.2, 1.0, 2.0, 4.0, 20.0 molar equivalents) were used to give overall trioctylphosphine oxide to copper complex ratios of 0.1, 0.5, 1.0, 2.0 and 10.0 to 1. Data are provided in Appendix 7.4.1.

The IR, UV/Vis and EPR spectra were recorded and are provided in Appendix 7.4.2.

5.5 Calculation of Association Constants

All data was plotted using Gnuplot, version 4.0. Fits were performed by implementation of the nonlinear least-squares Marquardt-Levenberg algorithm.

A summary of results is provided in Appendix 7.4.3.

5.5.1 TOPO-[Cu(19-H)$_2$] UV/Vis Job Plot

Solutions of TOPO and [Cu(**19**-H)$_2$] in *n*-heptane (0.4 mM) were mixed in glass vials to give molar ratios of TOPO to [Cu(**19**-H)$_2$] from 0 to 1.0 and *vice versa* in 5% increments. Experimental data are provided in Appendix 7.4.3.

5.5.2 TOPO-[Cu(19-H)$_2$] UV/Vis Titrations

A standard solution of [Cu(**19**-H)$_2$] (0.4 mM) was used to dissolve and make to volume samples of TOPO in volumetric flasks (50 ml). The molar equivalents of TOPO to [Cu(**19**-H)$_2$] were 0-2 in 0.2 intervals, 2.5-10 in 2.5 intervals, 10, 15, 20 and 50. Experimental data are provided in Appendix 7.4.3.

5.5.3 TOPO-19 NMR Titrations

A standard solution of TOPO (5.0 mM) in non-deuterated *n*-heptane was used to dissolve and make to volume samples of **19**. The molar ratio of **19** to TOPO was increased from zero in the stock solution to 2 in 0.1 molar equivalent intervals.

Portions (0.5 ml) of the resulting solutions were transferred to NMR tubes and the ^{31}P spectra measured and referenced to a H_3PO_4 external standard.

A standard solution of TOPO (10 mM) in deuterated toluene was used to dissolve and make to volume samples of **19**. The molar ratio of **19** to TOPO was increased from zero in the stock solution to 10 (0.025, 0.05, 0.10, 0.15, 0.20, 0.25, 0.50 and 1.0 molar equivalents). Portions (0.5 ml) of the resulting solutions were transferred to NMR tubes and the ^{31}P spectra measured and referenced to a H_3PO_4 external standard. Experimental data are provided in Appendix 7.4.3.

5.5.4 Sulfuric Acid Saturated TOPO-19 NMR Titrations

A standard solution of TOPO (5.0 mM) in non-deuterated *n*-heptane was stirred with sulfuric acid (1.0 M) for 16 hrs in a sealed glass jar. The phases were separated and a portion of the aqueous phase was back-titrated with sodium hydroxide. This procedure was repeated with fresh sulfuric acid solution until concordant back titration results were obtained (3 times) then repeated once more. The organic phase was filtered through phase separation filter paper to remove entrained aqueous phase. NMR titrations were repeated as Section 5.5.3. Experimental data are provided in Appendix 7.4.3.

5.6 EPR

EPR spectra of *n*-heptane solutions of [Cu(**19**-H)$_2$] and those with increasing quantities of modifier added (Chapter 4) were measured directly on extracts taken from the solvent extraction experiments. Spectra were measured in a flat quartz cell and *g*-values adjusted relative to the reference 2,2'-diphenyl-1-picrylhydrazyl (dpph) $g_{correct} = g_{expt}$ - 0.01135. Instrument parameters were not altered between measurements: centre field = 3288 G, sweep width = 600 G, gain = 80000, power = 32 mW, sweep time = 200s. Experimental data are provided in Appendix 7.4.2.

5.7 X-ray Crystallography

All crystal structures were solved by Mr. Fraser J. White at the University of Edinburgh Crystallography Service. Details of each solution, along with appropriate cif files, are located in Appendix 7.2.3. Data were collected on a 3 circle Bruker Smart Apex CCD diffractometer with graphite-monochromated Mo-Kα radiation (λ = 0.71073 Å) and equipped with an Oxford Cryosystems low temperature device operating at 150 K.

5.8 Magnetic Susceptibility

Magnetic susceptibility of a vacuum dried polycrystalline sample of [Cu(**L2**-2H)$_2$] (21.2 mg) in the 5-300 K temperature range under an applied field of 1.0 T. Data are provided in Appendix 7.2.5.

5.9 References

1. R. Aldred, R. Johnston, D. Levin and J. Neilan, *J. Chem. Soc., Perkin Trans. 1*, 1994, 1823-1831.
2. J. A. Ruell, E. De Clercq, C. Pannecouque, M. Witvrouw, T. L. Stup, J. A. Turpin, R. W. Buckheit, Jr. and M. Cushman, *J. Org. Chem.*, 1999, **64**, 5858-5866.
3. K. S. Putt, G. W. Chen, J. M. Pearson, J. S. Sandhorst, M. S. Hoagland, J. T. Kwon, S. K. Hwang, H. Jin, M. I. Churchwell, M. H. Cho, D. R. Doerge, W. G. Helferich and P. J. Hergenrother, *Nature Chem. Bio.*, 2006, **2**, 543-550.
4. Q. Wang, C. Wilson, A. J. Blake, S. R. Collinson, P. A. Tasker and M. Schroder, *Tetrahedron Lett.*, 2006, **47**, 8983-8987.
5. D. C. R. Henry, PhD Thesis, The University of Edinburgh, 2007.
6. R. S. Forgan, PhD Thesis, The University of Edinburgh, 2008.

Chapter 6 : Conclusions

This thesis considers options to improve the efficiency of recovery of copper in solvent extraction processes which currently use the commercial reagent 5-nonylsalicylaldoxime (**P50**). Initially it was proposed to do this by:

- increasing molar transport efficiency using novel trinucleating copper extractants to form $[Cu_3(\mathbf{L}\text{-}3H)_2]$ and,
- investigating the interactions between modifiers and commercial salicylaldoxime extractants and their copper complexes to define their mode of action with a view to rationalising the design and application of modifiers.
- Early success in developing polynucleating extractants led to a third area of work to develop extractants for copper *salts*, in particular copper(II) sulfate for application to process feed solutions for recently developed sulfate leaching processes.[1] These new reagents operate more efficiently than the prototype reagents[2, 3] because they transfer two mol of copper(II) sulfate into the organic phase in each neutral complex $[Cu_2(L)_2(SO_4)_2]$.

The new triacidic ligands **L4**-**L13** discussed in Chapter 2 have been demonstrated[4, 5] to triple molar transport and increase mass transport by between 1.7 and 2.5 fold for **L10** and **L6** respectively relative to the commercial extractant **P50**. Solvent extraction experiments have also demonstrated that the new triacidic ligands can double the molar transport of phenolic oxime reagents when used in an equimolar blend through formation of a ternary $[Cu_2(L\text{-}3H)(\mathbf{P50}\text{-}H)]$ complex. A 1:1 blend of **L6** with **P50** increased the mass transport of copper by 1.8 fold relative to **P50** alone.

Before the new triacidic ligands were designed, it was important to understand the binding mode of the previously studied[6] dinucleating ligands (**1**-**6**). To investigate this, efforts were made to isolate single crystals of the dinuclear copper complex for X-ray structure determination. The lipophilic, nonyl and heptyl, groups of ligand **3** were replaced with, methyl and *t*-butyl groups respectively to yield **L2**. The resulting copper complex $[Cu_2(\mathbf{L2}\text{-}2H)_2]$ confirmed that the atom which bridged the copper centres was the phenolate oxygen atom rather than the amidate oxygen atom, see Figure 6.1.

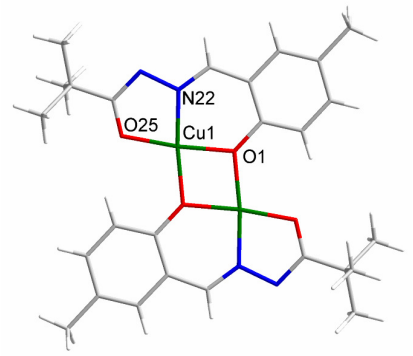

Figure 6.1: X-ray structure of phenolate bridged dinuclear copper complex $[Cu_2(\mathbf{L2}\text{-}2H)_2]$.

An understanding of the copper bridging motif in ligands **1**-**6** indicated that incorporation of an additional acidic functional group into the 3-position of the salicylaldehyde precursors should result in a linear trinuclear copper complex. Introducing a carboxylic acid group yielded 3-formyl-5-alkylsalicylic acid precursors which were used in the synthesis of the triacidic ligands **L4**-**L13**. Solvent extraction experiments carried out for octanoic hydrazone functionalised ligands **L6** and **L7** indicate that they extract three mol of copper per two mol of ligand to form complexes of the type $[Cu_3(\mathbf{L}\text{-}3H)_2]$. The copper loading profile shows evidence for a three step loading process which is consistent with the formation of mono-, di-, and tri-nuclear complexes of the form $[Cu(\mathbf{L}\text{-}H)_2]$, $[Cu_2(\mathbf{L}\text{-}2H)_2]$, $[Cu_3(\mathbf{L}\text{-}3H)_2]$.

Definition of the *structure* of the mono-, di-, and tri-nuclear complexes formed in *solution* is challenging. Mass spectroscopy proved invaluable in confirming the ligand:metal stoichiometry and molecular formulae of the mono-, di-, and tri-nuclear copper complexes formed in the organic extracts. The distinctive isotopic distributions patterns obtained for these complexes due to the relative abundance of copper 63/65 isotopes of 69/31% correlated well with those simulated. Efforts to isolate single crystals of trinuclear copper complexes of the triacidic ligands for X-ray structure determination were not as successful as those for isolation of the dinuclear complex $[Cu_2(\mathbf{L2}\text{-}2H)_2]$. Although a single crystal of the stoichiometry $[Cu_3(L\text{-}3H)_2]$ was not obtained, six X-ray structures were determined which demonstrate that the mode of binding intended through ligand design could result in a linear trinuclear copper complex.

Unfortunately, the limited solubility of the trinuclear copper complexes restricted solvent extraction studies to the 5-alkyl-3-octanoylhydrazonosalicylic acid ligands **L6** and **L7**. The limited solubility in chloroform will undoubtedly translate to very poor solubility in hydrocarbons solvents therefore these ligands are unlikely to be applied in a commercial process. However, blending the triacidic reagents in equimolar quantities with phenolic oximes to form ternary dinuclear copper complexes may find application as the dinuclear copper complexes are anticipated to have greater solubility than the trinuclear complexes.

Although the first objective of this thesis has been met by increasing the molar and mass transport efficiencies of copper solvent extraction relative to the current commercial reagents, their application in industrial processes is unlikely. This is not only due to the limited solubility of the resulting complexes in hydrocarbon solvents but also due to the large pH-swing (0.5-4.5) required to fully load and strip the copper from the complex.

In order to accomplish the third objective of this thesis (Chapter 3), anion binding sites were incorporated into the diacidic salicylaldehyde hydrazone ligand structure used in Chapter 2. Amine groups were used to created polytopic zwitterionic multiloading metal salt extractants which have the potential to extract two mol of copper and sulfate per two mole of ligand into a water-immiscible solvent *via* the formation of $[Cu_2(L)_2(SO_4)_2]$. It was hoped that incorporation of piperazinomethyl groups into the acyl group of the hydrazone (**L14** and **L15**) or in the 3-position of the salicylaldehyde (**L16** and **L17**) would result in formation of $[Cu_2(L)_2(SO_4)_2]$ complexes with the desired 2:2:2 stoichiometry. However, the resulting copper complexes had poor solubility in chloroform.

Solvent extraction results for 3,5-bis((dihexylamino)methyl)salicylaldehyde hydrazone (**L20**) demonstrate the formation of $[Cu_2(\mathbf{L20})_2(SO_4)_2]$ over a relatively narrow pH range (2.0-2.5). Solvent extraction results for the mono-amine analogue, 3-bis(dihexylamino)methyl)-5-*t*-octylsalicylaldehyde hydrazone (**L19**), are consistent with formation of $[Cu_2(\mathbf{L19}\text{-}H)_2(SO_4)]$ as **L19** has half the sulfate carrying capacity of **L20**. This complex was stable over a greater than expected pH range (1.5-5.5) and

L19 exhibited a lower $pH_{½}$ than **P50** in chloroform which indicates that it is a stronger extractant.

The promising extraction properties displayed by **L19** led to further studies to investigate its potential industrial applicability. **L19** was found to be hydrolytically stable to sulfuric acid at an industrially relevant concentration (150 g L^{-1}) and was successfully recycled through 4 consecutive load/strip cycles. Unfortunately, metal selectivity tests indicated that **L19** extracted *ca.* 10% iron and 90% copper when contacted with a mixed metal feed solution containing, Fe(III), Co(II), Ni(II), Cu(II) and Zn(II). Similar studies should be repeated for **L20** in case it displays greater selectivity for copper over iron.

L19 and **L20** were found to be soluble in kerosene at 0.1 M concentrations. The copper complex of **L19** was not very soluble but did dissolve upon addition of a few volume percent of decanol. Commercial phenolic oximes are generally used at concentrations of 0.1-0.3 M, therefore the ligands could be industrially applicable. The absolute solubilities of the ligands in kerosene was not determined because the quantities of ligand required to do this were not available and difficulties which would be encountered when recovering the ligand from the high boiling point solvent deterred the use of the ligand for such studies.

Results obtained for ligands **L19** and **L20** are promising and a more exhaustive study of their industrial applicability is required to establish their potential. The high molecular weights of these ligands means that they do not increase copper mass transport efficiency relative to the commercial reagent **P50**, in fact a decrease of 8 and 20% are calculated for **L19** and **L20** respectively. Nevertheless they do double the molar transport and are capable of extracting metal *salts*; therefore, direct comparison of copper mass transport efficiencies is not appropriate.

The other objective of this thesis (Chapter 4) was to investigate the mode of action of modifiers in copper extraction processes which use the conventional salicylaldoxime reagents. Modifiers increase the effective mass transport in load/strip processes by increasing the $pH_{½}$ value of the reagent to a more industrially relevant pH under strip conditions which results in more copper being stripped from the organic phase than

would be achieved without the use of a more concentrated sulfuric acid solution. The effect of the modifiers, 2-ethylhexanol and trioctylphosphine oxide (TOPO), on the extractive abilities of 5-*t*-octylsalicylaldoxime (**19**) in *n*-heptane were investigated at different equilibrium pH values. Both were found to depress copper loading more at low pH (≤ 2.2) than at high pH (> 3.1). TOPO depressed copper loading to a greater extent than 2-ethylhexanol.

An adduct was identified in the organic phase when TOPO was used as the modifier at high pH (3.1) in the presence of base in the aqueous phase. IR, UV/Vis and EPR results are consistent with formation of a 5-coordinate adduct of the form [Cu(**19**-H)$_2$•TOPO]. UV/Vis titrations of TOPO with [Cu(**19**-H)$_2$] and ^{31}P NMR titrations of **19** with TOPO and with TOPO saturated with sulfuric acid gave similar association constants. As a consequence it is very difficult to define which equilibria process TOPO perturbs most to assist copper stripping. EPR analysis of [Cu(**19**-H)$_2$•TOPO] show that the copper and nitrogen coupling constants measured by EPR are reduced relative to those in [Cu(**19**-H)$_2$]. These observations suggest that the copper complex may be more susceptible to dissociation of the copper-oxygen and copper-nitrogen bonds by protonation of the phenolate oxygen atom, making the complex more kinetically labile.

The observations made in Chapter 4 suggest that 2-ethylhexanol and TOPO perturb the extraction equilibrium in different ways. It is theorised that 2-ethylhexanol associates more readily with the free ligand than the copper complex while TOPO associates approximately equally with both. It is anticipated that the associative interaction with the ligand is the dominant equilibrium process at lower pH values when there is free ligand available and provides the driving force for the depression in copper loading. Whilst at high pH, the ligand is fully loaded and there is no free ligand for the modifier to associate with. In the case of TOPO, the Lewis basic oxygen atom interacts with the Lewis acidic copper centre to form an adduct which is more kinetically labile than the parent complex. It is thought that such adduct formation is not observed with 2-ethylhexanol because the alcohol oxygen atom is not sufficiently electronegative.

A greater understanding of the options to increase mass transport efficiency in copper recovery processes by solvent extraction has been reached by completion of this thesis. The evidence gathered suggests that when more than two copper cations are extracted into a water-immiscible phase, limited solubility of the resulting complex becomes a problem as demonstrated for the trinuclear copper complexes studied in Chapter 2. This does not appear to be such a problem for the dinucleating metal salt reagents discussed in Chapter 3 but further work needs to be carried out to investigate their industrial applicability. Although the mode by which extraction modifiers interact with species in the organic phase at a molecular level has not been fully elucidated, evidence has been obtained for modifiers forming adducts with both ligands and copper complexes.

6.1 References

1. D. Dreisinger, *Hydromet.*, 2006, **83**, 10-20.
2. D. J. White, N. Laing, H. Miller, S. Parsons, S. Coles and P. A. Tasker, *Chem. Commun.*, 1999, 2077-2078.
3. S. G. Galbraith, P. G. Plieger and P. A. Tasker, *Chem. Commun.*, 2002, 2662-2663.
4. R. J. Gordon, J. Campbell, D. K. Henderson, D. C. R. Henry, R. M. Swart, P. A. Tasker, F. J. White, J. L. Wood and L. J. Yellowlees, *Chem. Commun.*, 2008, 4801-4803.
5. R. J. Gordon, J. Campbell, D. C. R. Henry, R. M. Swart, P. A. Tasker, F. J. White, J. L. Wood and L. J. Yellowlees, ISEC 2008, Tuscon, Arizona, 2008.
6. J. L. Wood, PhD Thesis, The University of Edinburgh, 2005.

Chapter 7 Appendix

7.1 Publications

Polyacidic Multiloading Metal Extractants, Ross J. Gordon, John Campbell, David K. Henderson, Dorothy C. R. Henry, Ronald M. Swart, Peter A. Tasker, Fraser J. White, Jenny L. Wood, and Lesley J. Yellowlees, *Chem. Commun*., 2008, 4801.

Polyacidic Extractants to Improve Mass Transport Efficiencies of Base Metals, R. J. Gordon, J. Campbell, D. C. R. Henry, R. M. Swart, P. A. Tasker, F. J. White, J. L. Wood, and L. J. Yellowlees. *International Solvent Extraction Conference Proceedings*, Tucson, Arizona, 2008, 1475.

7.2 Supplementary Data and Contents of Appendix CD

Chapter 1

7.1.1 Figures and Schemes

Chapter 2

7.2.1 Complex Characterisation

7.2.2 Solvent Extraction Data

7.2.3 Crystallographic Data

L2

$C_{13}H_{16}N_2O_2$, *F*w = 232.28, orthorhombic, space group P_{nma}, a = 10.7453(3), b = 6.7631(2), c = 16.8374(5) Å and $\alpha = \beta = \gamma = 90(0)°$, U = 1223.60(6) Å^3, Z = 4, λ = 0.71073 Å, D_{calc} = 1.261 Mgm^{-3}, μ(Mo-Kα) = 0.086 mm^{-1}, F(000) = 496. Data were

collected using a colourless plate oil coated crystal of dimension 0.33 x 0.24 x 0.08 mm using the φ/ω method ($2.25 \leq \theta \leq 30.47°$). Of a total of 12735 reflections collected 1932 were independent. The structure was solved by direct methods (Shelxs Sheldrick) and refined by full-matrix least-squares on F^2 to final values of $R1$ = 0.0827 (for 1856 data with $F>4\sigma F$) and Rw = 0.1892. Goodness of fit on F^2 = 1.228 parameters. Largest difference between peak and hole in the final difference map were 0.478 and -0.573 eÅ^{-3}.

Cu_2(**L2**-2H)$_2$

$C_{28}H_{34}C_{l6}Cu_2N_4O_4$, Fw = 830.37, triclinic, space group $P\bar{1}$, a = 5.9794(3), b = 9.9352(5), c = 15.3792(9) Å and α = 98.853(4), β = 94.933(4), γ = 103.343(4)°, U = 871.33(8) Å^3, Z = 1, λ = 0.71073 Å, D_{calc} = 1.582 Mgm^{-3}, μ(Mo-Kα) = 1.719 mm^{-1}, F(000) = 422. Data were collected using a green needle oil coated crystal of dimension 0.54 x 0.05 x 0.04 mm using the sphere ω scans method ($1.35 \leq \theta \leq 25.03°$). Of a total of 8149 reflections collected 3052 were independent. The structure was solved by direct methods (Shelxs Sheldrick) and refined by full-matrix least-squares on F^2 to final values of $R1$ = 0.0957 (for 2750 data with $F>4\sigma F$) and Rw = 0.2094. Goodness of fit on F^2 = 1.303 parameters. Largest difference between peak and hole in the final difference map were 1.053 and -1.163 eÅ^{-3}.

16•DMSO

$C_{22}H_{28}N_2O_8S_2$, Fw =512.58, monoclinic, space group $P2^1/c$, a = 10.1188(5), b = 11.0055(5), c = 11.1339(5) Å and α = 90, β = 96.868(3), γ = 90°, U = 1231.00(10) Å^3, Z = 2, λ = 0.71073 Å, D_{calc} = 1.383 Mgm^{-3}, μ(Mo-Kα) = 0.265 mm^{-1}, F(000) = 540. Data were collected using a pale yellow rod oil coated crystal of dimension 0.43 x 0.26 x 0.14 mm using the θ/ω method ($2.03 \leq \theta \leq 30.43°$). Of a total of 13426 reflections collected 3544 were independent. The structure was solved by direct methods (Shelxs Sheldrick) and refined by full-matrix least-squares on F^2 to final values of $R1$ = 0.0510 (for 2384 data with $F>4\sigma F$) and Rw = 0.1321. Goodness of fit

on F^2 = 1.057 parameters. Largest difference between peak and hole in the final difference map were 0.437 and -0.257 eÅ^{-3}.

L5•CH_3OH

$C_{18}H_{28}N_2O_5$, *F*w = 352.42, monoclinic, space group $P2^1/c$, a = 12.0497(4), b = 17.1021(5), c = 10.1171(3) Å and α = 90, β = 111.718(2), γ = 90°, *U* = 1936.89(10) Å^3, *Z* = 4, λ = 0.71073 Å, D_{calc} = 1.209 Mgm^{-3}, μ(Mo-Kα) = 0.088 mm^{-1}, F(000) = 760. Data were collected using a pale yellow block, oil coated crystal of dimension 0.48 x 0.35 x 0.26 mm using the ω method ($1.82 \leq \theta \leq 30.50°$). Of a total of 18816 reflections collected 5587 were independent. The structure was solved by direct methods (Shelxs Sheldrick) and refined by full-matrix least-squares on F^2 to final values of *R*1 = 0.0786 (for 4593 data with $F>4\sigma F$) and *Rw* = 0.1707. Goodness of fit on F^2 = 1.128 parameters. Largest difference between peak and hole in the final difference map were 0.535 and -0.305 eÅ^{-3}.

L5•C_2H_5OH

$C_{19}H_{30}N_2O_5$, *F*w = 366.45, monoclinic, space group $P2^1/c$, a = 11.5437(15), b = 19.427(3), c = 9.9438(13) Å and α = 90, β = 111.834(9), γ = 90°, *U* = 2070.0(5) Å^3, *Z* = 4, λ = 0.71073 Å, D_{calc} = 1.176 Mgm^{-3}, μ(Mo-Kα) = 0.085 mm^{-1}, F(000) = 792. Data were collected using a colourless block, oil coated crystal of dimension 0.43 x 0.23 x 0.13 mm using the ω method ($1.90 \leq \theta \leq 25.02°$). Of a total of 19757 reflections collected 3653 were independent. The structure was solved by direct methods (Shelxs Sheldrick) and refined by full-matrix least-squares on F^2 to final values of *R*1 = 0.0737 (for 2563 data with $F>4\sigma F$) and *Rw* = 0.2121. Goodness of fit on F^2 = 1.060 parameters. Largest difference between peak and hole in the final difference map were 0.461 and -0.311 eÅ^{-3}.

L6•py

$C_{22}H_{29}N_3O_4$, *F*w = 399.48, triclinic, space group $P\bar{1}$, a = 8.4017(4), b = 9.0644(4), c = 14.9898(7) Å and α = 98.588(3), β = 104.368(3), γ = 96.169(3)°, *U* = 1080.95(9) Å^3, *Z* = 2, λ = 0.71073 Å, D_{calc} = 1.227 Mgm^{-3}, μ(Mo-Kα) = 0.085 mm^{-1}, F(000) = 428. Data were collected using a colourless block, oil coated crystal of dimension 0.73 x 0.33 x 0.20 mm using the φ/ω method ($2.30 \leq \theta \leq 30.54°$). Of a total of 22690 reflections collected 6267 were independent. The structure was solved by direct methods (Shelxs Sheldrick) and refined by full-matrix least-squares on F^2 to final values of $R1$ = 0.0701 (for 4398 data with $F>4\sigma F$) and Rw = 0.1766. Goodness of fit on F^2 = 1.057 parameters. Largest difference between peak and hole in the final difference map were 0.357 and -0.302 eÅ^{-3}.

L11

$C_{19}H_{21}NO_4$, *F*w = 327.37, monoclinic, space group *C*2/*c*, a = 16.3335(6), b = 17.8346(6), c = 13.1446(5) Å and α = 90, β = 113.367(2), γ = 90°, *U* = 3515.0(2) Å^3, *Z* = 8, λ = 0.71073 Å, D_{calc} = 1.237 Mgm^{-3}, μ(Mo-Kα) = 0.087 mm^{-1}, F(000) = 1392. Data were collected using a red block, oil coated crystal of dimension 0.52 x 0.52 x 0.42 mm using the φ/ω method ($2.72 \leq \theta \leq 27.01°$). Of a total of 27933 reflections collected 3847 were independent. The structure was solved by direct methods (Shelxs Sheldrick) and refined by full-matrix least-squares on F^2 to final values of $R1$ = 0.0523 (for 3202 data with $F>4\sigma F$) and Rw = 0.1513. Goodness of fit on F^2 = 1.099 parameters. Largest difference between peak and hole in the final difference map were 0.336 and -0.423 eÅ^{-3}.

[Cu(**L5**-H)$_2$]

$C_{34}H_{46}CuN_4O_8$, *F*w = 824.38, triclinic, space group $P\bar{1}$, a = 13.8188(7), b = 14.6597(7), c = 22.3253(11) Å and α = 70.937(3), β = 73.965(3), γ = 71.718(3)°, *U* = 3982.0(3) Å^3, *Z* = 4, λ = 0.71073 Å, D_{calc} = 1.375 Mgm^{-3}, μ(Mo-Kα) = 0.616 mm^{-1}, F(000) = 1740. Data were collected using a green block, oil coated crystal of

dimension 0.24 x 0.21 x 0.12 mm using the φ/ω method ($0.98 \leq \theta \leq 25.03°$). Of a total of 53332 reflections collected 14063 were independent. The structure was solved by direct methods (Shelxs Sheldrick) and refined by full-matrix least-squares on F^2 to final values of $R1 = 0.0555$ (for 10776 data with $F>4\sigma F$) and $Rw = 0.1445$. Goodness of fit on $F^2 = 1.037$ parameters. Largest difference between peak and hole in the final difference map were 0.626 and -0.518 eÅ^{-3}.

[Cu(**L4**-2H)(H_2O)]

$C_{14}H_{18}CuN_2O_5$, *F*w = 357.84, monoclinic, space group *C*2/*c*, a = 37.1378(12), b = 6.5536(2), c = 36.1806(12) Å and $\alpha = 90$, $\beta = 90.907(2)$, $\gamma = 90°$, $U = 8804.8(5)$ Å^3, $Z = 16$, $\lambda = 0.71073$ Å, $D_{calc} = 1.080$ Mgm^{-3}, μ(Mo-Kα) = 1.009 mm^{-1}, F(000) = 2960. Data were collected using a green needle, oil coated crystal of dimension 0.33 x 0.08 x 0.06 mm using the φ/ω method ($1.10 \leq \theta \leq 25.03°$). Of a total of 36899 reflections collected 7776 were independent. The structure was solved by direct methods (Shelxs Sheldrick) and refined by full-matrix least-squares on F^2 to final values of $R1 = 0.0685$ (for 6325 data with $F>4\sigma F$) and $Rw = 0.1647$. Goodness of fit on $F^2 = 1.076$ parameters. Largest difference between peak and hole in the final difference map were 0.774 and -0.758 eÅ^{-3}.

[Cu(**L5**-H)(H_2O)][ClO_4]

$C_{17}H_{25}ClCuN_2O_9$, *F*w = 500.38, monoclinic, space group $P2^1/n$, a = 9.4842(3), b = 9.0628(3), c = 25.8018(8) Å and $\alpha = 90$, $\beta = 97.7040(10)$, $\gamma = 90°$, $U = 2197.73(12)$ Å^3, $Z = 4$, $\lambda = 0.71073$ Å, $D_{calc} = 1.512$ Mgm^{-3}, μ(Mo-Kα) = 1.165 mm^{-1}, F(000) = 1036. Data were collected using a green block, oil coated crystal of dimension 0.55 x 0.44 x 0.24 mm using the φ/ω method ($1.59 \leq \theta \leq 29.54°$). Of a total of 23487 reflections collected 5539 were independent. The structure was solved by the heavy (Dirdif 99) method and refined by full-matrix least-squares on F^2 to final values of $R1 = 0.0422$ (for 5146 data with $F>4\sigma F$) and $Rw = 0.1052$. Goodness of fit on $F^2 = 1.167$ parameters. Largest difference between peak and hole in the final difference map were 0.623 and -0.649 eÅ^{-3}.

$[Cu_2(\mathbf{L11}\text{-}2H)_2]$

Crystal data were twinned. $C_{19}H_{19}CuNO_4$, *F*w = 388.89, triclinic, space group $P\bar{1}$, a = 6.8829(7), b = 9.6493(10), c = 12.3771(12) Å and α = 88.498(6), β = 83.850(6), γ = 83.339(6)°, *U* = 811.70(14) Å^3, *Z* = 2, λ = 0.71073 Å, D_{calc} = 1.591 Mgm^{-3}, μ(Mo-Kα) = 1.370 mm^{-1}, F(000) = 402. Data were collected using a yellow plate, oil coated crystal of dimension 0.54 x 0.21 x 0.01 mm using the sphere method ($1.65 \leq \theta \leq 26.37°$). Of a total of 3802 reflections collected 3802 were independent. The structure was solved by direct methods (Shelxs Sheldrick) and refined by full-matrix least-squares on F^2 to final values of $R1$ = 0.0865 (for 3091 data with $F>4\sigma F$) and Rw = 0.2302. Goodness of fit on F^2 = 1.093 parameters. Largest difference between peak and hole in the final difference map were 1.820 and -1.073 eÅ^{-3}.

$[Cu_6(\mathbf{L6}\text{-}3H)_2(\mathbf{L6}\text{-}2H)_2(MeO)_2(MeOH)_6\bullet 6(MeOH)]$

$C_{82}H_{136}Cu_6N_8O_{30}$, *F*w = 2095.23, triclinic, space group $P\bar{1}$, a = 12.6441(3), b = 13.2751(3), c = 15.0230(4) Å and α = 104.936(2), β = 94.422(2), γ = 92.036(2)°, *U* = 2425.17(10) Å^3, *Z* = 1, λ = 0.71073 Å, D_{calc} = 1.435 Mgm^{-3}, μ(Mo-Kα) = 1.371 mm^{-1}, F(000) = 1098. Data were collected using a green block, oil coated crystal of dimension 0.30 x 0.18 x 0.18 mm using the φ/ω method ($1.59 \leq \theta \leq 26.06°$). Of a total of 33179 reflections collected 9561 were independent. The structure was solved by direct methods (Shelxs Sheldrick) and refined by full-matrix least-squares on F^2 to final values of $R1$ = 0.0679 (for 5900 data with $F>4\sigma F$) and Rw = 0.2036. Goodness of fit on F^2 = 1.044 parameters. Largest difference between peak and hole in the final difference map were 1.089 and -0.778 eÅ^{-3}.

$[Cu_{10}(\mathbf{L5}\text{-}3H)_4(OH)_4(CH3COO)_4(MeOH)_2\bullet 11(H_2O),3(MeOH)]$

$C_{81}H_{148}Cu_{10}N_8O_{46}$, *F*w = 2605.47, triclinic, space group $P\bar{1}$, a = 12.7080(10), b = 14.8129(12), c = 16.8881(11) Å and α = 115.562(5), β = 95.165(5), γ = 93.821(6)°, *U* = 2836.5(4) Å^3, *Z* = 1, λ = 0.71073 Å, D_{calc} = 1.525 Mgm^{-3}, μ(Mo-Kα) = 1.921 mm^{-1}, F(000) = 1348. Data were collected using a green block, oil coated crystal of

dimension 0.30 x 0.27 x 0.21 mm using the sphere (omega scans) method ($1.35 \leq \theta \leq 25.12°$). Of a total of 27866 reflections collected 10026 were independent. The structure was solved by direct methods (Shelxs Sheldrick) and refined by full-matrix least-squares on F^2 to final values of $R1 = 0.0814$ (for 5283 data with $F>4\sigma F$) and $Rw = 0.2255$. Goodness of fit on $F^2 = 0.933$ parameters. Largest difference between peak and hole in the final difference map were 1.900 and -1.514 eÅ^{-3}.

7.2.4 Figures and Schemes

7.2.5 Magnetic Susceptibility Data

7.2.6 EPR Spectra of Copper Complexes of **L7**

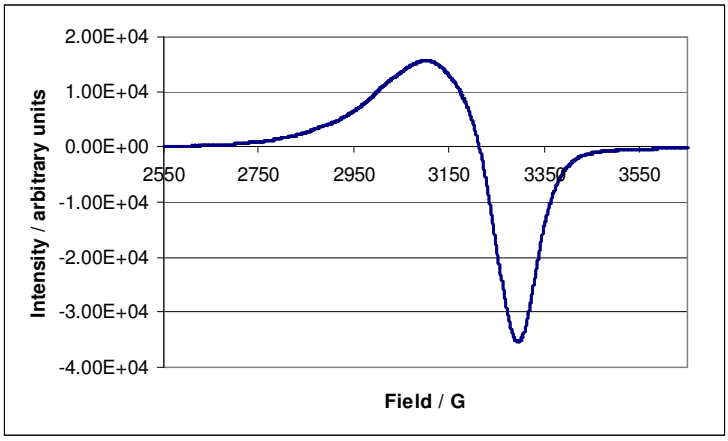

Figure 7.1: X-Band EPR spectra of [Cu(**L7**-H)$_2$] at 140 K.

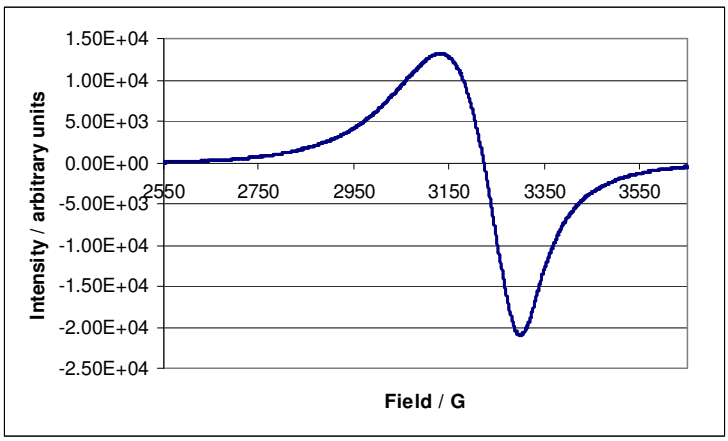

Figure 7.2: X-Band EPR spectra of [Cu$_2$(**L7**-2H)$_2$] at 140 K.

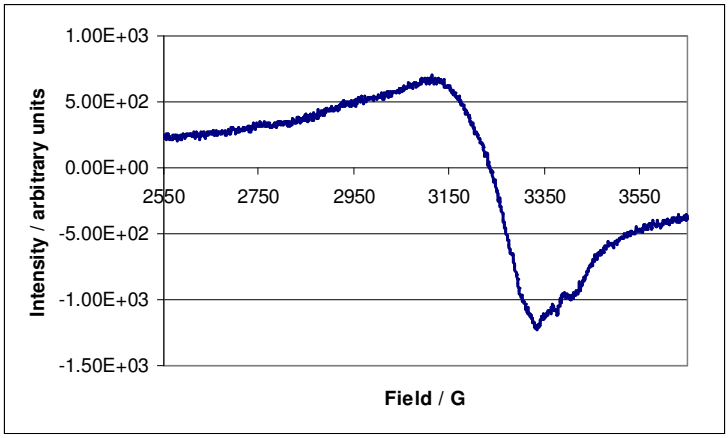

Figure 7.3: X-Band EPR spectra of $[Cu_3(\mathbf{L7}\text{-}3H)_2]$ at 140 K.

Chapter 3

7.3.1 Complex Characterisation

7.3.2 Solvent Extraction Data

7.3.3 Figures and Schemes

Chapter 4

7.4.1 Solvent Extraction Data

7.4.2 Complex Characterisation

7.4.3 Association Constant Data

7.4.3.1 Association Constant Data Fitting Curves

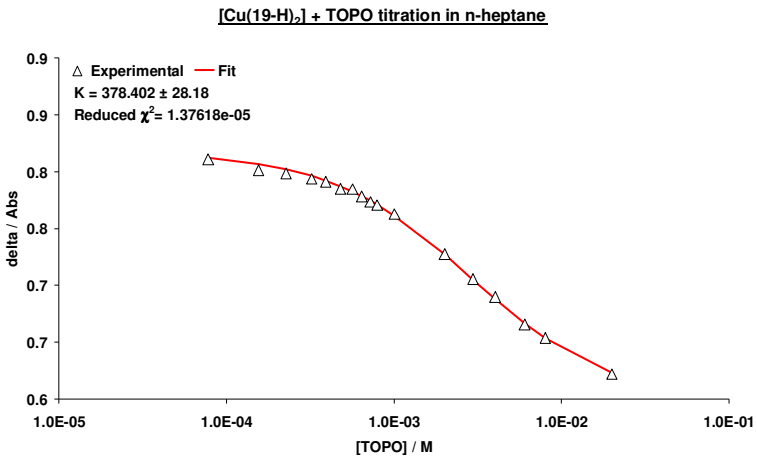

Figure 7.4: Association constant data fitting for the UV/Vis titration of an *n*-heptane solution of [Cu(**19**-H)$_2$] with increasing molar equivalents of TOPO.

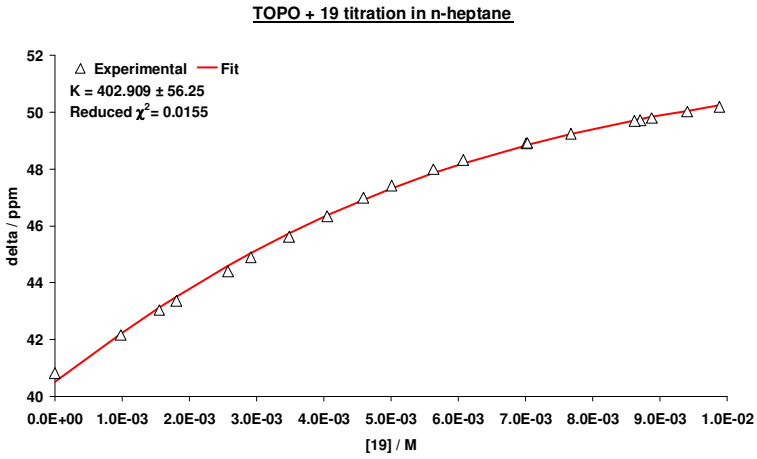

Figure 7.5: Association constant data fitting for the ^{31}P NMR titration of an *n*-heptane solution of TOPO with increasing molar equivalents of **19**.

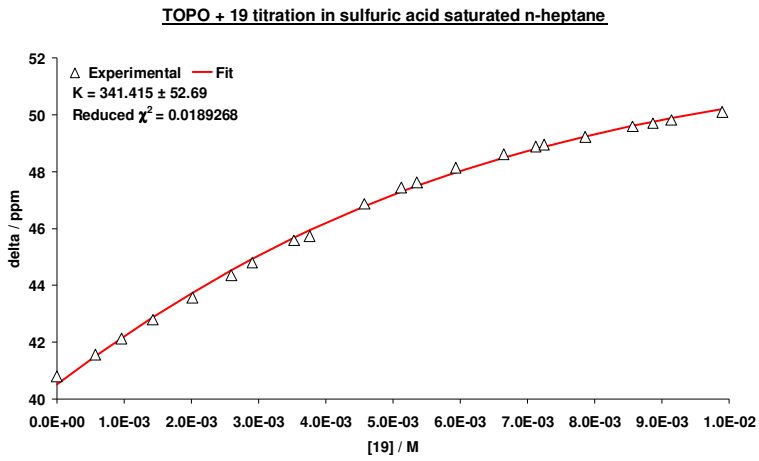

Figure 7.6: Association constant data fitting for the ^{31}P NMR titration of a sulphuric acid saturated *n*-heptane solution of TOPO with increasing molar equivalents of **19**.

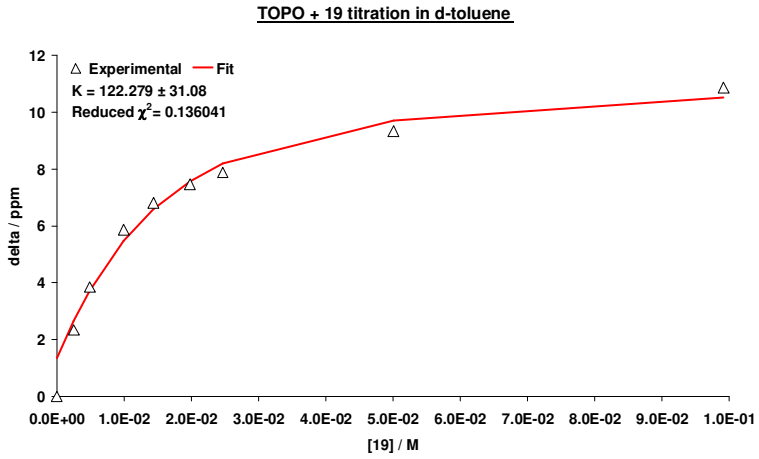

Figure 7.7: Association constant data fitting for the ^{31}P NMR titration of a d-toluene solution of TOPO with increasing molar equivalents of **19**.

7.4.4 Molecular Modelling

7.4.5 Figures and Schemes